Landau-gauge Green's functions in unquenched lattice QCD

Maria B. Parappilly

Supervisors: Prof. Anthony G. Williams and
A/Prof. Derek B. Leinweber

A Thesis presented for the degree of
Doctor of Philosophy

Centre for the Subatomic Structure of Matter
University of Adelaide
Adelaide
2006

To the honor and memory of my father P. J. Francis.

Abstract

Most previous lattice calculations have been done in quenched QCD, where the effects of fermion vacuum fluctuations are neglected in the creation of the gluon field configurations. The sea-quark masses may be thought of as infinite in the quenched approximation. Due to computational resource issues, the quenched approximation provided the basis for the vast majority of lattice calculations until relatively recently. In order to meaningfully test QCD against experimental observation, realistic simulations with the dynamical sea-quarks are needed. Computing resources becoming available now are powerful enough to treat up, down and strange quarks dynamically.

A major component of this work consists of full lattice QCD calculations of some of the fundamental quantites of QCD. We are computing the gluon and quark propagators in full QCD and investigating the effects of finite sea-quark masses on these. We have used the configurations generated by the MILC collaboration to do nonperturbative simulations with $2 + 1$ flavors of dynamical quarks. We have performed extensive simulations with realistic quark vacuum polarization (quark loops) to evaluate the effect of unquenching.

We use an improved staggered fermion action "AsqTad" in the dynamical simulations. Current simulations with dynamical staggered quarks have the benefits of both good chiral properties at moderate lattice spacing and being computationally inexpensive. A highlight of this study is the first results for gluon and quark propagators in Landau gauge with 2+1 flavors of dynamical quarks. A comparative study of quenched and unquenched results for both quark and gluon propagators, which probes the effects of dynamical sea-quarks is a significant part of this work.

In the second part of this thesis, we study the scaling behavior of the quark and gluon propagator in Landau gauge with $2 + 1$ flavors of dynamical quarks on two lattices with different lattice spacings and similar physical volumes in order to test whether we are close to the continuum limit for these lattices. We compare the mass function and wave renormalization function for two different lattice spacings and find them to be consistent within errors. The Asqtad quark propagator shows good scaling behavior as does the gluon propagator for the lattice spacings considered. The work carried out in this thesis provides a clear understanding of the role of dynamical sea-quarks on the Landau-gauge Green's functions.

Testing of the violation of positivity of the gluon propagator comes in the third part of this thesis. Correlation functions play an important role in the nonperturbative studies of the gluon propagator and confinement. Violation of positivity is considered to be a sufficent condition for confinement. An infrared suppressed propagator always violates reflection positivity and we found explicit evidence for this in our study.

Statement of Originality

This work contains no material which has been accepted for the award of any other degree or diploma in any university or other tertiary institution and, to the best of my knowledge and belief, contains no material previously published or written by another person, except where due reference has been made in the text.

I give consent for this copy of my thesis, when deposited in the University library, to be available for loan and photocopying.

Maria Parappilly

Acknowledgements

This thesis would never have come into existence if my principal supervisor Tony Williams had not given me moral support at times of distress during my candidature. I am eternally grateful for the friendship and support I have received from him throughout the three years I have spent on this work.

I wish to thank my supervisors Derek Leinweber and Tony Williams for their continued assistance, support and encouragement. Thanks to Tony in providing a motivating, enthusiastic, and critical atmosphere during the many discussions we had. I also acknowledge Derek Leinweber who as my co-supervisor provided many constructive comments along the way.

The help of Patrick Bowman made my transition into the graduate program an effortless one. Special thanks to Jianbo Zhang, with whom I worked on the major part of this thesis, and who was always there to help when I got stuck. I also want to thank Patrick Fitzhenry for his help in computing the majority of this work on the Hydra supercomputer. Sincere thanks also to Ben Lasscock for all the help provided. Thanks also to Andre Sternbeck for his colloboration on positivity violation studies.

Working at the CSSM was great. I thank everyone especially Sara, Sharon and Ramona for making the place friendly and welcoming. Needless to say, I am grateful to all my friends and colleagues in the CSSM who have always been there for me. And a special thanks to Sisters of St. Anne's girls high school, Kerala, India for being a strong influence during my formative years. Thanks to Anisha, my best friend who did the proof reading.

Last but not least I would like to thank my family. Special thanks to my husband Boy and my wonderful daughter Aline for putting up with me and my long hours of work. This wouldn't be possible without them. Mum, my strength comes from you. And a special mention to all the members of my family back home.

Contents

List of Figures

List of Tables

Introduction

The standard model describes the interactions of the fundamental constituents of matter. The standard model, based on the gauge group $SU(3) \otimes SU(2) \otimes U(1)$, is one of the great successes of the gauge theory revolution. The universe appears to be governed by four kinds of forces: strong, electromagnetic, weak and gravitational. The particles undergoing strong forces (nuclear forces) are known as hadrons. The key to the understanding of the strong interaction is the representation of all hadrons as composite of basic fermions called quarks and antiquarks within the theory known as Quantum Chromodynamics (QCD). The description of matter in terms of quarks and leptons, QCD and Electroweak (EW) Theory with their gauge field quanta is referred to as the Standard Model of particle physics. It is a powerful tool to understand the hadron spectrum, their internal structures and their interactions. Hadron interactions occur through the interactions of their quark and gluon components. The strength of these interactions is characterized by the so-called coupling constant. When the forces are weak, the predictions of the theory can be worked out in terms of an expansion in powers of the coupling constant, which is referred to as perturbation theory.

Quantum chromodynamics, called QCD, is the theory of strong interactions. It is a non-abelian variant of QED (Quantum ElectroDynamics), the quantum gauge theory which describes the interaction between electrons and photons. QED is referred to as an abelian gauge theory, since the group structure is $U(1)$ and since the elements of this group all commute with each other. Non-abelian gauge theories are built on group structures [*e.g.* $SU(N)$] whose elements do not commute. QCD, the gauge field theory which describes the interaction of quarks and gluons, is one of the components of the $SU(3) \otimes SU(2) \otimes U(1)$ Standard Model. The theoretical picture of the strong interactions began with the identification of elementary fermions, called quarks, that make up the proton and other hadrons. The strong interaction is associated with the unbroken non-abelian symmetry group $SU(3)$. QCD is a non-abelian gauge field theory describing the strong interaction between quarks and antiquarks with the gluons being the quanta of the QCD gauge fields.

Non-abelian gauge field theories, formulated in 1954 by C.N. Yang and R.L. Mills, are non-abelian quantum versions of Maxwell's theory of electromagnetism. In formulation, QCD and QED are strikingly similar. Both are gauge-invariant quantum field theories. The coupling constant of QCD characterizes the strength of the interaction between quarks and gluons in a similar manner to the fine structure constant in QED. The smallness of the QED fine structure constant, $\alpha \approx 1/137$, guarantees the prediction of physical quantities with high precision using perturbation theory. QCD has been shown to be an asymptotically free gauge field theory, where the interaction between quarks and gluons becomes weaker in the short-distance limit.

Perturbation theory is extremely successful in Quantum Electrodynamics and is

useful in the high energy regime of Quantum Chromodynamics, but no matter what the coupling, some features of a theory, such as spontaneous symmetry breaking, can not appear at any finite order in perturbation theory. If the coupling that characterises a theory is strong, which is the case in QCD at intermediate to low energies, then the perturbative series will converge poorly, or not at all. In such a case we must turn to nonperturbative methods.

1.1 Quarks and gluons

Quarks, invented in 1964 by M. Gell-Mann and G. Zweig, are basic to the understanding of hadron spectroscopy. The simple and elegant theory of QCD is formulated in terms of quarks and gluons. Quarks are the building blocks of protons, neutrons and related subatomic particles. There are six quarks: up, down, strange, charm, bottom and top. Protons and neutrons are bundles of 3 quarks and any number of quark-antiquark pairs. Quarks and gluons experience and transmit strong forces which are described by a theoretical concept called color. "Color" is a conserved quantum number which is absent in leptons. QCD has three different kinds of charge, 'color' where as in QED there is only one kind of charge. Color charges of QCD have nothing to do with physical colors. Rather, they have properties analogous to electric charge. A quark of a given flavor has three different color states. Conventionally, they are labeled red, blue and green. Antiquarks have the corresponding anticolors. Triplets of quarks containing equal portions of the three colors are color neutral or 'white'.

The fundamental idea of QCD is that the color charges of quarks act as the sources of the strong, so-called chromodynamic forces between quarks just like electric charge between charged particles. At a qualitative level, it successfully accounts for many observed phenomena. Color-induced interactions between quarks are mediated by *gluons*, the massless spin-1 gauge bosons of QCD. Quarks can change their color state after emitting or absorbing gluons. Due to color conservation, gluons also carry color quantum numbers and hence as a result they also interact with each other. This self interaction of gluons makes QCD very different from QED where photons can not interact directly. Thus the standard theory of hadronic interactions is based on quarks interacting with non-abelian gauge fields. The non-abelian nature of the theory means that the gluons couple to themsleves.

This thesis is organized as follows:

The principal of gauge invariance is a most significant underlying concept and it is one basic property QCD has in common with QED. QCD also has other "internal" symmetries which are explained in the 2nd Chapter. The extraordinary thing about quarks and gluons is that they are never seen as free particles in nature. Indeed, no object with color charge has ever been seen. This property is called confinement. It implies that all observable particles with strong interactions have zero color charge. Confinement is also discussed in Chapter 2. Numerical simulations of lattice QCD allow us to study quark confinement. Some results leading to confinement of gluons

are presented in Chapter 8. Some results from perturbative QCD are also discussed briefly in Chapter 2. The proton is made up of two up quarks and a down quark ($2m_u + m_d \simeq 12$ MeV). The mass of the proton is 938 MeV. Where does the proton mass (938 MeV $\gg$ 12 MeV) come from? Infact, the proton mass comes from the current quarks acquiring mass through dynamical mass generation, which is a form of spontaneous symmetry breaking. Dynamical mass generation and chiral symmetry breaking are discussed in Chapter 2.

In the mathematical formulation of QCD, the basic quantities are quark and gluon fields, which are functions of the space-time coordinates. Discretization of space-time is introduced to allow numerical treatment. This procedure turns differential operators into finite difference operators and the fields are defined either on the links or on the points of a space-time lattice. Quantization is acheived by Feynman's path integral representation.

The primary role of the lattice is to provide a non-perturbative regularisation. It provides a minimum wavelength through the lattice spacing a, *i.e.,* a maximum momentum of π/a. I have described the principles of lattice calculations, the use of path integrals, the gauge fixing, the standard Wilson actions, and improved lattice actions in Chapter 3. Techniques involving the staggered fermion formalism as well other method for putting fermions on the lattice are also briefly explained in this chapter.

The quenched approximation, in which the effect of quark loops is neglected, reduces the computational time for numerical simulations dramatically, and hence has been used in many of the previous studies. The quenched approximation ignores the fermion contribution to the path integral. Unquenched QCD (full QCD) corresponds to the real world, though it is computationally expensive. Computing resources avaliable now are powerful enough to treat up, down and strange quarks dynamically. We may also assume that up and down quarks are degenerate, since this reduces the computational costs of simulations to minimum. The quenched approximation can be safely applied for the heavier quarks, namely charm, bottom and top quarks [Kan] for the typically low energies considered here. There are three physical sources of systematic errors in any lattice calculation. They are finite volume, quark masses $m_q a$ and the nonzero lattice spacing. The quenched approximation where it used is the main algorithmic source of systematic error [Got97].

The main focus of this thesis is the results for two-point Greens functions in full QCD. We compute full QCD calculations for a number of reasons:

- To describe the real world with the inclusion of dynamical quarks.
- To investigate the effect of dynamical sea-quarks on the gluon and quark propagators.
- To reduce the systematic errors due to the quenched approximation.

Simulating with light dynamical quarks for full QCD calculations is a difficult task. Also lattice simulations with light fermions are computationally demanding. Incorporating fermions into the functional integral demands significant additional effort. The computational cost of Monte Carlo simulations in a box of length L with

lattice spacing a and quark mass m_q scales approximately as [FGMS03, DeG04]

$$(L/a)^4(1/a)^2(1/m_q)^3. \tag{1.1}$$

The first term in parentheses takes account of the number of sites, the second term gives the cost of "critical slowing down"- the extent to which successive configurations are correlated [DeG04]. This occurs because the Monte Carlo acceptance probability diminishes with decreasing lattice spacing. The third term gives the cost of inverting the fermion propagator. This makes it too expensive at present to let the u and d quarks be as light as they are in nature. The numerical cost increases substantially with decreasing quark masses as the CPU time for unquenched simulations increases as quark mass decreases. So unquenched simulations are typically performed using light quark masses (u and d) with masses larger than half of the strange quark mass. Improved Kogut-Susskind staggered fermion actions are less expensive than the Wilson-type of action to simulate with on both coarse and fine lattices. The lightest dynamical quark masses are obtained with staggered fermions. We have performed dynamical fermion simulations with staggered fermions (two light and a heavier strange quark), where the strange quark has its physical value.

We have performed calculations of the quark and gluon propagator in quenched and full QCD on coarse and fine lattices with similar physical volumes. In Chapter 4, I have explained the basics of the gluon propagator, the lattice implementation and the calculation of the gluon propagator both in quenched and full QCD. The effect of dynamical sea-quarks on gluon propagator can be clearly seen. The comparison of quenched and full QCD results for the gluon propagator is the highlight of this chapter. We have also studied the sea quark mass dependence on the gluon propgator. These results for the nonperturbative study of the gluon propagator both in quenched and unquenched QCD is obtained from high statistics lattice simulations.

In Chapter 5, we study the role of dynamical sea-quarks on the quark propagator. The quark propagator results also shows us that the degree of mass generation is diminished when we include the sea-quarks in the calculation. Quenched and unquenched results are also presented for a comparitive study. We also study the sea-quark mass dependence of the quark propagator.

Chapter 6 deals with the computation of the gluon and quark propagator on a fine lattice. The results reveal that the effect of sea-quarks are very much similar to the case of the coarse lattice.

In Chapter 7, we study the scaling behavior of gluon and quark propagators by working on two different sets of lattices with different lattice spacings. We find good scaling overall for the lattice spacings considered.

We test positivity of the gluon propagator as a test of whether or not the gluon is confined in Chapter 8. We calculate the real space propagator (Schwinger function) on both fine and coarse lattices. When the Schwinger function becomes negative, reflection positivity becomes violated, which is a sufficent condition for gluon confinement. Positivity violation for the gluon propagator has been studied in the quenched case before but we are doing the first test of positivity for the gluon propagator in full lattice QCD here.

Chapter 9 closes with the conclusions and remarks on the work presented in this thesis and with a discussion of possible future studies.

2

QCD and perturbative QCD

In QED, perturbative calculations of quantities of physical interest are possible because of the smallness of the electron photon coupling constant $e \sim 0.303$, ($\alpha = \frac{e^2}{4\pi} = 1/137$). This success arises from the fact that the increasingly complicated higher-order terms become decreasingly important. The smallness of the coupling constant in QED gave physicists confidence that perurbation theory was a reliable approximation to the theory. In contrast to QED, the strongly interacting particles, "the hadrons" have a coupling constant of order 1 meaning that perturbation theory is not useful in predicting the spectrum of strongly interacting particles.

In the late fifties and sixties it was generally believed that the strong interactions of hadrons may not be described in any sense by the perturbative method of quantum field theory. Accordingly, formulations based on the perturbative method were discarded in the theory of strong interactions and suitable formulations independent of the perturbative approach were sought. Perturbation theory can not be expected to provide us with detailed information about strong coupling problems such as quark confinement and dynamical chiral symmetry breaking.

After years of struggle, a theory has emerged to give us the best understanding of the strong interactions and this theory is referred to as QCD. The principal breakthrough which eventually led to quantum chromodynamics was the discovery of the property of asymptotic freedom of non-abelian gauge theories like QCD for which Gross, Politzer and Wilczek received the 2004 Nobel prize in Physics. QCD is an asymptotically free theory and using that property one can safely use perturbation theory to discuss short-distance interactions. In QCD, the coupling constant at typical energies available in present-day accelerators is $\alpha_s \backsim \frac{1}{10}$.

The perturbative treatment of QCD is allowed for very large mometum transfers. However, in many body problems of the hadron system, a non-perurbative treatment of QCD is necessary. Techniques of nonperturbative QCD are also important for physics beyond the Standard Model. In the low-energy region where the coupling constant g is large and perturbation theory fails, it is possible to use Lattice QCD to carry out a first-principles exploration of the non perturbative behavior of QCD. To date, the testing of QCD against experimental studies is restricted to the domain of high-energy scattering where perturbation theory can be applied.

In 1974, Wilson proposed a formulation of quantum chromodynamics (QCD) on a discrete space-time lattice. Via the functional integral formalism one could non-perturbatively regularize QCD by introducing such a lattice. The lattice was constructed through the introduction of the lattice spacing a. Then we can formulate QCD on lattice such that when we take $a \to 0$ we recover the standard continuum form of QCD. Clearly, there are many such discretisations possible with correct continuum limit. Obviously those discretisations which are cheap to compute and with the fastest convergence to the continuum limit are preferred.

For any theory to provide a successful description of strong interactions it should simultaneously exhibit the phenomena of confinement at large distances and asymptotic freedom at short distances.

2.1 QED and the gauge principal

The principle of gauge invariance is one of the most significant concepts used in modern particle physics. The basic method of gauge theory is to ensure that the Lagrangian describing the interaction of particle wave functions, remain invariant under certain symmetry transformations which reflect conservation laws observed in nature. The Lagrangian density for the free electromagnetic field (in usual Minkowski space) is

$$\mathcal{L}_{\text{em}} = -\frac{1}{4}F_{\mu\nu}F^{\mu\nu}, \tag{2.1}$$

where $F_{\mu\nu} = \partial_\mu A_\nu - \partial_\nu A_\mu$ is the electromagnetic field tensor and A_μ is the electromagnetic vector potential. The Lagrangian density of the free Dirac field is given by

$$\mathcal{L}_{\text{free}} = \bar{\psi}(i\,\partial\!\!\!/ - m)\psi = \bar{\psi}(i\gamma^\mu\partial_\mu - m)\psi\,, \tag{2.2}$$

where ψ is the fermion field and m is the fermion mass. The full Lagrangian for charged Dirac fermions interacting with the electromagnetic field is

$$\mathcal{L}_{\text{QED}} = \bar{\psi}(i\,\partial\!\!\!/ - m)\psi - \frac{1}{4}F_{\mu\nu}F^{\mu\nu} - e\bar{\psi}\gamma^\mu\psi A_\mu. \tag{2.3}$$

The group we consider here is the Abelian group $U(1)$ which denotes the shift in the phase of the electron. Under a global phase transformation $\psi(x) \to e^{i\alpha}\psi(x)$ for a constant phase α, we see that the Dirac density is invariant. A gauge transformation is a local phase transformation, $\alpha \to \alpha(x)$. Under such a gauge transformation $\psi(x) \to e^{i\alpha(x)}\psi(x)$, the Dirac Lagrangian density is changed by the transformation and is not invariant due to the derivative. The invariance under gauge transformations of the fermions thus requires a compensating gauge transformation of the electromagnetic field.

$$A_\mu \to A_\mu - \frac{1}{e}\partial_\mu\alpha(x). \tag{2.4}$$

With the requirement that the electromagnetic (photon) field transform in this way we see that the sum of the first and third terms in Eq. (2.3) are now gauge invariant. It is easily seen that the photon Lagrangian density is itself gauge invariant and needed to introduce a photon kinetic term. Hence, the requirement of the gauge invariance for the Dirac fermion field has lead directly to the QED Lagrangian density of Eq. (2.3). This resulted simply from the requirement that the local $U(1)$ phase invariance of the Dirac fermion (the electron) be generalized to a local phase invariance. We can express things in a more compact form by introducing the gauge covariant derivative

$$D_\mu \equiv \partial_\mu + ieA_\mu(x). \tag{2.5}$$

The QED Lagrangian density can then be written more simply as

$$\mathcal{L}_{\rm QED} = \bar{\psi}(i \not{D} - m)\psi - \frac{1}{4}F_{\mu\nu}F^{\mu\nu}. \tag{2.6}$$

This Lagrangian is then invariant under $U(1)$ *gauge transformations* by construction. Indeed, it is important to emphasize that the most successful theory in physics, QED, follows trivially from the requirement that electrons be locally phase invariant, *i.e.*, $U(1)$ gauge invariant.

2.2 QCD and nonabelian gauge invariance

Quantum chromodynamics is correspondingly defined as a field theory by its own Lagrangian density. QCD is based on the extension of the idea explained above, but with the $U(1)$ gauge group replaced by the $SU(3)$ group of phase transformations on the quark color fields. Notations and conventions in this section follow [PS]. The Lagrangian density for the free fermion field, $\psi(x)$, in Minkowski space is given by (supressing the spinor, flavor and color indices as is standard)

$$\mathcal{L}_{\rm free}(x) = \bar{\psi}(i \not{\partial} - m)\psi(x), \tag{2.7}$$

and is invariant under global gauge tranformations,

$$\psi(x) \to G\psi(x), \;\; \bar{\psi}(x) \to \bar{\psi}(x)G^{\dagger}, \tag{2.8}$$

where $G \in SU(N)$, where $N = 3$ for QCD. The $U(1)$ version of G is $e^{i\alpha}$. The principle of gauge invariance states that $\mathcal{L}(x)$ should also be invariant under *local* $SU(3)$ *gauge transformations*,

$$\psi(x) \to G(x)\psi(x), \;\; \bar{\psi}(x) \to \bar{\psi}(x)G^{\dagger}(x). \tag{2.9}$$

However, we can see that $\mathcal{L}_{\rm free}(x)$ is not locally gauge invariant as

$$\mathcal{L}_{\rm free}(x) \to \mathcal{L}'_{\rm free}(x) = \bar{\psi}(x)(i \not{\partial} - m)\psi(x) + \bar{\psi}(x)G^{\dagger}(x)\left[\not{\partial} G(x)\psi(x)\right]. \tag{2.10}$$

The problem is that ∂_μ now acts non-trivially on $G(x)$. We can resolve this problem by introducing a gauge covariant derivative in analogy with the $U(1)$ case,

$$D_\mu = \partial_\mu - ig_s A_\mu, \tag{2.11}$$

where g_s is the QCD ("strong") coupling, the gluonic field $A_\mu(x) = A^a_\mu T_a(x)$ contains the eight gluon vector fields A^a_μ, and T_a are the eight generators of $SU(3)$. In analogy with Eq. (2.4) the gauge field $A_\mu(x)$ is then required to tranform under an $SU(3)$ gauge transformation as

$$A_\mu(x) \to G(x)\left(A_\mu(x) + \frac{1}{ig_s}\partial_\mu\right)G^{\dagger}(x). \tag{2.12}$$

As $G(x)G^\dagger(x) = 1$, we have $\big(\partial_\mu G(x)\big)G^\dagger(x) = -G(x)\big(\partial_\mu G^\dagger(x)\big)$ and hence the covariant derivative tranforms as

$$D_\mu\psi(x) \to G(x)D_\mu\psi(x), \tag{2.13}$$

and thus as a result of our definition, Eq. (2.12), we see that

$$\mathcal{L}(x) = \bar{\psi}(x)(i\not{D} - m)\psi(x)\,, \tag{2.14}$$

is invariant under local $SU(N)$ gauge tranformations, with $N = 3$ for QCD. Hence we see that in QCD the gauge group is $SU(3)$ (non-abelian), and the quarks (ψ) and gluons (A_μ) belong to the fundamental and adjoint representations of $SU(3)$ respectively. We also have $A_\mu(x) \equiv A^a_\mu(x)T_a(x)$, where we have eight gluon fields $A^a_\mu(x)$ and T_a with $a = 1, ..., 8$ are the eight generators of $SU(3)$. Again we must add a kinetic term for the gluon field which is itself gauge invariant and hence the final $SU(3)$ gauge invariant QCD Lagrangian is given by

$$\mathcal{L} = \bar{\psi}(x)(i\not{D} - m)\psi(x) - \frac{1}{2}\mathrm{tr}F_{\mu\nu}(x)F^{\mu\nu}(x) \tag{2.15}$$

where $F_{\mu\nu} = \partial_\mu A_\nu - \partial_\nu A_\mu + g_s[A_\mu, A_\nu]$ is the antisymmetric field tensor, which satisfies $[D_\mu, D_\nu] = -ig_sF^{\mu\nu}$. It is straightforward to verify that the 2$^{\text{nd}}$ of Eq. (2.15) is invariant under the gauge transformation of Eq. (2.12). The important new feature of the Lagrangian Eq. (2.15) is that it includes cubic and quadratic self-interactions among the gauge fields through the gluon kinetic term $\frac{1}{2}\mathrm{tr}F_{\mu\nu}F^{\mu\nu}$. The self-interactions have arisen from the need to write down a kinetic term (quadratic in A), which is gauge-invariant under a nonabelian gauge transformation.

2.3 Gauge fixing

The gauge invariance of $\mathcal{L}(x)$, where the gauge field has the freedom of gauge transformations, actually makes it somewhat difficult to quantize the theory. One way of getting rid of this difficulty is to eliminate the freedom of the gauge transformation by imposing constraints on the field A^a_μ. This problem is solved by adding to $\mathcal{L}(x)$ *gauge-fixing* and *ghost* densities $\mathcal{L}_{\text{gauge}}$, $\mathcal{L}_{\text{ghost}}$ The most common choice being the covariant gauge fixing

$$\mathcal{L}_{\text{gauge}} = -\frac{\lambda}{2}\sum_\mu \big[\partial_\mu A_\mu(x)\big]^2,\ 1 < \lambda < \infty, \tag{2.16}$$

where the parameter λ is effectively a Lagrangian multiplier. It is customary to write

$$\lambda = \frac{1}{2\alpha}\,, \tag{2.17}$$

where the parameter α is called the gauge parameter. Eq. (2.16) defines the set of "covariant" gauges, the most familiar of these being the Feynman gauge ($\alpha = 1$) and Landau gauge ($\alpha = 0$).

As a covariant constraint, we may choose the Lorentz condition

$$\partial_\mu A^\mu = 0\,. \tag{2.18}$$

By the constraint of Eq. (2.18), the arbitrariness of the field A^a_μ due to the freedom of gauge transformations is eliminated. Hence a constraint such as Eq. (2.18) is called a gauge fixing condition. We will see that the Lorentz gauge condition is automatically a result of working in the Landau gauge limit, $\alpha \to 0$, of the covariant gauges. The Landau/Lorentz gauge has many Gribov copies[1] per gauge orbit.

It will be useful to describe the usual gauge-fixing arguments and Fadeev-Popov anasatz. The following discussion closely follows that in [Wil03].

The standard lattice definition of QCD is equivalent to the choice of a Gribov copy free gauge-fixing. This follows since there is a negligible chance of selecting two gauge-equivalent configurations (strictly zero except for numerical round-off error) in any finite ensemble of gauge field configurations. Calculations of *physical observables* are unaffected by arbitrary gauge transformations on the configurations in such an ensemble, since observables are by definition gauge invariant. A lattice QCD calculation using an ideal gauge-fixed ensemble will give a result for a gauge-invariant (i.e., physical) quantity which is identical to doing no gauge fixing at all, i.e., equivalent to the standard lattice calculation of physical quantities.

We begin by reviewing the standard arguments for constructing QCD perturbation theory, which use the Faddeev-Popov gauge fixing procedure to construct the perturbative QCD gauge-fixed Lagrangian density. The naive Lagrangian Eq. (2.15) is neither gauge-fixed nor renormalized, however it is invariant under local $SU(3)_{\text{color}}$ gauge transformations $G(x)$. For arbitrary, small $\omega^a(x)$ we have

$$G(x) \equiv \exp\left\{-ig_s\left(\lambda^a/2\right)\omega^a(x)\right\} \in SU(3)\,, \tag{2.19}$$

where the $\lambda^a/2 \equiv T^a$ are the generators of the gauge group $SU(3)$ and the index a runs over the eight generator labels $a = 1, 2, ..., 8$.

Consider some gauge-invariant Green's function (for the time being we shall concern ourselves only with gluons)

$$\langle\Omega|\; T(\hat{O}[A])\;|\Omega\rangle = \int \mathcal{D}A\; O[A]\; e^{iS[A]} \Big/ \int \mathcal{D}A\; e^{iS[A]}\,, \tag{2.20}$$

where $O[A]$ is some gauge-independent quantity depending on the gauge field, $A_\mu(x)$. We see that the gauge-independence of $O[A]$ and $S[A]$ gives rise to an infinite quan-

[1] An ideal gauge-fixing condition, $F[A] = 0$, defines a surface called the Fundamental Modular Region (FMR) that intersects each gauge orbit once and only once and typically where possible contains the trivial configuration $A_\mu = 0$. A non-ideal gauge-fixing condition, $F'[A] = 0$, defines a surface or surfaces which intersect the gauge orbit more than once. These multiple intersections of the non-ideal gauge fixing surface(s) with the gauge orbit are referred to as Gribov copies.

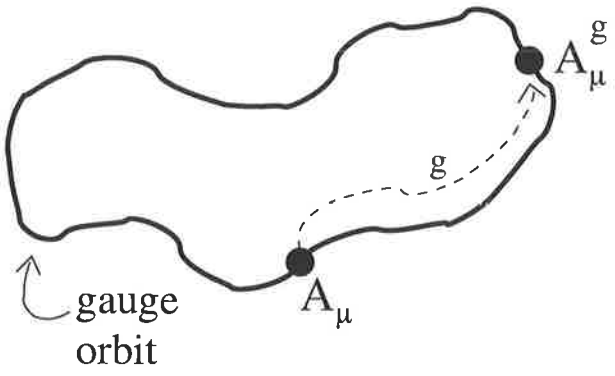

Fig. 2.1: Gauge orbit containing A_μ and showing the effect of A_μ on the gauge transformation G. Figure courtesy of [Wil03].

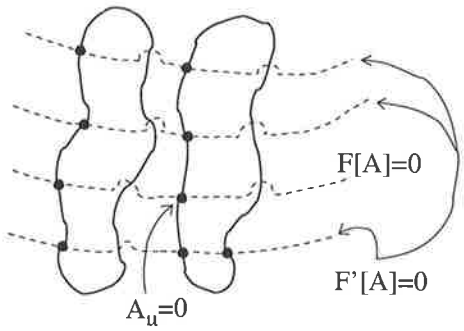

Fig. 2.2: Ideal, $F[A]$, and non-ideal, $F'[A]$, gauge-fixing. Figure taken from [Wil03].

tity in both the numerator and denominator, which must be eliminated by gauge-fixing. The Minkowski-space Green's functions are defined as the Wick-rotated versions of the Euclidean ones.

The gauge orbit for some configuration A_μ is defined to be the set of all of its gauge-equivalent configurations. Each point A_μ^G on the gauge orbit is obtained by acting upon A_μ with the gauge transformation G. By definition the action, $S[A]$, is gauge invariant and so all configurations on the gauge orbit have the same action, e.g., see the illustration in Fig. 2.1.

By definition an ideal gauge fixing is free from Gribov copies, *i.e.*, the multiple intersection points of a gauge-fixing surface with the closed gauge-orbit of gauge-equivalent field configurations. The ideal gauge-fixing surface $F[A] = 0$ specifies the FMR for that gauge choice and by definition the corresponding gauge-fixing surface intersects every gauge orbit once and only once. Fig. 2.2 is a depiction of these surfaces represented as dashed lines intersecting the gauge orbits within this configuration space. Typically the gauge fixing condition depends on a space-time coordinate, (e.g., Lorentz gauge, axial gauge, *etc.*), and so we write the gauge fixing condition more generally as $F([A]; x) = 0$.

Let us denote one arbitrary gauge configuration per gauge orbit, A_μ^0, as the origin

for that gauge orbit, i.e., corresponding to G equal to identity ($\omega^a(x) = 0$) on that orbit. Then each gauge orbit can be labelled by A^0_μ and the set of all such A^0_μ is equivalent to one particular, complete specification of the gauge. Under a gauge transformation, G, we move from the origin of the gauge orbit to the configuration, A^G_μ, where by definition

$$A^0_\mu \xrightarrow{G} A^G_\mu = GA^0_\mu G^\dagger - (i/g_s)(\partial_\mu G)G^\dagger. \tag{2.21}$$

Let us denote for each gauge orbit the gauge transformation, $\tilde{G} \equiv \tilde{G}[A^0]$, as the transformation which takes us from the origin of that orbit, A^0_μ, to the corresponding configuration on the FMR, $A^{\rm FMR}_\mu \equiv A^{\tilde{G}}_\mu$, which is specified by some assumed ideal gauge fixing condition

$$F([A^G]; x) = 0.$$

In other words, an ideal gauge fixing has a unique $\tilde{G}$ which satisfies

$$F([A^G]; x)|_{G=\tilde{G}} = 0\,,$$

and hence specifies the FMR as $A^{\tilde{G}} \equiv A^{\rm FMR}_\mu \in$ FMR. Note then that we have

$$\begin{aligned} \int \mathcal{D}A &= \int \mathcal{D}A^0 \int \mathcal{D}G\,, \\ &= \int \mathcal{D}A^{\rm FMR} \int \mathcal{D}(G - \tilde{G})\,. \end{aligned} \tag{2.22}$$

The *inverse Faddeev-Popov determinant* is defined as the integral over the gauge group of the gauge-fixing condition, i.e.,

$$\begin{aligned} \Delta_F^{-1}[A^{\rm FMR}] &\equiv \int \mathcal{D}G\ \delta[F[A]] \\ &= \int \mathcal{D}G\ \delta(G - \tilde{G}) \left|\det\left(\frac{\delta F([A]; x)}{\delta G(y)}\right)\right|^{-1}. \end{aligned} \tag{2.23}$$

Let us define the matrix $M_F[A]$ as

$$M_F([A]; x, y)^{ab} \equiv \delta F^a([A]; x)/\delta G^b(y)\,. \tag{2.24}$$

Then the *Faddeev-Popov determinant* for an arbitrary configuration A_μ can be defined as

$$\Delta_F[A] \equiv |\det M_F[A]|\,,$$

since

$$\begin{aligned} \Delta_F^{-1}[A^{\rm FMR}] &\equiv \Delta_F^{-1}[A^{\tilde{G}}] \\ &= \int \mathcal{D}G\ \delta(G - \tilde{G})\Delta_F^{-1}[A]. \end{aligned} \tag{2.25}$$

By definition, we have

$$\begin{aligned} 1 &= \int \mathcal{D}G\ \Delta_F[A]\ \delta[F[A]] \\ &= \int \mathcal{D}(G-\tilde{G})\ \Delta_F[A]\ \delta[F[A]] \end{aligned} \tag{2.26}$$

and hence

$$\begin{aligned} \int \mathcal{D}A^{\mathrm{FMR}} &\equiv \int \mathcal{D}A^{\mathrm{FMR}} \int \mathcal{D}(G-\tilde{G})\ \Delta_F[A]\delta[F[A]] \\ &= \int \mathcal{D}A\ \Delta_F[A]\delta[F[A]]. \end{aligned} \tag{2.27}$$

Since for an ideal gauge-fixing there is one and only one $\tilde{G}$ per gauge orbit, such that $F([A];x)|_{\tilde{G}} = 0$, then $|\det M_F[A]|$ is non-zero on the FMR. The *first Gribov horizon* is defined to be those configurations with $\det M_F[A] = 0$ which lie closest to the FMR. By definition the determinant can change sign on or outside this horizon. Clearly, the FMR is contained within the first Gribov horizon and for an ideal gauge fixing, since the sign of the determinant cannot change, we can replace $|\det M_F|$ with $\det M_F$.

These results are generalizations of results from ordinary calculus, where $|\det(\partial f_i/\partial x_j)|^{-1}_{\vec{f}=0} = \int dx_1 \cdots dx_n\, \delta^{(n)}(\vec{f}(\vec{x}))$ and if there is one and only one $\vec{x}$ which is a solution of $\vec{f}(\vec{x}) = 0$ then the matrix $M_{ij} \equiv \partial f_i/\partial x_j$ is invertible (i.e., non-singular) on the hypersurface $\vec{f}(\vec{x}) = 0$ and hence $\det M \neq 0$.

2.3.1 Faddeev-Popov technique and standard gauge fixing

Let us now assume that we have a family of *ideal* gauge fixings $F([A];x) = f([A];x) - c(x)$ for any Lorentz scalar $c(x)$ and for $f([A];x)$ being some Lorentz scalar function, (e.g., $\partial^\mu A_\mu(x)$ or $n^\mu A_\mu(x)$ or similar or any nonlocal generalizations of these). Therefore, using the fact that we remain in the FMR and can drop the modulus on the determinant, we have $\int \mathcal{D}A^{\mathrm{FMR}} = \int \mathcal{D}A\ \det M_F[A]\ \delta[f[A]-c]$. Since $c(x)$ is an arbitrary function, we can define a new "gauge" as the Gaussian weighted average

over $c(x)$, i.e.,

$$\begin{aligned}\int \mathcal{D}A^{\rm FMR} &\propto \int \mathcal{D}c \exp\left\{-\frac{i}{2\alpha}\int d^4x\, c(x)^2\right\}\int \mathcal{D}A\ {\rm det}M_F[A]\ \delta[f[A]-c] \\ &\propto \int \mathcal{D}A\ {\rm det}M_F[A] \exp\left\{-\frac{i}{2\alpha}\int d^4x f([A];x)^2\right\} \\ &\propto \int \mathcal{D}A\mathcal{D}\chi\mathcal{D}\bar{\chi}\ \exp\left\{-i\int d^4x d^4y\ \bar{\chi}(x)M_F([A];x,y)\chi(y)\right\} \\ &\quad \times\exp\left\{-\frac{i}{2\alpha}\int d^4x f([A];x)^2\right\}, \end{aligned} \tag{2.28}$$

where we have introduced the anti-commuting ghost fields χ and $\bar{\chi}$. Note that this kind of ideal gauge fixing does not choose just one gauge configuration on the gauge orbit, but rather is some Gaussian weighted average over gauge fields on the gauge orbit. We then obtain for an arbitrary Green's function

$$\langle\Omega|\ T(\hat{O}[...])\ |\Omega\rangle = \frac{\int \mathcal{D}\psi\mathcal{D}\bar{\psi}\mathcal{D}A\mathcal{D}\chi\mathcal{D}\bar{\chi}\ O[...]\ e^{iS_{\rm QCD}[...]}}{\int \mathcal{D}\psi\mathcal{D}\bar{\psi}\mathcal{D}A\mathcal{D}\chi\mathcal{D}\bar{\chi}\ e^{iS_{\rm QCD}[...]}}, \tag{2.29}$$

where we have defined the QCD action, $S_{\rm QCD}$, in Eq. (2.29) with a form determined by the exponents in Eq. (2.28), *i.e.*,

$$\begin{aligned} S_{\rm QCD}[\psi,\bar{\psi},A_\mu,\chi,\bar{\chi}] &= \int d^4x\left[-\frac{1}{2}{\rm tr}F_{\mu\nu}F^{\mu\nu}-\frac{1}{2\alpha}\left(f([A];x)\right)^2+\sum_f \bar{\psi}_f(i\not{D}_\mu-m_f)\psi_f\right] \\ &\quad +\int d^4y\ \bar{\chi}(x)M_F([A];x,y)\chi(y)\,. \end{aligned} \tag{2.30}$$

First consider the standard covariant gauge, which we obtain by taking $f([A];x) = \partial_\mu A^\mu(x)$ and by *neglecting* the fact that this is known to lead to Gribov copies. We need to evaluate $M_F[A]$ in the vicinity of the gauge-fixing surface (specified by $\tilde{G}$):

$$M_F([A];x,y)^{ab} = \frac{\delta F^a([A];x)}{\delta G^b(y)} = \frac{\delta[\partial_\mu A^a_\mu(x)-c(x)]}{\delta G^b(y)} = \partial^x_\mu\frac{\delta A^a_\mu(x)}{\delta G^b(y)]}\,. \tag{2.31}$$

Under an infinitesimal gauge transformation about the FMR, $\delta G \equiv G-\tilde{G}$, we have $(A^{\tilde{G}})_\mu \to (A^{\tilde{G}+\delta G})_\mu$, where

$$(A^{\tilde{G}+\delta G})^a_\mu(x) = (A^{\tilde{G}})^a_\mu(x) + g_s f^{abc}\omega^b(x)A^c_\mu(x) - \partial_\mu\omega^a(x) + \mathcal{O}(\omega^2) \tag{2.32}$$

and hence near the gauge fixing surface (i.e., for small fluctations along the orbit around $A^{\rm FMR}_\mu$) using

$$M_F([A];x,y)^{ab} \equiv \partial^x_\mu[\delta A^a_\mu(x)/\delta(\delta\omega^b(y))]|_{\omega=0}\,,$$

we find

$$M_F([A];x,y)^{ab} = \partial^x_\mu\left([-\partial^{x\mu}\delta^{ab}+g_s f^{abc}A^c_\mu(x)]\delta^{(4)}(x-y)\right). \tag{2.33}$$

We then recover the standard covariant gauge-fixed form of the QCD Lagrangian

$$\mathcal{L}_{\rm QCD}[\psi,\bar{\psi},A_\mu,\chi,\bar{\chi}] = -\frac{1}{2}{\rm tr}F_{\mu\nu}F^{\mu\nu} - \frac{1}{2\alpha}\left(\partial_\mu A^\mu\right)^2 + \sum_f \bar{\psi}_f(i\not{D} - m_f)\psi_f + (\partial_\mu\chi_a^*)(\partial_\mu\delta^{ab} - g_s f^{abc}A_\mu^c)\chi_b\,. \quad (2.34)$$

where index f corresponds to quark flavors and where the QCD action is $S_{QCD} = \int d^4x\,\mathcal{L}_{\rm QCD}$. χ_a^* and χ_b are the scalar ghost and antighost fields. In the quantization procedure, ghost fields anticommute, despite their spin [B+95]. In an $SU(N)$ theory, the ghost fields ensure that the gauge fixing does not spoil the unitarity of the "physical" S matrix that governs the scattering of quarks and gluons in the perturbation theory. This Lorentz covariant set of naive gauges corresponds to a Gaussian weighted average over generalized Lorentz gauges, where the gauge parameter α is the width of the Gaussian distribution over the configurations on the gauge orbit. Setting $\alpha = 0$ we see that the width vanishes and we obtain Landau gauge (equivalent to Lorentz gauge, $\partial^\mu A_\mu(x) = 0$). Choosing $\alpha = 1$ is referred to as "Feynman gauge" and so on.

Because of gauge fixing the new Lagrangian $\mathcal{L}_{\rm QCD}$ is by construction no longer gauge-invariant. A potentially troublesome phenomenon in gauge field theory is the *Gribov ambiguity*. Gauge-fixing is necessary to remove gauge transformations from the theory, because they represent nonphysical degrees of freedom. However, there will be some configurations related by local gauge transformations that satisfy the gauge condition. These are called Gribov copies and occur both in the continuum and on the lattice and are the multiple solutions to the gauge-fixing condition on a single gauge orbit.

The Faddeev-Popov technique can also be used to fix the gauge of lattice fields and this will discussed in more detail later. In the continuum theory we often use perturbative methods to calculate certain quantities. Gauge fixing is not needed for lattice studies of gauge invariant quantities as already discussed. But it is necessary for performing perturbation theory on the lattice and for studying gauge dependent quantities like the quark and gluon propagators on the lattice. If we use standard lattice gauge fixing, which neglects the fact that Gribov copies are present, then at large momenta $\int \mathcal{D}A$ will be dominated by configurations lying on the gauge-fixed surfaces in the neighbourhood of *each* of the Gribov copies [GPP+01, vB97, Neu87, Tes98] on the trivial orbit. These will all contribute equally and so in perturbation theory Gribov copies can be neglected.

2.4 QCD Feynman rules

Feynman diagrams in QCD are obtained by employing the quark-gluon propagators and vertices as the building blocks. The Feynman rules for the QCD Lagrangian can be derived from a functional integral over the fields $\psi\,,\bar{\psi}$ and A_μ. We have seen in the previous section that the action plus the gauge-fixing contribution becomes

Eq. (2.34). To extract the feynman rules from this action, we will decompose the lagrangian density into a free part and an interacting part,

$$\mathcal{L} = \mathcal{L}_0 + \mathcal{L}_1. \tag{2.35}$$

Note that for brevity the "Lagrangian density" will often simply be referred to as the "Lagrangian". Here the free Lagrangian $\mathcal{L}_0$ is made up of three parts [Mut87] each of which corresponds to the participating particles, *i. e.,* the gluons, Faddeev-Popov ghosts and the quarks,

$$\mathcal{L} = \mathcal{L}_0^{\mathrm{F}} + \mathcal{L}_0^{\mathrm{G}} + \mathcal{L}_0^{\mathrm{FP}}, \tag{2.36}$$

$$\mathcal{L}_0^{\mathrm{F}} = \bar{\psi}_f(x)(i \not{D}_\mu - m_f)\psi_f(x) \tag{2.37}$$

$$\mathcal{L}_0^{\mathrm{G}} = -\frac{1}{2}\mathrm{tr}F_{\mu\nu}(x)F^{\mu\nu}(x) - \frac{1}{2\alpha}(\partial_\mu A^\mu(x))^2 \tag{2.38}$$

$$\mathcal{L}_0^{\mathrm{FP}} = (\partial_\mu \chi^a)(\partial_\mu \chi_a^*)\,. \tag{2.39}$$

As Eq. (2.39) is of the form of the Lagrangian for massless charged scalar fields, we recognize that the Fadeev-Popov ghost is spin zero though it is fermionic owing to its nature as a Grassmann number. In Eq. (2.38) the gauge fixing term $\mathcal{L}_0^{\mathrm{GF}}$is included. The remaining part of the Lagrangian $\mathcal{L}$ after substracting $\mathcal{L}_0$ is the interaction Lagrangian $\mathcal{L}_1$ which amounts to

$$\begin{aligned}
\mathcal{L}_1 &= \mathcal{L}_1(A^a, \chi^a, \chi^{a^*}, \psi, \bar{\psi}) && (2.40)\\
&= -\frac{g_s}{2} f^{abc}(\partial_\mu A_\nu^a - \partial_\nu A_\mu^a) && (2.41)\\
&\quad -\frac{g_s^2}{4} f^{abe} f^{cde} A_\mu^a A_\nu^b A^{c\mu} A^{d\nu} && (2.42)\\
&\quad -g_s f^{abc}(\partial^\mu \chi^{a^*})\chi^b A_\nu^c + g\bar{\psi} T^a \gamma^\mu \psi A_\mu^a\,. && (2.43)
\end{aligned}$$

From this, we can read off Feynman rules for Yang-Mills theory: Wavy, dotted and solid lines represent the gluon, ghost and quark, respectively; the arrows on the ghost and quark line show a flow of the ghost and fermion number, respectively. The loop-sign factor is an extra minus sign needed for closed ghost and quark loops [Ynd]. The gluon, ghost and quark propagators are represented respectively by the functions given below:

$$D_{\mu\nu}^{ab}(x) = \delta^{ab} \int \frac{d^4k}{(2\pi)^4} \frac{e^{-ik.x}}{k^2 + i\epsilon}\left(g_{\mu\nu} - (1-\alpha)\frac{k_\mu k_\nu}{k^2}\right), \tag{2.44}$$

$$D^{ab}(x) = \delta^{ab} i \int \frac{d^4k}{(2\pi)^4} \frac{e^{-ik.x}}{k^2 + i\epsilon}, \tag{2.45}$$

$$S(x) = \int \frac{d^4p}{(2\pi)^4} \frac{i}{\not{p} - m} e^{-ip.x}\,. \tag{2.46}$$

Here α fixes the gauge where *e.g.,* $\alpha = 1$ is Feynman gauge and $\alpha = 0$ is Landau

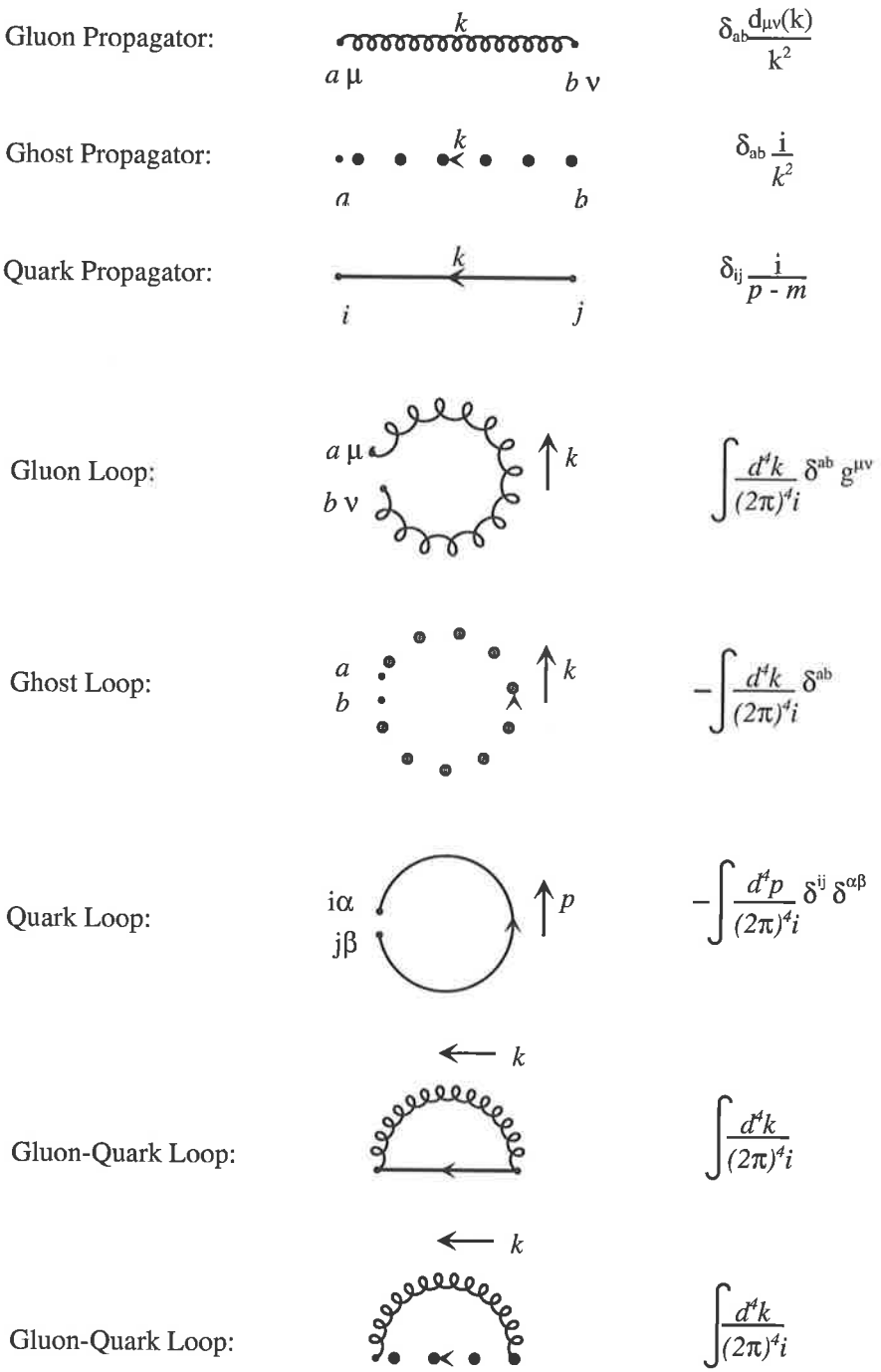

Fig. 2.3: QCD feynman rules.

3-gluon vertex:

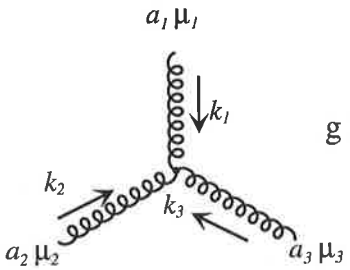

$g\, f^{a_1 a_2 a_3} V_{\mu_1 \mu_2 \mu_3}(k_1, k_2, k_3)$

4-gluon vertex:

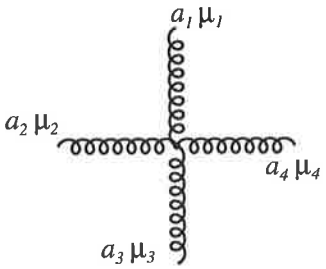

$-ig^2 W^{a_1 \ldots a_4}_{\mu_1 \ldots \mu_4}$

gluon-ghost vertex:

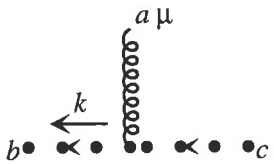

$-g f^{a\,b\,c}\, k_\mu$

gluon-quark vertex:

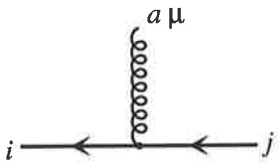

$ig\gamma_\mu\, T^a_{ij}$

Fig. 2.4: QCD feynman rules for vertices.

gauge. The factor (-1) associated with each quark and ghost loop is called the loop-sign factor. The loop-sign factor always accompanies a fermion loop integration. The measure for integration of each loop is given by $\int \frac{d^4k}{(2\pi)^4 i}$. The rules for loop integration are explained in Fig. 2.3. In the rules, δ^{ab}, δ^{ij}, $g_{\mu\nu}$ and $\delta^{\alpha\beta}$ represent the contraction of the group, Lorentz and spinor indices, respectively, at the point where the loop closes. Also $d_{\mu\nu}$ is given by

$$d_{\mu\nu} = g_{\mu\nu} - (1-\alpha)\frac{k_\mu k_\nu}{k^2}\,. \tag{2.47}$$

To obtain the Feynman rules for vertices, recall $\lambda^a/2 \equiv T^a$ which are the color matrices and the generators of the $SU(3)$ group explained in the previous section. The group structure is given by

$$[T^a, T^b] = i f^{abc} T^c\,,$$

where $a\,, b\,, c = 1, 2, ..., 8$ and the f^{abc} are the structure constants. They are anti-symmetric under the interchange of two indices:

$$f_{123} = 1\,, f_{147} = f_{246} = f_{257} = f_{345} = f_{516} = f_{637} = \frac{1}{2}\,, f_{458} = f_{678} = \frac{\sqrt{3}}{2}\,.$$

Feynman rules for the vertices are depicted in Fig. 2.4, where the functions V and W are well explained in [Mut98]. In evaluating Feynman diagrams that contain loops, divergent integrals over momenta occur. Divergences of perturbation theory are removed by absorbing them into the definition of the bare quantites through a renormalization procedure [BP93]. This is done by introducing a new dimensional scale μ, called the renormalization scale or point. The renormalized quantities in the theory, like the coupling constant g_s depend explicitly on μ. The renormalization of the coupling necessitates the introduction of a scale μ. This is the scale at which the physical parameters of the theory are fixed.

2.5 Results from perturbative QCD

In constructing a theory, the information about the properties of the coupling constants between the fields is of primary importance. The coupling constants depend on momenta. Studying the behaviour of the coupling at large momentum transfers ($|Q|^2 \to \infty$), in the so called asymptotic region is important. Asymptotic properties of the effective charges of abelian and non-abelian fields are different. In the case of abelian fields, the effective coupling constant grows like the log of a log with increasing Q^2, while for non-abelian gauge theories it decreases like a log. Asymptotically free fields play an important role in our understanding of the gauge theory of strong interactions.

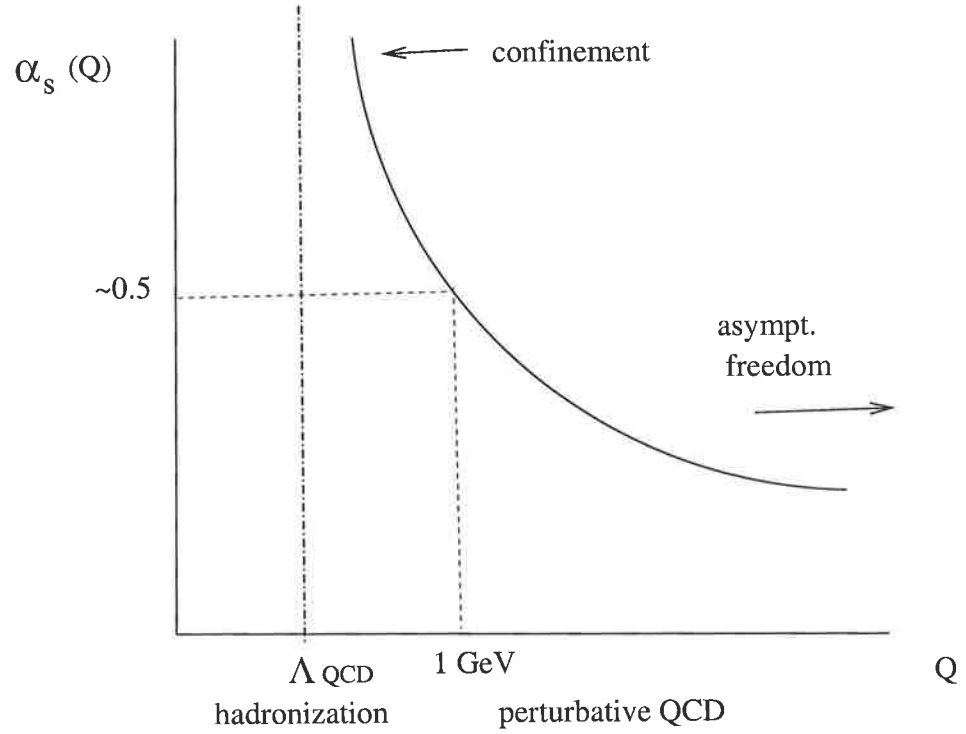

Fig. 2.5: Schematic view of running coupling constant. Figure taken from [Kho04]

2.5.1 Asymptotic freedom

Non-abelian gauge theories are asymptotically free. *Asymptotic freedom* is a feature of quantum chromodynamics (QCD), the quantum field theory of the interactions of quarks and gluons, which was discovered by David Gross, Frank Wilczek, and David Politzer in 1973. For this great discovery they won the Nobel prize in 2004. The QCD running coupling is defined as

$$\alpha_s(Q^2) = \frac{g_s^2(Q^2)}{4\pi}, \tag{2.48}$$

where α_s is small at large momentum transfers. The consistent use of the running coupling in perturbative expansions is possible for large Q where α_s is numerically small. So in an aymptotically free theory, there is no barrier to use perturbation theory at large momenta. At smaller scales, at $Q \lesssim 1$ GeV, α_s grows as shown in Eq. (2.5) and perturbation theory becomes useless. In QCD, perturbation theory is legimate in the large momentum region. At long distances (small momentum transfers), quarks and antiquarks interact and form hadrons. QCD is asymptotically free because the antiscreening of the gluons overcomes the screening due to quarks [Gro99]. Asymptotic freedom implies that the coupling $g_s \to 0$ as the momentum scale of the probe $\to \infty$. The renormalized coupling constant tends to be very small as the relevant momentum scale grows. We will see in the next section that at

large momenta, $q^2 = -Q^2$, the theory behaves as a free-field modulo logarithmic corrections. This is the celebrated property of *asymptotic freedom*. The β function in non-abelian theory is given by [Gro99]

$$\beta(\alpha) \equiv \mu \frac{d}{d\mu} \alpha(\mu)|_{\alpha_0} = \frac{\alpha^2}{\pi} b_1 + (\frac{\alpha^2}{\pi})^2 b_2 + \cdots , \tag{2.49}$$

where

$$b_1 = -\left[\frac{11}{6} C_A - \frac{2}{3} \sum_R N_f T_f\right] . \tag{2.50}$$

β function is the rate of change of renormalized coupling at scale μ corresponding to a fixed bare coupling g_0 [PS]. The bare Green's functions depends on the bare coupling g_0. The bare coupling constant is defined as

$$\alpha_0 = \frac{g_0^2}{4\pi} . \tag{2.51}$$

In the case of the $SU(3)$ gauge group such as QCD, $C_A = N = 3$, $T_f = \frac{1}{2}$ for each Dirac fermion, and N_f is the number of fermion and thus $b_1 = -[\frac{11}{2} - \frac{N_f}{3}]$. Thus one can tolerate as many as 16 triplets of quarks before losing asymptotic freedom. That is asymptotic behavior is possible only if there are a limited number of fermions in the theory (no more than 16 quark flavors in QCD). We see that as long as $11 - \frac{2}{3} N_f > 0$, the coupling constant decreases with μ! This is the statement of asymptotic freedom . The coupling constant will decrease at shorter distances with the result that one can use perturbation theory with confidence for short distance physics. On the other hand at large distances, the coupling constant increases leaving the domain where perturbative calculations can be trusted.

2.5.2 Running coupling constant for QCD

In QED, the coupling constant defined on the mass shell is small enough to guarantee the perturbative expansion meaningful at any achievable finite order of perturbation theory, although it should be noted that perturbative QED forms an asymptotic series. The increase of the effective charge prevents the separation of quarks to large distances in QCD. The charge the experimentalist measures depends on the Q^2 of the experiment; $\alpha(Q^2) \equiv \frac{e^2(Q^2)}{4\pi}$ is referred to as the "running coupling constant". The running coupling constant, $\alpha(Q^2)$ in QED describes how the effective charge depends on the seperation of the two charged particles. The effective coupling constant is reduced by the presence of this screening charge. In the large $Q^2 \equiv -q^2$ limit

$$\alpha(Q^2) = \frac{\alpha_0}{1 - \frac{\alpha_0}{3\pi} \log(\frac{Q^2}{M^2})} . \tag{2.52}$$

To eliminate explicit dependence of $\alpha(Q^2)$ on the cutoff M, we choose a reference momentum μ. The renormalization procedure is then to subtract $\alpha(\mu^2)$ from $\alpha(Q^2)$.

We find

$$\alpha(Q^2) = \frac{\alpha(\mu^2)}{1 - \frac{\alpha(\mu^2)}{3\pi}\log(\frac{Q^2}{\mu^2})}. \tag{2.53}$$

At large distances, the effective coupling constant α gets smaller in QED . The situation in QCD is different, where the net coupling constant gets larger at larger distances. The Q^2 behavior of the QCD coupling, $\alpha_s(Q^2)$ is different from that for $\alpha(Q^2)$. In the covariant gauge, the coefficient of $\log(\frac{Q^2}{\mu^2})$ is given by

$$+\frac{\alpha_s(\mu^2)}{4\pi}(11 - \frac{2}{3}N_f) \tag{2.54}$$

Combining Eq. (2.53) and Eq. (2.54), we obtain the QCD "running coupling constant"

$$\alpha_s(Q^2) = \frac{\alpha_s(\mu^2)}{1 + \frac{\alpha_s(\mu^2)}{4\pi}(11 - \frac{2}{3}N_f)\log(\frac{Q^2}{\mu^2})}. \tag{2.55}$$

The sign of the coefficient is the same as in QED, only in a world with more than 16 quark flavors. $\alpha_s(Q^2)$ decreases with increasing Q^2 and therefore becomes small for short-distance interactions. This is we say that QCD is "asymptotically free". From Eq. (2.55), we see that at sufficiently small Q^2, the effective coupling becomes large. It is customary to denote the Q^2 scale at which this happens by Λ, where

$$\Lambda^2 = \mu^2 \exp\left[\frac{-12\pi}{(33 - 2N_f)\alpha_s(\mu^2)}\right]. \tag{2.56}$$

the momentum scale Λ is often referred to as the QCD scale parameter ($\Lambda_{\rm QCD}$) and is the only adjustable parameter in QCD except for the quark masses. It then follows that Eq. (2.55) may be written as

$$\alpha_s(Q^2) = \frac{12\pi}{(33 - 2N_f)\log(\frac{Q^2}{\Lambda^2})}. \tag{2.57}$$

For Q^2 values much larger than Λ^2, the effective coupling is small and a perturbative description in terms of quarks and gluons interacting weakly makes sense. As $Q^2 \to \infty$, $\alpha_s \to 0$. For Q^2 of order Λ^2, quarks and gluons are seen to arrange themselves into strongly bound clusters, namely hadrons. Thus Λ, a free parameter is the boundary between a world of quasi-free quarks and gluons, and the world of pions, protons and so on.

2.5.3 Running mass

For asymptotically free theories, the leading log result for the running mass at $Q^2 \equiv -q^2 \gg \Lambda^2_{\rm QCD}$ is given by

$$M(Q^2) = \frac{\hat{m}}{\left[\frac{1}{2}\log(\frac{Q^2}{\Lambda^2_{\rm QCD}})\right]^{d_M}}, \tag{2.58}$$

where $\hat{m}$ (the mass analog of Λ) is the renormalisation group invariant mass parameter and $d_M = \frac{12}{(33-2N_f)}$ is the anomalous dimension of mass. The renormalised mass, m_μ, is related to $\hat{m}$ using Eq. (2.58) by

$$m_\mu \equiv M(\mu^2) = \frac{\hat{m}}{\left[\frac{1}{2}\log\left(\frac{\mu^2}{\Lambda^2_{\rm QCD}}\right)\right]^{d_M}}\,, \tag{2.59}$$

where the renormalisation point dependence is explicitly indicated. The asymptotic behavior of the running mass is in general gauge dependent [RW94].

2.6 Symmetries of QCD

In this section we discuss some symmetries of the QCD Lagrangian density. Chiral Symmetry and its dynamical breaking is important in the gluon and quark propagator studies. Chiral symmetry of the quark terms in the Lagrangian proves to be useful in generating low energy expansions of QCD [Fis03, Leu94, Man96, Eck98]. Chiral symmetry is one of the fundamental properties of the theory of particle physics. It follows from the invariance of the Lagrangian under independent global transformations on left and right handed fermion fields.

The quark part of the QCD Lagrangian from Eq. (2.15) is

$$\mathcal{L}_m = \bar{\psi}(i\not{D} - m)\psi\,, \tag{2.60}$$

where m is a diagonal matrix containing the masses of six different flavors of quarks. Since the up, down and strange quarks have relatively small masses, the real world has an approximate $SU(3)_{\rm flavor}$ chiral symmetry. In the chrial limit (the case of massless quarks), $m = 0$, the fermionic part of the QCD Lagrangian density in the continuum is

$$\mathcal{L}_{m=0} = \bar{\psi} i \not{D}\psi\,. \tag{2.61}$$

This Lagrangian is invariant under axial rotations

$$\psi(x) \to e^{i\alpha\gamma_5}\psi(x)\,,\ \bar{\psi}(x) \to \bar{\psi}(x)e^{i\alpha\gamma_5}. \tag{2.62}$$

This symmetry of the massless Lagrangian is called chiral symmetry. It is one of the most important symmetries of QCD and strong interactions. In the chiral case, the quark fields can be decomposed in terms of their helicity $\psi = \psi_{\rm left} + \psi_{\rm right}$,

$$\psi_{\rm left} = \frac{1-\gamma_5}{2}\psi\,,\ \psi_{\rm right} = \frac{1+\gamma_5}{2}\psi. \tag{2.63}$$

The resulting Lagrangian is symmetric under the global unitary flavor transformation $SU(3)_{\rm left} \times SU(3)_{\rm right} \times U(1)_{\rm left} \times U(1)_{\rm right}$, which generates the conserved

currents

$$j_\mu = \bar{\psi}\gamma_\mu\psi \tag{2.64}$$
$$j_\mu^5 = \bar{\psi}\gamma_\mu\gamma_5\psi \tag{2.65}$$
$$j_\mu^a = \bar{\psi}\gamma_\mu T^a\psi \tag{2.66}$$
$$j_\mu^{5a} = \bar{\psi}\gamma_\mu\gamma_5 T^a\psi\,, \tag{2.67}$$

where $T^a \equiv \lambda^a/2$ are generators of of the gauge group $SU(3)$ which we have seen in the earlier sections of this chapter. These currents are conserved on the classical level of the theory. In the presence of a non-vanishing mass matrix m, the divergences of these currents are given by

$$\partial^\mu j_\mu = 0\,, \tag{2.68}$$
$$\partial^\mu j_\mu^5 = 2i\bar{\psi}\gamma_5\psi - \frac{g^2}{16\pi^2}\epsilon^{\mu\nu\sigma\rho}F_{\mu\nu}^a F_{\sigma\rho}^a\,, \tag{2.69}$$
$$\partial^\mu j_\mu^a = \bar{\psi}[T^a, m]\psi\,, \tag{2.70}$$
$$\partial^\mu j_\mu^{5a} = \bar{\psi}\{T^a, m\}\psi. \tag{2.71}$$

Only one current is conserved and in the presence of nonzero quark mass it describes the baryon number conservation in strong interaction process. The second term of Eq. (2.69) expresses the anomalous nonconservation of the axial current, known as Adler-Bell-Jackiw anomaly. The vector current in Eq. (2.70) is conserved in the case of identical quark masses [Fis03] and describes the approximate flavor symmetry in the light quark sector of QCD.

If we have a non-vanishing quark mass matrix in the Lagrangian of QCD, the axial vector current Eq. (2.71) is no longer conserved and we say that the symmetry is broken. This is called *explicit chiral symmetry breaking* (ECSB). Since the masses of light quarks are light, we still expect approximate degenerate parity partners of the lowest lying hadron spectra, if the current masses are the only reason for the breaking of chiral symmetry. However, such parity partners are not observed in nature. The solution to this problem is dynamical chiral symmetry breaking. For QCD to describe the strong interactions observed in nature, it is crucial that chiral symmetry is broken. In the case of dynamically broken symmetry, the Lagrangian is invariant under the symmetry but the vacuum state is not. It can be shown that the case of dynamical symmetry-breaking leads to the occurance of zero-mass particles called Goldstone bosons. This is known as Goldstone's theorem. In any physical system in which the vacuum state breaks a symmetry there must exist a zero-mass, spinless boson carrying the quantum numbers of this symmetry transformation. These massless particles are called Goldstone bosons. In QCD, the pions are approximate Goldstone bosons arising from the dynamical symmetry breaking of chiral symmetry. Dynamical mass generation via the dynamical breaking of chiral symmetry gives rise to almost the entire nucleon mass.

The biggest advance of the early 1960's was the discovery of flavor symmetry of hadrons, $SU(3)$, by Gell-Mann and Yuval Neeman and then the beginning of the

understanding of dynamically broken chiral symmetry [Rob03]. Dynamical chiral symmetry breaking (DCSB) is fundamental to understanding the strong interaction spectrum. It explains how the strong interaction generates constituent quark masses of the order of several hundred MeV even in the chiral limit of zero bare quark masses in the Lagrangian. It is an essentially non-perturbative mechanism that give rise to a momentum dependent quark mass, $M(Q^2)$, in the chiral limit, that is large in the infrared but power suppressed in the ultraviolet. When there is no ECSB renormalised quark mass, we have exact chiral symmetry and $M(Q^2)$ is given by [RW94]

$$M(Q^2) \overset{Q^2\to\infty}{=} \frac{c}{Q^2}\left[\log\frac{Q^2}{\Lambda^2_{\rm QCD}}\right]^{d_M-1}, \tag{2.72}$$

where c is a constant independent of Q^2. In the limit of exact chiral symmetry ($m = 0$) in Landau gauge c satisfies

$$c \backsimeq -\frac{4\pi^2 d_M}{3}\frac{\langle\bar{q}q\rangle}{\left[\log(\mu^2/\Lambda^2_{\rm QCD})\right]^{d_M}}. \tag{2.73}$$

μ is the renormalization scale and $\langle\bar{q}q\rangle$ is the quark condensate which is a measure of the degree of dynamical chiral symmetry breaking. It is defined as $\langle\bar{q}q\rangle = \langle{\rm vac}| : \bar{q}(0)q(0) : |{\rm vac}\rangle$, where $|{\rm vac}\rangle$ refers to the nonperturbative vacuum and the normal ordering of the operators is with respect to the perturbative vacuum. The asymptotic form of the quark mass can be summarized as

$$M(Q^2) \overset{Q^2\to\infty}{=} \frac{c}{Q^2}\left[\log\frac{Q^2}{\Lambda^2_{\rm QCD}}\right]^{d_M-1} + m\left[\frac{\log(\mu^2/\Lambda^2_{\rm QCD})}{\log(Q^2/\Lambda^2_{\rm QCD})}\right]^{d_M}, \tag{2.74}$$

where for exact chiral symmetry ($m = 0$), the second term on the RHS is zero, while in the presence of ECSB ($m \neq 0$), the second term gives the dominant asymptotic behavior.

The physical QCD vacuum lies very close to a dynamically broken phase of an exact chiral symmetry [You04]. With the quark masses being so small on hadronic scales, explicit symmetry breaking is small and can be systematically treated as a perturbation.

2.7 Confinement

When the quark model of hadrons was first introduced by Gell-Mann and Zweig in 1964, an obvious question was "where are the quarks?". The absence of isolated quark states became a much more urgent issue with the success of the quark-patron model, and the introduction of quantum chromodynamics in 1972. Confinement requires that the fundamental excitations of QCD (quarks and gluons) can not

be observed although they underlie the interactions. The *confinement* phenomena expresses the fact that all physical states that are observed are color $SU(3)$ singlets.

The most elementary picture of confinement mechanism builds on the idea of a *flux-tube*. In QED with Abelian photons the force between e^+ and e^- is an attractive Colomb law. The fields spread out to infinity since the photon field does not couple to itself. However the QCD case is different. The non-abelian nature of the gluon field implies that it couples to itself. This leads to the result that the energy minimising configuration between a quark and an anti-quark is a tube of colored flux. Such a flux tube would then have a potential energy which is a linearly rising function of the distance between the two quarks. In other words, quarks would be confined, as the energy required to separate them is infinite.

In general, if the potential between two quarks is proportional to the distance between them, then the two quarks can never be separated:

$$\text{Confinement potential} : V(r) \sim \sigma r \,, \tag{2.75}$$

where σ is called the string tension. Furthermore, the string may break, creating a quark-antiquark pair held together by another string. Thus, they can be separated if they are bound by a linear potential but only in such a way that two new flux tubes are formed and the quarks stay confined.

In Euclidean space ($t \to -it_E$), we can study the Wilson loop $W(C)$ (see the section, QCD on a lattice in Chapter 3 for more details), where C is a rectangular loop with width R in one spatial direction and length T in the time direction. If the potential between the quarks grows lineraly with the distance of separation R [Kak], then the quarks are confined and we have

$$W(R,T) \to \exp(-\sigma RT) \tag{2.76}$$

in the limit of large Euclidean time T. Since the area of the Wilson loop is RT, the *area law* for the behavior of the Wilson loop for large T gives us confinement. The renormalization group approach gives us a compelling theoretical argument that the coupling constant is large at small energies *i.e.,* larger coupling constant at low energies is consistent with the idea that the quarks are permanently bound inside a hadron. At larger and larger distances, the coupling constant increases, so that at a certain point perturbative calculations can no longer trusted. Confinement is called "infrared slavery" which is the flip side of asymptotic freedom. Thus within one theory, we are able to interpret two divergent facts, that quarks appear to be confined at low energies but act as if they are approximately free particles at high energy.

The basic properties of confinement and approximate $SU(3) \otimes SU(3)$ flavor symmetry of light quarks qualitatively describe many features of the hadron spectrum and of other low energy strong interaction phenomena. But due to strong couplings, a precise quantitative description of these phenomena is difficult. This spoils to some extent even the predictions of perturbative QCD, because the confinement acts also on the initial and final states of every short distance process.

Confinement in QCD is related to the *violation of positivity*. In this thesis we provide evidence for the violation of positivity of the gluon propagator in Chapter 8. We find that the spectral function describing the gluon propagator is not positive definite. Color confinement in QCD requires no colored states to be present in the positive definite space of physical states defined by some suitable condition maintaining physical S-matrix unitarity.

The description of the long distance strong color force requires non-perturbative methods. One of the main motivations for the introduction of lattice gauge theory was the need to formulate QCD non-perturbatively in order to explain confinement. A successful calculation of low energy hadronic parameters in lattice QCD yields convincing evidence for QCD as the correct theory of strong interactions.

2.8 Schwinger functions

Quantum field theories can be described in terms of infinite hierarchies of functions. There are different but equivalent hierarchies, like the Wightman functions and Schwinger functions to mention only two possibilities.

The Wightman functions $W^n(x_1, ..., x_n)$ are defined as the vacuum expectation values of the product of field operators:

$$W^n(x_1, ..., x_n) := \langle \Omega | \Phi(x_1) ... \Phi(x_n) | \rangle \Omega \,. \tag{2.77}$$

The set of functions W^n has to satisfy the Wightman axioms in order to ensure that the W^n corresponds to a standard Garding-Wightman QFT and the additional constraint

$$\langle \Omega | A^* A | \Omega \rangle \geq 0 \quad \text{for all} \quad A = \sum_n \int \prod_k d^4 x_k f^n(x_1, ..., x_n) \Phi(x_1) ... \Phi(x_n) \,, \tag{2.78}$$

makes sure that the metric of the Hilbert space is positive semidefinite. It has been proven that the hiearchy of functions W^n contains the information that is necessary to reconstruct the Hilbert space and deduce the action. This is known as reconstruction theorem for the Wightman functions.

The Schwinger functions $S^n(x_1, ..., x_n)$ are defined as the Wightman functions for imaginary times:

$$S^n(x_1, ..., x_n) = W^n(-ix_1^{(4)}, \vec{x}_1, ..., -ix_n^{(4)}, \vec{x}_n) \,. \tag{2.79}$$

and they are the Euclidean Green's functions. These functions have some remarkable properties [Haa]:

(i) If we exclude the coincidence of points, *i.e.,* remain outside of the submanifold

$$\Delta = \{x_1, ..., x_n : x_k = x_j \ \text{for some} \, k \neq j\} \,, \tag{2.80}$$

then the S^n are analytic functions.

(*ii*) S^n is Euclidean invariant

$$S^n(gx_1, ..., gx_n) = S^n(x_1, ..., x_n)\,, \tag{2.81}$$

where $gx = Rx + a; R \in SO(4)$.

(*iii*) S^n is symmetric under permutations.

$$S^n(x_{P1}, ..., x_{Pn}) = S^n(x_1, ..., x_n)\,, \tag{2.82}$$

for any permutations,

$$\begin{pmatrix} 1..., n \\ P_1..., P_n \end{pmatrix}.$$

The Euclidean correlation functions can be continued back to Minkowski space if they obey a positivity condition. The conditions on the hierarchy $\{S^n\}$ which guarantee that their analytic continuation leads to distributions in Minkowski space satisfying the Wightman axioms have been found by Osterwalder and Schrader [Haa]. Their work shows that besides (*i*) to (*iii*) the essential requirement is *reflection positivity*. It is called Osterwalder-Schrader positivity or reflection positivity.

The Osterwalder-Schrader reflection positivity is the Euclidean counterpart of the positivity constraint of Eq. (2.78) and is defined as

$$\sum_{n,m} S^{n+m}\left(\Theta[f_n \otimes f_m]\right) \geq 0\,, \tag{2.83}$$

for all test functions f_n, f_m where the tensor product $f_n \otimes f_m$ understood as

$$[f_n \otimes f_m](x_1, ..., x_n, y_1, ..., y_m) := f_n(x_1, ..., x_n).f_m(y_1, ..., y_m)\,. \tag{2.84}$$

and the Θ-operation is defined as

$$\Theta f_n(x_1, ..., x_n) \equiv \bar{f}_n(\theta x_1, ..., \theta x_n) \text{ with } \theta x = \theta(x^4, \vec{x}) \equiv (-x^4, \vec{x})\,. \tag{2.85}$$

If the hierarchy S^n does satisfy Osterwalder-Schrader reflection positivity then the corresponding Hilbert space will have a positive semidefinite metric. A fundamental principle of quantum mechanics is the positivity of the norm in Hilbert space of states. Physically this expresses the possibility of probabilities. When translated to the condition of imaginary-time Green's functions, this physical positivity condition is known as reflection positivity. Violation of positivity is another condition for confinement. In this thesis we study whether or not the gluon propagator violates reflection positivity.

3

Lattice QCD

The lattice formulation of QCD was invented by Wilson in 1974. Lattice methods are presently the only way to compute masses and matrix elements beginning with the QCD Lagrangian, *i.e.,* from first principles. The lattice is a cutoff which regulates the ultraviolet divergences of quantum field theories. Other regularization schemes such as dimensional regularisation are often tied closely to perturbative expansions: one calculates a process to some order in a coupling constant, divergences are removed order by order in perturbation theory by absorbing them into the definition of the bare parameters of the theory [DeG96]. Several analytic approximation methods are available on the lattice: weak coupling expansions, strong coupling expansions and mean field approximation. However, Monte-Carlo numerical simulations are the only known first principles technique for studying QCD and allow us to bridge the gap between the strong and weak coupling regimes. Numerical simulations using lattice QCD allows us to address non-perturbative phenomena such as confinement and dynamical chiral symmetry breaking, to study full QCD (with the effect of dynamical sea-quarks), pure Yang-Mills QCD and the glueball spectrum, to compute static potential between quarks, the propagators, the running coupling constant starting from non-perturbative data and the parameters of the chiral Lagrangian and to learn more about the QCD vacuum, its topological properties and its condensates [Pen95]. The ultimate aim of numerical studies of QCD on the lattice is a quantitative understanding of the dynamics of strong interactions from first principles.

The principle of the method is to discretize space-time on a four-dimensional lattice. This amounts to excluding the high energy modes and including a cutoff. In an asymptotically free theory we can recover these modes by adjusting the coupling in a well-defined, controlled way by taking the limit of the discretization scale to zero [Wil99].

As space-time is to be discretized on a hypercubic lattice, contact with experiment only exists in the continuum limit, when the lattice spacing is taken to zero. The numerical implementation of the path integral approach requires the following five steps;
- Discretization of space-time;
- The transcription of the gauge and fermion degrees of freedom into lattice equivalents;
- Construction of the discretized action;
- Definition of the measure of integration in the path integral;
- The transcription of the continuum operators into discretized forms that can be used to probe the physics.

3.1 Overview of the lattice approach

Lattice QCD calculations are a non-perturbative implementation of quantum field theory using the feynman path integral approach.

In this Chapter I will describe the principles of lattice calculations, the use of path integrals, gauge-fixing, standard actions and improved staggered actions. Some basics of lattice formulation follows [Lep96]. A detailed and thorough study can be found in the texts by Heinz Rothe [Rot05], Montvay & Münster [MM] and Jan Smit [Smi02] and in the review articles [Gup97] and [Ric99]. We formulate quantum field theory on a finite lattice, calculate the desired observables using appropriate numerical techniques and then obtain the physical result by carefully taking the infinite volume and continuum ($a \to 0$) limits.

3.2 Gauge field basics

On the lattice, we sacrifice Lorentz invariance but preserve all internal symmetries-including local gauge invariance. This preservation is important for nonperturbative physics. In the infinite volume, continuum limit Lorentz invariance is recovered. For example gauge invariance is a property of the continuum theory which is highly relevant to nonperturbative physics, so maintaining it as we move to the lattice means that all of its consequences will be preserved. On the lattice, we replace the space-time coordinate x_μ by a set of integers n_μ ($x_\mu = an_\mu$, where a is the lattice spacing). The construction of the gauge field is more complicated. In the continuum, the gauge fields $A_\mu(x)$ carry 4-vector Lorentz indices, and mediate interactions between quarks. They carry a space-time index μ in addition to an internal symmetry index a, $(A^a_\mu(x))$. In the continuum a fermion moving from site x to y in the presence of gauge field $A_\mu(x) = A^a_\mu(x)T^a$ picks up a phase factor given by the path ordered product.

$$\psi(y) = \mathcal{P}e^{\int_x^y ig_s A_\mu(x)dx_\mu}\psi(x), \tag{3.1}$$

where the $\mathcal{P}$-operator path-orders the A_μ's along the integration path. Note that the ordering is important since T^a's and hence A_μ's do not commute .

We use U_μ's as dynamical variables in place of A_μ's on the lattice. The eight types of gluons that mediate interactions between quarks are written interms of the matrix $A_\mu(x)$ which we have seen in Chapter 2. Eq. (3.1) suggests that gauge fields are associated with links that connect sites on the lattice. So each link is associated with a path ordered product which is explained in the coming sections.

3.3 Field theory on a lattice

The functional integral in Minkowski space is not in general well-defined in the continuum and is not suited for numerical studies. Hence, most nonperturbative

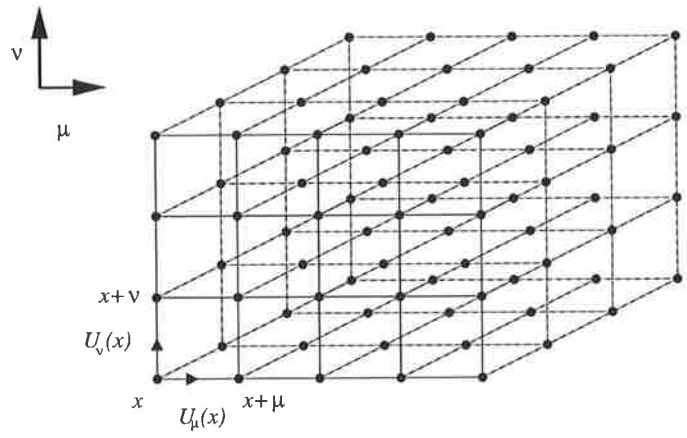

Fig. 3.1: A schematic of a lattice showing the association of the $SU(3)$ matrices $U_\mu(x)$ with the links of the lattice. Figure courtesy of [Ric99].

numerical studies using either Dyson-Schwinger equations or lattice simulations are carried out in Euclidean space. Indeed, even the contour integrals that underlie all perturbative calculations can be viewed as being carried out in Euclidean space with the results analytically continued to Minkowski space using Cauchy's theorem. We begin by formulating QCD in Euclidean space, which we accomplish by a Wick rotation from Minkowski space,

$$t \to -it_E, \tag{3.2}$$

where t is Minkowski-space time and t_E is its Euclidean counterpart. Note that the wick rotation takes the trace of the evolution operator into the partition function of statistical mechanics, $\mathrm{tr}\,(\mathrm{e}^{-\mathrm{i}\hat{\mathrm{H}}\mathrm{t}}) \to \mathrm{tr}\,(\mathrm{e}^{-\hat{\mathrm{H}}\mathrm{t}_\mathrm{E}})$ when we identify t_E with $\beta = \frac{1}{kT}$, where k is Boltzmann constant and T is the temperature.

The Euclidean action and functional integral are obtained from the Minkowski space equivalents by the analytic continuations

$$\int d^4x \to -i \int d^4x^E\,, \tag{3.3}$$

$$\gamma^\mu \partial_\mu \to i\gamma^E \cdot \partial^E\,, \tag{3.4}$$

$$\gamma^\mu A_\mu \to -i\gamma^E \cdot A^E\,, \tag{3.5}$$

$$A^\mu B_\mu \to -iA^E \cdot B^E\,. \tag{3.6}$$

where $a \cdot b = \sum_{i=1}^{4} a_i b_i$, and the Euclidean Dirac gamma matrices, γ_μ^E, have the properties

$$\{\gamma_\mu^E, \gamma_\nu^E\} = 2\delta_{\mu\nu}. \tag{3.7}$$

The Euclidean γ_5 matrix can be written as

$$\gamma_5^E = -\gamma_1^E \gamma_2^E \gamma_3^E \gamma_4^E\,. \tag{3.8}$$

The proper Green's functions of the Minkowski-space theory are Wick-rotated versions of their Euclidean space counter parts.

Let us recall that the gauge fields $A_\mu(x)$ are 3×3 matrices

$$A_\mu(x) = A^a_\mu(x) T^a, \tag{3.9}$$

where the $T^a, a = 1, \ldots, 8$ are the generators of SU(3), satisfying

$$[T^a, T^b] = i f^{abc} T^c, \tag{3.10}$$

$$\mathrm{tr}\,(T^a T^b) = \frac{1}{2}\delta^{ab}. \tag{3.11}$$

The structure of the $SU(3)$ group is captured in the real numbers f^{abc}, which are the $SU(3)$ structure constants. We will now work exclusively in Euclidean space. The field-strength tensor is

$$F^a_{\mu\nu} \equiv \partial_\mu A^a_\nu - \partial_\nu A^a_\mu + g_s f^{abc} A^b_\mu A^c_\nu\,, \tag{3.12}$$

and it is straightforward to see that

$$\frac{1}{2}\mathrm{tr} F_{\mu\nu} F_{\mu\nu} = \frac{1}{4} F^a_{\mu\nu} F^a_{\mu\nu}\,, \tag{3.13}$$

where

$$F_{\mu\nu} = F^a_{\mu\nu} T^a = \partial_\mu A^a_\nu - \partial_\nu A^a_\mu + i g_s \left[A_\mu(x), A_\nu(x)\right],$$

and in terms of which the Euclidean continuum action is

$$S = \int d^4x \, \frac{1}{2}\mathrm{tr}\left(F_{\mu\nu} F_{\mu\nu}\right). \tag{3.14}$$

In the lattice approximation, we only know the fields on the lattice sites or on the lattice links. Thus all derivatives in field equations, the action, and the like must be converted to finite differences. For example, the second derivative of a scalar field ϕ at some point x_j on the lattice is given approximately by

$$\frac{\partial^2 \phi(x_j)}{\partial x^2} = \Delta^{(2)}_x \, \phi(x_j) + \mathcal{O}(a^2)\,, \tag{3.15}$$

where

$$\Delta^{(2)}_x \, \phi(x) \equiv \frac{\phi(x+a) - 2\phi(x) + \phi(x-a)}{a^2}. \tag{3.16}$$

A quantum field theory involving the field ϕ is defined in continuum Euclidean space by an action, $S_E[\phi]$ from which a generating functional,

$$\mathcal{Z}[\eta_i] = \frac{1}{Z}\int \mathcal{D}\phi e^{-S_E[\phi] + \int d^4x \phi(x)\eta(x)}\,, \tag{3.17}$$

may be constructed and from which all physical quantities can be obtained. The $\eta(x)$ is the source term and the normalisation is

$$Z = \int \mathcal{D}\phi e^{-S_E[\phi]}. \tag{3.18}$$

The elements of the field theory – the n-point Green's functions – are constructed from Eq. (3.17) by differentiating the generating functional with respect to the source, then setting those sources to zero. For n differentiations we obtain from this approach the n-point Euclidean Green's function.

$$\begin{aligned} G_n(x_1, x_2, \cdots, x_n) &= \langle \phi(x_1)\phi(x_2)\cdots\phi(x_n)\rangle \\ &= \frac{1}{Z}\int \mathcal{D}\phi\phi(x_1)\phi(x_2)\cdots\phi(x_n)e^{-S_E[\phi]}. \end{aligned} \tag{3.19}$$

3.4 QCD on a lattice

The continuum action for the Yang-Mills theory in Euclidean space is

$$S_{\mathrm{E}}^{\mathrm{YM}} = \int d^4x \frac{1}{2}\sum_{\mu,\nu} \mathrm{tr}\, F_{\mu\nu}(x)F_{\mu\nu}(x)\,, \tag{3.20}$$

where

$$F_{\mu\nu}(x) = \partial_\mu A_\nu(x) - \partial_\nu A_\mu(x) + ig_s\big[A_\mu(x), A_\nu(x)\big]. \tag{3.21}$$

is the field tensor, a traceless 3×3 hermitian matrix. This is just the gluon part of the QCD action.

The gauge fields, A_μ specified by variables on the links joining the sites, are acted upon by gauge transformations, $G(x) \in \mathrm{SU(N)}$ such that

$$A_\mu(x) \to A_\mu^G(x) = G(x)(A_\mu(x) + i\partial_\mu)G^\dagger(x), \tag{3.22}$$

In the continuum, the "*link variable*" on the link joining a site x to one at $x + a\hat{\mu}$ is determined by the line integral of A_μ along the link:

$$U_\mu(x) \equiv \mathcal{P}\exp\left(-ig_s\int_x^{x+a\hat{\mu}} A(y)\cdot dy\right), \tag{3.23}$$

where the $\mathcal{P}$-operator path-orders the A_μ's along the integration path. and where $\hat{\mu}$ denotes the unit vector in the Euclidean space-time direction μ. We use U_μ's in place of A_μ's on the lattice. The U_μ's of Eq. (3.23) can equally well be written as

$$U_\mu(x) = \mathcal{P}\exp\Big\{iag_s\int_0^1 A_\mu(x + at\hat{\mu})dt\Big\}. \tag{3.24}$$

Note that for a smooth field $A_\mu(x)$ and a small enough "a", we have $U_\mu(x) \simeq e^{iag_sA_\mu(x)}$. The *lattice spacing*, a, is the distance between sites on the lattice. It

is the smallest unit of length in a lattice regularized theory. So $U_\mu(x)$ is the link connecting lattice sites x and $x + a\hat{\mu}$ and represented pictorially by a directed line from x to $x + \hat{\mu}$, where this line is the integration path for the line integral in the exponent of $U_\mu(x)$:

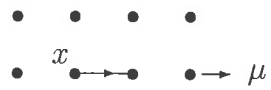

$U_\mu(x)$

The figures in this section are taken from [Lep98]. In the conjugate matrix $U_\mu^\dagger(x)$ the direction of the line integral is flipped and so we represent $U_\mu^\dagger(x)$ by a line going backwards from $x + \hat{\mu}$ to x:

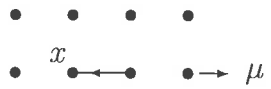

$U_\mu^\dagger(x)$

The links are unitary, *i.e.*, $U_\mu^\dagger = U_\mu^{-1}$, and as the inverse of a link is just the link coming back, it follows that

$$U_\mu^\dagger(x) = U_{-\mu}(x + a\hat{\mu})\,. \tag{3.25}$$

The links obey the simple gauge transformation law

$$U_\mu^G(x) = G(x)U_\mu(x)G_\mu^\dagger(x + a\hat{\mu})\,. \tag{3.26}$$

A Wilson loop function,

$$W(\mathcal{C}) \equiv \frac{1}{3}\mathrm{tr}\mathcal{P}e^{-i\oint_c gA\cdot dx}\,, \tag{3.27}$$

for any closed path $\mathcal{C}$ built of links on the lattice can be computed from the path-ordered product of the U_μ's and $U_\mu^\dagger$'s associated with each link. For example, if $\mathcal{C}$ is the loop

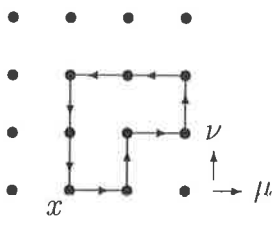

then

$$W(\mathcal{C}) = \frac{1}{3}\mathrm{tr}\left(U_\mu(x)U_\nu(x + a\hat{\mu})\ldots U_\nu^\dagger(x)\right)\,. \tag{3.28}$$

It will be shown that the trace of any closed loop of links is gauge invariant. The most basic Wilson loop (1x1) is called the *plaquette*, and it is defined to be

$$P_{\mu\nu}(x) = U_\mu(x)U_\nu(x + a\hat{\mu})U_\mu^\dagger(x + a\hat{\mu} + a\hat{\nu})U_\nu^\dagger(x)\,, \tag{3.29}$$

where $P_{\mu\nu}(x)$ is the product of the link variables around the small sqaure at the site x in the $\mu\nu$ plane. It can be shown, by pairwise application of Eq. (3.24) and the Baker-Campbell-Hausdorff formula (see below) that

$$P_{\mu\nu}(x) \simeq \exp\Big\{ig_s a^2\Big(\partial_\mu A_\nu(x) - \partial_\nu A_\mu(x) + ig_s\big[A_\mu(x), A_\nu(x)\big]\Big)\Big\}\,, \tag{3.30}$$

where the term in exponential looks like the field strength tensor, Eq. (3.21). The simplest lattice gauge action is thus

$$S_G[U] = \frac{\beta}{2N}\sum_{\text{plaquettes}} \text{tr}\Big\{1 - \frac{1}{2}\big(P_{\mu\nu} + P_{\mu\nu}^\dagger\big)\Big\}\,, \tag{3.31}$$

$$= S_E^{\text{YM}} + \text{higher order terms.} \tag{3.32}$$

The coupling constant of the theory has been absorbed into the parameter,

$$\beta = \frac{2N}{g_s^2} = \frac{6}{g_s^2}\,, \tag{3.33}$$

giving Eq. (3.32) a form that emphasises the analogy with statistical physics (c.f., $\beta = \frac{1}{kT}$).

Our lattice gauge theory is now defined by the generating functional

$$\mathcal{Z} = \frac{1}{Z}\int \mathcal{D}U e^{-S_G[U]+\text{sources}}\,, \tag{3.34}$$

in terms of the link variables, U_μ. The measure,

$$\mathcal{D}U = \prod_{x,\mu} dU_\mu(x)\,, \tag{3.35}$$

which properly defines integration over a compact group element is called the *Haar measure*. Its properties

$$\int \mathcal{D}U = \int \mathcal{D}(UV) = \int \mathcal{D}(VU) \quad \forall V \in G\,, \tag{3.36}$$

$$\int \mathcal{D}U = 1\,, \tag{3.37}$$

$$\int \mathcal{D}U\, V = 0 \quad \forall V \in G\,. \tag{3.38}$$

ensure gauge invariance of the path integral. The normalisation in Eq.(3.34) is, of course,

$$Z = \int \mathcal{D}U e^{-S_G[U]}\,. \tag{3.39}$$

The discretization acts as an ultraviolet cutoff, $p_{\text{max}} = \frac{\pi}{a}$, so loops will be finite if perturbation theory is applied to the lattice generating functional. Furthermore,

the lattice formulation maintains exact gauge invariance, unlike field theory with a naïve UV cutoff [Mut98]. As the elements of the gauge field, the links, are written in terms of a complex exponential, e.g., $U_\mu \equiv e^{i\phi_\mu}$, they are bounded above and below. The gauge group is thus seen to be compact. Eq. (3.32) is only one of the many possible lattice actions that reduce to the desired continuum action. The simplicity of this particular action, the Wilson action, is attractive and its locality makes it computationally efficient.

3.5 Relation to the continuum

Observables in lattice gauge theory need to be related to the continuum physical world to recover meaningful results for the continuum theory. In order to obtain the theory in the continuum, the lattice spacing has to taken to zero; at the same time, the cut-off necessarily goes to infinity and we have to construct renormalized physical quantities that remain finite in the continuum limit [Nec03]. It is also important to know the behavior of physical quantities in the continumm limit so that we will be able to judge whether lattice quantum chromodynamics goes over into continumm theory of strong interactions of hadrons as $a \to 0$. In practice, quantities of interest calculated at different values of lattice spacing a, need to be extrapolated to $a = 0$. We have seen that the Lattice formulation creates an approximation to a continuum theory that is UV regulated and maintains exact gauge invariance. Now we shall more thoroughly explore its relation to the continuum theory.

Define $\phi_\mu(x)$ in terms of the link variables by

$$U_\mu(x) = e^{ig_s\phi_\mu(x)} \in SU(N)\,, \tag{3.40}$$

where $\phi_\mu(x)$ is $N \times N$ complex matrix and can be thought of the lattice gauge field on a hypercubic lattice. From Eq. (3.23) and Eq. (3.24) we see that for a continuous $A_\mu(x)$ in the limit $a \to 0$, that $\phi_\mu(x) \to aA_\mu(x)$. Note that g_s and $\phi_\mu(x)$ are dimensionless. Gauge transformations, $G(x) \in SU(N)$, act upon the links as

$$U^G_\mu(x) = G(x)U_\mu(x)G^\dagger(x + a\hat{\mu})\,. \tag{3.41}$$

which, to leading order in g_s, corresponds to

$$\phi^G_\mu(x) = G(x)(\phi_\mu(x) + i\partial_\mu)G^\dagger(x)\,. \tag{3.42}$$

where $G^\dagger(x + a\hat{\mu})$ has been expanded about x. This has the same form as the gauge transformation for continuum fields. One can construct a gauge invariant action from any closed loops of link variables, the simplest of which is the plaquette,

$$\begin{aligned} P_{\mu\nu}(x) &= U_\mu(x)U_\nu(x + a\hat{\mu})U^\dagger_\mu(x + a\hat{\mu} + a\hat{\nu})U^\dagger_\nu(x) \\ &= e^{ig_s\phi_\mu(x)}e^{ig_s\phi_\nu(x+a\hat{\mu})}e^{-ig_s\phi_\mu(x+a\hat{\mu}+a\hat{\nu})}e^{-ig_s\phi_\nu(x)}\,. \end{aligned} \tag{3.43}$$

To demonstrate this, we gauge transform each link in the plaquette using Eq. (3.41) to give

$$\begin{aligned} P^G_{\mu\nu}(x) &= G(x)U_\mu(x)G^\dagger(x+a\hat{\mu}) \times G(x+a\hat{\mu})U_\nu(x+a\hat{\mu})G^\dagger(x+a\hat{\mu}+a\hat{\nu}) \\ &\quad \times \big(G(x+a\hat{\nu})U_\mu(x+a\hat{\nu})G^\dagger(x+a\hat{\mu}+a\hat{\nu})\big)^\dagger \times \big(G(x)U_\nu(x)G^\dagger(x+a\hat{\mu}+a\hat{\nu})\big)^\dagger \\ &= G(x)P_{\mu\nu}(x)G^\dagger(x)\,. \end{aligned}$$

As we have already seen, it is the trace of $P_{\mu\nu}$ that occurs in the action, so an action composed of traces over plaquettes is automatically gauge invariant, since by the property of the trace $\mathrm{tr}\,[\mathrm{G(x)}\cdots,\mathrm{G^\dagger(x)}] = \mathrm{tr}\,[\cdots]$.

This result can be readily seen to apply to a closed loop of any size and shape.

As the fields ϕ_μ are complex matrices, they are in general not commuting and so we need to use the Baker-Campbell-Hausdorff formula

$$e^A e^B = e^{A+B+\frac{1}{2}[A,B]+\cdots} \tag{3.44}$$

to express the plaquette in terms of the gauge fields. Each commutator carries one additional power of the coupling, g_s, and one additional power of lattice spacing a (recall $\phi_\mu(x) \sim a$) and so expansion to one commutator will be sufficient for our purposes here. Applying Eq. (3.44) pairwise we obtain

$$\begin{aligned} P_{\mu\nu}(x) = \exp\Big\{ & ig_s\Big(\phi_\mu(x) + \phi_\nu(x+a\hat{\mu}) - \phi_\mu(x+a\hat{\nu}) - \phi_\nu(x)\Big) \\ & - \frac{g_s^2}{2}\Big(\big[\phi_\mu(x),\phi_\nu(x+a\hat{\mu})\big] + \big[\phi_\mu(x+a\hat{\nu}),\phi_\nu(x)\big] - \big[\phi_\mu(x),\phi_\mu(x+a\hat{\nu})\big] \\ & - \big[\phi_\mu(x),\phi_\nu(x)\big] - \big[\phi_\nu(x+a\hat{\mu}),\phi_\mu(x+a\hat{\nu})\big] - \big[\phi_\nu(x+a\hat{\mu}),\phi_\nu(x)\big]\Big)\Big\} + \mathcal{O}(g_s^3)\,. \end{aligned} \tag{3.45}$$

As the links are $SU(N)$ matrices, any product of the links such as $P_{\mu\nu}$, is also an element of $SU(N)$, [see Eq. (3.43)]. In analogy with Eq. (3.40) we can define $\Phi_{\mu\nu}(x)$ as

$$P_{\mu\nu} = e^{ig_s\Phi_{\mu\nu}(x)}. \tag{3.46}$$

Note that $\Phi_{\mu\nu}$ is dimensionless. We can expand the $\phi_\mu(x)$ fields by performing a one dimensional Taylor expansion about x, where ∂_μ^n is the n^{th} partial derivative in the μ direction, *i.e.*,

$$\phi_\mu(x+a\hat{\nu}) = \phi_\mu(x) + a\partial_\nu\phi_\mu(x) + \frac{a^2}{2}\partial_\nu^2\phi_\mu(x) + \cdots\,. \tag{3.47}$$

To best demonstrate how this discussion relates to a corresponding continuum theory, we will expand the vector fields, ϕ_μ about the midpoint of the plaquette

$$\tilde{x} = x + \frac{a(\hat{\mu}+\hat{\nu})}{2}\,. \tag{3.48}$$

Hence, for example, if we have

$$\phi_\mu(x + a\hat{\nu}) = \phi_\mu(\tilde{x}) + \frac{a}{2}\partial_\nu\phi_\mu(\tilde{x}) - \frac{a}{2}\partial_\mu\phi_\mu(\tilde{x}) + \cdots ,$$

then at the midpoint we get

$$\phi_\mu(\tilde{x} + a\hat{\nu}) = \phi_\mu(\tilde{x}) + a\partial_\nu\phi_\mu(\tilde{x}) - a\partial_\mu\phi_\mu(\tilde{x}) + \cdots . \tag{3.49}$$

Combining Equations (3.45) with (3.49) gives us

$$\begin{aligned}\Phi_{\mu\nu}(x) &= \phi_\mu(\tilde{x}) + \phi_\nu(\tilde{x}) - \phi_\mu(\tilde{x}) - \phi_\nu(\tilde{x}) + a\partial_\mu\phi_\nu(\tilde{x}) - a\partial_\nu\phi_\mu(\tilde{x}) + \mathcal{O}(a^2) \\ &\quad + \frac{ig_s}{2}\big([\phi_\mu(\tilde{x}), \phi_\nu(\tilde{x})] + [\phi_\mu(\tilde{x}), \phi_\nu(\tilde{x})] - [\phi_\mu(\tilde{x}), \phi_\mu(\tilde{x})] \\ &\quad - [\phi_\mu(\tilde{x}), \phi_\nu(\tilde{x})] - [\phi_\nu(\tilde{x}), \phi_\mu(\tilde{x})] - [\phi_\nu(\tilde{x}), \phi_\nu(\tilde{x})]\big) \\ &= a\big(\partial_\mu\phi_\nu(\tilde{x}) - \partial_\nu\phi_\mu(\tilde{x})\big) + ig_s[\phi_\mu(\tilde{x}), \phi_\nu(\tilde{x})]\big) \\ &\quad + \frac{a^3}{24}\big(\partial_\mu^3\phi_\nu(\tilde{x}) - \partial_\nu^3\phi_\mu(\tilde{x})\big) + \mathcal{O}(a^5).\end{aligned} \tag{3.50}$$

Now we construct a lattice gauge action

$$S[U] = \frac{\beta}{2N}\sum_x \mathrm{tr}\Big\{1 - \frac{1}{2}(P_{\mu\nu} + \text{h.c.})\Big\} \tag{3.51}$$

$$= \sum_x \mathrm{tr}\Big\{\big(\Phi_{\mu\nu}(x)\big)^2 - \frac{g_s^2}{2}\big(\Phi_{\mu\nu}(x)\big)^4 + \mathcal{O}(g_s^4)\Big\}. \tag{3.52}$$

which has, to lowest order in lattice coupling and spacing, the same form as the continuum gauge action, Eq. (3.20). Note that "h.c." is shorthand for hermitian conjugate.

This action, Eq. (3.51), is called the *Wilson action*. We now have a gauge theory on a discretized Euclidean space. It remains to relate our theory to the continuum. The lattice gauge fields are related to the continuum fields through

$$\phi_\mu(x) = \int_0^1 A_\mu(x + at\hat{\mu})dt \tag{3.53}$$

$$\simeq aA_\mu(x)\,. \tag{3.54}$$

which means that from Eq. (3.50)

$$a^{-2}\Phi_{\mu\nu}(x) = F_{\mu\nu}(x) + \mathcal{O}(a^2) + \mathcal{O}(a^2 g_s^2)\,. \tag{3.55}$$

Thus

$$\frac{1}{2}a^4 g_s^2 \sum_x \mathrm{tr}\big\{\Phi_{\mu\nu}^2(x)\big\} \xrightarrow[a\to 0]{} \frac{1}{2}\int d^4x\, \mathrm{tr}\big\{F_{\mu\nu}^2(x)\big\}\,. \tag{3.56}$$

So we recover the continuum Yang-Mills action as the lattice spacing goes to zero. Therefore in the limit $a \to 0$ the lattice action $S[U]$ tends to the conntiuum action.

If D denotes a dimensionless observable, then its expectation value on the lattice differs from the value in the continuum by dimensionless corrections of order a^n and higher :

$$D^{\text{lat}} = D^{\text{cont}} + \mathcal{O}(a^n), \tag{3.57}$$

where the power n depends on the chosen discretization of the QCD action. The correction term for typical values of a can be quite large, and an extrapolation to the continuum limit is then required to obtain the required result [SW02]. If n is large, the rate of convergence to the continuum limit is more rapid, which is the case by construction for improved actions. Improved actions are necessarily more non-local and so are slightly more expensive to compute with.

3.6 Lattice gauge-fixing

Gauge fixing in Yang-Mills theories is well understood in the perturbation regime where Gribov copies can be neglected. For the calculation of physical observables it is not necessary to fix the gauge provided that one never includes two gauge equivalent fields in the Monte carlo estimate of integration over the gauge fields. This is automatic as the probability of accessing two gauge-equivalent fields in a finite ensemble is utterly negligible. However, gauge fixing is necessary to study the Green's functions of fundamental quantities such as the gluon and quark propagators and the quark gluon vertex. Common gauge choices are covariant gauge, maximal axial gauge ($\eta_\mu A_\mu = 0$ where η in Minkowski space is a fixed time-like vector) and Coloumb gauge.

The quark propagator and gluon propagator are gauge dependent and we work in the Landau gauge for ease of comparison with other studies. Landau gauge is a smooth gauge that preserves the Lorentz invariance of the theory, so it is a popular choice. Landau gauge corresponds to the Lorentz gauge fixing condition $\partial_\mu A_\mu(x) = 0$. Lattice gauge fixing is achieved by maximising a functional [BBL+99] whose extremum in the continuum implies the gauge fixing condition, $\partial_\mu A_\mu(x) = 0$. The usual Landau gauge fixing functional is

$$\mathcal{F}_1^G[\{U\}] = \sum_{\mu,x} \frac{1}{2} \text{tr} \left\{ U_\mu^G(x) + U_\mu^G(x)^\dagger \right\}, \tag{3.58}$$

where the superscript G denotes that $\mathcal{F}_1^G$ varies as G moves along the orbit of gauge equivalent configurations defined by Eq. (3.41) and

$$G(x) = \exp\left\{ -i \sum_a \omega^a(x) T^a \right\}. \tag{3.59}$$

We have seen from Eq. (3.58) that $\mathcal{F}_1^G$ is a functional of the links U and hence the functional of the gauge transformation G. For maximising the lattice functional, consider the variation of Eq. (3.58) under gauge transformations. A maximum

of the functional implies the continuum Landau gauge. By taking the functional derivative of Eq. (3.58), we obtain

$$\frac{\delta \mathcal{F}_1^G}{\delta \omega^a(x)} = \frac{1}{2} i \sum_\mu \mathrm{tr} \left\{ \left[U_\mu^G(x-\hat{\mu}) - U_\mu^G(x) - \left(U_\mu^G(x-\hat{\mu}) - U_\mu^G(x) \right)^\dagger \right] T^a \right\} . \quad (3.60)$$

We have seen that the gauge links $U_\mu(x)$ are defined by Eq. (3.24). Connection with the continuum is made by Taylor-expanding $A_\mu(x + a\hat{\mu}t)$ about x, integrating term-by-term, and then expanding the exponential, typically to leading order in g_s, noting that errors are of $\mathcal{O}(g_s^2 a^2)$. Expanding Eq. (3.60), we obtain

$$\begin{aligned} \frac{\delta \mathcal{F}_1^G}{\delta \omega^a(x)} = g_s a^2 \sum_\mu \mathrm{tr} \{ & [\partial_\mu A_\mu(x) \\ & + \frac{1}{12} a^2 \partial_\mu^3 A_\mu(x) + \frac{a^4}{360} \partial_\mu^5 A_\mu(x) + \mathcal{O}(a^6) \Big] T^a \Big\} + \mathcal{O}(g_s^3 a^4) . \end{aligned} \quad (3.61)$$

An extremum of Eq. (3.58) implies that $\frac{\delta \mathcal{F}_1^G}{\delta \omega^a(x)}$ and hence implies that

$$\sum_\mu \partial_\mu A_\mu(x) = \sum_\mu \left\{ -\frac{a^2}{12} \partial_\mu^3 A_\mu(x) - \mathcal{H}_1 \right\} , \quad (3.62)$$

where $\mathcal{H}_1$ represents $\mathcal{O}(a^4)$ and higher-order terms. Clearly in the continuum limit, Eq. (3.62) becomes $\partial_\mu A_\mu(x) = 0$ as desired. The "one-link" functional can be generalised to functionals using "n-link" terms:

$$\mathcal{F}_n^G = \sum_{x,\mu} \frac{1}{2n^2} \mathrm{tr} \{ U_{n\mu}^G(x) + \mathrm{h.c.} \} , \quad (3.63)$$

where

$$U_{n\mu}^G(x) = U_\mu^G(x) + U_\mu^G(x + a\hat{\mu}) \cdots U_\mu^G\left(x + (n-1)a\hat{\mu}\right) . \quad (3.64)$$

Taking the functional derivative yields

$$\begin{aligned} \frac{\delta \mathcal{F}_n^G}{\delta \omega^a(x)} &= \frac{1}{2n^2} i \sum_\mu \mathrm{tr} \left\{ [U_{n\mu}^G(x-\hat{\mu}) - U_{n\mu}^G(x) - \mathrm{h.c.}] T^a \right\} \\ &= g a^2 \left(\sum_\mu \mathrm{tr} \left\{ \left[\partial_\mu A_\mu(x) + \frac{2}{(na)^2} \left\{ \frac{(na)^4}{4!} \partial_\mu^3 A_\mu(x) \right. \right. \right. \right. \\ &\quad \left. \left. \left. \left. + \frac{(na)^6}{6!} \partial_\mu^5 A_\mu(x) + \cdots \right\} \right] T^a \right\} + \mathcal{O}(g_s^2 a^2) \right) \end{aligned} \quad (3.65)$$

and so we can approach the condition $\partial_\mu A_\mu(x) = 0$ more rapidly in the continuum limit by choosing an appropriate n-link functional.

3.6.1 Tadpole improvement and improved Landau gauge fixing

We are using improved Landau-gauge-fixing functional, $\mathcal{F}^G_{\rm Imp} \equiv \frac{4}{3}\mathcal{F}^G_1 - \frac{1}{12u_0}\mathcal{F}^G_2$ to remove $\mathcal{O}(a^2)$ errors arising from the the gauge fixing condition, where $\mathcal{F}^G_2$ is a two-link functional of the form of Eq. (3.63). Here we are taking a linear combination of one-link ($\mathcal{F}^G_1$) and two-link functionals. The mean field (tadpole) improvement parameter u_0 is defined by

$$u_0 = \left(\frac{1}{3}\mathcal{R}e\,\mathrm{tr}\langle P_{\mu\nu}\rangle\right)^{\frac{1}{4}}. \tag{3.66}$$

Tadpole improvement is the first step in a systematic procedure for improving the action. The $u_0's$ cancel lattice tadpole contributions. The small bare coupling in the traditional lattice theory is a symptom of the "tadpole problem" [Lep98]. We have seen from Eq. (3.24) that all gluonic operators in lattice QCD are built from the link operator $U_\mu(x)$. The leading term in the Lagrangian that couples quarks and gluons contains the usual vertex $\bar{\psi}gA\cdot\gamma\psi$. In addition, it contains vertices with any additional powers of agA_μ. Consider

$$U_\mu(x) = e^{iag_sA_\mu(x)} = 1 + iag_sA_\mu - \frac{a^2g_s^2}{2}A^2(x) + \cdots \tag{3.67}$$

The $\mathcal{O}(g_s^2)$ term corresponds to a gluonic tadpole diagram. Pairs of A_μ's generate ultraviolet divergent factors of $\frac{1}{a^2}$ that cancel extra $a's$. But the contributions generated by the extra vertices are suppressed by powers of g_s^2, and turn out to be uncomfortably large in typical lattice simulations. These are the tadpole contributions. The next term $\frac{a^4g_s^4}{4!}A_\mu^4$ is also poorly suppressed.

The mean value u_0 accounts for these tadpole contributions by dividing every link operator by u_0. That is, in every lattice operator we replace

$$U_\mu(x) \to \frac{U_\mu(x)}{u_0}, \tag{3.68}$$

where u_0 is computed numerically in a simulation. We adopt a "steepest decents" approach [D+88] to perform gauge fixing. The gauge transformation is $G(x) = \exp\{-i\alpha\sum_\mu \partial_\mu A_\mu(x)\}$. To maximise, for example $\mathcal{F}^G_1$, we use Eq. (3.65) to derive the gauge transformation

$$G_1(x) = \exp\left\{\frac{\alpha}{2}\Delta_1(x)\right\}, \tag{3.69}$$

where α is a tuneable step-size parameter and

$$\Delta_1(x) \equiv \frac{1}{u_0}\sum_\mu [U_\mu(x-\hat{\mu}) - U_\mu(x) - \mathrm{h.c.}]_{\rm traceless}, \tag{3.70}$$

where the subscript, "traceless" denotes the substraction of the average of the color-trace from each of the diagonal color elements.

This gauge transformation is calculated for every link on the lattice, and then applied as in Eq. (3.26). This procedure is repeated until the convergence criterion is met (as discussed below). For α small enough, it is possible to show that the functional, Eq. (3.58), monotonically increases with each iteration and that the convergence criterion will be satisfied within a finite number of iterations.

Similarly, $\Delta_2(x)$ and $\Delta_{\text{Imp}}(x)$ are obtained from the functional derivatives of $\mathcal{F}_2$ and $\mathcal{F}_{\text{Imp}}$ respectively.

$$\begin{aligned}\Delta_2(x) \equiv \frac{1}{u_0^2}\sum_\mu \Big[& U_\mu(x-2\hat{\mu})U_\mu(x-\hat{\mu}) \\ & -U_\mu(x)U_\mu(x+a\hat{\mu}) - \text{h.c.}\Big]_{\text{traceless}} ,\end{aligned} \tag{3.71}$$

and

$$\Delta_{\text{Imp}}(x) \equiv \frac{4}{3}\Delta_1(x) - \frac{1}{12}\Delta_2(x) . \tag{3.72}$$

The resulting gauge transformation is

$$\begin{aligned} G_i(x) &= \exp\left\{\frac{\alpha}{2}\Delta_i(x)\right\} \\ &= 1 + \frac{\alpha}{2}\Delta_i(x) + \mathcal{O}(\alpha^2) , \end{aligned} \tag{3.73}$$

where the index i is either 1, 2 or Imp. At each iteration $G_{\text{Imp}}(x)$ is unitarised through an orthonormalisation procedure. For a given functional $\mathcal{F}_i^G$, the gauge fixing algorithm proceeds by calculating the relevant Δ_i in terms of the mean-field-improved links, and then applying the associated gauge transformation, Eq. (3.73), to the gauge field. The algorithm using conjugate gradient Fourier acceleration is implemented in parallel, updating all links simultaneously, and is iterated until the Lattice Landau gauge condition

$$\theta_{\text{Imp}} = \frac{1}{VN_c}\sum_x \text{tr}\left\{\Delta_{\text{Imp}}(x)\Delta_{\text{Imp}}(x)^\dagger\right\} , \tag{3.74}$$

is satisfied with accuracy of $\theta_i < 10^{-12}$.

A configuration fixed by $\Delta_1(x)$ will satisfy Eq. (3.62). Substituting Eq. (3.62) into Eq. (3.71) yields

$$\begin{aligned}\Delta_2(x) &= -2iga^2\sum_\mu\left\{-\frac{a^2}{12}\partial_\mu^3 A_\mu(x) + \frac{a^2}{3}\partial_\mu^3 A_\mu(x) - \mathcal{H}_1 + \mathcal{H}_2\right\} \\ &= -2iga^2\sum_\mu\left\{\frac{a^2}{4}\partial_\mu^3 A_\mu(x) - \mathcal{H}_1 + \mathcal{H}_2\right\} ,\end{aligned} \tag{3.75}$$

where $\mathcal{H}_1$ represents $\mathcal{O}(a^4)$ and higher order terms. Collecting terms of $\mathcal{O}(a^6)$ and higher to $\mathcal{H}_i$ where the index i is either 2 or Imp. Similarly,

$$\Delta_{\text{Imp}}(x) = -2iga^2 \sum_{\mu} \Big\{ -\frac{a^2}{12} \partial_\mu^3 A_\mu(x) - \mathcal{H}_1 + \mathcal{H}_{\text{imp}} \Big\} . \tag{3.76}$$

Since the improved measure has no $\mathcal{O}(a^2)$ error of its own, Eq. (3.76) provides an estimate of the absolute size of these discretisation errors.

3.6.2 The Improved gauge action

The lattice regularization of field theory provides a unique tool to study its non-perturbative behavior. The determination of physical quantities from the lattice results in systematic uncertainties, if the lattice spacing is finite. One can simply make the lattice spacing smaller and smaller until a safe extrapolation to the continuum limit is obtained. Very fine lattices require time-consuming and demanding computation [Pap98]. A more efficient approach is to improve the discretization procedure according to some theoretical precription and so more rapidly approach the continuum limit. That theories can be constructed by this was shown by Symanzik many years earlier.

In Wilson's formulation of lattice QCD, the discretization effects are of the order of a^2, which can be large. An improved version of the Wilson's action gives discretization errors of $\mathcal{O}(a^4)$ or higher. The improvement method by Symanzik [Sym83] consists in adding irrelevant terms to the standard action with appropriately chosen coefficients to cancel the lattice artifacts in the n-point Green's functions up to a given order in a^2. These irrelevant terms vanish in the contiuum limit.

The $\mathcal{O}(a^2)$ tadpole-improved gauge action is defined as

$$\begin{aligned} S_G = & \frac{5\beta}{3} \sum_{\text{pl}} \frac{1}{N_c} \text{tr} \Big\{ 1 - \frac{1}{2} \big(P_{\mu\nu} + P_{\mu\nu}^\dagger \big) \Big\} \\ & - \frac{\beta}{12 u_0^2} \sum_{\text{rect}} \frac{1}{N_c} \text{tr} \Big\{ 1 - \frac{1}{2} \big(R_{\mu\nu} + R_{\mu\nu}^\dagger \big) \Big\} , \end{aligned} \tag{3.77}$$

where $\sum_{\text{rect}}$ includes both the 1×2 and the 2×1 "rectangle operators" *i.e.*,

$$\begin{aligned} R_{\mu\nu}^{1\times 2}(x) &= U_\mu(x) U_\nu(x + a\hat{\mu}) U_\nu(x + a\hat{\nu} + a\hat{\mu}) U_\mu^\dagger(x + 2\hat{\nu}) U_\nu^\dagger(x + a\hat{\nu}) U_\nu^\dagger(x) , \\ R_{\mu\nu}^{2\times 1}(x) &= U_\mu(x) U_\mu(x + a\hat{\mu}) U_\nu(x + 2\hat{\mu}) U_\mu^\dagger(x + a\hat{\mu} + a\hat{\nu}) U_\mu^\dagger(x + a\hat{\nu}) U_\nu^\dagger(x) . \end{aligned}$$

Thus we cancel $\mathcal{O}(a^2)$ errors in the Wilson action Eq. (3.52) by adding another Wilson loop. The action based on these loops has $\mathcal{O}(a^2)$ errors. But adding these terms to the Wilson action in the right combination, the $\mathcal{O}(a^2)$ terms can be cancelled whilst keeping the correct continuum limit. The inclusion of the rectangular Wilson loop is known as Symanzik improvement. Since in the continuum limit $u_0 \to 1$ we

see that Eq. (3.77) reproduces the continuum action as $a \to 0$, provided β takes the standard value of $\frac{2N_c}{g^2}$. The improved action in Eq .(3.77) also has shown to have excellent rotational symmetry.

3.7 Fermions

The formulation of fermion fields on the lattice has been a huge problem. Lattice fermion actions are constructed by a suitable discretization. Fermions are represented on the lattice by anticommuting spinors ψ on the lattice sites. Lattice fermion actions are constructed by a suitable discretization of the covariant Dirac operator. The simplest is

$$D_\mu(x,y) = \frac{1}{2a}(U_\mu(x)\delta_{y,x+\hat{\mu}} - U^\dagger_\mu(x-\mu)\delta_{y,x-\hat{\mu}})\,, \tag{3.78}$$

which is equivalent to Eq. (2.11) up to terms of $\mathcal{O}(a^2)$. This "naïve" Dirac operator is, however, problematic on a lattice. Fermions will play an important role in this study. They are an integral part of field theories in general and QCD in particular, so it is important to discuss their lattice implementation. In Euclidean space, free fermions are represented by the action

$$S^E_F[\overline{\psi},\psi] = \int d^4x \overline{\psi}(x)(\gamma_\mu\partial_\mu + m)\psi(x)\,, \tag{3.79}$$

where γ_μ are the 4×4 Dirac matrices in their Euclidean form. Lattice fermion actions are constructed using Eq. (3.78). Such an action may be written in terms of a fermion matrix

$$S_F[\overline{\psi},\psi] = \sum_{x,y} \overline{\psi}_\alpha(x) K_{\alpha\beta}(x,y)\psi_\beta(y)\,, \tag{3.80}$$

where the fermion and antifermion fields, ψ and $\overline{\psi}$ respectively, dwell on the lattice sites x and y. The simplest discretisation, where the derivative is replaced by a finite difference, leads to the famous "doubling problem". Each species of continuum fermion becomes 2^d species of lattice fermion, where d is the number of space-time dimensions. One popular choice of discretisation is the Wilson fermion action where

$$K_{\alpha\beta}(x,y) = (m + \frac{4r}{a})\delta_{xy}\delta_{\alpha\beta} - \frac{1}{2a}\sum_{\mu,x}\left[(r-\gamma_\mu)_{\alpha\beta}\delta_{y,x+\hat{\mu}} + (r+\gamma_\mu)_{\alpha\beta}\delta_{y,x-\hat{\mu}}\right]\,, \tag{3.81}$$

which solves the doubling problem at the cost of chiral symmetry. The 15 unwanted quark flavors gain masses proportional to the cutoff. The real number, $r \neq 0$, is typically set to one. The gauge interaction is introduced by including the gauge fields in the Dirac operator, analogously to the continuum case where the derivative

is replaced by a covariant derivative. The finite difference operators in Eq. (3.81) become

$$\delta_{y,x+\hat{\mu}} \to U_\mu(x)\delta_{y,x+\hat{\mu}} \tag{3.82}$$

$$\delta_{y,x-\hat{\mu}} \to \delta_{y,x-\hat{\mu}}U_\mu^\dagger(x-\hat{\mu})\,. \tag{3.83}$$

and the Wilson fermion action is equivalent to the continuum fermion action to $\mathcal{O}(a)$ (c.f. $\mathcal{O}(a^2)$ for the Wilson gauge action).

When the fermion part is added to the lattice gauge action, the fermionic fields, being Grassman variables, can be integrated out. Hence, for an arbitrary n-point Green's function of the Lattice QCD fields, i.e. gauge links, quarks and anti-quarks

$$G_n = \langle \psi_1\psi_2\cdots\overline{\psi}_1\overline{\psi}_2\cdots U_1\cdots\rangle\,, \tag{3.84}$$

where we have omitted spinor and space-time indices and the fields are understood to be at arbitrary coordinates,

$$G_n = \frac{\int \mathcal{D}U\langle\psi\cdots\overline{\psi}\cdots\rangle_{\rm SF}U\cdots\ {\rm det}Ke^{-S_G}}{\int \mathcal{D}U\ {\rm det}Ke^{-S_G}}\,, \tag{3.85}$$

where

$$\langle\psi\cdots\overline{\psi}\cdots\rangle_{\rm SF} = \frac{\int \mathcal{D}\overline{\psi}\mathcal{D}\psi\psi\cdots\overline{\psi}\cdots e^{-S_F}}{\int \mathcal{D}\overline{\psi}\mathcal{D}\psi e^{-S_F}}\,. \tag{3.86}$$

Computing the determinant of the fermion matrix, det$K$, is extremely expensive. For this reason, many lattice simulations have used the ansatz

$${\rm det}K = 1\,. \tag{3.87}$$

which is equivalent to ignoring all fermion loops in the theory. This is called the quenched approximation. The quenched approximation while convenient does not correspond to the real world, It may turn out that the effects of vacuum polarization do not influence the hadron spectrum significantly. Only a calculation in full QCD can provide us with an answer to how quenched QCD result are modified by the presence of dynamical quarks. It is commonly believed that while the quenched approximation is reasonable for heavy quarks it fails badly for physical mass quarks.

3.8 Unquenched QCD

The quenched approximation ignores the fermion contribution to the path integral, *i.e.*, detK = 1. Because of the appearance of the fermionic determinant, the times required for numerical simulations in full QCD are much much larger than in quenched QCD. The limitations of computer power was the main reasons for quenched QCD calculations. Physically, the quenched approximation corresponds to quenched QCD which is not real-world QCD. In unquenched QCD, we need to

evaluate the determinant of the fermion matrix. Until the mid-nineties it was essentially impossible. Though the quenched approximation can cause uncontrollable ten or twenty percent errors, it makes things faster. Physically, it amounts to neglecting dynamical fermions in the simulation. As people started to remove the quenched approximation another problem came up. Evaluating the determinant gets slower as we go to smaller and smaller quark masses as discussed in the introduction. This forces us to work at unphysical values of the up and down quark masses. That is the situation today. Simulations are forced to use masses that are larger than the physical up and down quark masses and we need to extrapolate to the physical limit (which is near $m = 0$). So it is possible to simulate with dynamical fermions, but, for the most part, we simulate at unphysical masses. We set valence and sea-quark mass values equal and recover the real theory, namely "full QCD" by attempting to extrapolate to the physical mass regime. The Kogut-Susskind formulation of lattice fermions is attractive for full QCD simulations due to the reduction of the degrees of freedom which reduces the compuational efforts [B+00b]. In this work, we carried out full QCD simulations with $2 + 1$ flavors of dynamical sea-quarks using the improved staggered fermion action.

3.9 Lattice fermion action

Lattice fermion actions are constructed by a suitable discretisation of the covariant Dirac operator. The simplest is Eq. (3.78), and it corresponds to action which describes 16 degenerate types of fermions. These degenerate types are called "tastes". So the naive discritization of lattice fermions induces 16 tastes. So if we take Dirac equation, and construct a "naive" approximation to it, we find that the theory describing a single quark is actually describing 16 identical copies of quark. Obviously we don't want to simulate 16 degenerate quarks, we want to simulate one quark, so we need to figure out some method of getting rid of the other 15 tastes.

3.10 Staggered fermion Action

The majority of Dynamical Monte Carlo simulations have been carried out with Kogut-Susskind fermions. This approach reduces the number of tastes through a technique called "staggering". It puts the four spin components of the Dirac spinor on different sites of the lattice. The staggered fermion action posseses a continous axial flavor symmetry in the limit of vanishing fermions. This allows us to study spontaneous chiral symmetry breaking and the associated Goldstone phenomenon with out having to tune any parameters, as would be required in the case for Wilson fermions. In the case of staggered fermions the chiral limit just corresponds to setting the quark masses to zero. On the other hand, for Wilson fermions chiral symmetry is explicitely broken by the fermionic action. Staggered fermions are cheaper to simulate on big lattices. The number of degrees of freedom for Wilson fermions

is much larger than for Kogut-Susskind fermions. Consequently simulations with Wilson fermions have been performed on much smaller lattices than those using staggered fermions.

Consider the naïve quark action Eq. (3.78) at tree-level, i.e., with $U_\mu(x) = 1$ everywhere. In momentum space, the propagator is

$$S_0(p) = \frac{1}{\sum_\mu \gamma_\mu \sin(p_\mu) + m_0}, \tag{3.88}$$

where the lattice momentum

$$p_\mu = \frac{2\pi n_\mu}{aL_\mu} \qquad n_\mu \in \left(\frac{-L_\mu}{2}, \frac{L_\mu}{2}\right), \tag{3.89}$$

covers the first Brillouin zone. In the massless case, this propagator has a pole at $p_\mu = 0, \pi$ for each μ. So a mode with momentum near zero will describe a low momentum continuum quark, but so will a mode with momentum near π [BHL$^+$05]. That means the naïve quark action describes $2^d = 16$ species of degenerate fermions. This is the (in)famous "doubling problem." Note that QCD only has asymptotic freedom for $N_f < \frac{33}{2}$, and 16 flavors is rather close to this transition. Another consequence of doubling is the loss of the axial anomaly. In continuum QCD, the axial symmetry is broken by quantum effects, but on the lattice the doublers of the naïve quark action conspire such that the symmetry breaking terms exactly cancel.

As with gauge actions, there are many possible lattice fermion actions that reduce the desired continuum action. The best know solution to the doubling problem is the Wilson fermion action, which uses a chiral symmetry breaking term to give the doublers mass of $\mathcal{O}(a^{-1})$ (the cutoff). This is described in many places [Rot05]. Here we will briefly discuss the other main type of lattice fermion action, the Kogut–Susskind or staggered action. The discussion below follows that of [Rot05, BHL$^+$05, B$^+$98].

The principle observation that leads to the staggered formalism is that the doubling problem occurs at the edge of the Brillouin zone. If the available momenta only spanned half the Brillouin zone, there would be no problem. The difficulties lie in recovering the correct theory in the continuum limit. Halving the Brillouin zone is equivalent to doubling the "effective" lattice spacing, so imagine a situation where the field of a particular fermion species is spaced out by two links in every direction. We shall see how it is possible to reduce the 2^d Dirac spinors – each with $2^{d/2}$ components – to $2^{d/2}$ by distributing the degrees of freedom across the hybercube. This process is called "spin diagonalisation." For concreteness, we shall restrict ourselves to $d = 4$ (Euclidean) space-time dimensions.

Consider the local change of variables

$$\begin{aligned} \psi(x) &= \Gamma(x)\chi(x) \\ \overline{\psi}(x) &= \overline{\chi}(x)\Gamma^\dagger(x), \end{aligned} \tag{3.90}$$

where $\Gamma(x)$ is a unitary 4×4 matrix that satisfies

$$\Gamma^{\dagger}(x)\gamma_{\mu}\Gamma(x + a\hat{\mu}) = \eta_{\mu}(x). \tag{3.91}$$

This is accomplished by

$$\Gamma(x) = \gamma_1^{x_1}\gamma_2^{x_2}\gamma_3^{x_3}\gamma_4^{x_4}, \tag{3.92}$$

where the staggered phases are: $\eta_{\mu}(x) = (-1)^{\sum_{\nu<\mu} x_{\nu}}$. Explicitly

$$\begin{aligned}
\eta_1(x) &= 1 \\
\eta_2(x) &= (-1)^{x_1} \\
\eta_3(x) &= (-1)^{x_1+x_2} \\
\eta_4(x) &= (-1)^{x_1+x_2+x_3}.
\end{aligned}$$

Note that Eq. (3.90) is satisfied if χ is a Grassman variable with just one component (although it could have more). We can now write the Kogut–Susskind action as

$$S = \frac{1}{2}\sum_{x,\mu}\eta_{\mu}(x)\overline{\chi}(x)D_{\mu}\chi(x) + m\sum_{x}\overline{\chi}(x)\chi(x), \tag{3.93}$$

where D is the lattice covariant derivative given in Eq. (3.78). The Dirac structure has been completely absorbed into the staggered phases, η.

To see more clearly what has been done, consider the staggered action in terms of the hypercubes. We re-label the position vector

$$x_{\mu} = 2h_{\mu} + \rho_{\mu}, \tag{3.94}$$

where $h_{\mu} = 0, \cdots, \frac{L_{\mu}}{2} - 1$ and $\rho_{\mu} = 0, 1$. Then we define

$$\chi_{\rho}(h) = \chi(x). \tag{3.95}$$

giving us a relationship between the single component Grassman fields on a lattice with spacing a and 16 component Grassman fields on a lattice with spacing $2a$. From these components one then constructs the 4 flavored, 4 component Dirac fields by taking the appropriate linear combinations:

$$\psi_{\alpha}^{f}(h) = \mathcal{N}\sum_{\rho}(\Gamma_{\rho})_{\alpha f}\chi_{\rho}(h), \tag{3.96}$$

where the Γ_{ρ} are now

$$\Gamma_{\rho} = \gamma_1^{\rho_1}\gamma_2^{\rho_2}\gamma_3^{\rho_3}\gamma_4^{\rho_4} \tag{3.97}$$

and $\mathcal{N}$ is a normalisation. So spin-diagonalisation has reduced our 16 Dirac fields to four distributed around a hypercube and the continuum spin-flavors are reconstructed from linear combinations of the staggered. One major advantage of the staggered formulation over the Wilson is that it retains a U(1) x U(1) chiral symmetry. It is not the same symmetry as continuum QCD, but it protects the theory

from additive mass renormalisation and ensures that the pion is a genuine Goldstone boson.

We will work mostly in momentum space, so it will be necessary to construct the Fourier transform of the staggered action. In analogy to the "blocking" we performed in coordinate space, we write

$$k_\mu = \frac{2\pi n_\mu}{L_\mu} \quad | \quad n_\mu = 0, \ldots, L_\mu - 1 \tag{3.98}$$

as $k_\mu = p_\mu + \pi\alpha_\mu$, where

$$p_\mu = \frac{2\pi m_\mu}{L_\mu} \quad | \quad m_\mu = 0, \ldots, \frac{L_\mu}{2} - 1 \tag{3.99}$$

$$\alpha_\mu = 0, 1, \tag{3.100}$$

(α is like ρ above) and define $\int_k \equiv \frac{1}{V}\sum_k$. Then we have

$$\int_k = \int_p \sum_{\alpha_\mu=0}^{1} \tag{3.101}$$

$$\chi(x) = \int_k e^{ik\cdot x}\chi(k) = \int_p \sum_\alpha e^{i(p+\pi\alpha)\cdot x}\chi_\alpha(p)\,. \tag{3.102}$$

Using

$$\overline{\delta}_{\alpha\beta} = \Pi_\mu \delta_{\alpha_\mu\beta_\mu|\bmod 2} \tag{3.103}$$

$$\theta_\nu(\mu) = \begin{cases} 1 & \text{if } \nu < \mu \\ 0 & \text{otherwise} \end{cases}, \tag{3.104}$$

we can define

$$(\overline{\gamma}_\mu)_{\alpha\beta} = (-1)^{\alpha_\mu}\overline{\delta}_{\alpha+\theta(\mu),\beta} \tag{3.105}$$

where the $\overline{\gamma}_\mu$ satisfy

$$\{\overline{\gamma}_\mu, \overline{\gamma}_\nu\}_{\alpha\beta} = 2\delta_{\mu\nu}\overline{\delta}_{\alpha\beta} \tag{3.106}$$

$$\overline{\gamma}_\mu^\dagger = \overline{\gamma}_\mu^T = \overline{\gamma}_\mu^* = \overline{\gamma}_\mu, \tag{3.107}$$

forming a "staggered" Dirac algebra. Putting all this together, we can derive a momentum space expression for the KS action,

$$S = \int_p \sum_{\alpha\beta} \overline{\chi}_\alpha(p)\Big[i\sum_\mu (\overline{\gamma}_\mu)_{\alpha\beta}\sin(p_\mu) + m\overline{\delta}_{\alpha\beta}\Big]\chi_\beta(p)\,. \tag{3.108}$$

This will be very convenient as it casts the action into a familiar form.

3.10.1 Improved staggered fermion action

Due to the large computational requirements, full QCD lattice simulations typically use improved actions, which allow better physics to be extracted from simulations at moderate lattice spacings. The standard staggered-fermion action has leading errors of the order of a^2, unlike the Wilson formulation which has an order a artifact, which can be cancelled by the "clover" improvement. A third nearest neighbor coupling introduced by Naik cancelled order "a^2" violations of rotational symmetry in the free quark propagator [Lep96].

In the standard KS action, the derivative term is estimated by a simple nearest-neighbours finite difference. This can improved by the addition of a three-link, next-to-nearest-neighbours piece, called the Naik term [Nai89]. The coefficients are chosen to eliminate $\mathcal{O}(a^2)$ errors, improving the rotational symmetry of the action. This resulting Naik action is

$$\begin{aligned} S_N = \frac{1}{2}\sum_{x;\mu} \eta_\mu(x)\overline{\chi}(x)\Big[& c_1\big(U_\mu(x)\chi(x+\hat{\mu}) - U_\mu^\dagger(x-\hat{\mu})\chi(x-\hat{\mu})\big) \\ & + c_2\big(U_\mu(x)U_\mu(x+\hat{\mu})U_\mu(x+2\hat{\mu})\chi(x+3\hat{\mu}) \\ & - U_\mu^\dagger(x-\hat{\mu})U_\mu^\dagger(x-2\hat{\mu})U_\mu^\dagger(x-3\hat{\mu})\chi(x-3\hat{\mu})\big)\Big] + m\sum_x \overline{\chi}(x)\chi(x)\,. \end{aligned} \tag{3.109}$$

At tree-level, this action is $\mathcal{O}(a^2)$ accurate when $c_1 = \frac{9}{8}$ and $c_2 = -\frac{1}{24}$. We can see that the standard Kogut-Susskind action (recall Eq. (3.93)) is obtained with coefficients $c_1 = 1$ and $c_2 = 0$. Thus we find that the conventional "one-link" quark action has $c_1 = 1$ and $c_2 = 0$ and the "Naik" action has $c_1 = \frac{9}{8}$ and $c_2 = -\frac{1}{24}$.

Such an action was tested in [B+98]. Flavor symmetry breaking in this action is still large, but this can be reduced by "fattening" with three, five and seven link terms [KO99, LS99]. The result of this fattening is to reduce the coupling of the quarks to hard gluons with momentum of the order of the cutoff, as this type of gluon exchange results in the flavor-changing interactions that give rise to flavor symmetry breaking. These terms can, however, introduce errors into the low-momentum behaviour of the quark propagator, but these are compensated for by the addition of a planar three-link Lepage term [Lep99].

The quark action that will be of particular interest to us is the AsqTad quark action. It is a type of fat-link staggered action using three-link, five-link and seven-link terms to cancel $\mathcal{O}(a^2)$ errors and improve flavor symmetry. There are a number of ingredients to this improvement. Complete details of the formulation of the AsqTad action can be found in [KO99]. All coefficients are tadpole improved, producing the rather sophisticated "AsqTad" (a^2, tadpole improved) action. In this thesis, the essential aspect of the AsqTad is its tree-level form.

At tree-level (*i.e.*, no interations, links set to the identity), the staples in this action make no contribution, and the action reduces to the Naik action. We can perform the same analysis as discussed in the previous section to derive the momentum

space action which has the tree-level form

$$S = \int_p \sum_{\alpha\beta} \overline{\chi}_\alpha(p) \Big[i \sum_\mu \left(\overline{\gamma}_\mu\right)_{\alpha\beta} \sin(p_\mu) \Big(\frac{9}{8} \sin(p_\mu) - \frac{1}{24} \sin(3p_\mu) \Big) + m\overline{\delta}_{\alpha\beta} \Big] \chi_\beta(p) \,, \tag{3.110}$$

from which the kinematic momentum can be obtained. This is described in the next Chapter.

4

Unquenched gluon propagator

The study of the gluon propagator-the most fundamental quantity of QCD and its infrared behavior provides a powerful tool for understanding QCD and the physics of confinement in non-abelian gauge theories. Perturbatively the gluon is expected to behave like a massless particle. But in the real world such behavior is not possible at large distances due to the color confinement of QCD. There were many studies dealing with the infrared behavior of QCD towards the end of the seventies and the method (truncated Scwinger-Dyson Equations) used in all these approaches is more or less the same [Had]. Lattice QCD- the nonperturbative calculational method-allows a direct probe into the behavior of the gluon propagator in the infrared.

The gluon propagator, the most basic quantity of QCD, has been subject to much calculation and speculation since the origin of the theory. In particular there has long been interest in the infrared behavior of the Landau gauge gluon propagator as a probe into the mechanism of confinement [Man99].

In this thesis, we present the first results of gluon propagator calculation using $2+1$ flavors of dynamical quarks–two light and one strange, and quenched simulation for comparison. One way of studying the effects of dynamical sea-quarks is to calculate in quenched and full QCD, using same fermion action in both cases, for the same set of lattice with same lattice spacing. This comparison study clearly reveals the effect of dynamical sea-quarks on the gluon propagator. We study the gluon propagator in Landau gauge using configurations generated by the MILC collaboration [BO01] available from the Gauge Connection[1]. These use "AsqTad" improved staggered quarks, giving us access to relatively light sea quarks. We analysed the gluon propagator in Landau gauge with an improved action on a $20^3 \times 64$ lattice in quenched unquenched set of lattices. We find that the addition of dynamical quarks preserves the qualitative features of the gluon dressing function $q^2D(q^2)$ in the quenched case – enhancement for intermediate infrared momenta followed by suppression in the deep infrared – but produces a clearly visible effect. A significant suppression of the infrared enhancement with respect to the quenched case is observed. It is interesting to compare these results to those of a recent Dyson-Schwinger equation study [ADFM04].

The highlight of our work is the comparitive study of gluon propagator including and neglecting quark masses in the calculation. Since the gluon propagator is gauge dependent, its properties can be studied only after fixing the gauge.

Some authors have argued it to be infrared finite [Gri78, Sti86, Zwa91] while others favored infrared singular [Man79, BP95]. There is a long history of its study on the lattice, in quenched QCD [MO87, BPS94, MMS95, Ma00, B$^+$99, B$^+$00a, NF00, BBL$^+$01, LRG02, LSWP99, LSWP98, BHLW02, BBLW00] and in quenched $SU(2)$ [Cuc98, CMT03]. The restriction to quenched lattice gauge theory calcula-

[1] http://www.qcd-dmz.nersc.gov

tions has been due to the lack of sufficient computational resources. The quenched theory differs from full QCD only in the relative weighting of the background gauge configurations (due to the fermion determinant), but the evaluation of the Green's functions is otherwise the same. In the quenched approximation the fermion determinant is replaced by unity and this corresponds to the complete suppression of all quark loops. The dynamics of the gluon field depends upon the determinant of the Dirac operator. The removal of quark loops is equivalent to the limit where all sea-quark masses are taken to infinity. In this chapter, we report the first results for the gluon propagator from an unquenched lattice computation.

4.1 The gluon propagator in the literature

The Greens functions of the fundamental fields such as gluon, ghost and quark propagators are gauge dependent. The gluon propagator is the gluon two point correlation function. The gluon propagator is the Fourier transform of the time-ordered matrix element of two gluon fields $A^a_\mu(x)$, where a runs from 1 to N^2-1 for $SU(N)$ group [Man99]

$$D^{ab}_{\mu\nu}(q) = -i \int d^4x e^{iq\cdot x} \langle 0|T(A^a_\mu(x)A^b_\nu(0))|0\rangle \,. \tag{4.1}$$

In covariant gauges, the propagator has the form

$$D^{ab}_{\mu\nu}(q) = -i\delta^{ab}\left[(\delta_{\mu\nu} - \frac{q_\mu q_\nu}{q^2})D(q^2) + \alpha\frac{q_\mu q_\nu}{q^2}D^L(q^2)\right], \tag{4.2}$$

where the parameter α specifies the gauge. In Landau gauge $\alpha = 0$. The Euclidean two-point Greens function in momentum space in the Landau gauge is given by

$$D^{ab}_{\mu\nu}(q) = \delta^{ab}(\delta_{\mu\nu} - \frac{q_\mu q_\nu}{q^2})D(q^2) \,. \tag{4.3}$$

To zeroth order in perturbation theory,

$$D_0(q^2) = -\frac{1}{q^2} \,.$$

$D(q^2)$ may be obtained from $D^{ab}_{\mu\nu}$ via

$$\begin{aligned} D(q^2) &= \frac{1}{8} \quad \frac{1}{3}\sum_{\mu\, a} D^{aa}_{\mu\mu}(q) \text{ for } q \neq 0 \,, \\ D(0) &= \frac{1}{8} \quad \frac{1}{4}\sum_{\mu\, a} D^{aa}_{\mu\mu}(q). \end{aligned} \tag{4.4}$$

The factor $\frac{1}{4}$ for zero momentum is due to an additional degree of freedom. In order to measure the propagtor on lattice, it is necessary to fix the gauge.

4.2 The gluon propagator on the lattice

The detailed study of the gluon propagator on the lattice can be found in [LSWP98, BHLW02, BBLW00, WBB+]. We have seen from the previous chapter that the gauge links $U_\mu(x)$ are expressed in terms of the continuum gluon fields as Eq. (3.24). From this, the dimensionless lattice gluon field $A^L_\mu(x)$ may be obtained from

$$A^L_\mu(x+\hat{\mu}/2) = \frac{1}{2ig_0}\big(U_\mu(x) - U^\dagger_\mu(x)\big) - \frac{1}{6ig_0}\mathrm{tr}\big(U_\mu(x) - U^\dagger_\mu(x)\big)\,, \tag{4.5}$$

which is accurate to $\mathcal{O}(a^2)$.

We calculate the gluon propagator in coordinate space

$$D^{ab}_{\mu\nu}(x,y) \equiv \langle\, A^a_\mu(x)\, A^b_\nu(y)\,\rangle\,, \tag{4.6}$$

using Eq. (4.5). To improve statistics, we use translational invariance and calculate

$$D^{ab}_{\mu\nu}(y) = \frac{1}{V}\Big\langle \sum_x A^a_\mu(x) A^b_\nu(x+y)\Big\rangle\,, \tag{4.7}$$

where here the angle brackets imply an ensemble average.

The scalar part of the gluon propagator is given by,

$$D(y) = \frac{1}{N_d - 1}\sum_\mu \frac{1}{N_c^2 - 1}\sum_a D^{aa}_{\mu\mu}(y), \tag{4.8}$$

which is then Fourier transformed into momentum space using

$$D(q) = \sum_y e^{i\hat{q}\cdot y} D(y), \tag{4.9}$$

On the lattice, due to periodic boundary conditions, the discrete momenta $\hat{q}$ available are

$$\hat{q}_\mu = \frac{2\pi n_\mu}{aL_\mu}, \qquad n_\mu \in \Big(-\frac{L_\mu}{2}, \frac{L_\mu}{2}\Big]\,, \tag{4.10}$$

where L_μ is the lattice length over direction μ.

The range of $\hat{q}$ is determined by the fact that our lattices have an even number of points in each direction and that we use periodic boundary conditions. Assuming that the deviations from the continuum are negligible, the scalar function $D(q^2)$ can be extracted from $D^{ab}_{\mu\nu}(q)$ using

$$D(q^2) = \frac{1}{3}\sum_\mu \frac{1}{8}\sum_a D^{aa}_{\mu\mu}(q). \tag{4.11}$$

This expression is also valid on a finite volume, provided q is not too close to zero [LSWP99]. The finite volume induces an effective mass $m \sim \frac{1}{L}$ which becomes significant for q sufficiently close to zero.

4.2.1 Tree-level correction

For $a \to 0$, the lattice propagator is related to the continuum propagator by (recall Eq. (3.57))

$$a^2 D(q^2) = a^2 D^{\text{cont}}(q^2) + \mathcal{O}(a^4)\,.$$

At tree level

$$D(q^2) = \frac{1}{q^2}\,, \tag{4.12}$$

The improved gauge action Eq. (3.77) together with the gluon field defined in Eq. (4.5) has the $\mathcal{O}(a^2)$ improved tree-level behavior

$$D^{-1}(p_\mu) = \frac{4}{a^2}\sum_\mu \left\{ \sin^2\left(\frac{p_\mu a}{2}\right) + \frac{1}{3}\sin^4\left(\frac{p_\mu a}{2}\right)\right\}, \tag{4.13}$$

where

$$p_\mu = \frac{2\pi n_\mu}{a L_\mu}, \qquad n_\mu \in \left(-\frac{L_\mu}{2}, \frac{L_\mu}{2}\right], \tag{4.14}$$

a is the lattice spacing and L_μ is the length of the lattice in the μ direction. As explained in [BBL+01] this suggests a "kinematic" choice of momentum,

$$q_\mu(p_\mu) \equiv \frac{2}{a}\sqrt{\sin^2\left(\frac{p_\mu a}{2}\right) + \frac{1}{3}\sin^4\left(\frac{p_\mu a}{2}\right)}, \tag{4.15}$$

ensuring that the lattice gluon propagator has the correct tree-level behavior.

Since QCD is asymptotically free, we expect that $q^2 D(q^2) \to 1$ up to logarithmic corrections as $q^2 \to \infty$. Hence, Fig. 4.1 and Fig. 4.3 present $q^2 D(q^2)$, which is expected to approach a constant up to logarithmic corrections as $q^2 \to \infty$. All figures have a cylinder cut imposed upon them, *i.e.*, all momenta must lie within a cylinder of radius two spatial momentum units centered about the lattice diagonal.

4.2.2 Renormalization

In the study of the gluon propagator [Wil98], we can see that the bare lattice gluon propagator $D(qa)$ is related to renormalised continuum propagator $D_R(q;\mu)$ by

$$D(qa) = Z_3(\mu, a) D_R(q;\mu), \tag{4.16}$$

for momenta, q, sufficiently small compared to the cutoff, a^{-1}. μ is the renormalization point. $D_R(q;\mu)$ only becomes truly independent of a when the cutoff is removed: in the limit that $a \to 0$. In a renormalizable theory such as QCD, renormalized quantities become independent of the regularization parameter in the limit where it is removed. Z_3 is then defined by some renormalization prescription.

We choose the momentum space subtraction (MOM) where the renormalisation constant $Z_3(\mu, a)$ is determined by imposing a renormalisation condition at some chosen renormalisation scale μ, e.g.,

$$D_R(q)|_{q^2=\mu^2} = \frac{1}{\mu^2}, \tag{4.17}$$

i.e., it takes the tree-level value at the renormalization point. We have chosen $\mu = 4$ GeV here.

The renormalized gluon propagator can be computed both non-perturbatively on the lattice and perturbatively in the continuum for choices of the renormalization point in the ultraviolet [LSWP99].

4.3 Details of calculation

The gluon propagator is gauge dependent, so the gauge configurations must be gauge fixed for its calculation. We work in the Landau gauge for ease of comparison with other studies. It is also the simplest covariant gauge to implement on the lattice. Landau gauge is a smooth gauge that preserves the Lorentz invariance of the theory, so it is a popular choice. It will be interesting to repeat this calculation for the Gribov-copy free Laplacian gauge, but that will be left for a future study. Similar calculations have been done in Laplacian gauge [ADFF02b, BHLW02].

We compute the lattice QCD gluon propagator in Landau gauge for 192 configurations quenched with $\beta = 8.0$ and for the unquenched set with four different light sea-quark masses (see Table 4.1 for the number of configurations and β values used) for the $20^3 \times 64$ lattice. The parameters are summarized in Table 4.1. The lattice spacing is approximately 0.125 fm [D$^+$04]. The configurations generated by the improved action Eq (3.77) are gauge fixed by maximising the improved gauge fixing functional $\mathcal{F}^G_{\rm Imp}$ discussed in the previous Chapter. The algorithm using conjugate gradient Fourier acceleration is implimented in parallel, updating all links simultaneously, and is iterated until the lattice Landau gauge condition is satisfied. The gluon propagator is plotted in units of GeV. Plotting the propagator multiplied by q^2 shows more detail of the infrared behavior.

The MILC configurations were generated with the $\mathcal{O}(a^2)$ one-loop Symanzik improved [Sym83] Lüscher–Weisz gauge action [LW85]. The dynamical configurations use the "AsqTad" quark action, an $\mathcal{O}(a^2)$ Symanzik improved staggered fermion action. β and the bare sea-quark masses are matched such that the lattice spacing is held constant. The lattices we consider all have the same dimensions. This means that all systematics are fixed; the only variable is the addition of the quark loops. The parameters are summarized in Table 4.1. The lattice spacing is approximately 0.125 fm [D$^+$04].

Table 4.1: Lattice parameters used in this study. The dynamical configurations each have two degenerate light quarks (up/down) and a heavier quark (strange). In physical units the bare masses range from $\sim$ 16 MeV to $\sim$ 79 MeV. The lattice spacing is $a \simeq 0.125$ fm.

	Dimensions	β	Bare Quark Mass	# Configurations
1	$20^3 \times 64$	8.00	quenched	192
2	$20^3 \times 64$	6.76	0.01, 0.05	193
3	$20^3 \times 64$	6.79	0.02, 0.05	249
4	$20^3 \times 64$	6.81	0.03, 0.05	212
5	$20^3 \times 64$	6.83	0.04, 0.05	337

4.4 Effects of dynamical quarks to gluon propagator

Lattice studies strongly suggest that the quenched gluon propagator is infrared finite [BBL+01]. As is customary, we will begin by considering the (necessarily finite) gluon dressing function, $q^2 D(q^2)$. In Fig. 4.1 we compare the well-known quenched dressing function with that for 2+1 flavor QCD. For the moment we only consider the lightest of our dynamical quarks as we expect that they will show the greatest difference from the quenched case.

The addition of dynamical quarks to the gauge fields produces a significant visible effect in the dressing function, in the region of infrared hump. We can clearly see the difference between quenched and unquenched gluon dressing function in this region. It is also very clear from the Fig. 4.1 that unquenching results in a reduction of around 30% at 1 GeV [P+06a].

We can see that the qualitative features of the propagator-enhancement of the intermediate infrared momenta followed by supression in the deep infrared are unchanged. Indeed there is a clear difference between quenched and dynamical quark behavior in the infrared region. The addition of quark loops to the gluon propagator softens the infrared enhancement without altering its basic features. The screening of dynamical sea quarks brings the $2 + 1$ flavor results significantly closer to the tree-level form, $q^2 D(q^2) = 1$. In Fig. 4.2, our results for gluon dressing function in quenched and full QCD are compared to the results obtained for the same from DSE approach. The screening effect from the quark loop is clearly visible in DSE results also. For momenta p larger than $p = 0.5$ GeV, the gluonic self interaction becomes less important in this region and the gluon dressing increases [FA05].

In Fig. 4.3, we show the gluon dressing function for the lightest and for the heaviest u and d quark masses in our set. These correspond to bare light-quark masses of $\simeq$ 16 MeV and $\simeq$ 63 MeV respectively; a factor of four difference. The

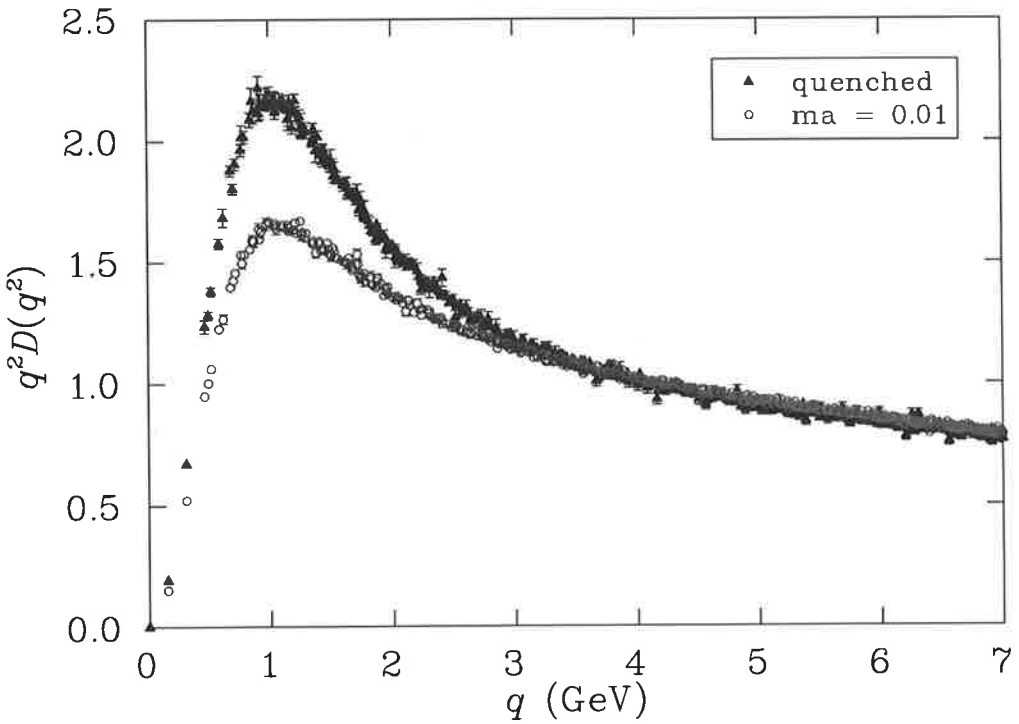

Fig. 4.1: Gluon dressing function in Landau gauge. Full triangles correspond to the quenched calculation, while open circles correspond to 2+1 flavor QCD. As the lattice spacing and volume are the same, the difference between the two results is entirely due to the presence of quark loops. The renormalization point is at $\mu = 4$ GeV. Data has been cylinder cut [LSWP99].

bare strange-quark mass is the same in both cases ($\simeq$ 79 MeV). The mass dependence of the gluon dressing function is only just detectable. We expect that increasing the sea-quark masses further will interpolate between the curves in Fig. 4.1. We see that the gluon propagator changes in the expected way. As the sea-quark mass increases, the curve moves towards the quenched result. However, for the range of bare quark masses studied here the change is relatively small. This transition would be better studied with heavier sea quarks.

Another view of the mass dependence of the gluon propagator is provided in Fig. 4.4. We choose one data point from the infrared hump ($q \simeq 1.12$ GeV) and plot it for each choice of bare light-quark mass. Although the variation in the propagator at this momentum is only 4.5% over the range of quark masses investigated here, the light sea-quark mass dependence is clearly resolved.

In Fig. 4.5, we present results for the gluon propagator, $D(q^2)$. The largest effects of unquenching are observed in the deep infrared. The shape of the curves suggest that the previous results indicating the infrared-finite nature of the quenched gluon

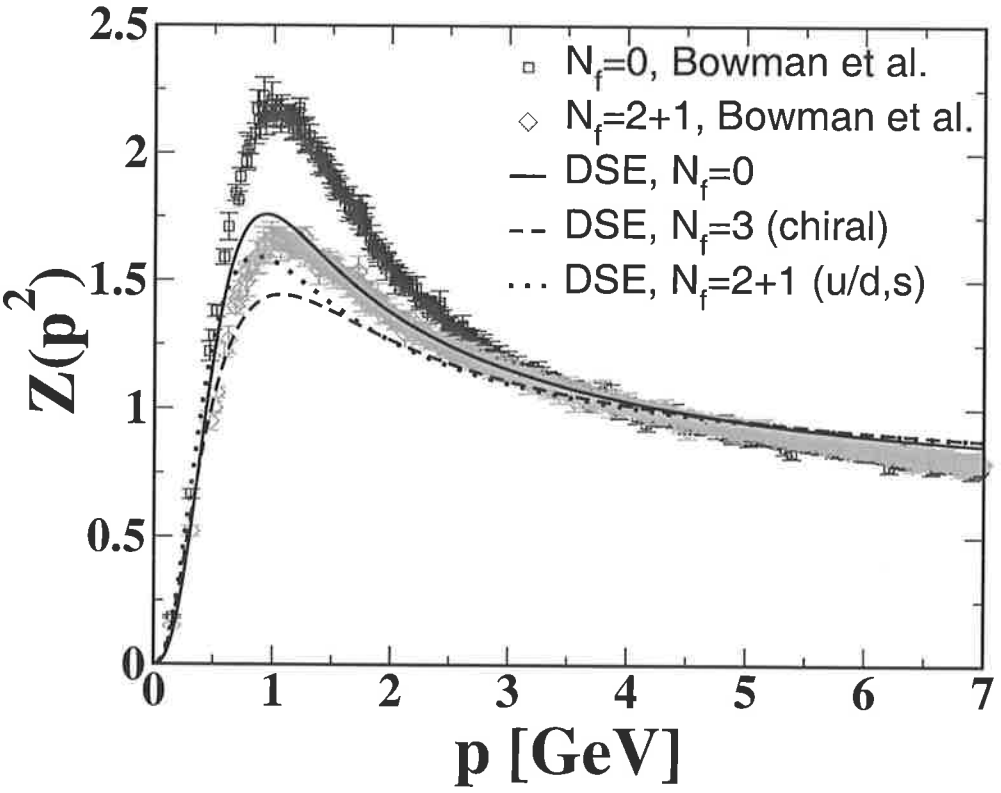

Fig. 4.2: Comparison of our results for the gluon dressing function in quenched and unquenched QCD to the corresponding result from the DSE approach [FA05].

propagator [BBL+01] are unchanged upon unquenching. The results suggest that the gluon propagator of QCD is infrared finite. It will be interesting to examine the behavior of $D(0)$ as a function of volume to elucidate this aspect of the gluon propagator further. Finally, in Fig. 4.6, the light sea-quark mass dependence of the renormalized gluon propagator is illustrated for a momentum point in the infrared region. To avoid finite volume artifacts, the second smallest nontrivial momentum is considered. Whereas the mass dependence of the propagator for the masses studied here is at the 4.5% level for $q \simeq 1.12$ GeV, the variance is larger in the infrared region at 6% for $q \simeq 0.31$ GeV.

4.5 Results

The addition of quark loops has a clear, quantitative effect on the gluon propagator. While its basic structure is qualitatively similar, there is significant screening of the propagator in the infrared. As anticipated, the effect is to suppress the non-abelian enhancement of the gluon propagator in the nonperturbative infrared-momentum region. This is relevant to analytic studies of the gluon propagator and confinement [ADFM04]. Despite the clear difference between the quenched and dynamical

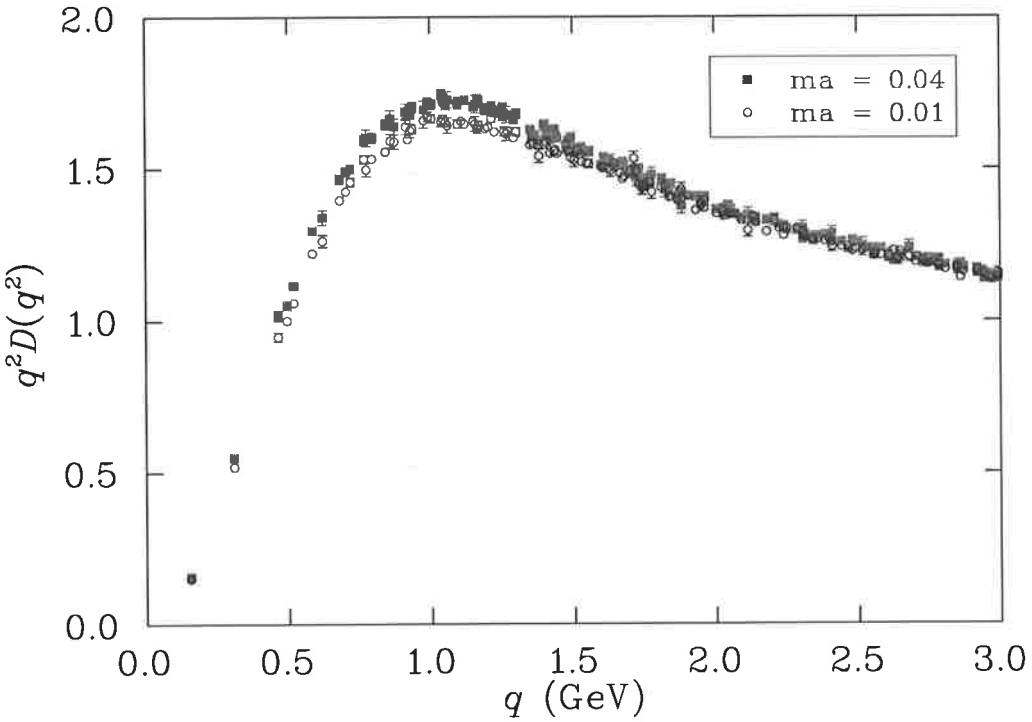

Fig. 4.3: The sea-quark mass dependence of the Landau gauge gluon propagator dressing function renormalized at $\mu = 4$ GeV. Filled squares correspond to u and d bare masses $\simeq 63$ MeV and bare s-quark mass $\simeq 79$ MeV. Open circles correspond to the same strange-quark mass, but with bare u and d masses $\simeq 16$ MeV. Data has been cylinder cut [LSWP99]. Increasing the sea-quark masses alters the results in the expected way, *i.e.* towards the quenched data.

results, we see little dependence on the dynamical quark mass for the range of available light sea-quark masses. The dependence that is observed is consistent with expectations.

We have also done calculations of gluon propagator on finer lattice which is discussed in Chapter 6. Calculations on finer lattices are currently underway to provide more information on the ultraviolet nature of the propagator and provide a test for finite lattice spacing artifacts.

We would like to extend the study to a wider range of dynamical masses to study both the chiral limit and the transition to the quenched limit. Finally, a study of the volume dependence of the propagator will provide valuable insights into the nature of the propagator at $q^2 = 0$.

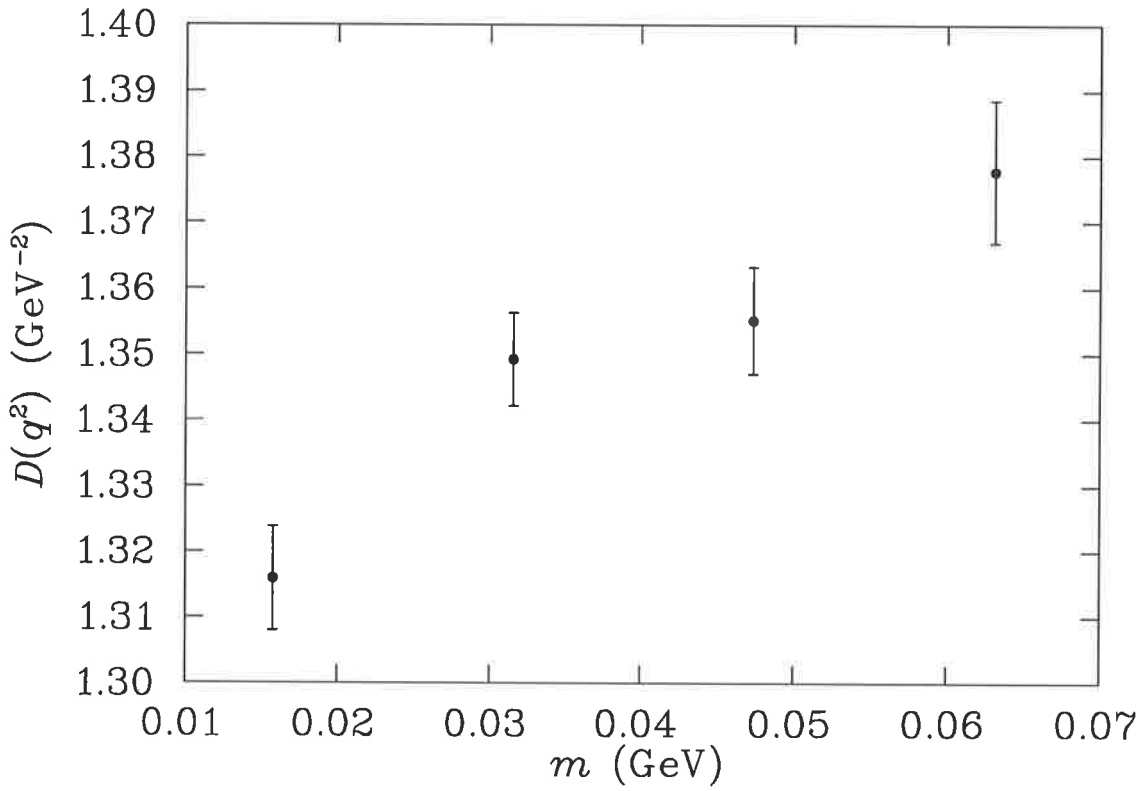

Fig. 4.4: The renormalized propagator at one momentum point in the infrared hump of the gluon dressing function ($q \simeq 1.12$ GeV) is shown here as a function of the bare light-quark mass.

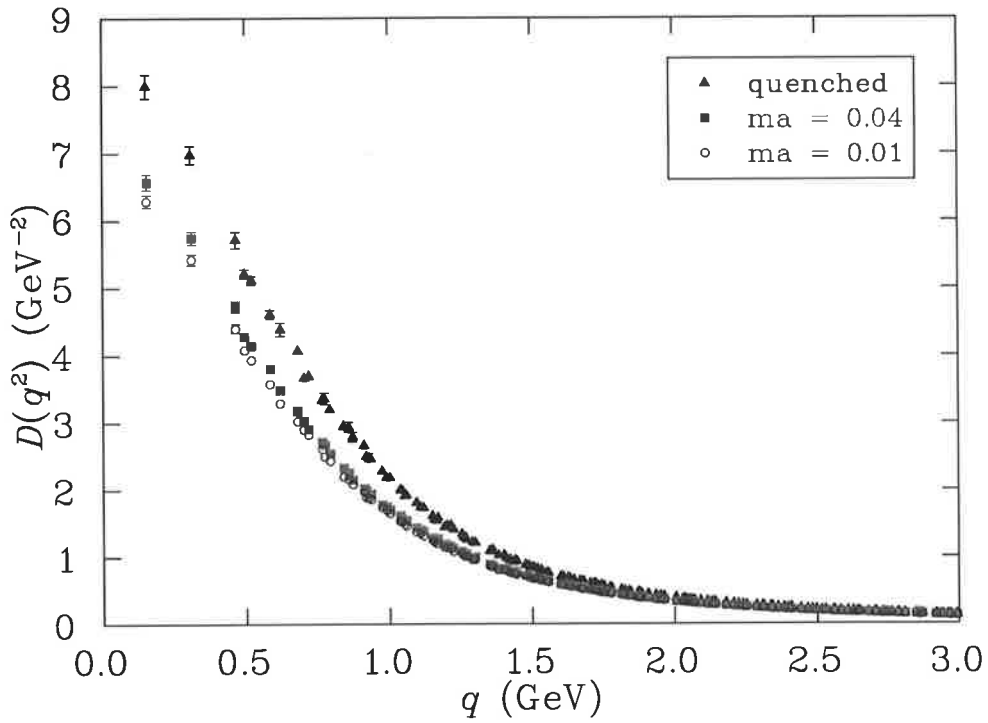

Fig. 4.5: The sea-quark mass dependence of the Landau gauge gluon propagator renormalized at $\mu = 4$ GeV. Filled triangles illustrate the quenched propagator while filled squares correspond to bare up/down masses $\simeq 63$ and bare strange-quark mass $\simeq 79$ MeV. Open circles correspond to lighter bare up/down masses $\simeq 16$ MeV but with the same strange quark mass. Data has been cylinder cut [LSWP99].

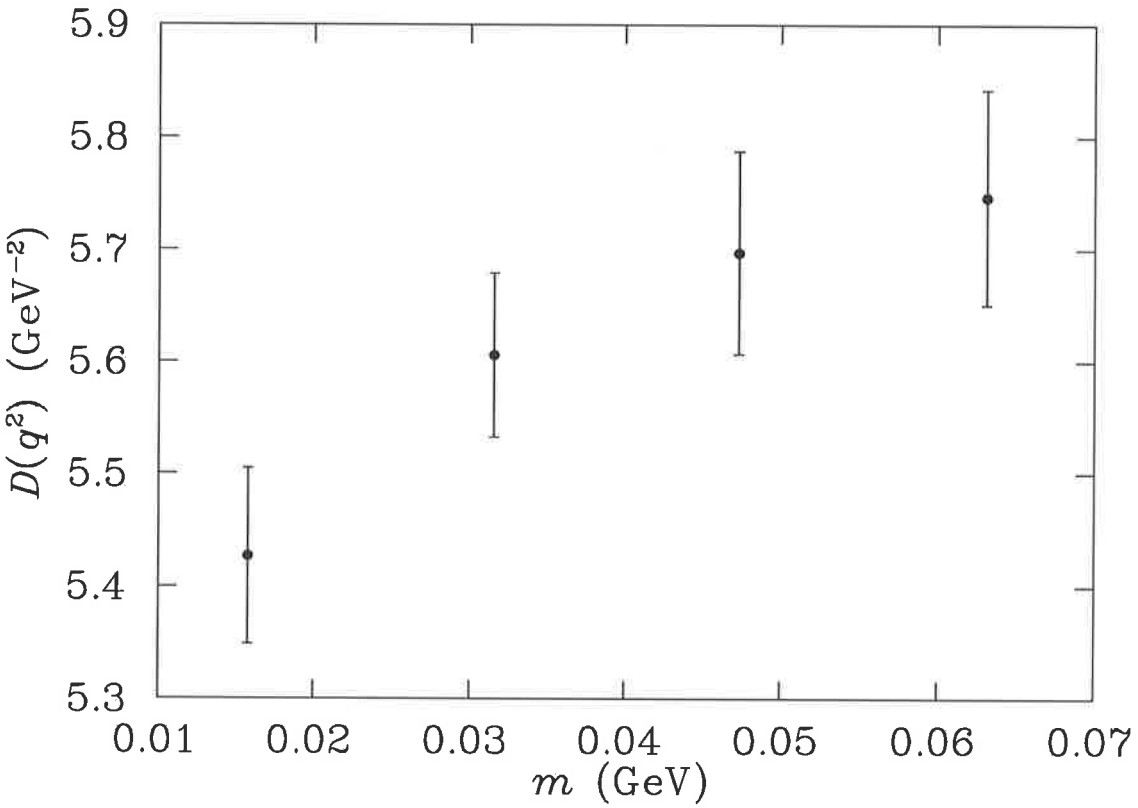

Fig. 4.6: The light sea-quark mass dependence of the renormalized gluon propagator at a momentum point in the infrared region ($q \simeq 0.31$ GeV).

5

Unquenched quark propagator

The quark propagator is the basic entity of QCD, though it is not directly observable in an experiment. But it has been the focus of many studies to gain better understanding of chiral symmetry breaking and the mechanisms by which it occurs [BMSY90]. In the low momentum region it exhibits dynamical chiral symmetry breaking and at high momentum it can be used to extract the running mass [BHW02]. It is an input in DSE based model calculations. The infrared structure of quark propagator gives insight to the dynamical mass generation. So quark propagator is interesting for studying the phenomenon of dynamical chiral symmetry breaking.

In this Chapter, we discuss unquenched calculation of the quark propagator in Landau gauge with $2+1$ flavors of dynamical quarks and report the first results for the quark propagator including dynamical quark effects. To verify the effect of dynamical sea quarks on the quark propagator, we have done a series of simulations of quenched QCD and $2+1$ flavor QCD with a range of quark masses. We study the quark propagator in quenched and full QCD using an improved staggered fermion action "AsqTad" which has $\mathcal{O}(a^4)$, $\mathcal{O}(a^2g^2)$ errors.

5.1 The quark propagator in literature

A "propagator" is the amplitude for a quark to move between space-time points. The quark propagator $S(x, y : A)$ for a quark mass m in the presence of a gluon field A_μ plays a central role in many investigations of lattice quantum chromodynamics. The quark propagator is defined by

$$S_{\alpha\beta} = -i\langle 0|T(\psi_\alpha(x)\bar{\psi}_\beta(y))|0\rangle\,, \tag{5.1}$$

where α and β are the spinor indices. $S(x, y : A)$ is a matrix and a given element of this matrix gives the amplitude of propagation of a quark with some spin, color and space-time point to another space-time point, spin and color.

At tree level ($A_\mu = 0$), the quark propagator is identified with the fermionic Greens function in Euclidean space,

$$(\not{\partial} + m)\Delta_f(x, y) = \delta^4(x - y)\,, \tag{5.2}$$

where m is the bare quark mass. In momentum space this equation is solved by,

$$\tilde{\Delta}_f(p) = \frac{1}{i\not{p} + m}. \tag{5.3}$$

$\tilde{\Delta}_f(p) \equiv S_{F0}(p)$ denotes the tree-level propagator in momentum space. Thus in the presence of gauge field interactions, we can define $S_F^{-1}(p)$ to be the Fourier transform

of the interacting fermionic Green's function,

$$(\not{D} + m)\Delta_f(x, y) = \delta^4(x - y). \tag{5.4}$$

In momentum space, the renormalised inverse quark propagator is

$$\begin{aligned} S_F^{-1}(p) &= S_{F0}^{-1}(p) - \Sigma(p) \\ &\equiv Z^{-1}(p^2)[i\ \not{p} + M(p^2)] \equiv i\ \not{p} A(p^2) + B(p^2), \end{aligned} \tag{5.5}$$

where

$$S_{F0}^{-1}(p) = i\ \not{p} + m \tag{5.6}$$

5.2 The quark propagator on the Lattice

The systematic study of the quark propagator on the lattice has also provided fruitful interaction with other approaches to hadron physics, such as instanton phenomenology [Dia03], chiral quark models [RAB03] and Dyson-Schwinger equation studies [BPRT03, ADFM04]. The lattice is a first principles approach and has provided valuable constraints for model builders. In turn, such alternative methods can provide feedback on regions that are difficult to access directly on the lattice, such as the deep infrared and chiral limits.

The quark propagator has previously been studied using Clover [SW01, SLW01], staggered [BHW02, BHLW03] and Overlap [BBL$^+$02, ZBL$^+$04] actions. For a review, see [BHL$^+$05]. All these actions have different systematic errors and the combination of these studies has given us an excellent handle on the possible lattice artifacts. In every case, however, they have been performed in the quenched approximation and have been restricted to modest physical volumes. The quark propagator is gauge dependent and we choose the ever popular Landau gauge.

We have seen from Chapter 3 that the n-point Green's functions $G_n(x_1 \cdots x_1)$ are obtained from the generating functional (recall Eq. (3.17)).

The quark propagator identified as two-point fermionic Green's function is given by

$$\begin{aligned} S(x, y) &= -1 \frac{\delta}{\delta\overline{\eta}(y)} \frac{\delta}{\delta\eta(x)} Z[\eta, \overline{\eta}]\Big|_{\eta=0,\overline{\eta}=0} \\ &= \frac{1}{Z[0]} \int \mathcal{D}\overline{\psi}\mathcal{D}\psi\mathcal{D}A_\mu \psi(y)\overline{\psi}(x) e^{-S_{\rm QCD}} \\ &= \langle \psi(y)\overline{\psi}(x) \rangle. \end{aligned} \tag{5.7}$$

Changing the variables

$$\overline{\psi} \to \overline{\psi}' = \overline{\psi} - \overline{\eta} K^{-1} \tag{5.8}$$

$$\psi \to \psi' = \psi - K^{-1}\eta\,, \tag{5.9}$$

and rewriting the fermionic part of the generating functional as

$$Z[\overline{\eta},\eta] = \frac{1}{Z[0]}\int \mathcal{D}\overline{\psi}'\mathcal{D}\psi' e^{\sum_x -\overline{\psi}' K\psi'} e^{\sum_x \overline{\eta}K^{-1}\eta}. \tag{5.10}$$

As in the continuum, we want the measure $\mathcal{D}U$ (see Chapter 3) to be gauge inavriant. As per the Grassman integration rules the measure is invariant under the above transformation, which enables us to write

$$Z[\overline{\eta},\eta] = \frac{1}{Z[0]}\det K e^{\sum_x \overline{\eta}K^{-1}\eta}. \tag{5.11}$$

The fermion matrix K (introduced in Chapter3) is a function of the gauge links in an interacting theory. Considering the full theory, we can write

$$Z[\overline{\eta},\eta,J_\mu] = \frac{1}{Z[0]}\int \mathcal{D}U \det K[U] e^{-S_G[U]-\sum_x \overline{\eta}K^{-1}\eta + J_\mu U_\mu}. \tag{5.12}$$

and

$$\left.\frac{\delta^2 Z}{\delta\eta(x)\delta\overline{\eta}(y)}\right|_{\overline{\eta}=0,\eta=0} = \frac{1}{Z[0]}\int \mathcal{D}U K[U]^{-1}\det K[U] e^{-S_G[U]}. \tag{5.13}$$

Now it is clear that the calculation of the quark propagator amounts to the inversion of the fermion matrix.

$$\langle\psi(y)\overline{\psi}(x)\rangle = K(x,y,U)^{-1}. \tag{5.14}$$

Equation (5.14) says that the quark propagator is calculated by inverting the fermion matrix. Lattice QCD allows a direct probe of the nonperturbative quark propagator.

To carry out simulations, we must select

- Lattice spacing (a) via coupling parameter $\beta \propto \frac{1}{g^2}$
- Grid size $(N_s^3 \times N_t)$
- Quark masses (m_u, m_d, m_s)
- The number of configurations averaged over.

To eliminate systematic errors, we must

- Take the continuum limit $a \to 0$

The lattice calculation of quark propagator requires the following steps [BHL+05];

- A statistical ensemble of lattice gauge configurations is generated by some method, quenched simulations using the pseudo heat-bath algorithm. Unquenched $(2+1$ flavor) simulations using the standard hybrid-molecular dynamics "R algorithm", with one pesudofermion field for runs with degenerate quarks and two pesudofermion fields for runs with different up and down and strange quark masses [GLT+87].
- Each configuration is gauge fixed: Landau gauge is selected.
- From the ensemble of configurations, on each configuration, the quark propagator is calculated by

$$\sum_y S(x,y)K(y,z) = \delta(x,z), \tag{5.15}$$

where K is the fermion matrix for the AsqTad quark action. The inversion is computed by a suitable method, in this case a multi-mass conjugate gradient algorithm [Jeg96].

- The propagator is Fourier transformed to momentum space.
- The result is averaged over all gauge configurations in the ensemble.

In the continuum, Lorentz invariance allows us to decompose the full propagator into Dirac vector and scalar pieces, so in momentum space

$$S^{-1}(p^2) = iA(p^2)\gamma \cdot p + B(p^2)\,, \tag{5.16}$$

or, alternatively,

$$S^{-1}(p^2) = Z^{-1}(p^2)[i\gamma \cdot p + M(p^2)]\,, \tag{5.17}$$

where $M(p^2)$ and $Z(p^2)$ are the nonperturbative mass and wave function renormalization functions, respectively. This is the bare propagator which, once regularized, is related to the renormalised propagator through the renormalisation constant

$$S(a;p^2) = Z_2(a;\mu)S^{\rm ren}(\mu;p^2), \tag{5.18}$$

where a is some regularisation parameter, *e.g.*, lattice spacing. Asymptotic freedom implies that, as $p^2 \to \infty$, $S(p^2)$ reduces to the free propagator

$$S^{-1}(p^2) \to i\gamma \cdot p + m, \tag{5.19}$$

up to logarithmic corrections. The mass function M is renormalization point independent and for Z we choose throughout this work the renormalization point as 3 GeV, where m is the bare quark mass.

We use an improved Kogut-Susskind quark action, "$a^2_{\rm tad}$" or "AsqTad" action which removes lattice artifacts up to order of a^2g^2. From Eq. (3.108) we write the tadpole improved, tree-level form of the KS quark propagator as

$$S^{-1}_{\alpha\beta}(p;m) = u_0 i \sum_\mu (\overline{\gamma}_\mu)_{\alpha\beta}\,, \sin(p_\mu) + m\overline{\delta}_{\alpha\beta} \tag{5.20}$$

where p_μ is the discrete lattice momentum given by

$$p_\mu = \frac{2\pi n_\mu}{aL_\mu} \qquad n_\mu \in \left(\frac{-L_\mu}{4}, \frac{L_\mu}{4}\right]. \tag{5.21}$$

and u_0- the mean field (tadpole) improvement parameter defined by Eq. (3.66). Lattice quark propagator got the correct continuum form,

$$\begin{aligned} S^{-1}_{\alpha\beta}(p) &= i\sum_\mu (\overline{\gamma}_\mu)_{\alpha\beta} \sin(p_\mu)A(p) + B(p)\overline{\delta}_{\alpha\beta} \\ &= Z^{-1}(p)\Big[i\sum_\mu (\overline{\gamma}_\mu)_{\alpha\beta} \sin(p_\mu) + M(p)\overline{\delta}_{\alpha\beta}\Big)\,. \end{aligned} \tag{5.22}$$

We define a new momentum variable for KS action,

$$q_\mu \equiv \sin(p_\mu). \tag{5.23}$$

We can then decompose the inverse propagator

$$Z^{-1}(q) = \frac{1}{16N_c iq^2}\mathrm{Tr}\{\overline{\gamma}\cdot qS^{-1}\} \tag{5.24}$$

$$M(q) = \frac{Z(q)}{16N_c}\mathrm{Tr}\{S^{-1}\}, \tag{5.25}$$

where the trace over the spin-flavor indices of the staggered quarks yields a factor of 16 and the factor N_c from the trace over color. In practice, we can calculate these quantities without inverting the propagator. For more details of calculation avoiding the inversion of the propagator see section 5.4 of this Chapter.

Comparing Eq. (5.17) and Eq. (5.22) we see that dividing out q^2 in Eq. (5.24) is analagous to dividing out p^2 in the continuum and ensures that that Z has the correct asymptotic behavior. So by considering the propagator as a function of q_μ, we ensure that the lattice quark propagator has the correct tree-level form, i.e.,

$$S^{\mathrm{tree}}(q_\mu) = \frac{1}{i\overline{\gamma}\cdot q + m}, \tag{5.26}$$

and retains its continuum behavior. We have seen from Chapter 4 that the same philosophy has been used in study of the gluon propagator as well. It has been also used in the previous studies of gluon propagator [LSWP99, BBL$^+$01] and Clover and Overlap quark propagators [SW01, SLW01, BBL$^+$02, ZBL$^+$04].

The AsqTad action obtained by adding a few terms to the conventional Kogut-Susskind action, namely three-link, five-link and seven-link staples and a third-neighbor coupling, removes all tree-level $\mathcal{O}(a^2)$ errors. From Eq. (3.110) we see that the quark propagator with this action has the tree-level form

$$S^{-1}_{\alpha\beta}(p;m) = u_0 i\sum_\mu (\overline{\gamma}_\mu)_{\alpha\beta}\sin(p_\mu)\left[1+\frac{1}{6}\sin^2(p_\mu)\right] + m\overline{\delta}_{\alpha\beta}\,. \tag{5.27}$$

As in the case of gluon propagator calculation which I have explained in the previous Chapter, we also use configurations generated by the MILC Collaboration [BO01] available from the Gauge Connection [GC]. These use "AsqTad", $\mathcal{O}(a^2)$ improved staggered quarks [KO99], giving us access to relatively light sea quarks. The computational expense using this action is quark mass dependent, and roughly a factor of 2.5 for the lightest quark masses we are using [B$^+$01]. In the quenched approximation, the quark propagator for this action has excellent rotational symmetry and is well behaved at large momenta [BHL$^+$04b]. We use quenched and dynamical configurations at the same lattice spacing and volume, which enables us to observe the relatively subtle effects of unquenching. These lattices are also somewhat larger than those of previous studies, giving us access to smaller momenta.

The formulation of the AsqTad fermion propagator calculations are performed on a $20^3 \times 64$ lattices. The tree-level quark propagator with the AsqTad action has the form

$$S^{-1}(p) = i \sum_{\mu} \overline{\gamma}_{\mu} q(p_{\mu}) + m, \tag{5.28}$$

where $q(p_{\mu})$ is the kinematic momentum given by [BHW02] so we repeat the above analysis, this time defining

$$q_{\mu} \equiv \sin(p_{\mu}) \left[1 + \frac{1}{6} \sin^2(p_{\mu})\right]. \tag{5.29}$$

The $\overline{\gamma}_{\mu}$ form a staggered Dirac algebra see Eq. (5.39). Having identified the kinematic momentum, we define the mass and renormalization functions by

$$S^{-1}(p) = Z^{-1}(q) \left[i \sum_{\mu} (\overline{\gamma}_{\mu}) q_{\mu}(p_{\mu}) + M(q) \right]. \tag{5.30}$$

Complete details of the extraction of the mass and renormalization functions from the AsqTad propagator are described in the upcoming section.

5.3 Details of the calculation

The quark propagator is gauge dependent and we work in the Landau gauge for ease of comparison with other studies. We used Symanzik improved gauge action. Landau gauge is a smooth gauge that preserves the Lorentz invariance of the theory, so it is a popular choice.

An improved Landau-gauge-fixing functional, $\mathcal{F}^G_{\text{Imp}} \equiv \frac{4}{3}\mathcal{F}^G_1 - \frac{1}{12u_0}\mathcal{F}^G_2$ is used where

$$\mathcal{F}^G_1[\{U\}] = \sum_{\mu,x} \frac{1}{2} \text{Tr} \left\{ U^G_{\mu}(x) + U^G_{\mu}(x)^{\dagger} \right\}, \tag{5.31}$$

$$\mathcal{F}^G_2 = \sum_{x,\mu} \frac{1}{2} \text{Tr} \left\{ U^G_{\mu}(x) U^G_{\mu}(x + \hat{\mu}) + \text{h.c.} \right\}. \tag{5.32}$$

More technical details of gauge fixing are explained in Chapter 3. As this gauge fixing Eq. (3.74) finds a local minimum of the gauge fixing functional, we are necessarily sampling from the first Gribov region. Our ensemble contains no gauge-equivalent configurations and hence has no Gribov copies as such. However, only our configurations are local minima and *absolute* minima and therefore are not from the Fundamental Modular Region (FMR) [Wil02]. However, they are necessarily from the first Gribov region, *i.e.*, the region containing the FMR and bounded by the surface where the Faddeev-Popov determinant first vanishes. It is known from previous $SU(3)$ studies that neither the gluon nor quark propagator display any obvious Gribov noise above and beyond the ensemble statistical noise and so we do not consider it further here [GPP+02, SIMPS05b, SIMPS05a]. It will be interesting to repeat this

Table 5.1: Lattice parameters used in this study. The dynamical configurations each have two degenerate light (up/down) quarks and a heavier (strange) quark. The lattice spacing is $a = 0.125(3)$ fm, where the uncertainty reflects the variation of a over the set of lattices considered in this analysis. Bare light quark masses $ma = 0.01, 0.02, 0.03, 0.04$ correspond to masses of $16 - 63$ MeV. The bare strange quark mass is $ma = 0.05$ or 79 MeV.

	Dimensions	β	Bare Quark Mass	# Config
1	$20^3 \times 64$	8.00	quenched	265
2	$20^3 \times 64$	6.76	16 MeV, 79 MeV	203
3	$20^3 \times 64$	6.79	32 MeV, 79 MeV	249
4	$20^3 \times 64$	6.81	47 MeV, 79 MeV	268
5	$20^3 \times 64$	6.83	63 MeV, 79 MeV	318

calculation for the Gribov-copy free Laplacian gauge, and to do a systematic search for Gribov noise in Landau gauge, but these are left for future studies.

The MILC configurations were generated with the $\mathcal{O}(a^2)$ one-loop Symanzik-improved Lüscher–Weisz gauge action [LW85]. The dynamical configurations use the AsqTad quark action [BO01], an $\mathcal{O}(a^2)$ Symanzik-improved staggered fermion action which removes lattice artifacts up to order a^2g^2. The dynamical configurations have two degenerate light fermions for the u and d quarks and a heavier one for the strange quark. The lighter u and d are taken to be of equal mass, as light of $\frac{1}{8}$ of the physical strange quark mass, while the third quark flavor has been kept close to the strange quark mass. Simulations at the physical light quark mass value has not been possible so far even with the improved "Asqad" quarks. Hence chiral extrapolations are needed to reach the physical value.

The simulation parameters are summarized in Table 5.1.

Weighting for the fermion determinants is provided by the so-called, "fourth root trick.". We have seen from Chapter 3 that a staggered fermion is a lattice formulation of four continuum flavors nowadays called "tastes". The fermion determinant for a single quark flavor in this framework is represented by a rooted determinant $\det(D_{\text{staggered}})^{\frac{1}{4}}$. There is concern that the use of the fourth root of the staggered fermion determinant to respresent the fermion determinant of a single sea-quark does not fit in an obvious way into the frame work of local lattice theory at non-zero lattice spacing. This raises the question of whether the dynamical staggered fermion formulation is a first principles approach to QCD or simply a phenomenological model which describes QCD well in a certain regime [Ber06]. Infact, such "rooted" staggered quarks have been used by the MILC colloboration for recent dynamical simulations, which are in good agreement with experiment for many simple hadronic quantities. This complex question will not be considered further here. We will proceed on the assumption that " fourth root trick." is meaningful.

5.4 Extraction of the scalar functions

The AsqTad quark action [KO99] is a staggered action using three-link, five-link and seven-link staples as a kind of "fattening" to minimize quark flavor (often referred to as "taste") changing interactions. The three-link Naik term [Nai89] is included to improve rotational symmetry by improving the finite difference operator, and the five-link Lepage term [Lep99] is included to correct errors at low momenta that may be introduced by the above mentioned staples. The coefficients are tadpole improved and chosen to remove all tree-level $\mathcal{O}(a^2)$ errors.

At tree-level (i.e. no interactions, links set to the identity) the staples in this action make no contribution, so the action Eq. (3.109) reduces to the tree-level Naik action,

$$S^{(0)} = \frac{1}{2}\sum_{x,\mu}\overline{\chi}(x)\eta_\mu(x)\Big[\frac{9}{8}\big(\chi(x+\mu)-\chi(x-\mu)\big) - \frac{1}{24}\big(\chi(x+3\mu)-\chi(x-3\mu)\big)\Big] + m\sum_x \overline{\chi}(x)\chi(x), \quad (5.33)$$

where the staggered phases are: $\eta_\mu(x) = (-1)^{\zeta^{(\mu)}\cdot x}$ and

$$\zeta_\nu^{(\mu)} = \begin{cases} 1 & \text{if } \nu < \mu \\ 0 & \text{otherwise.} \end{cases} \quad (5.34)$$

In momentum space, the quark propagator with this action has the tree-level form

$$S^{(0)^{-1}}_{\alpha\beta}(p;m) = i\sum_\mu(\overline{\gamma}_\mu)_{\alpha\beta}\Big[\frac{9}{8}\sin(p_\mu) - \frac{1}{24}\sin(3p_\mu)\Big] + m\overline{\delta}_{\alpha\beta}$$
$$= i\sum_\mu(\overline{\gamma}_\mu)_{\alpha\beta}\sin(p_\mu)\big[1+\frac{1}{6}\sin^2(p_\mu)\big] + m\overline{\delta}_{\alpha\beta}. \quad (5.35)$$

where the α, β are themselves four-vectors: $\alpha_\mu = 0, 1$, and likewise for β; thus the quark propagator in Eq. (5.35) is a 16×16 matrix. This familiar form is obtained by defining

$$\overline{\delta}_{\alpha\beta} = \Pi_\mu \delta_{\alpha_\mu \beta_\mu | \bmod 2} \quad (5.36)$$
$$(\overline{\gamma}_\mu)_{\alpha\beta} = (-1)^{\alpha_\mu}\overline{\delta}_{\alpha+\zeta^{(\mu)},\beta}. \quad (5.37)$$

The mod 2 in Eq. (5.36) ensures its validity in Eq. (5.37). The $\overline{\gamma}_\mu$ satisfy

$$\{\overline{\gamma}_\mu, \overline{\gamma}_\nu\}_{\alpha\beta} = 2\delta_{\mu\nu}\overline{\delta}_{\alpha\beta} \quad (5.38)$$
$$\overline{\gamma}_\mu^\dagger = \overline{\gamma}_\mu^T = \overline{\gamma}_\mu^* = \overline{\gamma}_\mu, \quad (5.39)$$

forming a "staggered" Dirac algebra.

Staggered actions are invariant under translations of $2a$, and the momentum on this blocked lattice is given by Eq. (3.99). We calculate the quark propagator in coordinate space,

$$G(x,y) = \langle \chi(x)\overline{\chi}(y)\rangle, \tag{5.40}$$

and obtain the quark propagator in momentum space by Fourier transform of $G(x,0)$. To write the Fourier transform of the staggered field we write the momentum on the lattice

$$k_\mu = \frac{2\pi n_\mu}{L_\mu} \quad | \quad n_\mu = 0,\ldots,L_\mu - 1 \tag{5.41}$$

so that $k_\mu = p_\mu + \pi\alpha_\mu$ and define $\int_k \equiv \frac{1}{V}\sum_k$. Then

$$\int_k = \int_p \sum_{\alpha_\mu=0}^{1}, \tag{5.42}$$

$$\chi(x) = \int_k e^{ik\cdot x}\chi(k) = \int_p \sum_\alpha e^{i(p+\pi\alpha)\cdot x}\chi_\alpha(p), \tag{5.43}$$

and

$$\begin{aligned} G(x,y) &= \sum_{\alpha\beta}\int_{p,l} \exp\left\{i(p+\alpha\pi)\cdot x - i(l+\beta\pi)\cdot y\right\} \\ &\qquad \times \langle \chi_\alpha(p)\overline{\chi}_\beta(l)\rangle \qquad (5.44)\\ &= \sum_{\alpha\beta}\int_p e^{ip(x-y)}e^{i\pi(\alpha\cdot x-\beta\cdot y)}S_{\alpha\beta}(p). \qquad (5.45) \end{aligned}$$

Now it will be convenient to re-write this

$$\begin{aligned} G(k) = G(l+\pi\delta) \equiv G_\delta(l) &= \sum_x e^{-ikx}G(x,0) \\ &= \sum_{\alpha\beta}\int_p \sum_x \exp\{-i(l+\pi\delta)x\} \\ &\qquad \times \exp\{i(p+\pi\alpha)x\}S_{\alpha\beta}(p) \\ &= \sum_{\alpha\beta}\int_p \delta_{pl}\overline{\delta}_{\alpha\delta}S_{\alpha\beta}(p) \qquad (5.46)\\ &= \sum_\beta S_{\delta,\beta}(l). \qquad (5.47) \end{aligned}$$

In the interacting case, the quark propagator asymptotically approaches its tree-level value due to asymptotic freedom. At finite lattice spacing the actual behavior is closer to

$$S(q;m) \to \frac{1}{u_0}S^{(0)}(q;m/u_0)\,, \tag{5.48}$$

where u_0 is the tadpole (or mean-field) improvement factor defined by

$$u_0 = (\langle \mathrm{Tr}\, U_{\mathrm{plaq}} \rangle)^{1/4}. \tag{5.49}$$

Assuming that the full lattice propagator retains its free form (in analogy to the continuum case) we write

$$S^{-1}_{\alpha\beta}(p) = i \sum_{\mu} (\overline{\gamma}_\mu)_{\alpha\beta} q_\mu(p_\mu) A(p) + B(p) \overline{\delta}_{\alpha\beta} \tag{5.50}$$

$$= Z^{-1}(p) \Big[i \sum_{\mu} (\overline{\gamma}_\mu)_{\alpha\beta} q_\mu(p_\mu) + M(p) \overline{\delta}_{\alpha\beta} \Big], \tag{5.51}$$

where q is the tree-level momentum, Eq. (5.29). Combining this with Eq. (5.46) above, we can extract the scalar functions (which we now write in terms of q) as follows:

$$G_\alpha(q) = Z(q) \frac{-i \sum_\mu (-1)^{\alpha_\mu} q_\mu + M(q)}{q^2 + M^2(q)}, \tag{5.52}$$

from which we obtain

$$\sum_\alpha \mathrm{Tr}\, G_\alpha(q) = 16 N_c \frac{Z(q) M(q)}{q^2 + M^2(q)}$$

$$= 16 N_c \mathcal{B}(q), \tag{5.53}$$

and

$$i \sum_\alpha \sum_\mu (-1)^{\alpha_\mu} q_\mu \mathrm{Tr}\, [G_\alpha(q)] = 16 N_c q^2 \frac{Z(q)}{q^2 + M^2(q)}$$

$$= 16 N_c q^2 \mathcal{A}(q). \tag{5.54}$$

Putting it all together we get

$$A(q) = Z^{-1}(q) = \frac{\mathcal{A}(q)}{\mathcal{A}^2(q) q^2 + \mathcal{B}^2(q_\mu)} \tag{5.55}$$

$$B(q) = \frac{M(q)}{Z(q)} = \frac{\mathcal{B}(p)}{\mathcal{A}^2(q) q^2 + \mathcal{B}^2(p)} \tag{5.56}$$

$$M(q) = \frac{\mathcal{B}(q)}{\mathcal{A}(q)}. \tag{5.57}$$

By calculating $\mathcal{A}, \mathcal{B}$ instead of A, B, we avoid inverting the propagator. We calculate the ensemble average of $\mathcal{A}$ and $\mathcal{B}$ and thence M and Z.

5.5 Quenched results

First we compare our quenched results to some previously published data obtained on a smaller lattice [BHLW03]. All the data illustrated in the following are cylinder cut [BBL+01]. This removes points most susceptible to rotational symmetry

breaking, making the data easier to interpret. As is well known, the definition of lattice spacing in a quenched calculation is somewhat arbitrary, and indeed the quoted estimate for our smaller ensemble is not consistent with that published for the MILC configurations. We determined a consistent value of the lattice spacing by matching the gluon propagator calculated on the old ensemble to that of the new ensemble [BHL$^+$04a]. This procedure yields a new nominal lattice spacing of $a = 0.105$ fm and physical volume of $1.7^3 \times 3.4$ fm^4 for the old lattices. Examining the quark propagator on the two quenched ensembles, shown in Fig. 5.1, we see that the agreement is excellent. This indicates that both finite volume and discretization effects are small. The flattening in the deep infrared of both scalar functions is a long-standing prediction of DSE studies [BPRT03].

We show results for the larger quenched lattice for a variety of bare quark masses in Fig. 5.2. Once again we see that for quark masses less than or approximately equal to that of the strange quark, the lowest momentum point of the mass function is insensitive to quark mass.

5.6 Effects of dynamical quarks

The difficulties with simulating dynamical fermions results most insight based on quenched approximation ignoring the dynamics of sea quarks. Sea quarks may be thought as infinite in quenched approximation. More over, the quenched approximation is very wrong in chiral limit where the sea quark masses are close to zero. Computing resources now available are powerful enough to begin treating up, down and strange quarks dynamically. Dynamical QCD is computationally expensive with the inculsion of sea quark loops. For the first time we will learn about the sea- quark mass dependence of the quark propagator.

We report the first results for the quark propagator including dynamical quark effects. We use configurations generated by the MILC Collaboration [BO01] available from the Gauge Connection [GC]. These use "AsqTad", $\mathcal{O}(a^2)$ improved staggered quarks [KO99], giving us access to relatively light sea quarks. In the quenched approximation, the quark propagator for this action has excellent rotational symmetry and is well behaved at large momenta [BHL$^+$04b]. We use quenched and dynamical configurations at the same lattice spacing and volume, which enables us to observe the relatively subtle effects of unquenching. These lattices are also somewhat larger than those of previous studies, giving us access to smaller momenta. We compare the scalar functions for the quenched and dynamical propagators. For a given bare mass, the running mass depends upon both the number of dynamical quark flavors and their masses. To make the most appropriate comparison we select a bare quark mass for the quenched case ($ma = 0.01$) and interpolate the dynamical mass function so that it agrees with the quenched result at the renormalization point, $q = 3$ GeV. The results are shown in Fig. 5.3. The necessary bare quark mass, $ma = 0.0087$, is a little smaller for the dynamical case.

The dynamical case does not differ greatly from the quenched case. For the

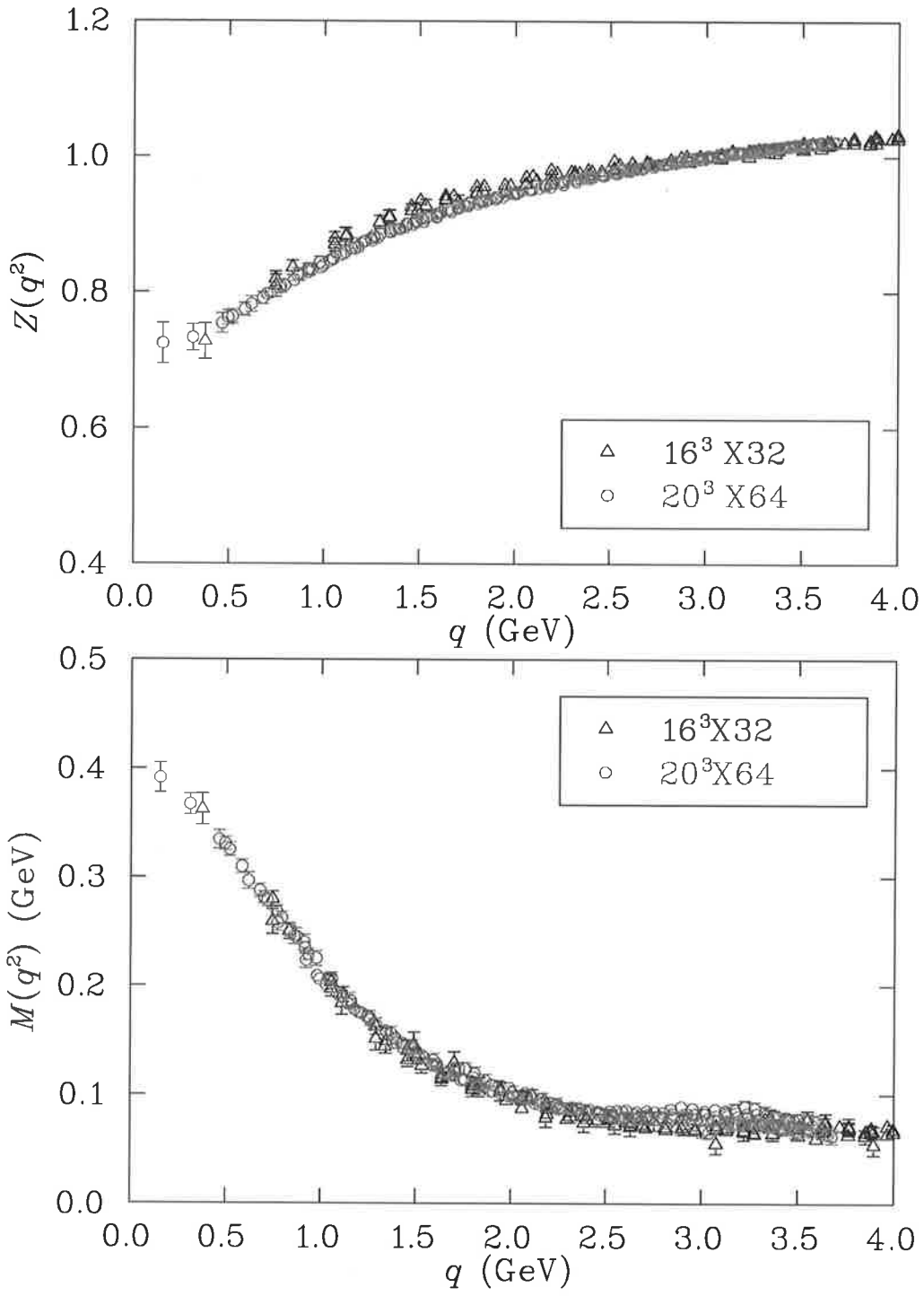

Fig. 5.1: Comparison of quenched wave-function renormalization and mass functions at approximately the same bare quark mass. The quark propagator from the $20^3 \times 64$ lattice with lattice spacing $a = 0.125$ fm at $m = 47$ MeV (open circles) is compared with the previously published quark propagator from a $16^3 \times 32$ lattice with lattice spacing $a = 0.105$ fm at $m = 45$ MeV (full triangles). The renormalization point for $Z(q^2)$ is set at $q = 3$ GeV.

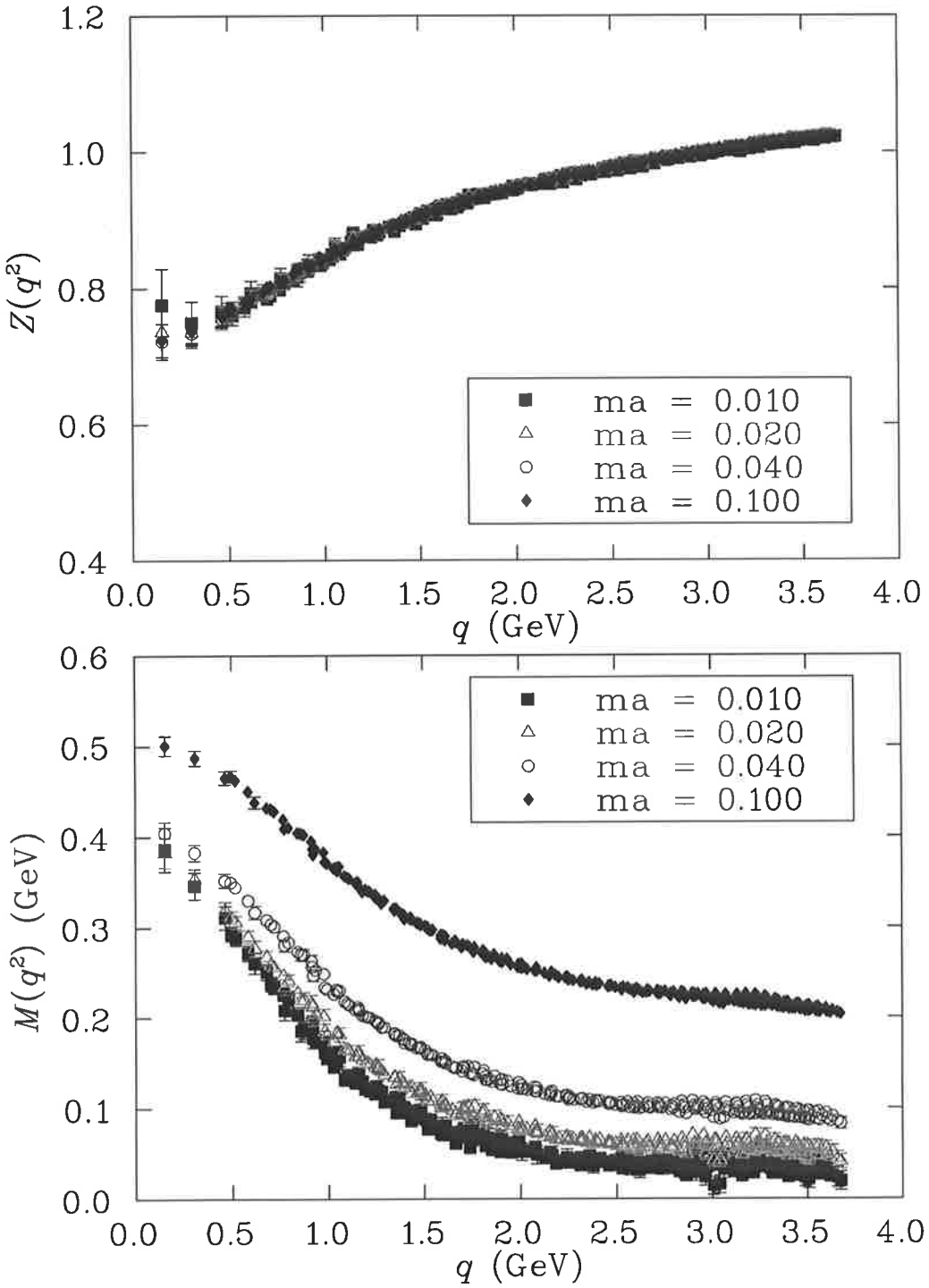

Fig. 5.2: The quenched renormalization function (top) and mass function (bottom) for a selection of quark masses, including $ma = 0.100$, about twice the strange quark mass. The renormalization point for $Z(q^2)$ is set at $q = 3$ GeV.

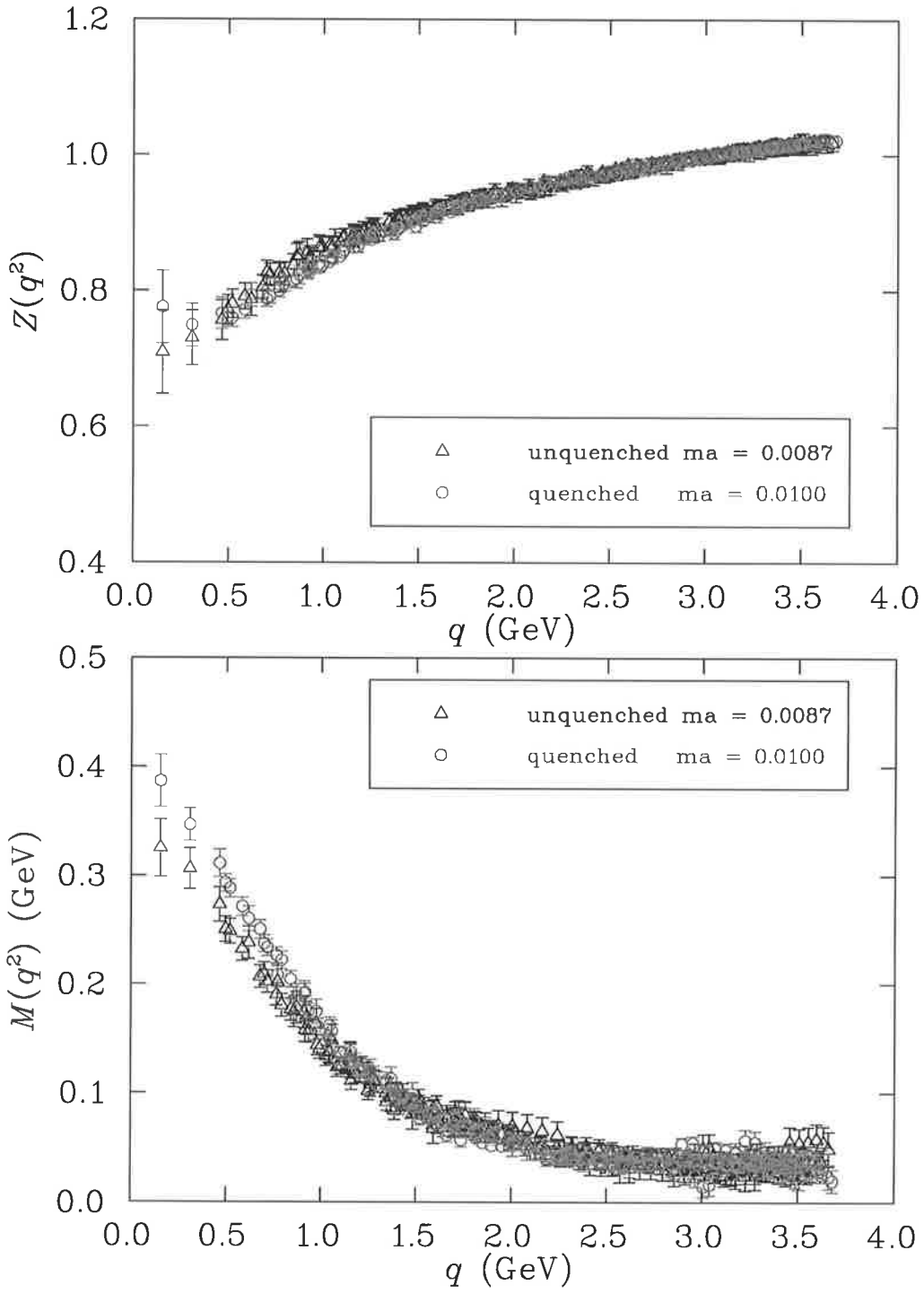

Fig. 5.3: Comparison of the unquenched (full QCD) and quenched quark propagator for non-zero quark mass. The mass function for the unquenched dynamical-fermion propagator has been interpolated so that it agrees with the quenched mass function for $ma = 0.01$ at the renormalization point, $q = 3$ GeV. For the unquenched propagator this corresponds to a bare quark mass of $ma = 0.0087$.

renormalization functions, there is no discernible difference between the quenched and unquenched cases. However the mass functions do reveal the effects of dynamical quarks. Dynamical mass generation is suppressed, in the infrared, in the presence of dynamical quarks relative to that observed in the quenched case when the mass functions are the same at the (UV) renormalization point. This is in accord with expectations as the dynamical quark loops act to screen the strong interaction. Further comparisons can be made in the chiral limit. In Fig. 5.4, both quenched and dynamical data have been extrapolated to zero bare quark mass by a fit linear in the quark mass. In the dynamical case, the extrapolation was done for the case when the valence and light sea quark masses are identical. As discussed above, for a given bare quark mass, the running mass is larger in full QCD than in quenched QCD. This is apparent from the fact that the bare mass must be chosen smaller in the dynamical case in order that the running masses agree at large momenta e.g., see Fig. 5.3. This is in qualitative agreement with perturbation theory. In the quenched case the mass runs more slowly than it does with three light quark flavors. Fig. 5.5 shows the mass and renormalization functions in the dynamical case for a variety of quark masses. Here the valence quark masses and the light sea quark masses are matched. The results show that the renormalization function is insensitive to the bare quark masses studied here. The renormalization function is infrared supressed. We have seen from the extraction of scalar function section in this Chapter that, the quark renormalization function is given by

$$Z(q) = \frac{\mathcal{A}^2(q)q^2 + \mathcal{B}^2(q_\mu)}{\mathcal{A}(q)} \,. \tag{5.58}$$

The denominator of this wave-function renormalization function increases as q approaches zero which causes the infrared supression. Even though the function $\mathcal{B}^2(q_\mu)$ in the numerator is like $\mathcal{A}^2(q)$, which is also an increasing function of q, as q approaches zero, it is almost constant as the bare quark mass decreases, in contrast to $\mathcal{A}^2(q)$ which increases when the bare quark mass decreased. The results for the mass function are ordered as expected with the larger bare quark masses, m, giving rise to a larger mass function. Our results for the scalar functions on the coarse lattice are in good agreement with the published results of [FN06]. Numerical simulations of lattice-QCD provide direct access to DSE calculations. We refer to Fig. 5.6, to make a comparitive study of our lattice results with the DSE approach of reproducing it from our full QCD gluon propagator data. The Dyson-Schwinger equations are a nonperturbative approach to study continuum QCD. The DSEs are useful tool and can be used directly to understand hadrons as bound states; the importance of dynamical chiral symmetry breaking (DCSB); and the confinement of quarks and gluons. The DSE for the dressed-quark propagator is given by [KR04]

$$S(p)^{-1} = Z_2\,(i\gamma\cdot p + m_{\rm bare}) + Z_1 \int_q^\Lambda g^2 D_{\mu\nu}(p-q)\frac{\lambda^a}{2}\gamma_\mu S(q)\Gamma^a_\nu(q;p)\,, \tag{5.59}$$

where $D_{\mu\nu}(k)$ is the dressed-gluon propagator, $\Gamma^a_\nu(q;p)$ is the dressed-quark-gluon vertex, $m_{\rm bare}$ is the Λ-dependent current-quark bare mass, and $\int_q^\Lambda := \int^\Lambda d^4q/(2\pi)^4$

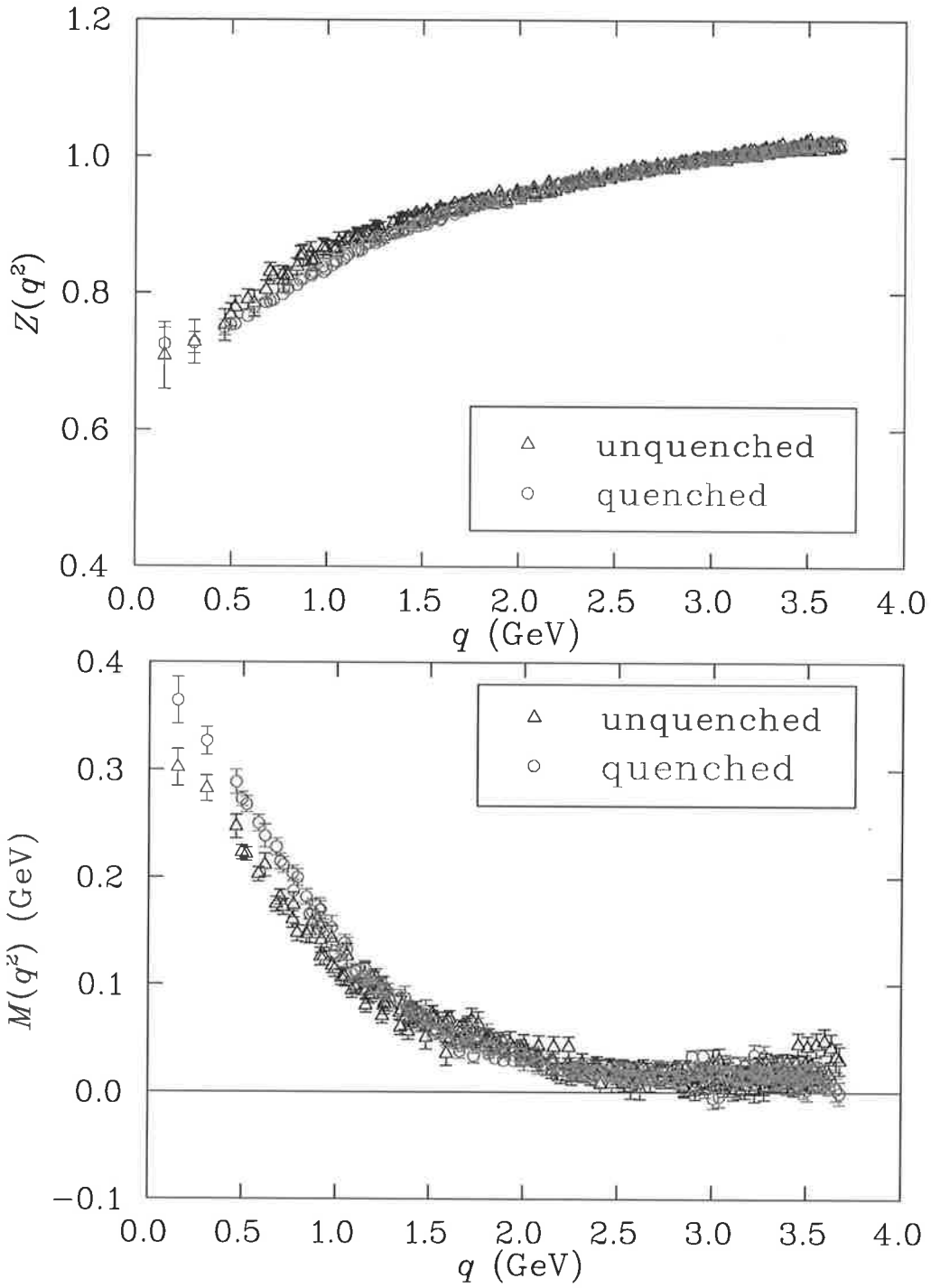

Fig. 5.4: Comparison of the unquenched (full QCD) and quenched quark propagator in the chiral limit. The renormalization function is renormalized at $q = 3$ GeV. Whereas little difference is observed in the renormalization function, the mass functions indicates that dynamical mass generation is suppressed by the addition of quark loops.

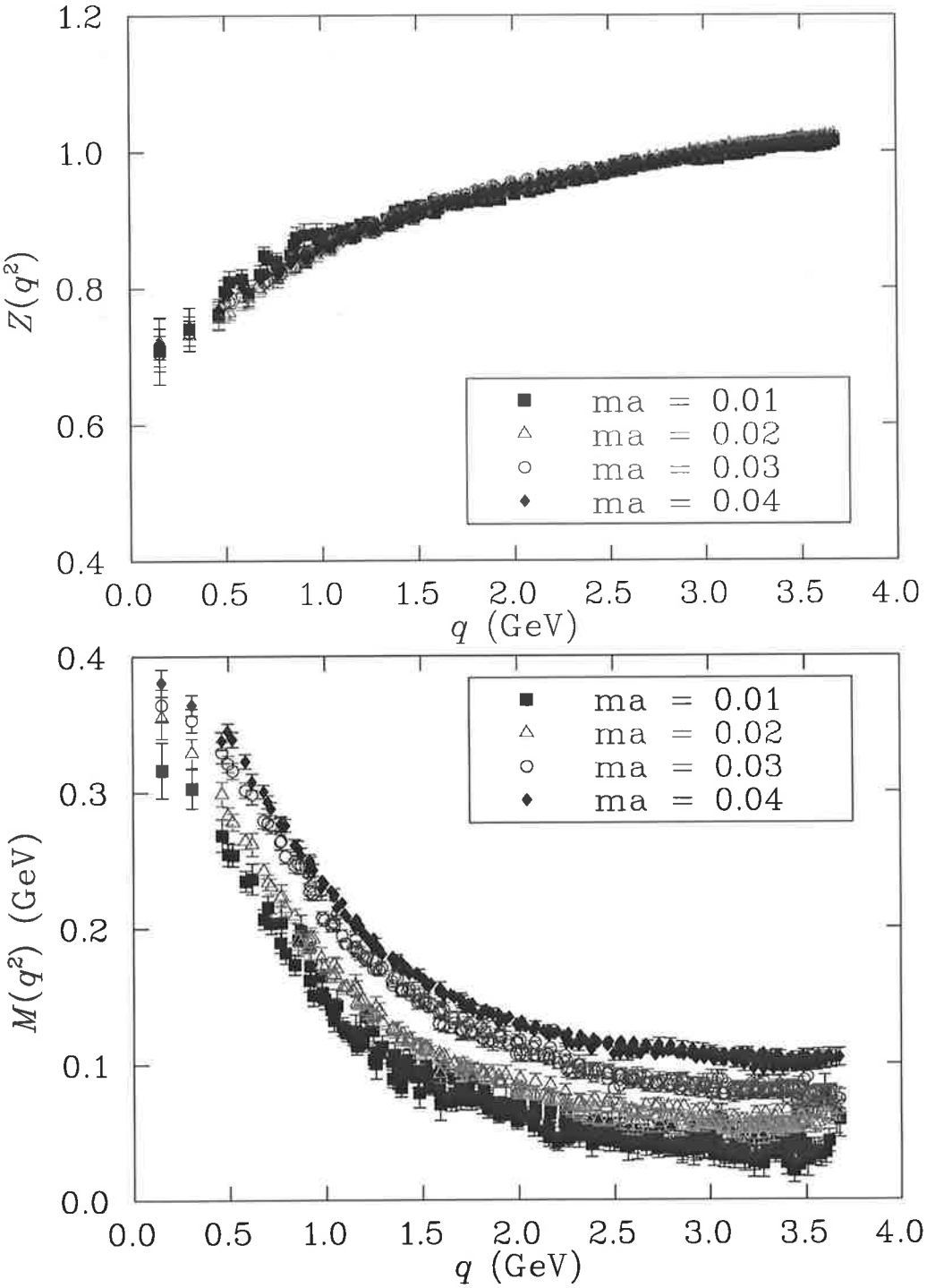

Fig. 5.5: Renormalization (top) and mass (bottom) functions for four different quark masses in full QCD, where the valence and light-sea masses are matched. The wave-function renormalization function Z is renormalized at $q = 3$ GeV.

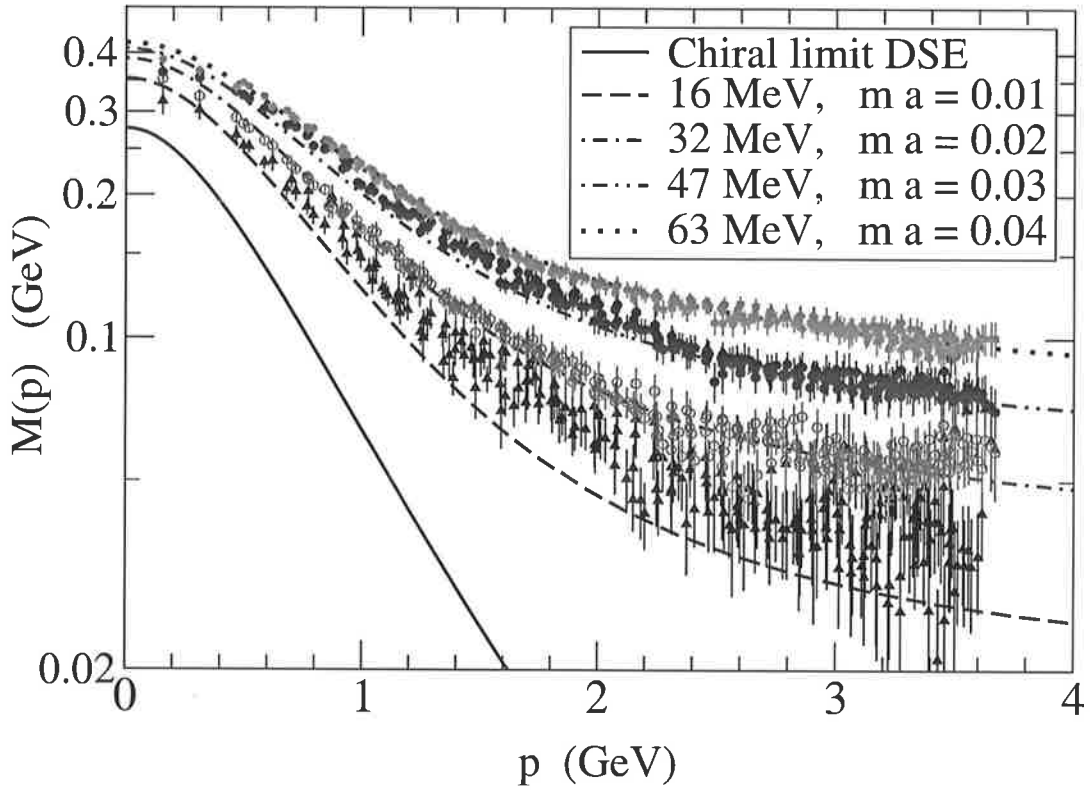

Fig. 5.6: Our full QCD lattice results reproduced via the continuum DSE [BT06].

represents a translationally-invariant regularisation of the integral. Here Λ the regularisation mass-scale, the $Z_i(\mu^2, \Lambda^2)$ are the quark-gluon-vertex and quark wave function renormalisation constants, which depend on Λ and the renormalisation point, μ. The lattice results for $S^{-1}(p)$ is given by Eq. (5.17). Comparison has been made by solving Eq. (5.59), with kernel factors $Z_1 g^2 D_{\mu\nu}(k)\Gamma^a_\nu(k;p)$ replaced by $D^{\rm lat}_{\mu\nu}(k)\frac{\lambda^a}{2}\gamma_\nu\Gamma^a_1(k^2)$. $D^{\rm lat}_{\mu\nu}(k)$ is a fit to our lattice gluon propagator data and $\Gamma^a_1(k^2)$ is a phenomenological vertex amplitude determined so that the DSE solution for $S(p)$ fits our data [BT06]. We can clearly seen from Fig. 5.6 that the lattice reults are in precise agreement with DSE results. Finally, we comment on the approach to the chiral limit. In Fig. 5.7, we show the mass function for five different momenta plotted as a function of the bare quark mass. The momenta considered include the lowest momentum of 0.155 GeV and 0.310, 0.495, 0.700 and 0.993 GeV to explore momentum dependent changes in the approach to the chiral limit. At larger momenta, the mass function is observed to be proportional to the bare quark mass. However, at small momenta, nonperturbative effects make this dependence more complicated. For example, a recent Dyson-Schwinger study predicts a downward turn as the bare mass approaches zero [BPRT03].

For the lowest momentum points, nonlinear behavior is indeed observed. For the quenched case, curvature in an upward direction is revealed as the chiral limit is approached, leading to the possibility of a larger infrared mass function for the

lightest quark mass, despite the reduction of the input bare quark mass. In contrast, a hint of downward curvature is observed for the most infrared points of the full QCD mass function as the chiral limit is approached. It is interesting that the nature of the curvature depends significantly on the chiral dynamics of the theory which are modified in making the quenched approximation. Similar behavior is observed in the hadron mass spectrum where the coefficients of chiral nonanalytic behavior can change sign in moving from quenched QCD to full QCD. [L$^+$04, YLTW02].

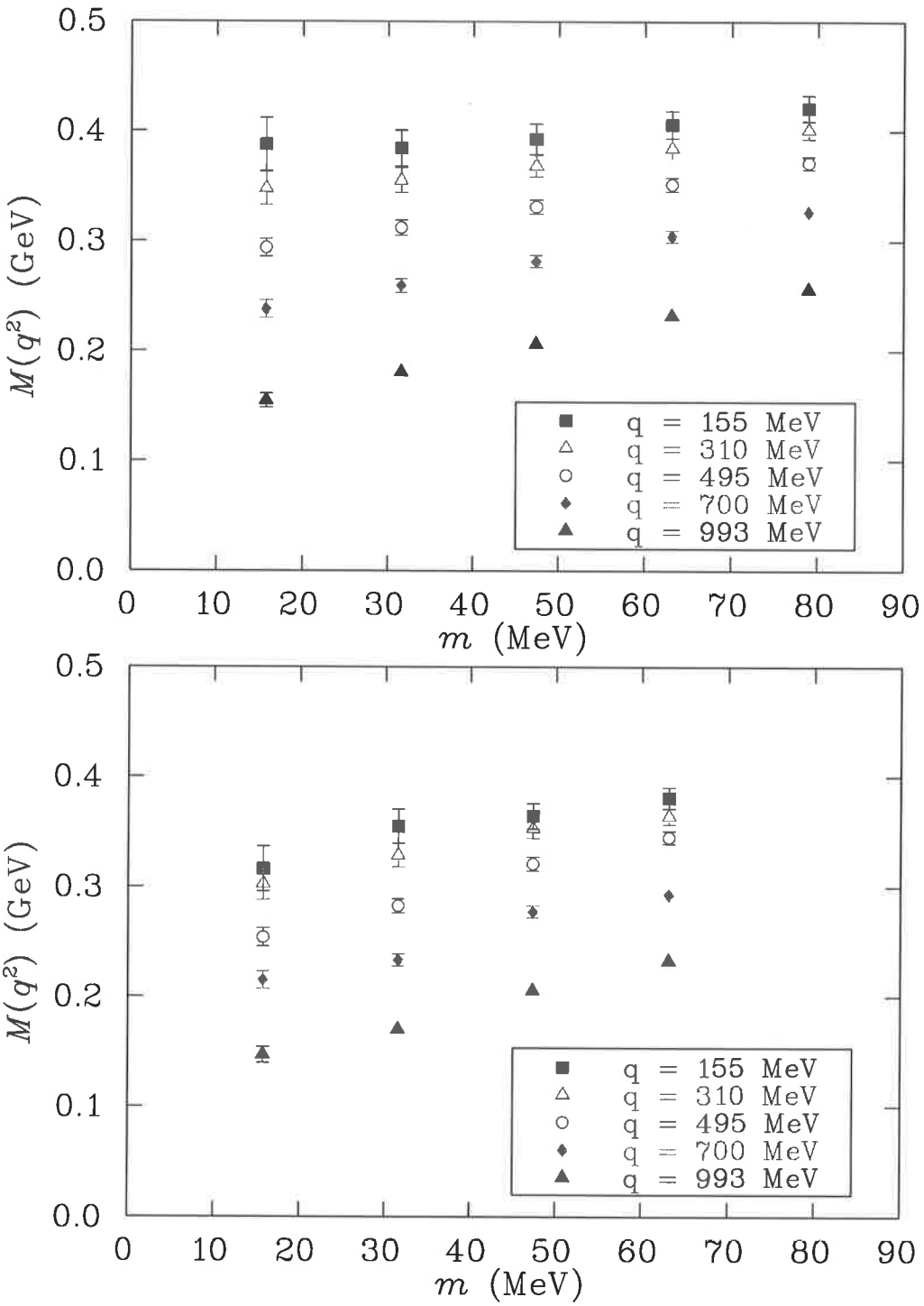

Fig. 5.7: The chiral limit approach of the mass function for selected momenta. Results from quenched QCD simulations are illustrated at top whereas full dynamical-fermion QCD results are illustrated at bottom. Non-linear behavior is observed for the lowest momentum points, in opposite directions for quenched and full QCD.

6

Comparison of unquenched and quenched quark and gluon propagator on a fine lattice

The n-point Green's functions are the building blocks of a field theory and in lattice the simplest are quark and gluon propagators. We can use them to study fundamental properties of QCD, both qualitative: dynamical mass generation, the transition from perturbative and nonperturbative regimes, confinement; and quantitative: quark and gluon condensates, running quark masses, running coupling [B$^+$]. The gluon and quark propagator contains valuable information about nonperturbative QCD. The systematic study of the quark propagator on the lattice has provided fruitful interaction with other approaches to hadron physics, such as instanton phenomenology [Dia03], chiral quark models [RAB03] and Dyson-Schwinger equation studies [BPRT03, ADFM04]. As a first principles approach lattice QCD has provided valuable constraints for model builders. In turn, such alternative methods can provide feedback on regions that are difficult to access directly on the lattice, such as the deep infrared and chiral limits.

Lattice QCD enables us to study the nonperturbative nature of QCD from the first principles. As space-time is replaced with a discretized lattice, physical results from the lattice simulations can be obtained once the effects of finite lattice spacing a and finite volume V are under control [Ma00]. One of the most important systematic errors comes from the finite lattice spacing which generates an errors of the order of $a\Lambda_{QCD}$.

In this chapter, we are presenting work clarifying the robustness of our earlier results on the gluon and quark propagators which we have studied in the previous chapters. We are extending our calculations on coarser lattices to a finer lattice. The infrared part of any lattice calculation may be affected by the finite volume of the lattice. Larger volumes mean either more lattice points with increased computational cost or coarser lattice with corresponding discretisation errors. The desire for minimizing discretization errors at reasonable physical volumes thus provides strong motivation for using improved actions.

We study the gluon and quark propagator on two lattices:coarse and fine and compare the results to see any effect of finite lattice spacing as well.

We have already seen the results for both propagators with and without the effects of dynamical sea-quarks on the coarse lattice which I have explained in Chapters 4 and 5. In this chapter we are performing a comparison of both quenched and full QCD results on a fine lattice with lattice spacing $a = 0.09$ fm and volume $(2.52\,\text{fm})^3$.

Table 6.1: Lattice parameters used in this study. The dynamical configurations each have two degenerate light quarks (up/down) and a heavier quark (strange). The light bare quark masses for the $28^3 \times 96$ lattice are 14.0 MeV and 27.1 MeV with a strange quark mass of 67.8 MeV. The lattice spacing is $a \simeq 0.09$ fm [A$^+$04a] for the $28^3 \times 64$ lattice.

	Dimensions	β	a	Bare Quark Mass	# Config
1	$28^3 \times 96$	8.40	0.086 fm	quenched	110
2	$28^3 \times 96$	7.09	0.086 fm	14.0 MeV, 67.8 MeV	108
3	$28^3 \times 96$	7.11	0.086 fm	27.1 MeV, 67.8 MeV	110

6.1 Gluon propagator on a fine lattice

We have performed calculations of the gluon propagator in Landau gauge for 110 configurations for quenched with $\beta = 8.4$ and for unquenched set with two different light sea-quark masses (see 6.1 for the number of configurations and β values used) for $28^3 \times 96$ lattice. The lattice spacing is approximately 0.09 fm. The technical details of gauge fixing and the lattice calculation of the gluon propagator are already explained in the previous chapters.

In Fig. 6.1, we present the behavior of gluon propagator in quenched and full lattice QCD for $28^3 \times 96$ lattice with lattice spacing $a = 0.09$ fm. The results are similar to our previous comparison of quenched and unquenched gluon dressing function $q^2D(q^2)$ on $20^3 \times 64$ lattice Fig. 4.1. The difference between quenched and dynamical quark behavior in the infrared region is significant. In quenched QCD, there are only gluon loops present. In the unquenched case, the addition of quark loops decreases the effect of the gluon loops at large momenta. The compelling evidence we have seen from Fig. 4.1 suggests that adding fermion loops suppresses the non-abelian effects as one might naively expect. In other words, the addition of sea-quark loops moves the result slighly back towards their tree-level form. The unquenching effect on the fine lattice is the same as that of coarse lattice which we have studied in chapter 4, showing around 30% of reduction in the dressing function.

6.1.1 Sea-quark mass dependence on gluon propagator

In Fig. 6.2, we are trying to see any mass dependence for the dressing function in the finer lattice with heavier light sea-quark mass ($m = 27.1$ MeV), lighter light sea-quark mass ($m = 14.0$ MeV). The bare strange-quark mass is the same in both cases ($m = 68$ MeV). As there is not much difference between both light quark masses we hardly seen any dependence in this case. But in our previous study,

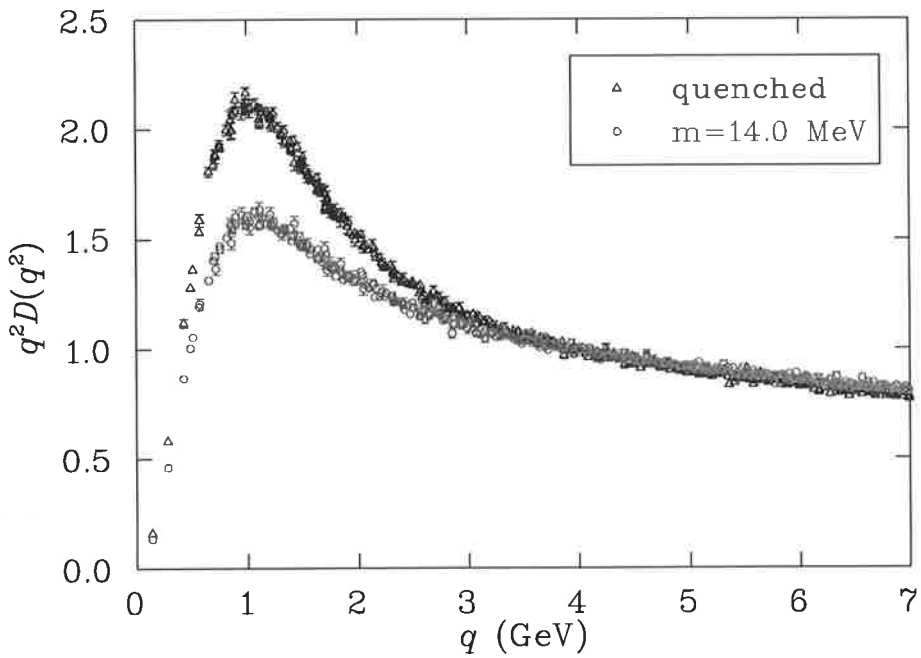

Fig. 6.1: Gluon dressing function in Landau gauge for the finer lattice $28^3 \times 96$. Full triangles correspond to the quenched calculation, while open circles correspond to 2+1 flavor QCD. The bare light quark mass is $m = 14.0$ MeV for the full QCD result. As the lattice spacing and volume are the same, the difference between the two results is entirely due to the presence of quark loops. The renormalization point is at $\mu = 4$ GeV. Data has been cylinder cut [LSWP99].

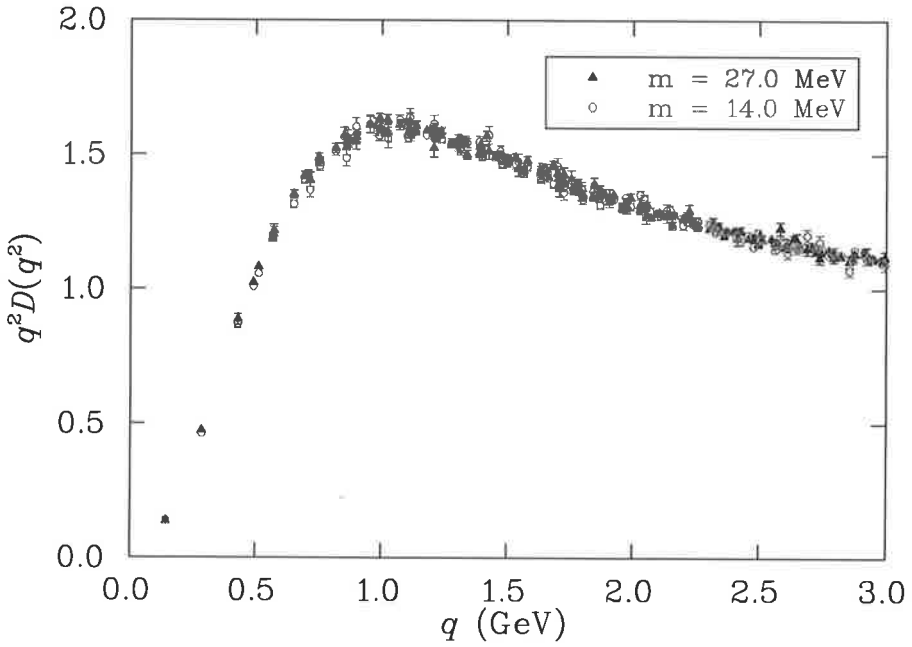

Fig. 6.2: The sea-quark mass dependence of the Landau gauge gluon dressing function $q^2D(q^2)$ renormalized at $\mu = 4$ GeV for the $28^3 \times 96$ lattice. Filled triangles correspond to bare light quark mass $\simeq 27$ MeV and bare strange-quark mass $\simeq 68$ MeV. Open circles correspond to the same strange-quark mass, but with bare light quark mass $\simeq 14$ MeV. Data has been cylinder cut [LSWP99]. A little mass dependence is observed for this case. But it is clearly visible that increasing the sea-quark masses alters the results in the expected way, *i.e.*, towards the quenched data and agrees with our previous study.

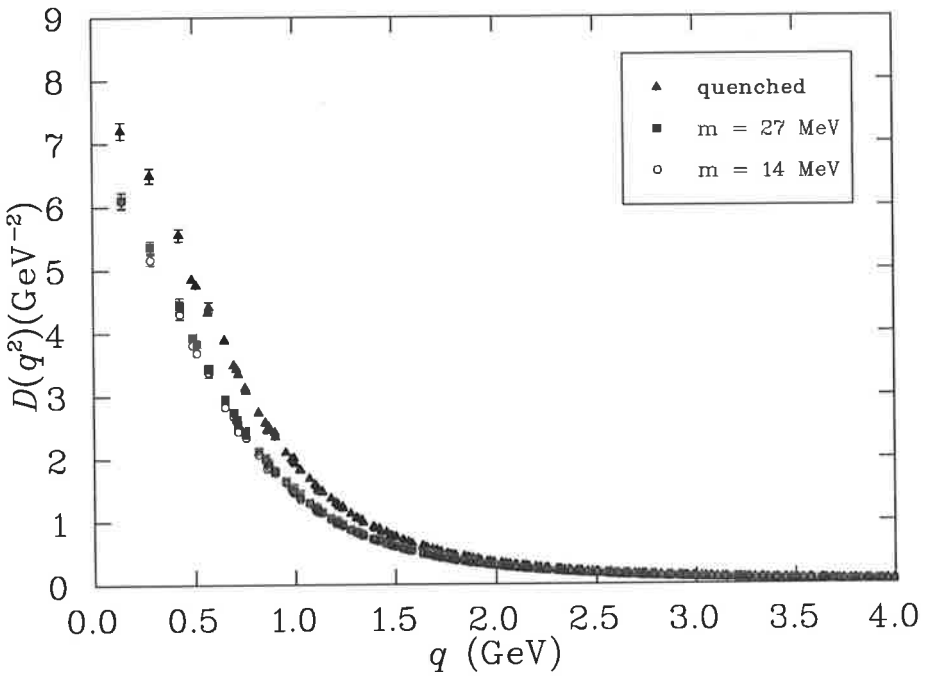

Fig. 6.3: The sea-quark mass dependence of the Landau gauge gluon propagator on a fine lattice. Filled triangles corresponds to the quenched gluon dressing function, while filled squares correspond to the bare light quark mass $\simeq$ 27 MeV and bare s-quark mass $\simeq$ 67.8 MeV. Open circles correspond to the same strange-quark mass, but with bare u and d masses $\simeq$ 14 MeV. Data has been cylinder cut [LSWP99].

recall Fig. 4.3, we have seen mass dependence as there is a a factor of four difference between the light quark masses chosen. As the sea-quark mass increases, the curve moves towards the quenched result. For the fine lattice, we have only two light sea-quark mass to compare the mass dependence so the sea-quark mass dependence is not that prominent compared to the results from the coarser lattice. It would be better studied with a range of heavy sea-quark masses for the fine lattice to see any significant effect.

In Fig. 6.3, we are highlighting the results of the quenched and unquenched gluon propagator, $D(q^2)$ for the fine $28^3 \times 96$ lattice. It is clear from the results that as the bare sea-quark mass increases, the result is moving towards the quenched result which is expected. The results (shape of the curve) indicates that the qualitative features of the quenched and unquenched gluon propagator are the same as Fig. 4.5.

6.2 Fine lattice quark propagator

We study the AsqTad quark propagator on a fine $28^3 \times 96$ lattice using the $\mathcal{O}(a^2)$ Symanzik improved gauge action for the quenched and unquenched set of lattices. We use 120 configurations for quenched set with $\beta = 8.4$. Full QCD simulations are run with two different set of light sea-quark masses (see Table 6.1 for the number of configurations and β values used). We will first report the results of quark propagator on a finer lattice, $28^3 \times 96$ with lattice spacing $a = 0.090$ fm. We explore two light sea quark masses, $ma = 0.0062$ ($m = 14.0$ MeV) and $ma = 0.0124$ ($m = 27.1$ MeV). The bare strange quark mass was fixed at $ma = 0.031$, or $m = 67.8$ MeV for $a = 0.09$ fm. The values of the coupling and the bare light sea-quark masses are matched such that the lattice spacing is held constant. The simulation parameters are summarized in Table 6.1 with the lattice spacings taken from [A+04a]. All the configurations we use in this study were generated by the MILC collaboration [BO01] available from the Gauge Connection [GC]. The dynamical configurations have two degenerate light fermions for the u and d quarks and a heavier one for the strange quark.

The computation of lattice quark propagator after gauge fixing the MILC configurations, extraction of scalar functions are described in detail in Chapter 5. In Fig. 6.4 we show the results of mass function $M(q^2)$ and wave-function renormalization function $Z(q^2)$ for the case of heavier light quark mass ($m = 27.1$ MeV) for a variety of valence quark masses. We set valence and sea masses equal to recover the true theory, namely "full QCD". In unquenched simulations, the valence quark mass can be different from the mass of dynamical sea-quarks which corresponds to "partially quenched" QCD.

In Fig. 6.4, just one valence quark mass $m = 27.1$ MeV is matched to the light sea-quark mass, this is the full QCD result. Filled squares in this figure correspond to full QCD result. It is also noted that one valence quark mass is matched with the strange quark mass $m = 67.8$ MeV which is also the full QCD result for the strange quark. The others are partially quenched results. Nevertheless, the data

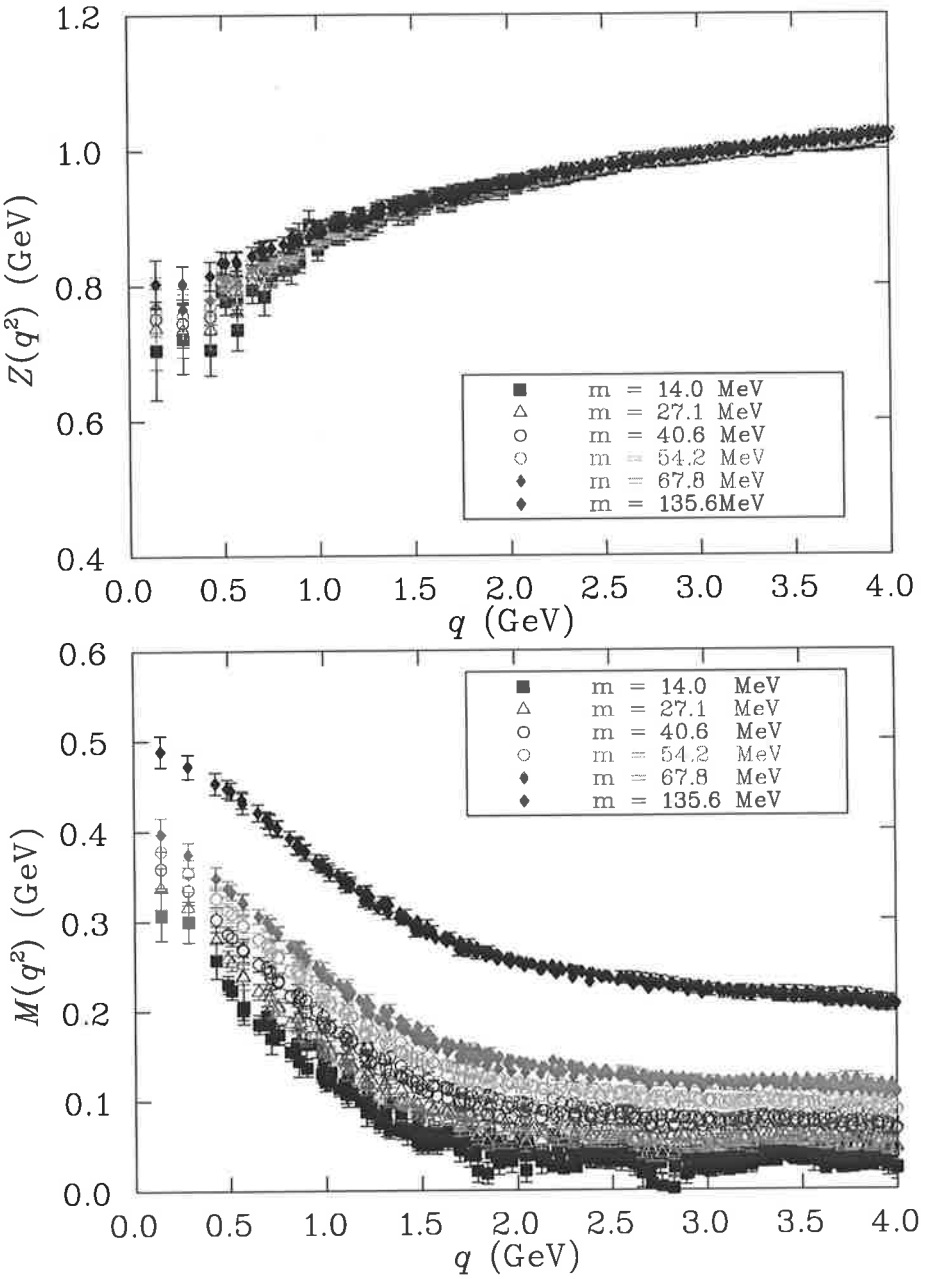

Fig. 6.4: The unquenched wave-function renormalization function $Z(q^2)$ and mass function $M(q^2)$ for a variety of valence quark masses, with light sea-quark mass fixed at $m = 27.1$ MeV

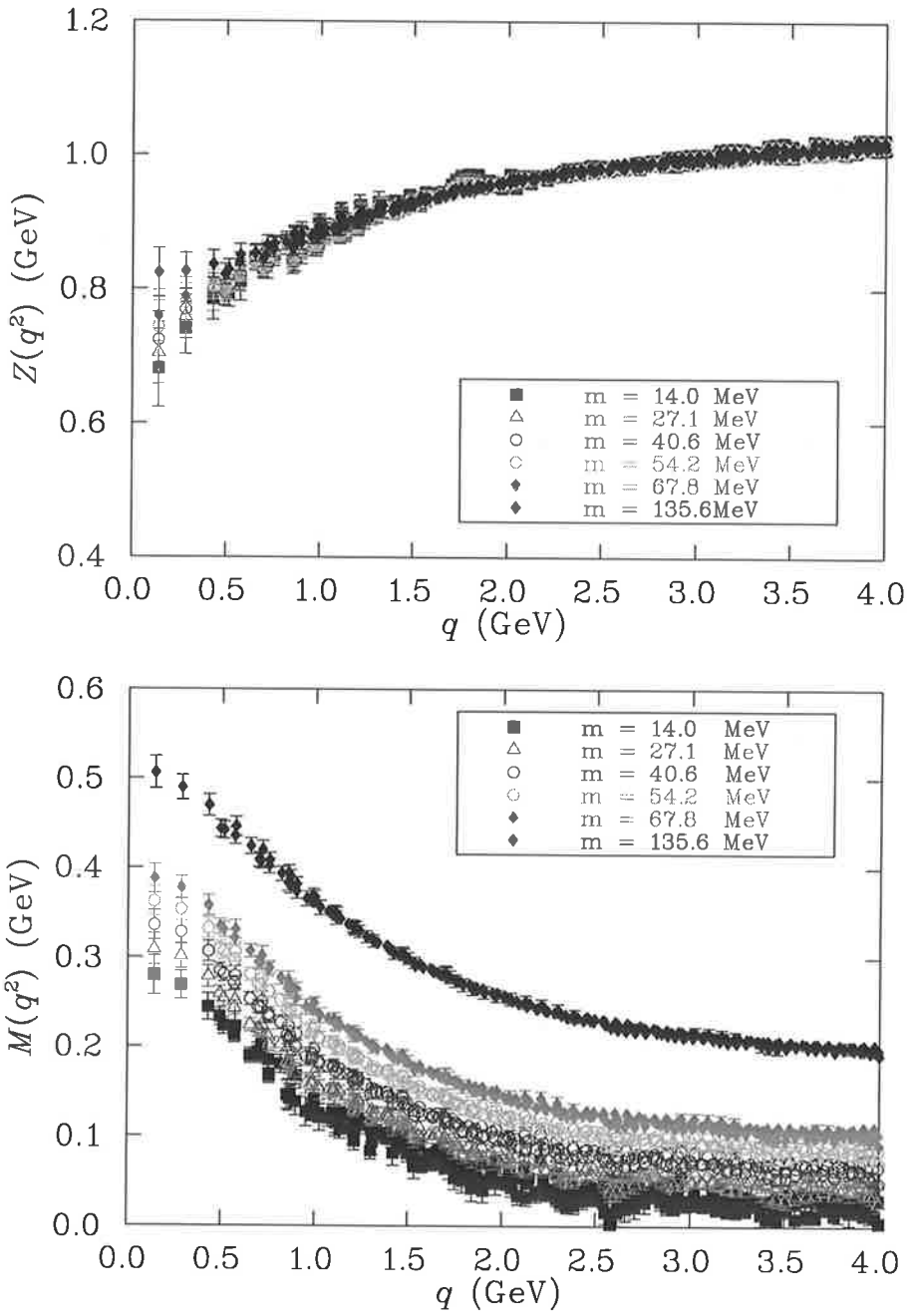

Fig. 6.5: The unquenched wave-function renormalization function $Z(q^2)$ and mass function $M(q^2)$ for a variety of valence quark masses (shown in the inset), with the light sea-quark mass fixed at $m = 14.0$ MeV. The renormalization function is renormalized at $q = 3.0$ GeV.

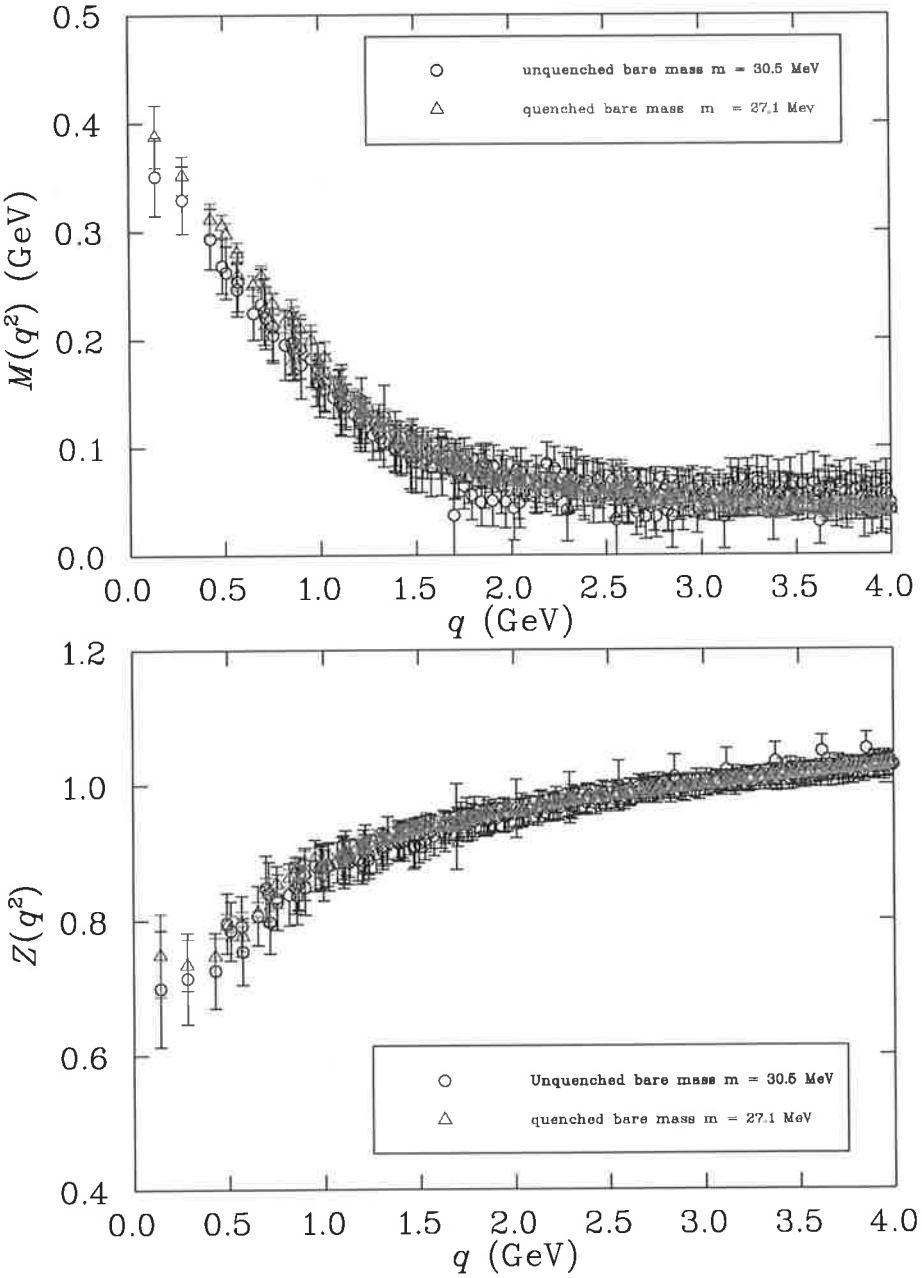

Fig. 6.6: Comparison of the unquenched (full QCD) and quenched quark propagator for non-zero quark mass. The mass function for the unquenched dynamical-fermion propagator has been interpolated so that it agrees with the quenched mass function for $m = 27.1$ MeV at the renormalization point, $q = 3$ GeV. For the unquenched propagator this corresponds to a bare quark mass of $m = 30.5$ MeV.

are ordered as we expected, i.e., the larger the bare valence quark mass, the higher is the $M(q^2)$. It is also in reasonable agreement with the behavior of $M(q^2)$ in the quenched case [B+05]. The wave-function renormalization function $Z(q^2)$, on the other hand, is infrared suppressed. The smaller the bare valence quark mass the more pronounced the dip at low momenta.

Fig. 6.5 is the same as Fig. 6.4 except the case sea-quark mass, which is lightest ($m = 14.0$ MeV) of our light sea-quark masses for a variety of valence quark masses. In these figures, one valence quark mass (14.0 MeV) is identical to the light sea quark mass, corresponding to the full QCD result. Others are partially quenched result except one more full QCD result for the strange quark mass $m = 67.8$ MeV which matches with the valence quark mass. Comparing Fig. 6.4 with Fig. 6.5, we see from the plots that for a given bare quark mass, the running mass depends upon both the valence quark mass and the sea-quark mass.

Next, we compare the scalar functions for the quenched and dynamical propagators on a fine lattice. For a given bare mass, the running mass depends upon both the number of dynamical quark flavors and their masses. To make the most appropriate comparison we select a bare quark mass for the quenched case ($m = 27.1$ MeV) and interpolate the dynamical mass function so that it agrees with the quenched result at the renormalization point, $q = 3$ GeV. The results are shown in Fig. 6.6. The necessary bare quark mass, $m = 30.5$ MeV, is a little higher for the dynamical case. Unfortunately we have only two sets of dynamical data to interpolate.

On the fine lattice also, the dynamical case does not differ greatly from the quenched case as we have seen on the coarse lattice. However, the effects of sea-quarks are clearly visible in the case of mass function. Dynamical mass generation is suppressed, in the infrared due to the presence of the sea-quarks. In the case of renormalization functions, there is not much discernable difference between the quenched and unquenched cases.

6.2.1 Sea-quark mass dependence on quark propagator

In Figs. 6.7 and 6.8 we instead hold the valence quark mass fixed and vary the sea quark mass. The top figures in both cases corresponds to the light sea-quark and seem to be noisier in each case. In this case our valence quark mass is the lightest ($m = 14.0$ MeV). The bottom one in both figures are clean where we used the heavier valence quark mass ($m = 135.6$ MeV). This also shows us that lighter quark masses are harder to simulate on the lattice. Clearly the dependence over this small range of sea quark masses is weak. Unfortunately we only have two dynamical sets to compare, and for the lightest valence quark the data are relatively noisy.

We have presented the first results for the gluon and quark propagator on a fine lattice in which the effects of $2 + 1$ dynamical quark flavors are taken into account. We have studied and analysed the gluon and quark propagator on a fine lattice with and with out the effect of dynamical sea-quarks. The comparison of quenched and

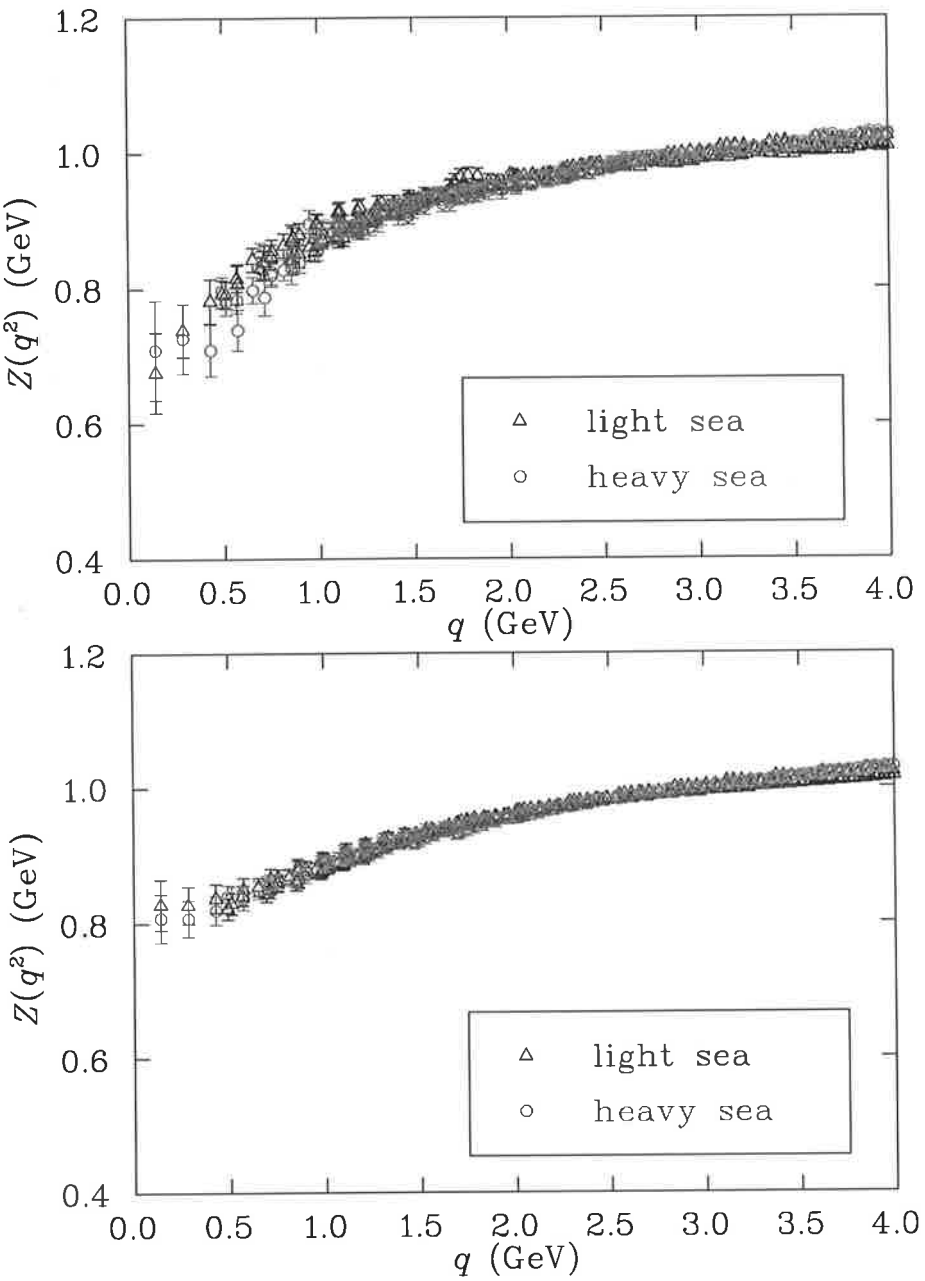

Fig. 6.7: The unquenched wave-function renormalisation function for the two different values of the light sea quark mass on the fine lattice (14.0 MeV and 27.1 MeV). The valence quark masses are $m = 14.0$ MeV (top) and $m = 135.6$ MeV (bottom), the lightest and heaviest in our current sample respectively. The renormalization function is renormalized at $q = 3.0$ GeV.

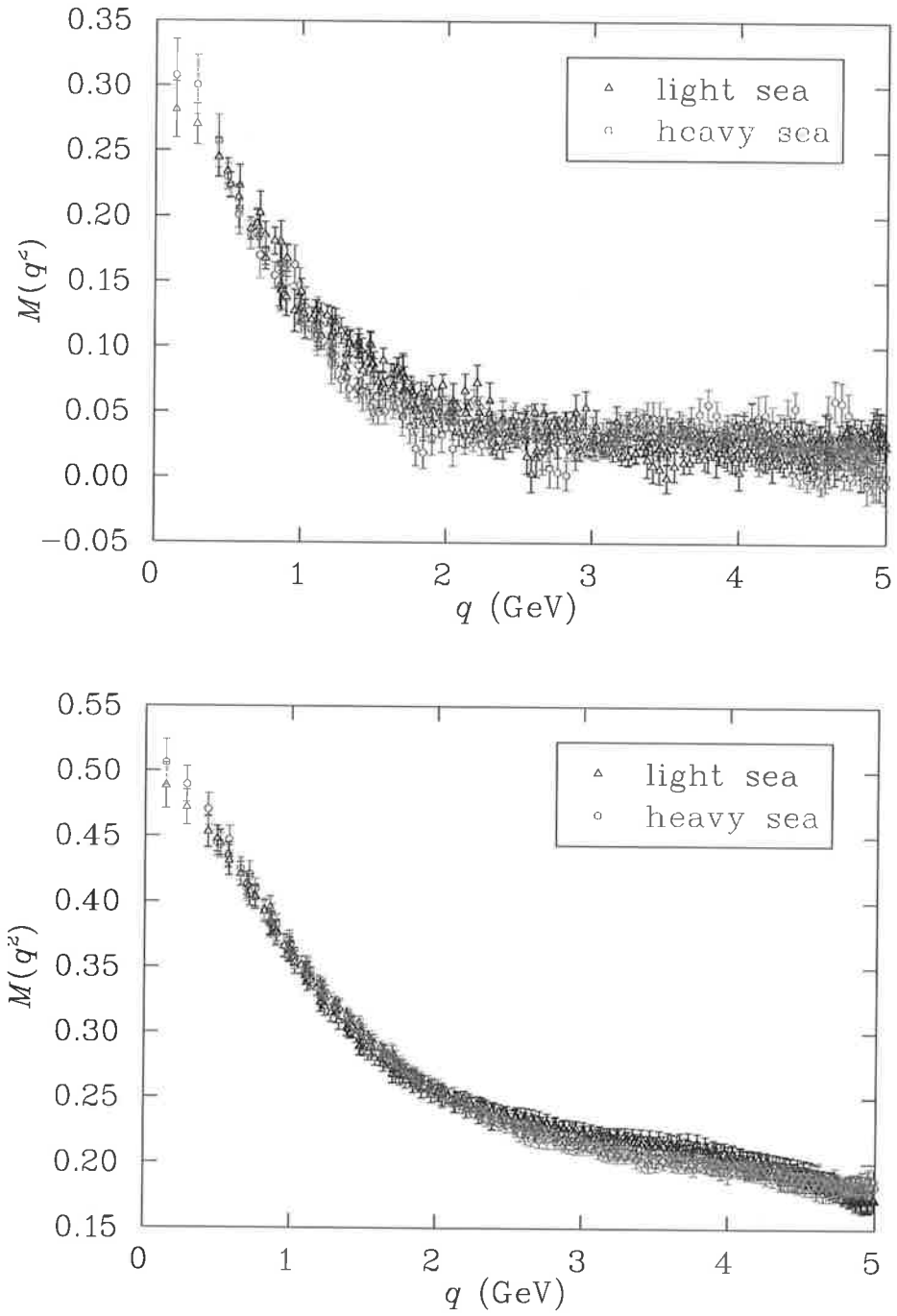

Fig. 6.8: The unquenched quark mass function for the two different values of the light sea quark mass on the fine lattice (14.0 MeV and 27.1 MeV). The valence quark masses are $m = 14.0$ MeV (top) and $m = 135.6$. MeV (bottom), the lightest and heaviest in our current sample respectively.

full QCD results for gluon propagator on the fine lattice is the same as the result we have seen from the coarse lattice. But we could not see as clearly the effect of sea-quark mass dependence on the fine lattice gluon propagator compared to the coarse lattice one. This may be due to the finer lattice being somewhat noisier. Moreover our range of dynamical sea-quarks is limited (2 set of masses) on a fine lattice compared to the coarse lattice calculation (4 set of masses). The results obtained for the AsTad quark propagator on a fine lattice are consistent with those from a coarse lattice. The qualitative effects of dynamical sea-quarks are the same in both cases.

Scaling behavior of the quark and gluon propagator in full QCD

7.1 Scaling behavior of the quark propagator

We study the scaling behavior of the quark propagator on two lattices with similar physical volume in Landau gauge with $2+1$ flavors of dynamical quarks in order to test whether we are close to the continuum limit for these lattices. We use configurations generated with an improved staggered ("AsqTad") action by the MILC collaboration. The calculations are performed on $28^3 \times 96$ lattices with lattice spacing $a = 0.09$ fm and on $20^3 \times 64$ lattices with lattice spacing $a = 0.12$ fm. We calculate the quark mass function, $M(q^2)$, and the wave-function renormalization function, $Z(q^2)$, for a variety of bare quark masses. Comparing the behavior of these functions on the two sets of lattices we find that both $Z(q^2)$ and $M(q^2)$ show little sensitivity to the ultraviolet cutoff suggesting that we are close to the continuum limit for these lattices.

In this study we focus on the Landau gauge quark propagator in full QCD, and extend our previous work [B+05] to a finer lattice with lattice spacing $a = 0.09$ fm [A+04a] but similar physical volume in order to test whether we are close to the continuum limit for these lattices. The scaling behavior of the momentum space quark propagator is examined by comparing the results on these two lattices. Our results show that there are no significant differences in the wave-function renormalization function and quark mass function on the two sets of lattices. Therefore the scaling behavior is good already at the coarser lattice spacing of $a = 0.12$ fm.

The configurations we use in this study were generated by the MILC collaboration [A+04a, BO01] and are available from the Gauge Connection [GC]. The dynamical configurations have two degenerate light fermions for the u and d quarks and a heavier one for the strange quark. Weighting for the fermion determinants is provided by the so-called, "fourth root trick." While the current numerical results [Dur05] provide compelling evidence that the fourth root trick gives an accurate estimate of the dynamical fermion weight, the formal issue of proving that this provides the determinant of a local fermion action from first principles remains unresolved.

The "Coarse" lattice spacing $a = 0.125$ fm and a wide range of sea-quark masses, with lowest up and down quark mass $m \simeq 16$ MeV about 3 times the physical value. The "fine" lattice spacing $a = 0.09$ fm and the lowest bare quark mass of $m = 14.0$ MeV about 5 times the physical value. These two lattices have simliar volume $\geq (2.5\,\mathrm{fm})^3$ [A+05].

Table 7.1: Lattice parameters used in this study. The dynamical configurations each have two degenerate light quarks (up/down) and a heavier quark (strange). The light bare quark masses for the $28^3 \times 96$ lattice are 14.0 MeV and 27.1 MeV with a strange quark mass of 67.8 MeV. For the $20^3 \times 64$ lattice the bare quark masses range from 15.7 MeV to 78.9 MeV. The lattice spacing is $a \simeq 0.12$ fm for the $20^3 \times 64$ lattice and $a \simeq 0.09$ fm [A+04a] for the $28^3 \times 96$ lattice.

	Dimensions	β	a	Bare Quark Mass	# Config
1	$28^3 \times 96$	7.09	0.086 fm	14.0 MeV, 67.8 MeV	108
2	$28^3 \times 96$	7.11	0.086 fm	27.1 MeV, 67.8 MeV	110
3	$20^3 \times 64$	6.76	0.121 fm	15.7 MeV, 78.9 MeV	203
4	$20^3 \times 64$	6.79	0.121 fm	31.5 MeV, 78.9 MeV	249
5	$20^3 \times 64$	6.81	0.120 fm	47.3 MeV, 78.9 MeV	268
6	$20^3 \times 64$	6.83	0.119 fm	63.1 MeV, 78.9 MeV	318

7.1.1 Details of the calculation

The MILC configurations were generated with the $\mathcal{O}(a^2)$ one-loop Symanzik-improved Lüscher–Weisz gauge action [LW85]. The dynamical configurations use the AsqTad quark action [Lep99], an $\mathcal{O}(a^2)$ Symanzik-improved staggered fermion action which removes lattice artifacts up to order a^2g^2. The AsqTad action is a good candidate for a fermion action to be used in dynamical simulations [KO99]. The study of the AsqTad action also shows highly improved chiral symmetry.

We refer to the $a = 0.09$ fm lattice as the "fine" lattice and the $a = 0.12$ fm one as the "coarse" lattice.

We explore two light quark masses, $ma = 0.0062$ ($m = 14.0$ MeV) and $ma = 0.0124$ ($m = 27.1$ MeV). The bare strange quark mass was fixed at $ma = 0.031$, or $m = 67.8$ MeV for $a = 0.09$ fm. The values of the coupling and the bare light quark masses are matched such that the lattice spacing is held constant. The simulation parameters are summarized in Table 7.1 with the lattice spacings taken from [A+04a].

7.1.2 Heavy and light quark scaling behavior

Here we work on two lattices with different lattice spacing but similar physical volume. We compare the wave-function renormalization function $Z(q^2)$ and mass function $M(q^2)$ for two lattices with different lattice spacing a in full lattice QCD.

In Fig. 7.1, we show the quark propagator from the fine lattice for full QCD (light sea-quark mass and valence quark mass equal) with the light quark mass set to $m = 27.1$ MeV. This is compared with data from the coarse lattice by a simple linear interpolation from the four different data sets so the running masses are the

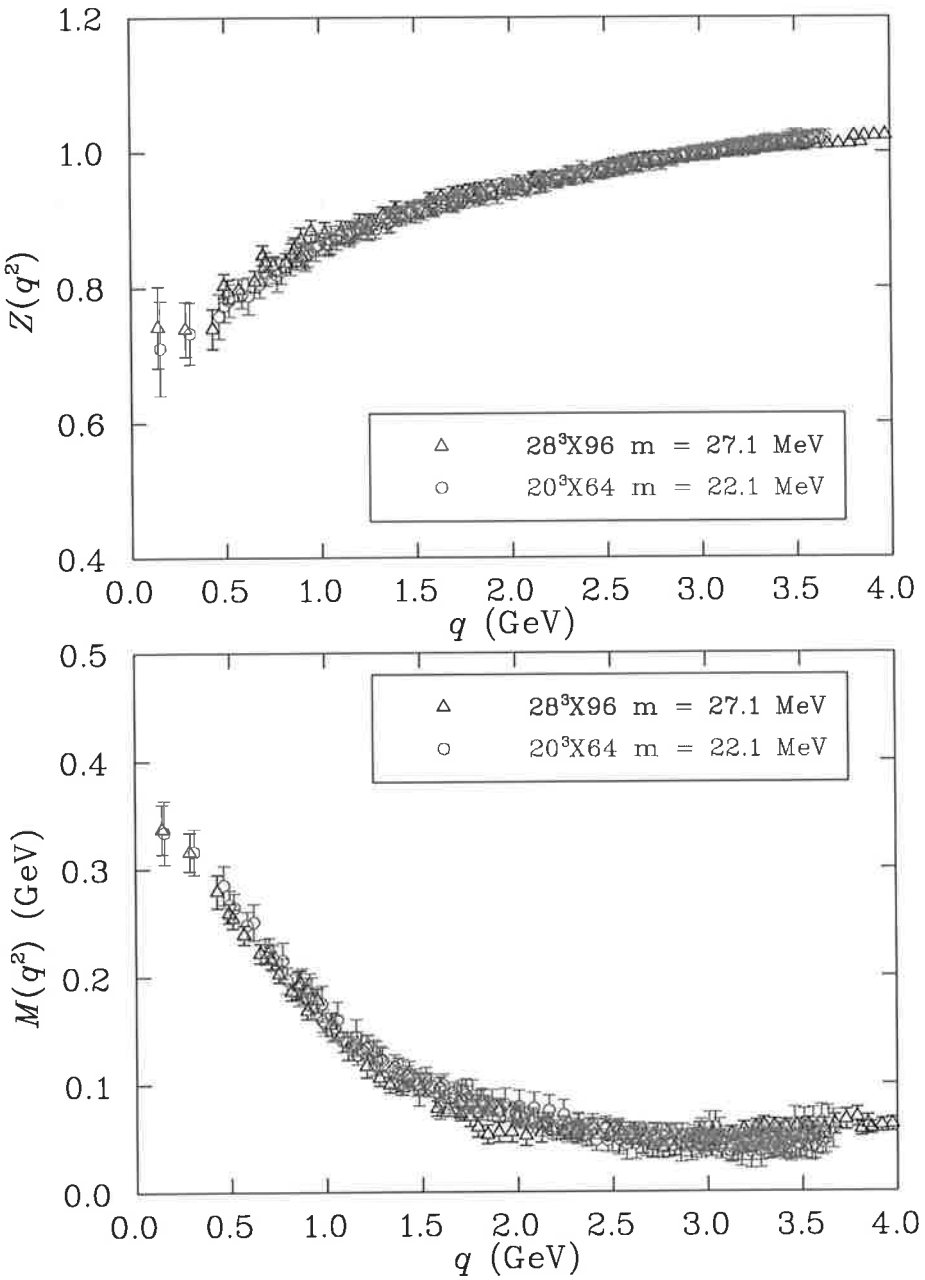

Fig. 7.1: Comparison of wave-function renormalization function $Z(q^2)$ and mass function $M(q^2)$ for two different lattices. Triangles correspond to the quark propagator at bare quark mass $m = 27.1$ MeV from $28^3 \times 96$ with lattice spacing $a = 0.09$ fm. The open circles are the data from $20^3 \times 64$ with lattice spacing $a = 0.12$ fm obtained by interpolating four different set of light quark masses making the $M(q^2)$ value matched for both lattices at $q = 3.0$ GeV. The renormalization point for $Z(q^2)$ is set at $q = 3.0$ GeV for both lattices.

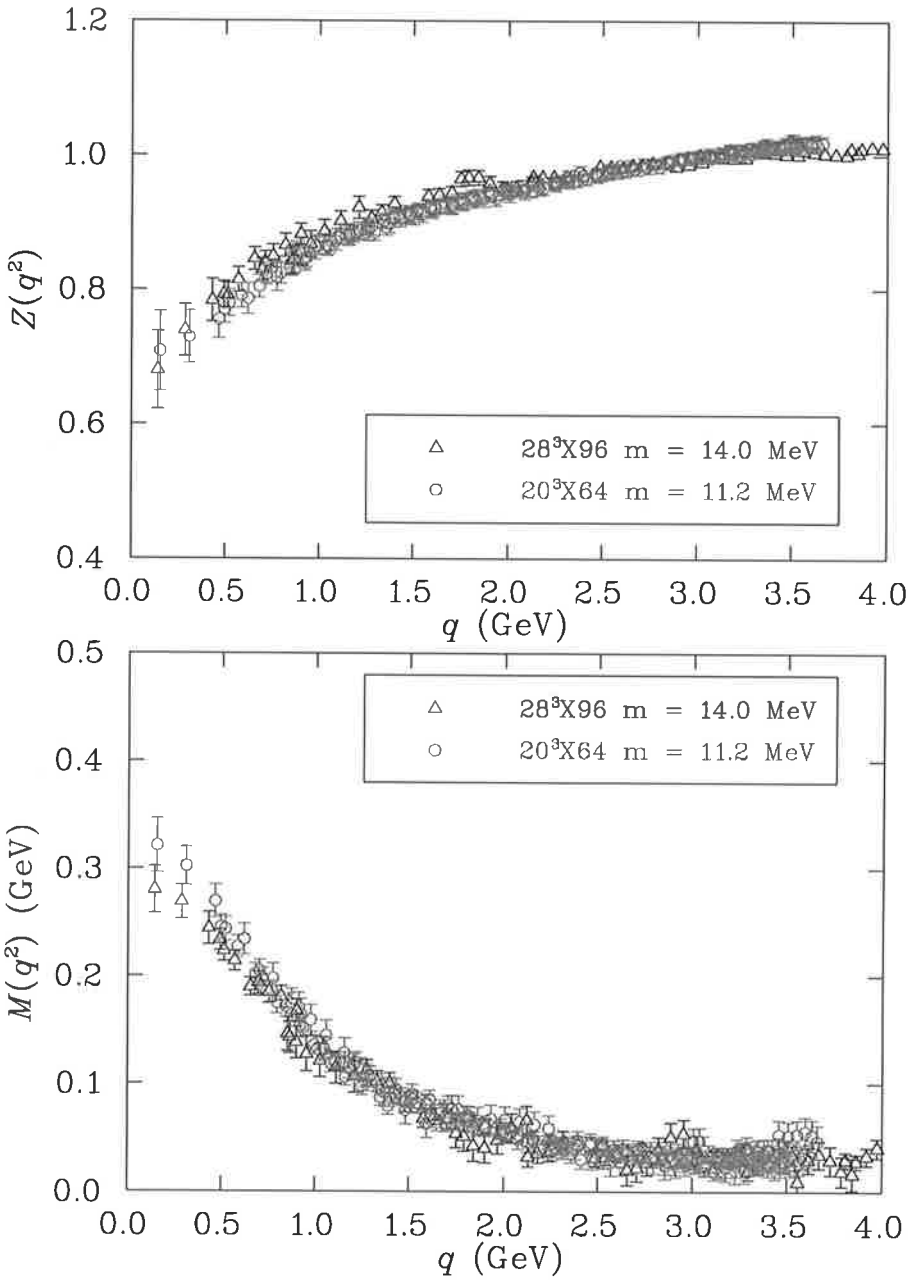

Fig. 7.2: This figure is same as Fig. 7.1, except the light bare quark mass of $28^3 \times 96$ with lattice spacing $a = 0.09$ fm is $m = 14.0$ MeV. The renormalization point is set at $q = 3.0$ GeV for both lattices.

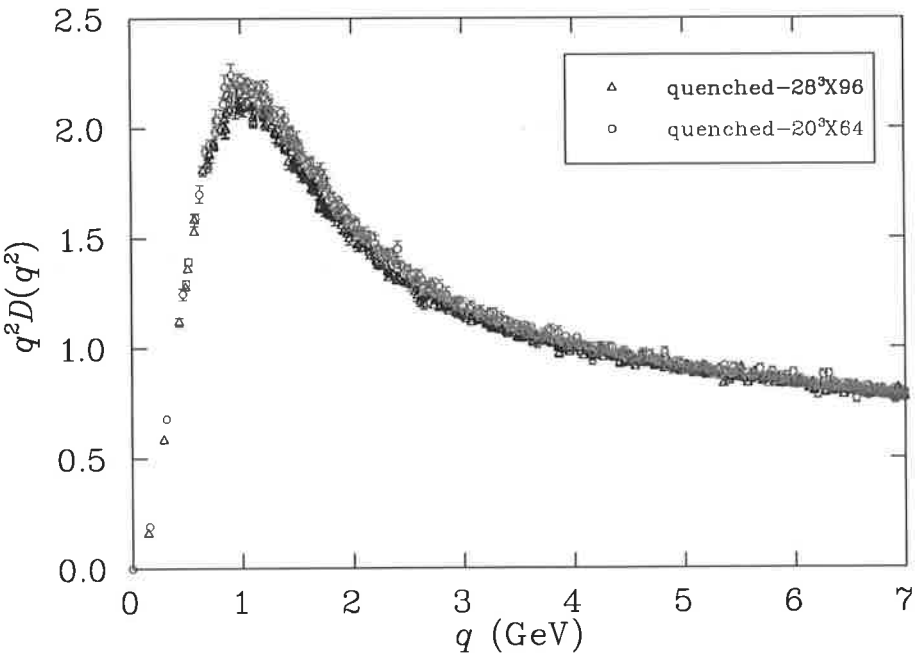

Fig. 7.3: The scaling behavior of gluon propagator dressing function renormalized at $\mu = 4$ GeV for the quenched case. Triangles corresponds to gluon propagator of $28^3 \times 96$ lattice. The open circles is the gluon propagator data from $20^3 \times 64$ lattice. Good scaling is observed.

same at $q^2 = 3.0$ GeV. Good scaling is observed. The wave function renormalization function also shows good scaling behavior. Bare masses are obtained by matching $M(q^2)$ at renormalization point of $q = 3.0$ GeV.

Fig. 7.2 repeats this for the lighter sea quark, $m = 14.0$ MeV. In this case the bare quark masses are lighter, so we are close to chiral limit. The quark propagators are in excellent agreement, showing no dependence on the lattice spacing. Our calculation scaling well suggesting that we are close to the continuum limit.

7.2 Scaling behavior of the gluon propagator

In this study we focus on Landau gauge gluon propagator in full QCD, and extend our previous work [BHL$^+$04a] to a finer lattice with lattice spacing $a = 0.09$ fm [A$^+$04b] and similar physical volume, and study the scaling behavior of the momentum space gluon propagator by comparing the results on these two lattices. The improved computational resources currently available makes this big lattice size simulations possible for gluon propagator. There have been few studies of the scaling behavior of gluon propagator [AdFF02a]. The renormalised propagator should become independent of lattice spacing as we approach the continuum limit [Wil98]. We can see this expected result in our study of scaling behavior of the renormalised

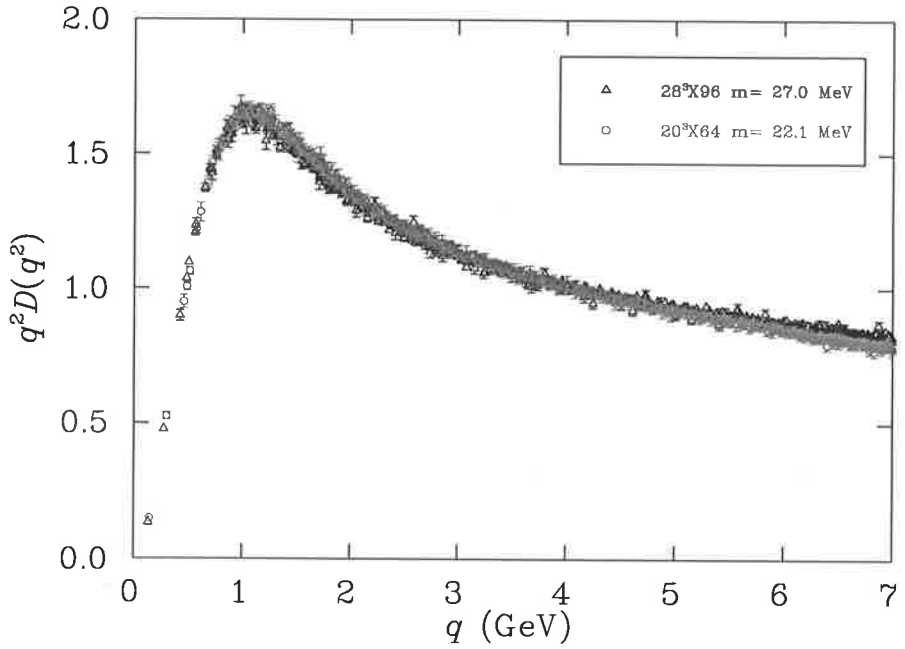

Fig. 7.4: The scaling behavior of the renormalized propagator in full QCD at $\mu = 4$ GeV. Triangles corresponds to gluon dressing function from $28^3 \times 96$ with lattice spacing $a = 0.09$ fm for quark mass $m = 27.0$ MeV. The open circles is the data from $20^3 \times 64$ with lattice spacing $a = 0.125$ fm for quark mass $m = 22.1$ MeV which is matched value calculated from the interpolated data for a set of quark masses. A small violation is seen in the large momentum region.

propagator for the quenched case in Fig. 7.3. Here we work on two lattices with different lattice spacings and similar physical volumes. 150 configurations are used for $28^3 \times 96$ lattice with lattice spacing a =0.09 fm and 192 configurations are used for $20^3 \times 64$ lattice with lattice spacing a =0.125 fm. The propagator is renormalised at $\mu = 4$ GeV. These two sets of data almost lie on the same curve again indicating that good scaling is found for the quenched results.

7.2.1 Heavy and light quark scaling behavior

We now turn to a study of the scaling behavior of the renormalised propagator in full QCD for both lattices. In Fig. 7.4, we are making a comparison for results from $28^3 \times 96$ lattice for light bare quark mass $m = 27.0$ MeV and that from $20^3 \times 64$ lattice with the matched bare quark mass $m = 22.1$ MeV which was obtained fom our previous calculation [P$^+$06b] after interpolating four set of light quark masses. The data agree within error bars. Some very small systematic difference at the highest momenta is suggested, but since this is where the discretization errors will be greatest it is not at all surprising.

We also repeated this full QCD scaling by choosing lighter light quark mass

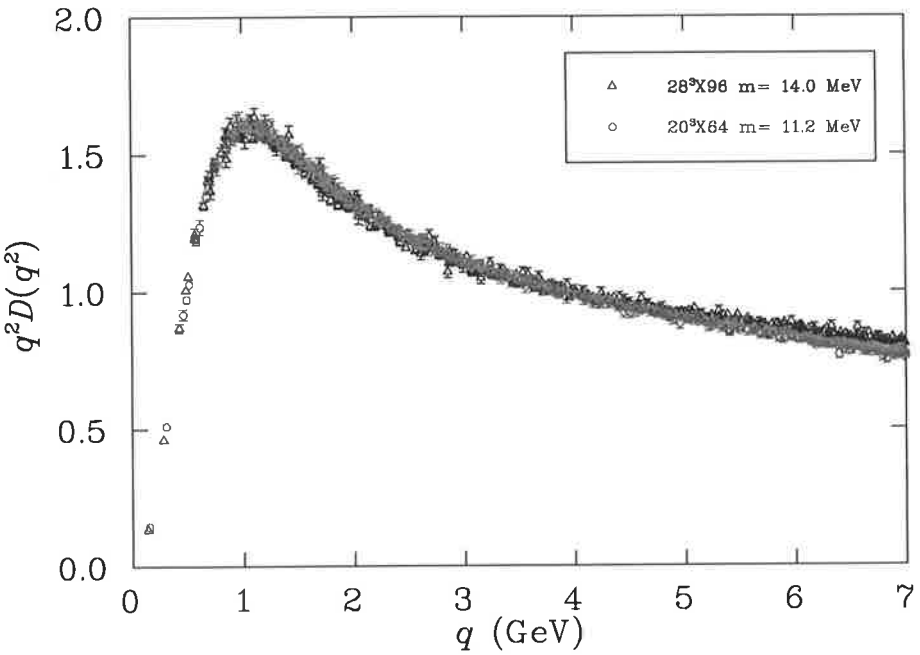

Fig. 7.5: This figure is same as Fig. 7.4, except the bare light quark mass of $28^3 \times 96$ with lattice spacing $a = 0.09$ fm is $m = 14.0$ MeV and that for $20^3 \times 64$ lattice is $m = 11.2$ MeV which is matched to the bare quark mass from the previous calculation

.

$m = 14.0$ MeV for finer lattice and for coarse lattice with matched quark mass $m = 11.20$ MeV calculated from our previous study which is plotted in Fig. 7.5. The unquenched result looks the same as in Fig. 7.4 with a little violation of scaling in large momentum region.

In this study we performed a systematic comparison of the AsqTad quark propagator in full QCD for two lattices with different lattice spacing in order to establish how close these lattices are to the scaling region and hence to the continuum limit.

We compared the two functions $Z(q^2)$ and $M(q^2)$ on fine and coarse lattices and found them to be consistent within errors. We can thus deduce that for both lattices we are close to the scaling region for the quark propagator, which for example makes these lattices suitable for future studies attempting to determine quark masses [BGLM00].

Our comparitive study of gluon propagator on a fine and coarse lattice shows good scaling behavior as well. The addition of quark loops has a clear, quantitative effect on the gluon propagator on the fine lattice in agreement with what is seen on the coarse lattice. Excellent scaling behavior is observed for the gluon dressing function both in quenched and unquenched case. Our calculation demonstrates good scaling for gluon propagator on both lattices in quenched and unquenched QCD.

8

Violation of positivity

Lattice QCD has enjoyed considerable success in predicting the origin of the masses of the strongly interacting particles observed in nature. QCD should be able to predict the bound state spectrum of hadrons built from quarks and gluons, which are confined permanently within the hadrons. Lattice Landau gauge and other related gauge fixing methods are known to violate spectral positivity [AO04]. Gauge fixing is an important technique in studying confinement for lattice studies. As we have seen from previous chapters, the gluon propagator is a gauge dependent quantity. It has been known that non-abelian gauge field propagators show a violation of spectral positivity.

The gluon propagator is the most basic quantity of QCD. There has been considerable interest in the study of the behavior of gluon propagator. The infrared behavior is an excellent probe into the mechanism of confinement [Man99] and as input for many other calculations. The ultraviolet bahavior has been used to calculate the running coupling constant of QCD [B$^+$99]. The gluon propagator is gauge dependent and one needs to fix the gauge to do lattice calculations. Landau gauge is the simplest covariant gauge to implement efficiently on the lattice. It will be interesting to repeat this calculation for the Gribov-copy free Laplacian gauge, but that will be left for a future study.

The infrared behavior of the Green's functions is related to confinement as supported by the studies done in Refs. [LRG02, GLR04]. A detailed non-perturbative study of the gluon propagator is essential to understand the phenomena of confinement. As gluons control the inter-quark dynamics, we expect that gluon propagators will manifest confining behavior in the small momentum region. There has been considerable interest in the possible violation of spectral positivity for QCD and its relation to confinement. The Landau gauge gluon propagator is predicted to vanish at zero momentum [Zwa91, Zwa94]. This implies that the real space propagator violates reflection positivity. There are earlier indications of the non-positivity of the gluon spectral density from the two sources of non-perturbative results, lattice simulations [FN04] as well as from the DSE studies [AvS01].

Correlation functions play an important role in non-perturbative studies of the gluon propagator and confinement. One possible manifestation of confinement is that the correlation functions are given by entire functions in the momentum space, *i.e.*, no singularities are present in any region of the complex p^2-plane of the 2-point correlation functions.

We perform studies of the positivity of the gluon spectral function in Landau gauge in quenched QCD as well as in full QCD. We find a violation of spectral positivity for the gluon propagator in both cases. The positivity test also shows good scaling on our comparison of the real space propagator on two different sets of lattices with different lattice spacing.

8.1 The covariant description of confinement

Covariant quantum theories of gauge fields require indefinite metric spaces [vSA00]. This implies that apart from positivity, most other properties of a local quantum field theory, and most important properties of Green's functions and amplitudes, remain valid in such a formulation [AvS01]. In QCD, colored states are expected to exist in the indefinite metric space of asymptotic states.

We know from perturbation theory that covariant gauges contain states of negative norm. Ignoring the positivity of the representation space implies some modifications to the standard framework of quantum field theory. These modifications to the standard framework of quantum field theory are necessary to accomodate confinement in QCD.

8.2 Gluon confinement and positivity

We have seen from Chapter 2 that Wightman functions contain important informations and from them the Hilbert space can be constructed (recall the reconstruction theorem). Wightman used positive energy to formulate analytic continuation of expectation of Minkowski field theories to Euclidean space. The reconstruction of Garding-Wightman quantum field theory from the corresponding Euclidean Greens function is possible if and only if they obey the Euclidean Osterwalder-Schrader axioms [TCM05]. Among the axioms, a fundamental role is played by the axiom of reflection positivity which is a requirement for establishing the Euclidean counterpart to the positive definiteness of the norm in the Hilbert space of the corresponding Garding-Wightman quantum field theory. This positivity condition involves the arbitrary partial sums of the n-point correlation function [AvS01]. This axiom for the special case of 2-point correlation function $\tilde{D}(x-y)$, is

$$\int d^4x d^4y f^*(-x_0, \boldsymbol{x}) \tilde{D}(x-y) f(-y_0, \boldsymbol{y}) \geq 0\,, \tag{8.1}$$

where $f(-x_0, \boldsymbol{x})$ is a fast decreasing complex test function, a so-called Schwartz function and f^* is its complex conjugate. For more details see section 5.3.4 of [AvS01]. This is the necessary and sufficient condition for the existence of $K\ddot{a}llen-Lehmann$ representation of $\tilde{D}(x-y)$, *i.e.*, a spectral representation of the propagator with positive spectral function. In other words this condition is necessary for interpreting the fields in terms of stable particles. Thus, a violation of Eq. (8.1) implies that the Euclidean 2-point function cannot represent the correlation of a physical particle. This can be viewed as one manifestation of confinement.

The connection between positivity and the Euclidean correlation function is specified clearly in [A+97]. The spectral representation for the Euclidean propagator

$D(p)$ in momentum space can be written as

$$D(p^2) = D(p_0^2, \vec{p}^{\,2}) = \int_0^\infty ds \frac{\rho(s)}{p^2 + s} \quad , \text{where } p^2 = p_0^2 + \vec{p}^{\,2} \,. \tag{8.2}$$

The Fourier transform is

$$D(t, \vec{p}^{\,2}) = \int_{-\infty}^{\infty} \frac{dp_0}{2\pi} D(p_0^2, \vec{p}^{\,2})\, e^{ip_0 t} \,. \tag{8.3}$$

Inserting Eq. (8.2) in the Fourier transform of the Euclidean propagator (Eq. (8.3)), and making use of the fact that

$$\int_{-\infty}^{\infty} \frac{dp_0}{2\pi} \frac{e^{-ip_0 t}}{p_0^2 + \omega^2} = \frac{1}{2\omega} e^{-\omega t} \,, \text{with } \omega = \sqrt{\boldsymbol{p}^2 + s} \,, \tag{8.4}$$

we can then obtain

$$D(t, \vec{p}^{\,2}) = \int_0^\infty ds\, \rho(s) \frac{1}{2\omega} e^{-\omega t} \,. \tag{8.5}$$

Since $s = \omega^2 - \vec{p}^{\,2}$, it follows that $ds = 2\omega d\omega$. Substituting for s and ds in Eq. (8.5), we find

$$D(t, \vec{p}^{\,2}) = \int_{\sqrt{\boldsymbol{p}^2}}^\infty d\omega\, \rho(\omega^2 - \boldsymbol{p}^2)\, e^{-\omega t} \,. \tag{8.6}$$

For a positive spectral function we have by definition, $\rho(s) \geq 0$ and hence we see that $D(t, \vec{p}^{\,2}) \geq 0$ from which Eq. (8.1) readily follows and vice versa. Thus the statement of reflection positivity is equivalent to a positive spectral density $\rho(s)$. This implies that the temporal correlator at zero spatial momentum $D(t, \boldsymbol{p} = 0)$ can be written as

$$C(t) \equiv D(t, 0) = \int_0^\infty d\omega\, \rho(\omega^2)\, e^{-\omega t}. \tag{8.7}$$

The behavior of $D(t, \boldsymbol{p} = 0)$ provides direct insight into mass-like properties associated with the fields. A positive density $\rho(\omega^2)$ clearly implies that

$$C(t) > 0 \,. \tag{8.8}$$

Having $C(t) > 0$ for all t does not guarantee the positivity of $\rho(\omega^2)$ [CMT05]. On the other hand, finding $C(t) < 0$ for some value of t implies that $\rho(\omega^2)$ can not be positive for all ω^2 suggesting confinement for the corresponding particle.

It is obvious from Eq. (8.2) that for a free particle of mass m, one has

$$\rho(s) = \delta(s - m^2) \tag{8.9}$$

and hence from Eq. (8.5), we obtain

$$\begin{aligned} C(t) \equiv D(t,0) &= \int_0^\infty ds\, \delta(s-m^2) \frac{1}{2\omega}\, e^{-\omega t} \\ &= \int_0^\infty 2\omega d\omega \frac{1}{2\omega}\, e^{-\omega t}|_{s=m^2} \\ &= -\frac{1}{m} e^{-mt}\,. \end{aligned} \tag{8.10}$$

It is easy to see from Eq. (8.10), that the Schwinger function decays exponentially

$$C(t) \backsim e^{-mt}\,, \tag{8.11}$$

and is positive definite. Therefore a free propagator satisfies reflection positivity.

8.3 Violation of reflection positivity

An infrared suppressed propagator always violates reflection positivity [AvS01]. This follows from Eq. (8.2), where we observe that the only way of inducing a decrease of $D(p^2)$ with decreasing p^2 is by having $\rho(s)$ take negative values for some range of s. Indeed, we will see numerical evidence for this simple observation in this study. The positivity violation in the spectral function of the propagator leads to the color confinement of degrees of freedom. If a certain degree of freedom has negative norm contributions in its propagator, it can not describe a physical asymptotic state. Therefore negative norm contributions to the spectral function signal the absence of asymptotic states from the physical part of the state space of QCD and is a sufficient condition for the confinement.

On the lattice , the real space propagator can be evaluated using the discrete Fourier transform

$$C(t) = \frac{1}{N} \sum_{k_0=0}^{N-1} e^{-2\pi i k_0 t/N}\, D(p_0, 0)\,, \tag{8.12}$$

where N is the number of points per lattice side, p_0 is the Euclidean time component of the lattice momentum, k_0 is an integer and $D(p_0)$ is the propagator in momentum space.

When a real space propagator $C(t)$ (Schwinger function) becomes negative, reflection positivity becomes violated, which means that gluon is confined and no more a physical particle. Such a violation of positivity is considered as a sufficient condition of confinement [FN04].

8.4 The results

The MILC configurations were generated with the $\mathcal{O}(a^2)$ one-loop Symanzik improved [Sym83] Lüscher–Weisz gauge action [LW85]. We use configurations generated by MILC collaboration available from the Gauge Connection [GC]. The dynamical configurations use the "AsqTad" quark action, an $\mathcal{O}(a^2)$ Symanzik improved staggered fermion action. The coupling β and the bare sea-quark masses are matched such that the lattice spacing is held constant. The lattices we considered all have the similar physical volumes. The parameters are summarized in Table 7.1.

8.4.1 Evidence for violation of positivity

It has been demonstrated in quenched QCD that the gluon propagator violates spectral positivity [AO03]. The explicit evidence for the non-positivity of the real space lattice Landau gauge propagator in three-dimensional pure $SU(2)$ case is found in [CMT05]. We investigate the positivity violation case in full QCD on a fine lattice. First we give the result for the $20^3 \times 64$ lattice for both quenched and unquenched case. In Fig. 8.1, the real space propagator $C(t)$ for $20^3 \times 64$ lattice plotted as a function of dimensionful t for a set of sea quark masses in unquenched case and quenched case. It is clear that positivity is convincingly violated in both cases.

In Fig. 8.2, the real space propagator $C(t)$ for the $28^3 \times 96$ lattice is plotted as a function of dimensionful t for a set of sea quark masses in full QCD and in the quenched case. It shows that the real space propagator $C(t)$ is negative for a range of values of t, showing a violation in positivity.

Next, we aim to study the analytic structure of the gluon propagator in the time like momentum by taking the absolute value of the Schwinger function in unquenched QCD. This is the first result for positivity violation for the gluon propagator with the effect of dynamical fermions. Compelling evidence for the non-positivity of the gluon propagator has been presented in the $SU(2)$ case and in the three-dimensional Yang-Mills theory [LRG02, CMT03]. In Fig. 8.3, we are doing a comparison study of the absolute value of the Schwinger function from our full and quenched QCD simulations with the numerical results from DSE calculations. It is clear from the figure that the zero crossing occurs at $t \approx 5\,\mathrm{GeV}^{-1} \approx 1$ fm. This is roughly the size of the hadron and hence the correct scale at which the gluon screening should occur. As our bare quark mass is the heaviest $m = 63.0$ MeV, our zero crossing slightly deviates from $t \approx 5\,\mathrm{GeV}^{-1}$ which is in accord with the $N_f = 0$ result from the DSE calculation. The result is consistent, as the bare quark mass increases, the result will move towards the quenched case. The comparison of the quenched result ($N_f = 0$) shows similar behavior.

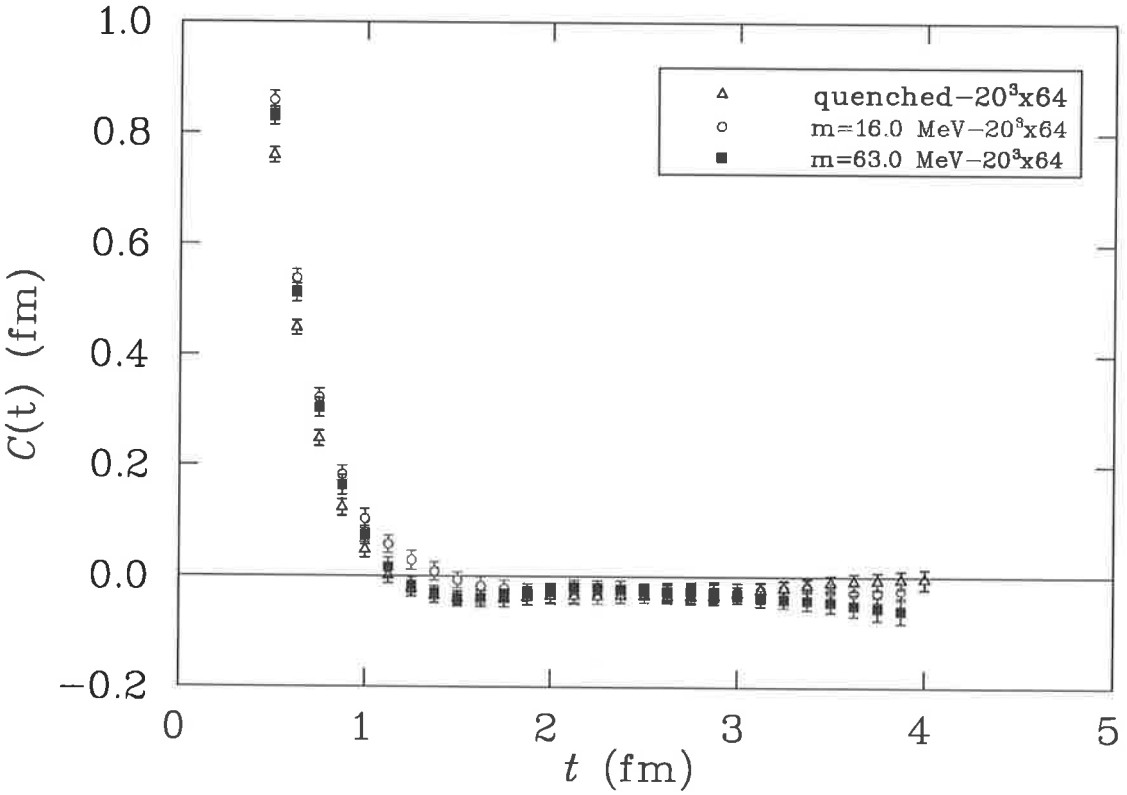

Fig. 8.1: The real space propagator $C(t)$ for $20^3 \times 64$ lattice plotted as a function of dimensionful t for two bare light sea quark masses in unquenched and quenched cases. It is clear from the plot that positivity is violated in both cases.

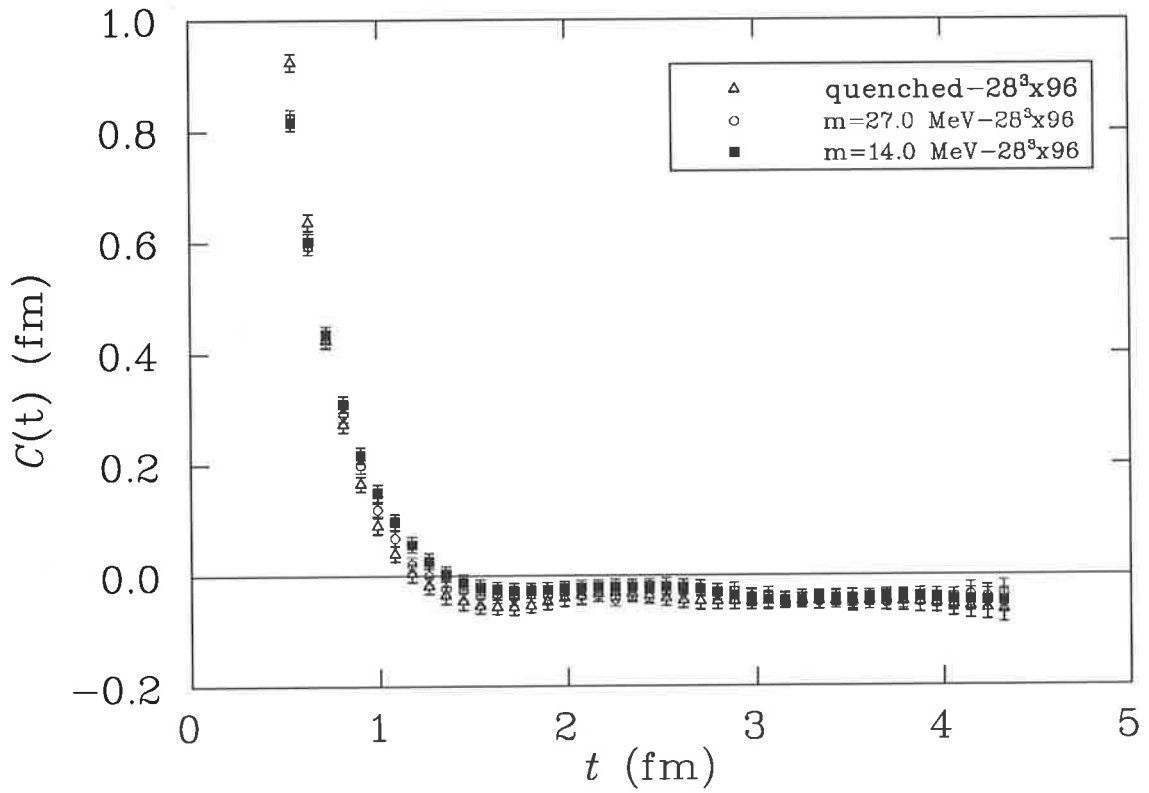

Fig. 8.2: The real space propagator $C(t)$ for $28^3 \times 96$ lattice plotted as a function of dimensionful t for two bare light sea quark masses in unquenched and quenched cases. It is clear from the plot that $C(t)$ is negative for a range of values of t.

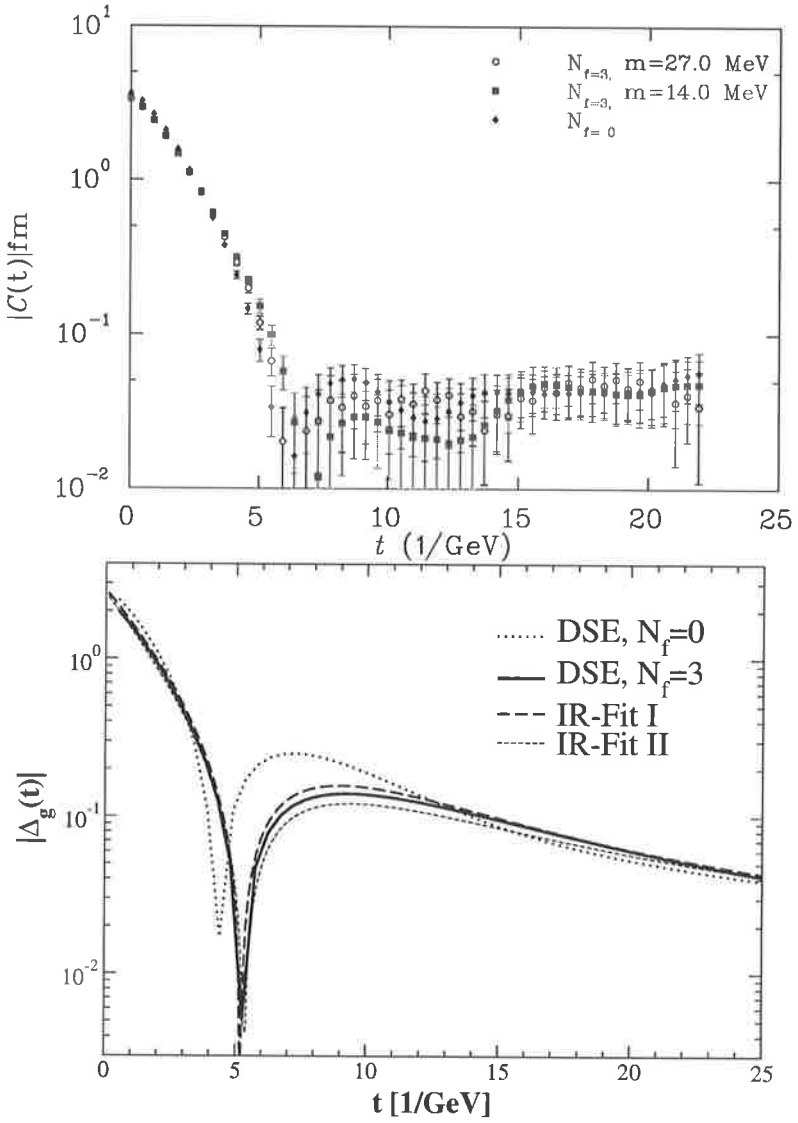

Fig. 8.3: The top figure corresponds to the absolute value of the gluon Schwinger function from our fine lattice calculations in quenched QCD as well as in full QCD. The bare quark masses for full QCD simulations are $m = 63.0$ MeV and $m = 16.0$ MeV respectively. The bottom figure shows the numerical results for the absolute value of the Schwinger function from the DSE result compared to the fits in the infrared. Bottom figure taken from [ADFM04].

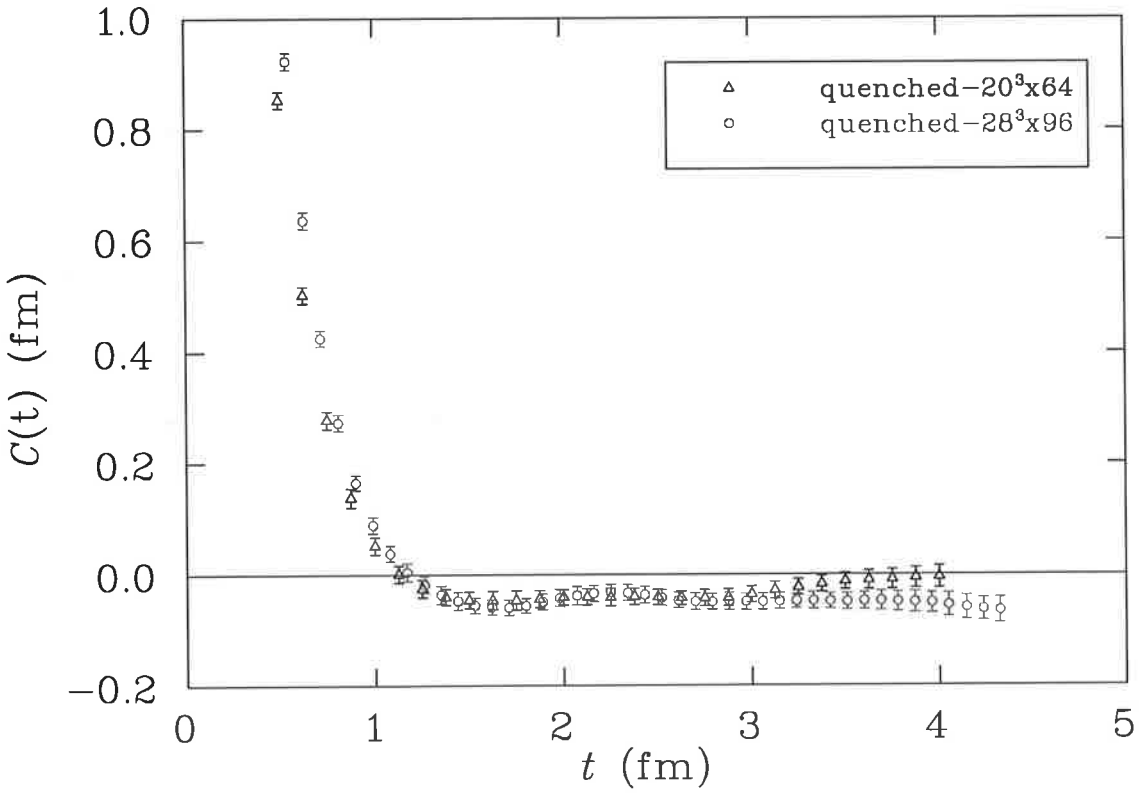

Fig. 8.4: The scaling behavior of the real space propagator $C(t)$ as a function of dimensionful t for two set of lattices in the quenched case. Triangles correspond to $20^3 \times 64$ lattice while open circles correspond to $28^3 \times 96$ lattice. It is clear that $C(t)$ is negative for medium and large values of t and violates positivity. Good scaling is observed for the quenched case.

8.4.2 Scaling violation in positivity

We now turn to study the scaling behavior of the real space Landau gauge gluon propagator. We have calculated the real space propagator on a fine and coarse lattices and thereby analysed a scaling of violation in positivity of both cases. In Fig. 8.4, we studied the real space propagator $C(t)$ as a function of dimensionful t for two set of lattices in quenched case. Triangles corresponds to $20^3 \times 64$ lattice while open circles corresponds to $28^3 \times 96$ lattice. It is clear that $C(t)$ is negative for medium and large values of t and violates positivity. Good scaling is observed for the quenched case. In Fig. 8.5, the unquenched real space propagator from both lattices plotted as a function of dimensionful t. A reflection positivity violation has already been observed in the unquenched gluon propagator [FN05]. Our unquenched lattice simulation result for both lattices also agree as seen in Fig. 8.5. The filled triangles correspond to $C(t)$ for light quark mass $m = 27.1$ MeV from the $28^3 \times 96$ lattice. The open circles correspond to $C(t)$ data obtained by interpolating four sets of light quark masses from the $20^3 \times 64$ lattice by matching the mass function on

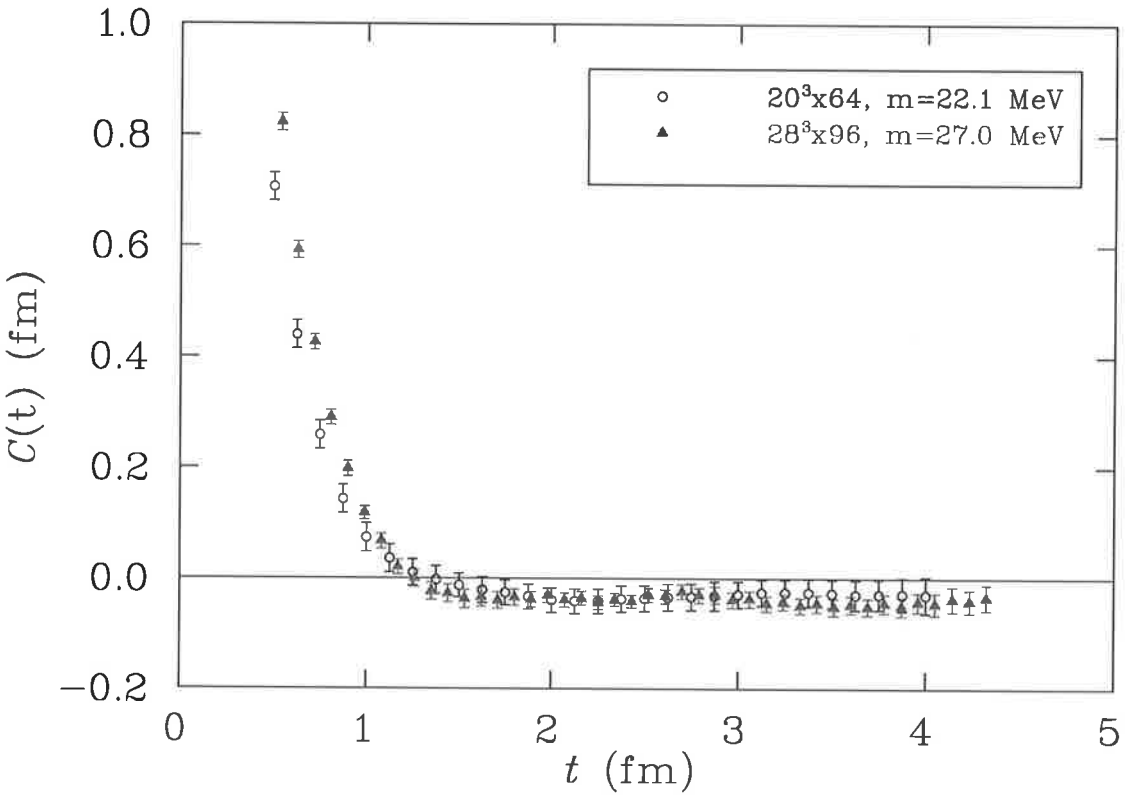

Fig. 8.5: The unquenched real space propagator $C(t)$ from both lattices plotted as a function of dimensionful t. The filled triangles correspond to $C(t)$ for the light quark mass $m = 27.1$ MeV from the $28^3 \times 96$ lattice. The open circles correspond to $C(t)$ data obtained by interpolating four sets of light quark masses from the $20^3 \times 64$ lattice by matching the mass function on two lattices at $q = 4$ GeV which was calculated in Ref. [P$^+$06b]. Good scaling is observed for full QCD as it was for the quenched case.

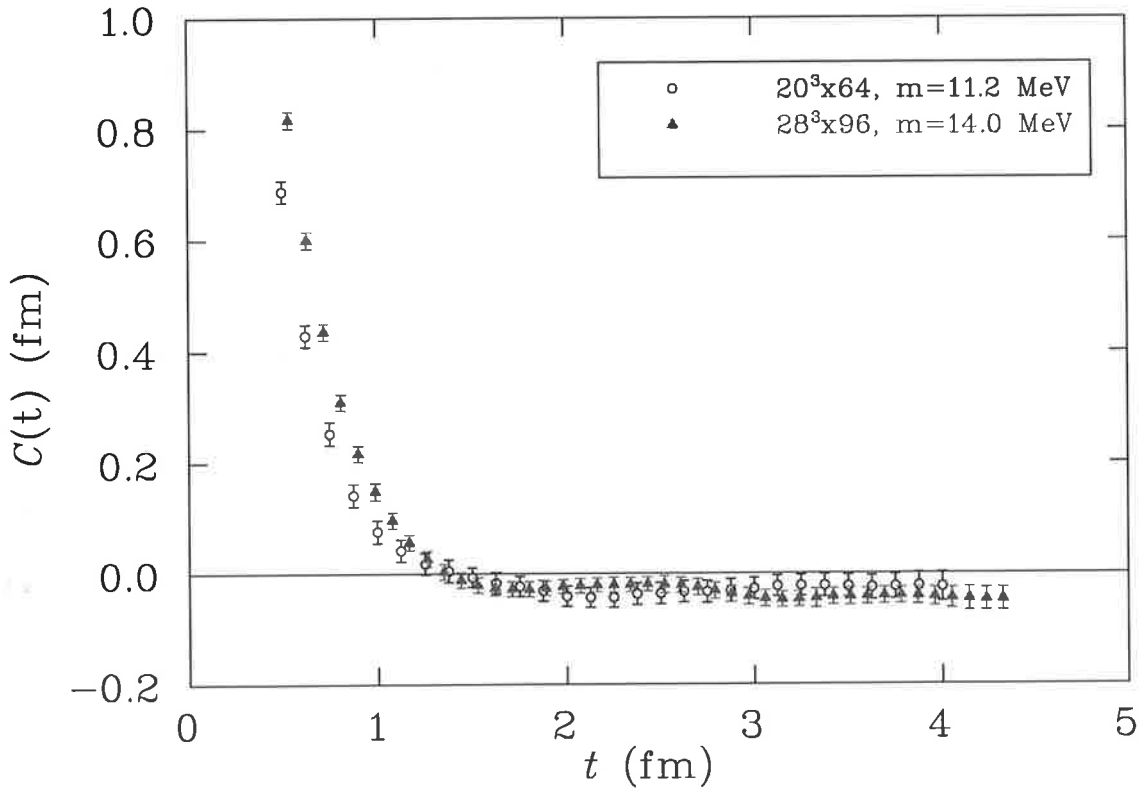

Fig. 8.6: This figure is same as Fig 8.5 except that here the light bare quark mass is $m = 14.0$ MeV for $28^3 \times 96$ lattice. While very small scaling violtions may be inferred, the scaling is on the whole very good.

two lattices at $q = 4$ GeV which was calculated in Ref. [P+06b]. We also studied the scaling behavior of the real space propagator in the unquenched case for the lightest bare sea quark mass for the $28^3 \times 96$ lattice which is $m = 14.0$ MeV, (see Fig. 8.6).

So in summary, we have seen good scaling for the real space propagator. The violation of positivity of the gluon propagator has been investigated by calculating and analyzing the real space propagator both in quenched and unquenched cases. The Landau gauge gluon propagator displays positivity violation. Our results signal a strong violation of reflection positivity for the gluon propagator both in quenched and full QCD. We have also calculated the real space propagator on a fine and coarse lattice to verify whether the non-positivity behavior of the real space propagator is scaling approximately. We have found resonable scaling in the reflection positivity violation of the real space propagator.

9

Conclusions

Quantum Chromodynamics (QCD) provides the framework for the understanding of the strong interactions. To date it has provided a very successful theory which has been tested by confronting experiment in both the perturbative and non-perturbative regimes. The ultimate aim of lattice QCD simulations is to numerically resolve the dynamics of quarks and gluons inside the nucleon and to either verify or disprove that QCD is indeed the fundamental theory of the strong interactions.

The gluon dynamics clearly depends on the sea-quarks. Most numerical simulations in the past have been done in "quenched approximation," where the determinant is simply replaced by one. To study the effect of all fermion loops, we have done simulations in "full QCD," where the sea-quark masses and valence quark masses are equal.

Full QCD simulation is the current critical task of lattice QCD. Simulating with dynamical sea-quarks enables us for the first time, to study hadron physics based on the principles of QCD without any approximation. Up to now most intensive studies have been done in the quenched approximation. Moreover, quenched approximation is one of the main sources of systematic uncertanties in lattice calculation.

It has been a long standing goal to perform non-perturbative simulations in full QCD. We have used configurations generated by the MILC collaboration and available from the "NERSC Gauge Connection" to achieve this goal. The development in recent years of an improved staggered fermion formulation has made full QCD lattice simulations possible. Employing an improved staggered formalism, the so-called "AsqTad" fermions, simulations with the light u and d quarks, taken to be of equal mass, as light as $\frac{1}{8}$ of the physical strange quark mass have been achieved by MILC, while the mass of the third quark flavor has been kept close to the strange quark mass [Hel06].

Unquenched calculations are done with improved staggered quarks. Numerical simulations of dynamical fermions within the framework of the staggered formalism are both computationally less expensive and phenomenologically successful. Using the staggered fermion formulation, various collaborations have performed high-precision lattice QCD calculations that are in excellent agreement with experimentally known measurements. However, this success is clouded by the problematic issue of the validity of the fourth root trick. Though, Wilson fermions avoids the theoretical uncertanity involved with the fourth root trick, it demands greater computational cost since the lattice spacing needs to be much finer.

Many non-perturbative studies have been done for the gluon and quark propagator in quenched QCD. However, for technical and computational reasons, simulations with dynamical sea-quarks could not be performed before. We have calculated the fundamental quantities of QCD with the effects of three light quark flavors. First we have calculated the gluon propagator with the effect of $2+1$ flavors of dynamical

sea-quarks using MILC configurations generated with the $\mathcal{O}(a^2)$ one-loop Symanzik improved [Sym83] Lüscher–Weisz gauge action [LW85]. The dynamical configurations use the "AsqTad" quark action, an $\mathcal{O}(a^2)$ Symanzik improved staggered fermion action. We performed simulations on a $20^3 \times 64$ lattice with lattice spacing $a = 0.125$ fm with lighter up, down and strange quark masses. For a comparitive study of quenched and unquenched gluon propagators, we also computed the gluon propagator in quenched QCD as well. The unquenching effect on the gluon propagator is clearly visible. We found compelling evidence that adding fermion loops slightly supresses the non-perturbative effects of the gluon loops. The screening of dynamical sea quarks brings the $2+1$ flavor results significantly closer to the tree-level form. We also studied the sea-quark mass dependence of the Landau gauge gluon propagator by analysing the gluon dressing function for the lightest and for the heaviest u and d quark masses in our set. These correspond to bare light-quark masses of $\simeq$ 16 MeV and $\simeq$ 63 MeV respectively; a factor of four difference. The bare strange-quark mass is the same in both cases ($\simeq$ 79 MeV). We found that as the sea-quark mass increases, the result moves toward the quenched result which is expected.

The effects of dynamical sea-quarks were also studied on the quark propagator. We have calculated the quark propagator in momentum space using the AsqTad improved lattice fermion action which removes tree-level lattice artifacts to order (a^2), in quenched, partially quenched and unquenched QCD. We have seen that the AsqTad action provides the quark propagator with an improved rotational symmetry. We have calculated the wave-function renormalization function and mass function for a variety of sea-quark masses for both quenched and unquenched QCD. We also have compared the scalar functions for the quenched and dynamical propagators. For a given bare mass, the running mass depends upon both the number of dynamical quark flavors and their masses. To make the most appropriate comparison, we have selected a bare quark mass for the quenched case ($ma = 0.01$) and interpolated it with the dynamical mass function so that it agrees with the quenched result at the renormalization point, $q = 3$ GeV. We have found that the mass functions do reveal the effects of dynamical quarks. Dynamical mass generation is suppressed, in the infrared, in the presence of dynamical quarks relative to that observed in the quenched case. For the renormalization functions, there is no discernible difference between the quenched and unquenched cases. As for the gluon, the presence of dynamical quark loops has the effect of moving the mass function closer to its tree-level form.

Our QCD simulations with $2+1$ flavors of quarks clearly indicate the effects of dynamical quarks on the gluon and quark propagators. Our studies indicate that the effect of dynamical sea-quarks is greater on the gluon propagator than on the quark propagator. We have found compelling evidence for the effect of dynamical chiral symmetry breaking in the mass function. The scaling behavior of the AsqTad quark propagator has also been studied by extending the calculation to a finer lattice with lattice spacing $a = 0.09$ fm. We have also compared the mass function and wave-

renormalization function on two lattices with similar physical volume, with different lattice spacing a, with and without the effects of dynamical sea-quarks. The quark propagator from the fine lattice for full QCD (light sea-quark mass and valence quark mass equal) with the light quark mass set to $m = 27.1$ MeV, is compared with data from the coarse lattice by a simple linear interpolation from the four different data sets, so the running masses are the same at $q^2 = 3.0$ GeV. Good scaling is observed. The wave function renormalization function also shows good scaling behavior. Bare masses are obtained by matching $M(q^2)$ at renormalization point of $q = 3.0$ GeV. We found that the quark propagators are in excellent agreement, showing no discernbile dependence on the lattice spacing.

The statement that quarks and gluons are confined is an observational one, in that, to date no free quarks and gluons have ever been seen. The development of a detailed understanding of the confinement of quarks and gluons in QCD is a difficult problem. We have addressed the gluon confinement problem in this thesis by testing the positivity violation of the gluon propagator. We have demonstrated that the gluon propagator obtained from both quenched and unquenched lattices violates the Osterwalder-Schrader reflection positivity, which we can regard as a signal for confinement.

Quark and gluon propagators are two of the three non-perturbative quantities used as an input of DSE quark propagator calculation. One of the major goals of lattice QCD is the calculation of hadron masses from first principles. We have presented the first results for the quark propagator on a fine lattice with the AsqTad action. Our results for the quark propagator on a coarser lattice have recently been confirmed by [FN06]. We compared mass and wave-functions renormalization function on a fine and coarse lattice in which the effects of $2 + 1$ dynamical quark flavors are taken into account. We find that $Z(q^2)$ and $M(q^2)$ agree on both lattices indicating good scaling behavior for $a \leq 0.125$ fm. A scaling behavior study for gluon propagator is also performed on these lattices in a similar way. They are also in good agreement.

We would like to extend the study of quark and gluon propagator to a wider range of dynamical masses to study both the chiral limit and the transition to the quenched limit. In future, studying the quarks and their confinement by extending the present framework will be interesting. A study of the ghost propagator on fine lattice in unquenched QCD is currently underway.

Notations and conventions

Throughout this thesis, I use the natural units $\hbar = c = 1$ where $\hbar = h/2\pi$ with h the Planck constant and c the velocity of light. Energies and masses are given in GeV where 1 GeV $= 1.602 \times 10^{-7}$J. It is convenient to note that

$$1\,\mathrm{fm} = \frac{(\hbar c)}{0.197328\,\mathrm{GeV}} \tag{A.1}$$

Our metric in Minkowski space $\{x^\mu : \mu = 0, 1, 2, 3\}$ is given by

$$g^{\mu\nu} = \begin{pmatrix} 1 & 0 & 0 & 0 \\ 0 & 1 & 0 & 0 \\ 0 & 0 & -1 & 0 \\ 0 & 0 & 0 & -1 \end{pmatrix} \tag{A.2}$$

with

$$g^{00} = +1 = g^{11} = g^{22} = g^{33} = -1, \quad \text{otherwise} = 0. \tag{A.3}$$

The contravariant vectors of space-time coordinate and energy-momentum are given by

$$x^\mu = (ct, \boldsymbol{r}),\ p^\mu = (E/c, \boldsymbol{p}), \tag{A.4}$$

where t and $\boldsymbol{r}$ are the time and space coordinate respectively and E and $\boldsymbol{p}$ are the energy and momentum. Bold-faced symbols here represent three dimensional vectors. The contravariant vectors are

$$\begin{aligned} x_\mu &= g_{\mu\nu} x^\nu = (ct, -\boldsymbol{r}) \\ p_\mu &= g_{\mu\nu} p^\nu = (E/c, -\boldsymbol{p}). \end{aligned} \tag{A.5}$$

The contravariant vector of space and time differentiation is defined as

$$\partial^\mu \equiv \frac{\partial}{\partial x_\mu} = \left(\frac{\partial}{\partial t}, -\nabla\right), \tag{A.6}$$

with ∇ the gradient operation in three dimensional space.

A.1 Dirac matrices

The Dirac gamma matrix γ^μ, with $\mu = 0, \cdots, 3$ in Minkowski space satisfies the anticommutation relations

$$\{\gamma^\mu, \gamma^\nu\} = 2g^{\mu\nu}, \quad \gamma_5^2 = 1 \tag{A.7}$$

The matrix γ_5 is defined by

$$\gamma_5 = i\gamma^0\gamma^1\gamma^2\gamma^3 \tag{A.8}$$

and anticommutes with all γ^μ:

$$\{\gamma_5, \gamma^\mu\} = 0. \tag{A.9}$$

We use chiral basis for representation of the gamma matrices in this thesis. The Minkowski-space matrices are given by

$$\gamma^0 = \begin{pmatrix} 0 & 0 & -1 & 0 \\ 0 & 0 & 0 & -1 \\ -1 & 0 & 0 & 0 \\ 0 & -1 & 0 & 0 \end{pmatrix}, \quad \gamma^1 = \begin{pmatrix} 0 & 0 & 0 & 0 \\ 0 & 0 & 1 & 0 \\ 0 & -1 & 0 & 0 \\ -1 & 0 & 0 & 0 \end{pmatrix},$$
$$\gamma^2 = \begin{pmatrix} 0 & 0 & 0 & -i \\ 0 & 0 & i & 0 \\ 0 & i & 0 & 0 \\ -i & 0 & 0 & 0 \end{pmatrix}, \quad \gamma^3 = \begin{pmatrix} 0 & 0 & 1 & 0 \\ 0 & 0 & 0 & -1 \\ 1 & 0 & 0 & 0 \\ 0 & -1 & 0 & 0 \end{pmatrix},$$
$$\gamma^5 = \begin{pmatrix} 1 & 0 & 0 & 0 \\ 0 & 1 & 0 & 0 \\ 0 & 0 & -1 & 0 \\ -i & 0 & 0 & -1 \end{pmatrix}.$$

The Wick rotation

$$t \to -i\tau, \tag{A.10}$$

transforms vectors from Minkowski-space to Euclidean space with the metric given by the Kronecker symbol $\delta_{\mu\nu}$:

$$\delta_{\mu\nu} = \begin{cases} 1, & \text{for} \mu = \nu \\ 0, & \text{for} \mu \neq \nu. \end{cases} \tag{A.11}$$

and the Euclidean Dirac gamma matrices are chosen to be Hermitean, and are simply denoted by γ_μ^E $(\mu = 1, 2, 3, 4)$, have the properties

$$\{\gamma_\mu^E, \gamma_\nu^E\} = 2\delta_{\mu\nu}. \tag{A.12}$$

The Euclidean γ_5 matrix can be written as

$$\gamma_5^E = -\gamma_1^E \gamma_2^E \gamma_3^E \gamma_4^E \tag{A.13}$$

The connection between the Dirac matrices in Euclidean and Minkowski space is

$$\gamma_{1,2,3}^{\text{Euclidean}} = i\gamma^{1,2,3\,\text{Minkowski}} \tag{A.14}$$

$$\gamma_4^{\text{Euclidean}} = i\gamma^{4\,\text{Minkowski}} \equiv -\gamma^{0\,\text{Minkowski}} \tag{A.15}$$

The Euclidean Dirac gamma matrices are then given by

$$\gamma^4 = \begin{pmatrix} 0 & 0 & 1 & 0 \\ 0 & 0 & 0 & 1 \\ 1 & 0 & 0 & 0 \\ 0 & 1 & 0 & 0 \end{pmatrix}, \quad \gamma^1 = \begin{pmatrix} 0 & 0 & 0 & i \\ 0 & 0 & i & 0 \\ 0 & -i & 0 & 0 \\ -i & 0 & 0 & 0 \end{pmatrix},$$

$$\gamma^2 = \begin{pmatrix} 0 & 0 & 0 & 1 \\ 0 & 0 & -1 & 0 \\ 0 & -1 & 0 & 0 \\ 1 & 0 & 0 & 0 \end{pmatrix}, \quad \gamma^3 = \begin{pmatrix} 0 & 0 & i & 0 \\ 0 & 0 & 0 & -i \\ i & 0 & 0 & 0 \\ 0 & -i & 0 & 0 \end{pmatrix}$$

$$\gamma^5 = \begin{pmatrix} 1 & 0 & 0 & 0 \\ 0 & 1 & 0 & 0 \\ 0 & 0 & -1 & 0 \\ -i & 0 & 0 & -1 \end{pmatrix}.$$

A.2 Lattice notations

Vectors in the discrete space of the lattice theory are always denoted by x. Unit vectors are written as $\hat{\mu}$ with $\mu = 1, \cdots, 4$. and the lattice spacing, a, is usually implicit. If the lattice volume is finite, the lengths L_μ in the direction μ are denoted by L_t and $L_s = L_1 = L_2 = L_3$, where L_t is the lattice size in "time" and L_s in "space" direction. An $L^3 \times L_t$ lattice is considered to mean an L^3 spatial lattice and L_t Euclidean time slices. The spatial volume in lattice units is denoted by $L^3 = L_1 L_2 L_3$. The total number of lattice points is

$$V = L_1 L_2 L_3 L_t. \tag{A.16}$$

Group-theoretic quantities

B.1 The $U(1)$ group

The $U(1)$ group is a special case of the $SU(N)$ groups. It consists of the group of complex numbers on the unit circle.

B.2 The $SU(N)$ groups

The $SU(N)$ group consists of elements isomorphic to the $N \times N$ unitary matrices with unit determinant.

$$U \cdot U^{\dagger} = U^{\dagger} \cdot U\,, \ \det U = 1 \tag{B.1}$$

The matrices U in Eq. (B.1) form the fundamental representation of the $SU(N)$ group.

B.3 The $SU(2)$ group

The standard choice for the generators of the $SU(2)$ group are Pauli matrices.

$$\sigma^1 = \begin{pmatrix} 0 & 1 \\ 1 & 0 \end{pmatrix}, \quad \sigma^2 = \begin{pmatrix} 0 & -i \\ i & 0 \end{pmatrix}, \quad \sigma^3 = \begin{pmatrix} 1 & 0 \\ 0 & -1 \end{pmatrix}. \tag{B.2}$$

These matrices together with the unit matrix,

$$\mathbf{1} = \begin{pmatrix} 1 & 0 \\ 0 & 1 \end{pmatrix}, \tag{B.3}$$

form a basis of the complex 2×2 matrices.

B.4 The $SU(3)$ group

In this thesis, $SU(3)$ group play an important role. For $SU(3)$, $T^a = \frac{\lambda^a}{2}$, with

$$\lambda^j = \begin{pmatrix} \sigma^j & 0 \\ 0 & 0 \end{pmatrix}, \quad j = 1,2,3; \quad \lambda^4 = \begin{pmatrix} 0 & 0 & 1 \\ 0 & 0 & 0 \\ 1 & 0 & 0 \end{pmatrix}, \quad \lambda^5 = \begin{pmatrix} 0 & 0 & -i \\ 0 & 0 & 0 \\ i & 0 & 0 \end{pmatrix},$$

$$\lambda^6 = \begin{pmatrix} 0 & 0 & 0 \\ 0 & 0 & 1 \\ 0 & 1 & 0 \end{pmatrix}, \quad \lambda^7 = \begin{pmatrix} 0 & 0 & 0 \\ 0 & 0 & -i \\ 0 & i & 0 \end{pmatrix}, \quad \lambda^8 = \frac{1}{\sqrt{3}} \begin{pmatrix} 0 & 0 & 0 \\ 0 & 0 & -i \\ 0 & i & 0 \end{pmatrix}$$

We can introduce the matrices C^a with elements $C^a_{bc} = -if_{abc} \equiv -if^{abc}$

$$[T^a, T^b] = i\sum f^{abc}T^c\,, \quad [C^a, C^b] = i\sum f^{abc}C^c \tag{B.4}$$

and anticommutation relations are

$$\{T^a, T^b\} = \sum_c d^{abc}T^c + \frac{1}{3}\delta^{ab}\,. \tag{B.5}$$

The f are totally anti-symmetric, the $d_{abc} \equiv d^{abc}$ are totally symmetric, and the nonzero elements (up to permutations) are as follows:

$$\begin{aligned}
1 &= f_{123} = 2f_{147} = 2f_{246} = 2f_{257} = 2f_{345} \\
&= -2f_{156} = -2f_{367} = \frac{2}{\sqrt{3}}f_{458} = \frac{\sqrt{3}}{2}f_{678}; \\
\frac{1}{\sqrt{3}} &= d_{118} = d_{228} = d_{338} = -d_{888}\,, \\
\frac{-1}{2\sqrt{3}} &= d_{448} = d_{558} = d_{668} = d_{778}\,, \\
\frac{1}{2} &= d_{146} = d_{157} = d_{247} = d_{256} = d_{344} = d_{355} = d_{366} = -d_{377}.
\end{aligned}$$

For an arbitrary $SU(N)$ group, we define the invariants C_A, C_F, T_F by

$$\delta_{ab}C_A = \mathrm{tr}\, C^aC^b = \sum_{cc'} f^{acc'}f^{bcc'},$$

$$\delta_{ik}C_F = \left(\sum_a T^aT^a\right)_{ik} = \sum_{a,l} T^a_{il}T^a_{lk}\,,$$

$$\delta_{ab}T_F = \mathrm{tr}T^aT^b = \sum_{k,i} T^a_{ik}T^a_{kl}.$$

one has

$$C_A = N\,, \quad C_F = \frac{N^2-1}{2N}\,, \quad T_F = \frac{1}{2}. \tag{B.6}$$

Functional derivatives

Some basic results from multivariable calculus has been used in Section 2.3. Recall the identity

$$\int d^n f \delta^{(n)}(\vec{f}) = 1\,, \tag{C.1}$$

where $\vec{f}$ is a vector of real numbers with n components. Consider a situation where $\vec{f}$ is specified in terms of n variables $\vec{x}$, so that $\vec{f} = \vec{f}(x)$. We can make a change of integration variables from f to x in the following way,

$$\int d^n x \delta^{(n)}(\vec{f}(\vec{x})) \left|\det\left(\frac{\partial f_i}{\partial x_i}\right)\right|_{\text{f=0}} = 1\,, \tag{C.2}$$

where we have inserted the Jacobian determinant for this change of variables. This is true as long as $\vec{\text{f}}$ has one zero within the integration range, or equivalently, if this change of variables corresponds to a change of basis.

A functional is an application of the space of sufficiently smooth functions, {f(x)} into the complex numbers:

$$F : f \to F[f]\,.$$

We treat functionals $F[f, g, \cdots]$ in the same way. We may consider a functional as a generalization of an ordinary function in the following sense: divide the space of x values in N cells, and let each x_j lie one in each cell. Then $F[f]$ is the limit for vanishing cell size of $F_N(f_1, \cdots, f_j)$, $f_j \equiv f(x_j)$. The derivative $\frac{\partial F_N}{\partial f_j}$ is

$$\frac{\partial F_N(f_1, \cdots, f_j, \cdots)}{\partial f_j} = \lim_{\varepsilon \to 0} \frac{F_N(f_1, \cdots, f_j + \varepsilon, \cdots) - F_N(f_1, \cdots, f_j, \cdots)}{\varepsilon}\,,$$

i.e., it may be obtained by shifting $f_i \to f_i + \varepsilon\delta_{ij}$. So, in the limit, we can define [Ynd]

$$\frac{\partial F[f]}{\partial \delta f(y)} = \lim_{\varepsilon \to 0} \frac{F[f + \varepsilon\delta_y]}{\varepsilon}\,,$$

where δ_y is the delta function at y : $\delta_y(x) = \delta(x - y)$. For integral functionals:

$$F[f] = \int dx\, K_F(x) f(x);$$

then,

$$\frac{\partial F[f]}{\partial \delta f(y)} = K_F(y)$$

Taylor series can be generalizes to functional series. If $K_n(x_1, \cdots, x_n)$ are symmetric and we consider the functional

$$F[f] = \sum_{n=0}^{\infty} \frac{1}{n!} \int dx_1 \cdots dx_n K_n(x_1, \cdots, x_n) f(x_1) \cdots f(x_n) \,,$$

we may easily verify that

$$K_n(x_1, \cdots, x_n) = \frac{\delta^n F[f]}{\delta f(x_1), \cdots \delta f(x_n)} \,.$$

Functional integration obeys rules analogous to those of ordinary integration. We define, for example,

$$\int \prod_x df(x) F[f] \equiv \lim_{N \to \infty} \int df_1 \cdots df_N F_N(f_1, \cdots, f_N).$$

List of publications

D.1 Refereed journal publications

- "Unquenched gluon propagator in Landau gauge"
  P.O. Bowman, Urs M .Heller, D.B. Leinweber, M.B Parappilly, A.G Williams
  Phys.Rev.D**70**, 034509 (2004)
  arXive: hep-lat/0402032

- "Unquenched quark propagator in Landau gauge"
  P.O. Bowman, Urs M .Heller, D.B. Leinweber, M.B Parappilly, A.G Williams, J.Zhang
  Phys.Rev.D**71**, 054507 (2005)
  arXive: hep-lat/0501019

- "Scaling behavior of quark propagator in full QCD"
  Maria B. Parappilly, Patrick O. Bowman, Urs M. Heller, Derek B . Leinweber, Anthony G. Williams, J.B Zhang
  Phys.Rev.D**73**, 054504 (2006)
  arXive: hep-lat/0511007

D.2 Conference publications

- "QCD propagators : Some Results from the Lattice"
  P.O. Bowman, Urs M .Heller, D.B. Leinweber, M.B Parappilly and A.G Williams
  contributed to the proceedings of theWorkshop on Light-Cone QCD and Non-perturbative Hadron Physics (LC2005), Cairns, Australia, 7-15 July 2005.

- "Recent research higlights from the CSSM"
  B.G. Lasscock, M.B Parappilly, D.B. Leinweber and A.G Williams
  contributed to the proceedings of theWorkshop on Light-Cone QCD and Non-perturbative Hadron Physics (LC2005), Cairns, Australia, 7-15 July 2005.

- " Effects of dynamical sea-quarks on quark and gluon propagators"
  M.B Parappilly, P.O. Bowman, Urs M .Heller, D.B. Leinweber, A.G Williams, J.Zhang
  contributed to the proceedings Particles and Nuclei International Conference (PANIC 05), Santa Fe, New Mexico, 24-28 Oct 2005
  arXive:hep-lat/0601010

D.3 In prepartion

- "Scaling behavior and positivity violation of the gluon propagator in full QCD" M.B Parappilly, P.O. Bowman, Urs M.Heller, D.B. Leinweber, A.G Williams, J.Zhang

E

Refereed journal publications

Unquenched gluon propagator in Landau gauge

Patrick O. Bowman,[1,2] Urs M. Heller,[3] Derek B. Leinweber,[1] Maria B. Parappilly,[1] and Anthony G. Williams[1]
[1]*Special Research Centre for the Subatomic Structure of Matter and The Department of Physics, University of Adelaide, SA 5005, Australia*
[2]*Nuclear Theory Center, Indiana University, Bloomington, Indiana 47405, USA*
[3]*American Physical Society, One Research Road, Box 9000, Ridge, New York 11961-9000, USA*
(Received 12 March 2004; published 19 August 2004)

Using lattice quantum chromodynamics (QCD) we perform an unquenched calculation of the gluon propagator in Landau gauge. We use configurations generated with the AsqTad quark action by the MILC collaboration for the dynamical quarks and compare the gluon propagator of quenched QCD (i.e., the pure Yang-Mills gluon propagator) with that of 2+1 flavor QCD. The effects of the dynamical quarks are clearly visible and lead to a significant reduction of the nonperturbative infrared enhancement relative to the quenched case.

DOI: 10.1103/PhysRevD.70.034509 PACS number(s): 12.38.Gc, 11.15.Ha, 12.38.Aw, 14.70.Dj

I. INTRODUCTION

The gluon propagator, the most basic quantity of QCD, has been the subject of much calculation and speculation since the origin of the theory. In particular there has long been interest in the infrared behavior of the Landau gauge gluon propagator as a probe into the mechanism of confinement [1]. Some authors have argued it to be infrared finite [2–4] while others favored it as infrared singular [5,6]. There is a long history of its study on the lattice, in quenched QCD [7–19] and in quenched SU(2) [20,21]. The restriction to quenched lattice gauge theory calculations has been due to the lack of sufficient computational resources. The quenched theory differs from full QCD only in the relative weighting of the background gauge configurations (due to the fermion determinant), but the evaluation of the Green's functions is otherwise the same. In the quenched approximation the fermion determinant is replaced by unity and this corresponds to the complete suppression of all quark loops. The removal of quark loops is equivalent to the limit where all sea-quark masses are taken to infinity. In this paper, we report the first results for the gluon propagator from an unquenched lattice computation.

We study the gluon propagator in Landau gauge using configurations generated by the MILC collaboration [22] available from the Gauge Connection [28]. These use "AsqTad" improved staggered quarks, giving us access to relatively light sea quarks. We find that the addition of dynamical quarks preserves the qualitative features of the gluon dressing function $q^2D(q^2)$ in the quenched case—enhancement for intermediate infrared momenta followed by suppression in the deep infrared—but produces a clearly visible effect. A significant suppression of the infrared enhancement with respect to the quenched case is observed. It is interesting to compare these results to those of a recent Dyson-Schwinger equation study [23].

II. DETAILS OF THE CALCULATION

The gluon propagator is gauge dependent and we work in the Landau gauge for ease of comparison with other studies. It is also the simplest covariant gauge to implement on the lattice. Landau gauge is a smooth gauge that preserves the Lorentz invariance of the theory, so it is a popular choice. It will be interesting to repeat this calculation for the Gribov-copy free Laplacian gauge, but that will be left for a future study.

The MILC configurations were generated with the $\mathcal{O}(a^2)$ one-loop Symanzik improved [24] Lüscher-Weisz gauge action [25]. The dynamical configurations use the "AsqTad" quark action, an $\mathcal{O}(a^2)$ Symanzik improved staggered fermion action. β and the bare sea-quark masses are matched such that the lattice spacing is held constant. The lattices we consider all have the same dimensions. This means that all systematics are fixed; the only variable is the addition of quark loops. The parameters are summarized in Table I. The lattice spacing is approximately 0.125 fm [26].

In Landau gauge the gluon propagator is entirely transverse. In Euclidean space, in the continuum, the gluon propagator has the tensor structure

$$D_{\mu\nu}(q)=\left(\delta_{\mu\nu}-\frac{q_\mu q_\nu}{q^2}\right)D(q^2), \tag{1}$$

and at tree level

$$D(q^2)=\frac{1}{q^2}. \tag{2}$$

TABLE I. Lattice parameters used in this study. The dynamical configurations each have two degenerate light quarks (up/down) and a heavier quark (strange). In physical units the bare masses range from ~16 to ~79 MeV. The lattice spacing is $a \approx 0.125$ fm.

	Dimensions	β	Bare quark mass	Number of configurations
1	$20^3\times 64$	8.00	quenched	192
2	$20^3\times 64$	6.76	0.01, 0.05	193
3	$20^3\times 64$	6.79	0.02, 0.05	249
4	$20^3\times 64$	6.81	0.03, 0.05	212
5	$20^3\times 64$	6.83	0.04, 0.05	337

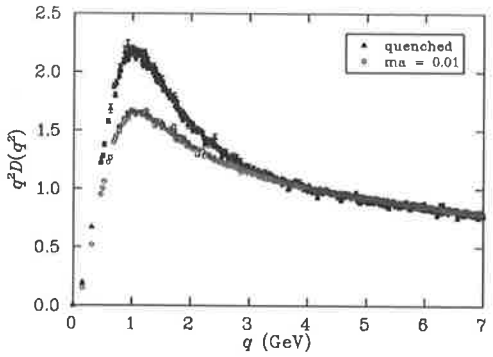

FIG. 1. Gluon dressing function in Landau gauge. Full triangles correspond to the quenched calculation, while open circles correspond to 2+1 flavor QCD. As the lattice spacing and volume are the same, the difference between the two results is entirely due to the presence of quark loops. The renormalization point is at $\mu = 4$ GeV. Data have been cylinder cut [16].

With this lattice gauge action the propagator at tree level is

$$D^{-1}(p_\mu) = \frac{4}{a^2} \sum_\mu \left\{ \sin^2\left(\frac{p_\mu a}{2}\right) + \frac{1}{3}\sin^4\left(\frac{p_\mu a}{2}\right) \right\}, \quad (3)$$

where

$$p_\mu = \frac{2\pi n_\mu}{a L_\mu}, \quad n_\mu \in \left(-\frac{L_\mu}{2}, \frac{L_\mu}{2} \right], \quad (4)$$

a is the lattice spacing and L_μ is the length of the lattice in the μ direction. As explained in Ref. [14], this suggests a "kinematic" choice of momentum,

$$q_\mu(p_\mu) \equiv \frac{2}{a} \sqrt{\sin^2\left(\frac{p_\mu a}{2}\right) + \frac{1}{3}\sin^4\left(\frac{p_\mu a}{2}\right)}, \quad (5)$$

ensuring that the lattice gluon propagator has the correct tree-level behavior.

The bare gluon propagator $D(q)$ is related to the renormalized propagator $D_R(q;\mu)$ through

$$D(q) = Z_3(\mu,a) D_R(q;\mu), \quad (6)$$

where μ is the renormalization point. In a renormalizable theory such as QCD, renormalized quantities become independent of the regularization parameter in the limit where it is removed. Z_3 is then defined by some renormalization prescription. We choose the momentum space subtraction (MOM) scheme where $Z_3(\mu,a)$ is determined by imposing the renormalization condition

$$D_R(q)|_{q^2=\mu^2} = \frac{1}{\mu^2}, \quad (7)$$

i.e., it takes the tree-level value at the renormalization point. In the following figures we have chosen $\mu = 4$ GeV.

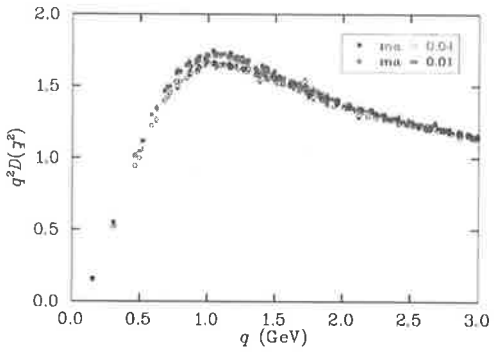

FIG. 2. The sea-quark mass dependence of the Landau gauge gluon propagator dressing function renormalized at $\mu = 4$ GeV. Filled squares correspond to u and d bare masses $\simeq 63$ MeV and bare s-quark mass $\simeq 79$ MeV. Open circles correspond to the same strange-quark mass, but with bare u and d masses $\simeq 16$ MeV. Data have been cylinder cut [16]. Increasing the sea-quark masses alters the results in the expected way, i.e., towards the quenched data.

III. SIMULATIONS RESULTS

Lattice studies strongly suggest that the quenched gluon propagator is infrared finite [14]. As is customary, we will begin by considering the (necessarily finite) gluon dressing function, $q^2D(q^2)$. In Fig. 1 we compare the well-known quenched dressing function with that for 2+1 flavor QCD. For the moment we only consider the lightest of our dynamical quarks as we expect that they will show the greatest difference from the quenched case.

Indeed there is a clear difference between quenched and dynamical quark behavior in the infrared region. The addition of quark loops to the gluon propagator softens the infrared enhancement without altering its basic features. The screening of dynamical sea quarks brings the 2+1 flavor results significantly closer to the tree-level form, $q^2D(q^2) = 1$.

In Fig. 2 we show the gluon dressing function for the lightest and for the heaviest u and d quark masses in our set. These correspond to bare light-quark masses of $\simeq 16$ MeV and $\simeq 63$ MeV, respectively; a factor of four difference. The bare strange-quark mass is the same in both cases ($\simeq 79$ MeV). The mass dependence of the gluon dressing function is only just detectable. We expect that increasing the

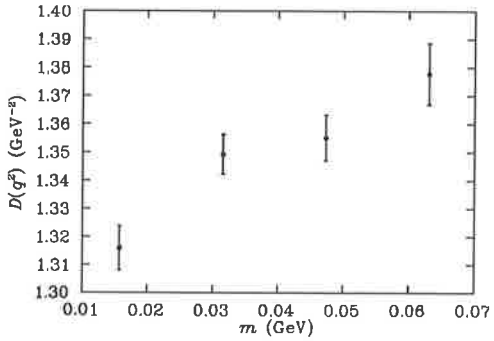

FIG. 3. The renormalized propagator at one momentum point in the infrared hump of the gluon dressing function ($q \simeq 1.12$ GeV) is shown here as a function of the bare light-quark mass.

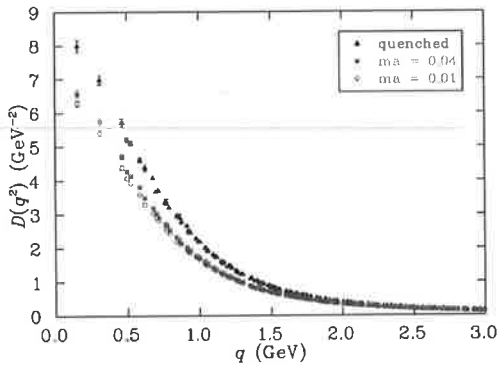

FIG. 4. The sea-quark mass dependence of the Landau gauge gluon propagator renormalized at $\mu=4$ GeV. Filled triangles illustrate the quenched propagator while filled squares correspond to bare up/down masses $\simeq 63$ and bare strange-quark mass $\simeq 79$ MeV. Open circles correspond to lighter bare up/down masses $\simeq 16$ MeV but with the same strange quark mass. Data have been cylinder cut [16].

sea-quark masses further will interpolate between the curves in Fig. 1. We see that the gluon propagator changes in the expected way. As the sea-quark mass increases, the curve moves toward the quenched result. However, for the range of bare quark masses studied here the change is relatively small. This transition would be better studied with heavier sea quarks.

Another view of the mass dependence of the gluon propagator is provided in Fig. 3. We choose one data point from the infrared hump ($q\simeq 1.12$ GeV) and plot it for each choice of bare light-quark mass. Although the variation in the propagator at this momentum is only 4.5% over the range of quark masses investigated here, the light sea-quark mass dependence is clearly resolved.

In Fig. 4 we present results for the gluon propagator, $D(q^2)$. The largest effects of unquenching are observed in the deep infrared. The shape of the curves suggest that previous results indicating the infrared-finite nature of the quenched gluon propagator [14] are unchanged upon unquenching. The results suggest that the gluon propagator of QCD is infrared finite. It will be interesting to examine the behavior of $D(0)$ as a function of volume to elucidate this aspect of the gluon propagator further.

Finally, in Fig. 5 the light sea-quark mass dependence of the renormalized gluon propagator is illustrated for a momentum point in the infrared region. To avoid finite volume artifacts, the second smallest nontrivial momentum is considered. Whereas the mass dependence of the propagator for the masses studied here is at the 4.5% level for $q\simeq 1.12$ GeV, the variance is larger in the infrared region at 6% for $q\simeq 0.31$ GeV.

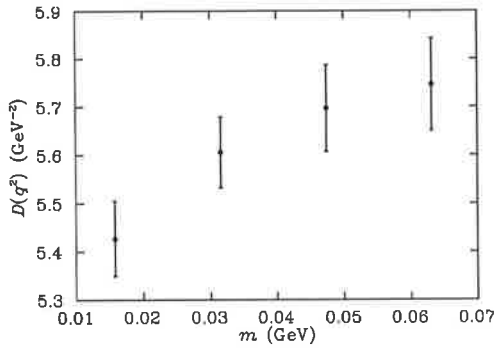

FIG. 5. The light sea-quark mass dependence of the renormalized gluon propagator at a momentum point in the infrared region ($q\simeq 0.31$ GeV).

In a recent Dyson-Schwinger equation (DSE) study [23,27] the inclusion of the quark DSE in the gluon DSE was found to slightly diminish its infrared enhancement. Osterwalder-Schrader positivity is still violated. Our results are consistent with the qualitative features of that prediction.

IV. CONCLUSIONS

The addition of quark loops has a clear, quantitative effect on the gluon propagator. While its basic structure is qualitatively similar there is significant screening of the propagator in the infrared. As anticipated, the effect is to suppress the non-Abelian enhancement of the gluon propagator in the nonperturbative infrared-momentum region. This is relevant to analytic studies of the gluon propagator and confinement [23]. Despite the clear difference between the quenched and dynamical results, we see little dependence on the dynamical quark mass for the range of available light sea-quark masses. The dependence that is observed is consistent with expectations.

Calculations on finer lattices are currently being made, which will provide more information on the ultraviolet nature of the propagator and provide a test for finite lattice spacing artifacts. We would like to extend the study to a wider range of dynamical masses to study both the chiral limit and the transition to the quenched limit. Finally, a study of the volume dependence of the propagator will provide valuable insights into the nature of the propagator at $q^2=0$.

ACKNOWLEDGMENT

This research was supported by the Australian Research Council and by grants of time on the Hydra Supercomputer, supported by the South Australian Partnership for Advanced Computing.

[1] J.E. Mandula, hep-lat/9907020 (1998).
[2] V.N. Gribov, Nucl. Phys. **B139**, 1 (1978).
[3] M. Stingl, Phys. Rev. D **34**, 3863 (1986).
[4] D. Zwanziger, Nucl. Phys. **B364**, 127 (1991).
[5] S. Mandelstam, Phys. Rev. D **20**, 3223 (1979).
[6] K. Buttner and M.R. Pennington, Phys. Rev. D **52**, 5220 (1995).
[7] J.E. Mandula and M. Ogilvie, Phys. Lett. B **185**, 127 (1987).

[8] C.W. Bernard, C. Parrinello, and A. Soni, Phys. Rev. D **49**, 1585 (1994).
[9] P. Marenzoni, G. Martinelli, and N. Stella, Nucl. Phys. **B455**, 339 (1995).
[10] J.P. Ma, Mod. Phys. Lett. A **15**, 229 (2000).
[11] D. Becirevic *et al.*, Phys. Rev. D **60**, 094509 (1999).
[12] D. Becirevic *et al.*, Phys. Rev. D **61**, 114508 (2000).
[13] H. Nakajima and S. Furui, Nucl. Phys. **A680**, 151 (2000).
[14] F.D.R. Bonnet, P.O. Bowman, D.B. Leinweber, A.G. Williams, and J.M. Zanotti, Phys. Rev. D **64**, 034501 (2001).
[15] K. Langfeld, H. Reinhardt, and J. Gattnar, Nucl. Phys. **B621**, 131 (2002).
[16] D.B. Leinweber, J.I. Skullerud, A.G. Williams, and C. Parrinello, Phys. Rev. D **60**, 094507 (1999).
[17] D.B. Leinweber, J.I. Skullerud, A.G. Williams, and C. Parrinello, Phys. Rev. D **58**, 031501 (1998).
[18] P.O. Bowman, U.M. Heller, D.B. Leinweber, and A.G. Williams, Phys. Rev. D **66**, 074505 (2002).
[19] F.D.R. Bonnet, P.O. Bowman, D.B. Leinweber, and A.G. Williams, Phys. Rev. D **62**, 051501(R) (2000).
[20] A. Cucchieri, Phys. Lett. B **422**, 233 (1998).
[21] A. Cucchieri, T. Mendes, and A.R. Taurines, Phys. Rev. D **67**, 091502(R) (2003).
[22] C.W. Bernard *et al.*, Phys. Rev. D **64**, 054506 (2001).
[23] R. Alkofer, W. Detmold, C.S. Fischer, and P. Maris, Phys. Rev. D **70**, 014014 (2004).
[24] K. Symanzik, Nucl. Phys. **B226**, 187 (1983).
[25] M. Luscher and P. Weisz, Chem. Phys. **97**, 59 (1985); **98**, 433(E) (1985).
[26] HPQCD, C.T.H. Davies *et al.*, Phys. Rev. Lett. **92**, 022001 (2004).
[27] C. Fischer and R. Alkofer, Phys. Rev. D **67**, 094020 (2003).
[28] http://www.qcd-dmz.nersc.gov

PHYSICAL REVIEW D 71, 054507 (2005)

Unquenched quark propagator in Landau gauge

Patrick O. Bowman,[1] Urs M. Heller,[2] Derek B. Leinweber,[3] Maria B. Parappilly,[3]
Anthony G. Williams,[3] and Jianbo Zhang[3]

[1]*Nuclear Theory Center, Indiana University, Bloomington Indiana 47405, USA*
[2]*American Physical Society, One Research Road, Box 9000, Ridge, New York 11961-9000, USA*
[3]*Special Research Centre for the Subatomic Structure of Matter and Department of Physics, University of Adelaide, Adelaide, SA 5005, Australia*

(Received 27 January 2005; published 18 March 2005)

We present an unquenched calculation of the quark propagator in Landau gauge with $2+1$ flavors of dynamical quarks. We use configurations generated with an improved staggered ("Asqtad") action by the MILC Collaboration. This quark action has been seen to have excellent rotational symmetry and scaling properties in the quenched quark propagator. Quenched and dynamical calculations are performed on a $20^3 \times 64$ lattice with a nominal lattice spacing of $a = 0.125$ fm. The matched quenched and dynamical lattices allow us to investigate the relatively subtle sea-quark effects, and even in the quenched case the physical volume of these lattices gives access to lower momenta than our previous study. We calculate the quark mass function and renormalization function for a variety of valence and sea-quark masses.

DOI: 10.1103/PhysRevD.71.054507 PACS numbers: 12.38.Gc, 11.15.Ha, 12.38.Aw, 14.65.−q

I. INTRODUCTION

Quantum chromodynamics is widely accepted as the correct theory of the strong interactions and the quark propagator is its most basic quantity. In the low momentum region it exhibits dynamical chiral symmetry breaking (which cannot be derived from perturbation theory) and at high momentum it can be used to extract the running quark mass [1]. In lattice QCD, quark propagators are tied together to calculate hadron masses and other properties. Lattice gauge theory provides a way to calculate the quark propagator directly, providing access to quantities such as operator product expansion (OPE) condensates [2]. In turn, such a calculation can provide technical insight into lattice gauge theory simulations.

The systematic study of the quark propagator on the lattice has also provided fruitful interaction with other approaches to hadron physics, such as instanton phenomenology [3], chiral quark models [4] and Dyson-Schwinger equation (DSE) studies [5,6]. The lattice is a first principles approach and has provided valuable constraints for model builders. In turn, such alternative methods can provide feedback on regions that are difficult to access directly on the lattice, such as the deep infrared and chiral limits.

The quark propagator has previously been studied using Clover [7,8], staggered [9,10], and Overlap [11,12] actions. For a review, see Ref. [13]. All of these actions have different systematic errors and the combination of these studies has given us an excellent handle on the possible lattice artifacts. In every case, however, they have been performed in the quenched approximation and have been restricted to modest physical volumes.

In this paper we report first results for the quark propagator including dynamical quark effects. We use configurations generated by the MILC Collaboration [14] available from the gauge connection [15]. These use "Asqtad," $\mathcal{O}(a^2)$ improved staggered quarks [16], giving us access to relatively light sea quarks. In the quenched approximation, the quark propagator for this action has excellent rotational symmetry and is well behaved at large momenta [1]. We use quenched and dynamical configurations at the same lattice spacing and volume, which enables us to observe the relatively subtle effects of unquenching. These lattices are also somewhat larger than those of previous studies, giving us access to smaller momenta.

II. DETAILS OF THE CALCULATION

The quark propagator is gauge dependent and we work in the Landau gauge for ease of comparison with other studies. Landau gauge is a smooth gauge that preserves the Lorentz invariance of the theory, so it is a popular choice. It will be interesting to repeat this calculation for the Gribov-copy free Laplacian gauge, and this is left for a future study.

The MILC configurations were generated with the $\mathcal{O}(a^2)$ one-loop Symanzik-improved Lüscher–Weisz gauge action [17]. The dynamical configurations use the Asqtad quark action, an $\mathcal{O}(a^2)$ Symanzik-improved staggered fermion action. They have two degenerate light fermions, for the u and d quarks, and a heavier one for the strange quark. We explore a variety of light quark masses, with the bare strange quark mass fixed at $ma = 0.05$, or $m = 79$ MeV for $a = 0.125$ fm [18]. In all cases the Asqtad action is also used for the valence quarks. The values of the coupling and the bare sea-quark masses are matched such that the lattice spacing is held constant. This means that all systematics are fixed; the only variable is the addition of quark loops. The simulation parameters are summarized in Table I.

On the lattice, the bare propagator $S(a; p^2)$ is related to the renormalized propagator $S^{\text{ren}}(\mu; p^2)$ through the renormalization constant

TABLE I. Lattice parameters used in this study. The dynamical configurations each have two degenerate light (up/down) quarks and a heavier (strange) quark. The lattice spacing is $a = 0.125(3)$ fm, where the uncertainty reflects the variation of a over the set of lattices considered in this analysis. Bare light quark masses $ma = 0.01, 0.02, 0.03, 0.04$ correspond to masses of 16–63 MeV. The bare strange quark mass is $ma = 0.05$ or 79 MeV.

	Dimensions	β	Bare quark mass	# Configuration
1	$20^3 \times 64$	8.00	quenched	265
2	$20^3 \times 64$	6.76	16 MeV, 79 MeV	203
3	$20^3 \times 64$	6.79	32 MeV, 79 MeV	249
4	$20^3 \times 64$	6.81	47 MeV, 79 MeV	268
5	$20^3 \times 64$	6.83	63 MeV, 79 MeV	318

$$S(a; p^2) = Z_2(a; \mu) S^{\text{ren}}(\mu; p^2). \quad (1)$$

In the continuum limit, Lorentz invariance allows one to decompose the full quark propagator into Dirac vector and scalar pieces

$$S^{-1}(p^2) = iA(p^2)\gamma \cdot p + B(p^2) \quad (2)$$

or, alternatively,

$$S^{-1}(p^2) = Z^{-1}(p^2)[i\gamma \cdot p + M(p^2)], \quad (3)$$

where $M(p^2)$ and $Z(p^2)$ are the nonperturbative mass and wave-function renormalization functions, respectively. Asymptotic freedom implies that, as $p^2 \to \infty$, $S(p^2)$ reduces to the free propagator

$$S^{-1}(p^2) \to i\gamma \cdot p + m, \quad (4)$$

up to logarithmic corrections. The mass function M is renormalization point independent and for Z we choose throughout this work the renormalization point as 3 GeV.

The tree-level quark propagator with the Asqtad action has the form

$$S^{-1}(p) = i\sum_\mu \overline{\gamma}_\mu q(p_\mu) + m, \quad (5)$$

where $q(p_\mu)$ is the kinematic momentum given by [9]

$$q_\mu \equiv \sin(p_\mu)\left[1 + \frac{1}{6}\sin^2(p_\mu)\right]. \quad (6)$$

The $\overline{\gamma}_\mu$ form a staggered Dirac algebra [see Eqs. (A5) and (A6)]. Having identified the kinematic momentum, we define the mass and renormalization functions by

$$S^{-1}(p) = Z^{-1}(q)\left[i\sum_\mu (\overline{\gamma}_\mu) q_\mu(p_\mu) + M(q)\right]. \quad (7)$$

Complete details of the extraction of the mass and renormalization functions from the Asqtad propagator are described in the appendix.

III. QUENCHED RESULTS

First we compare our quenched results to some previously published data obtained on a smaller lattice [10]. All the data illustrated in the following are cylinder cut [19]. This removes points most susceptible to rotational symmetry breaking, making the data easier to interpret. As is well known, the definition of lattice spacing in a quenched calculation is somewhat arbitrary, and indeed the quoted estimate for our smaller ensemble is not consistent with that published for the MILC configurations. We determined a consistent value of the lattice spacing by matching the gluon propagator calculated on the old ensemble to that of the new ensemble [20]. This procedure yields a new nominal lattice spacing of $a = 0.105$ fm and physical volume of $1.7^3 \times 3.4$ fm^4 for the old lattices. Examining the quark propagator on the two quenched ensembles,

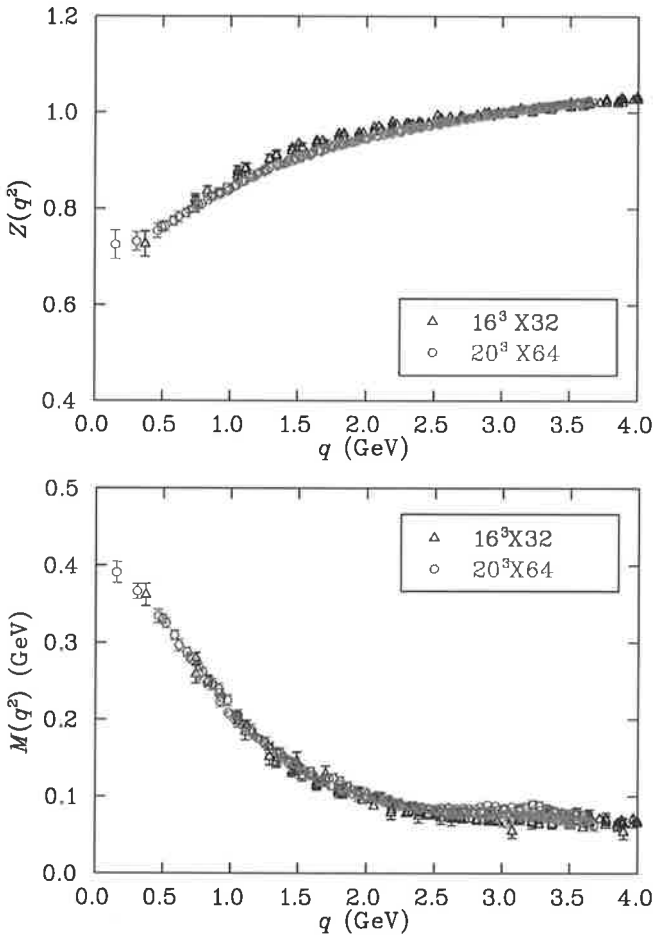

FIG. 1 (color online). Comparison of quenched wave-function renormalization and mass functions at approximately the same bare quark mass. The quark propagator from the $20^3 \times 64$ lattice with lattice spacing $a = 0.125$ fm at $m = 47$ MeV (open circles) is compared with the previously published quark propagator from a $16^3 \times 32$ lattice with lattice spacing $a = 0.105$ fm at $m = 45$ MeV (full triangles). The renormalization point for $Z(q^2)$ is set at $q = 3$ GeV.

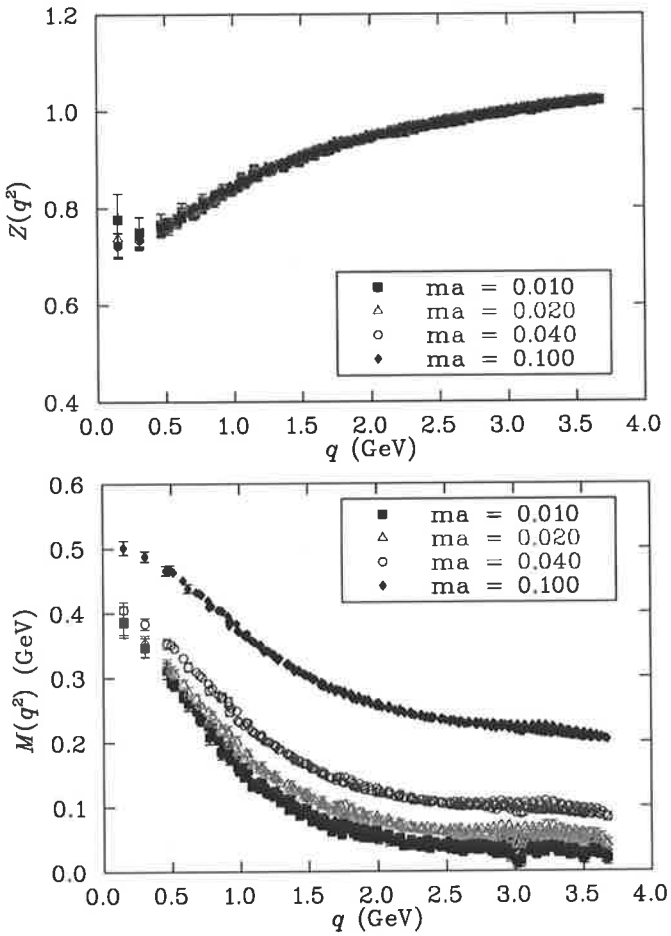

FIG. 2 (color online). The quenched renormalization function (top) and mass function (bottom) for a selection of quark masses, including $ma = 0.100$, about twice the strange quark mass. The renormalization point for $Z(q^2)$ is set at $q = 3$ GeV.

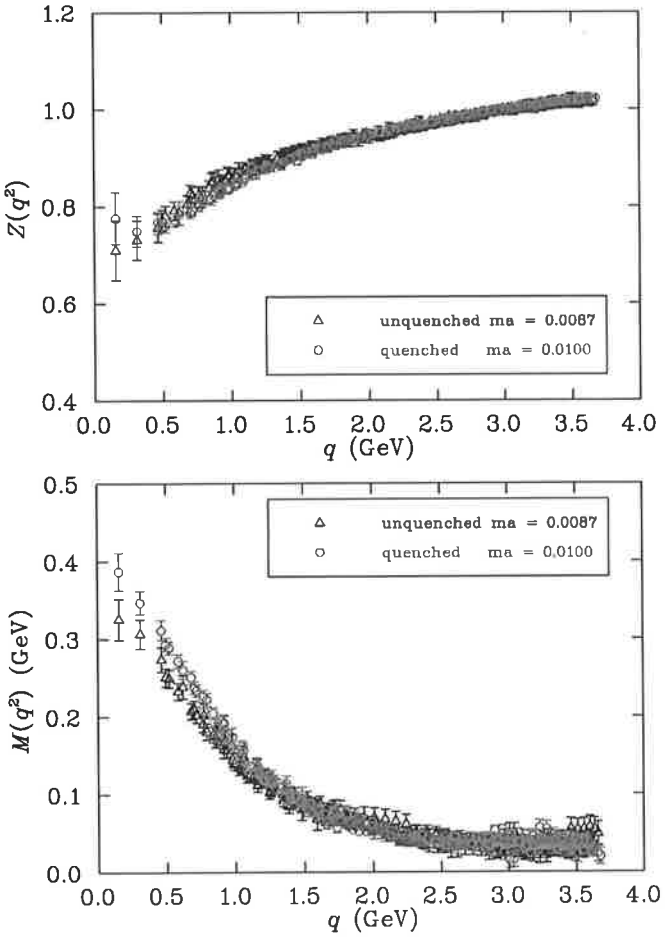

FIG. 3 (color online). Comparison of the unquenched (full QCD) and quenched quark propagator for nonzero quark mass. The mass function for the unquenched dynamical-fermion propagator has been interpolated so that it agrees with the quenched mass function for $ma = 0.01$ at the renormalization point, $q = 3$ GeV. For the unquenched propagator this corresponds to a bare quark mass of $ma = 0.0087$.

shown in Fig. 1, we see that the agreement is excellent. This indicates that both finite volume and discretization effects are small. The flattening in the deep infrared of both scalar functions is a long-standing prediction of DSE studies [5].

We show results for the larger quenched lattice for a variety of bare quark masses in Fig. 2. Once again we see that for quark masses less than or approximately equal to that of the strange quark, the lowest momentum point of the mass function is insensitive to quark mass.

IV. EFFECTS OF DYNAMICAL QUARKS

Here we compare the scalar functions for the quenched and dynamical propagators. For a given bare mass, the running mass depends upon both the number of dynamical quark flavors and their masses. To make the most appropriate comparison we select a bare quark mass for the quenched case ($ma = 0.01$) and interpolate the dynamical mass function so that it agrees with the quenched result at the renormalization point, $q = 3$ GeV. The results are shown in Fig. 3. The necessary bare quark mass, $ma = 0.0087$, is a little smaller for the dynamical case.

The dynamical case does not differ greatly from the quenched case. For the renormalization functions, there is no discernible difference between the quenched and unquenched cases. However the mass functions do reveal the effects of dynamical quarks. Dynamical mass generation is suppressed, in the infrared, in the presence of dynamical quarks relative to that observed in the quenched case when the mass functions are the same at the (UV) renormalization point. This is in accord with expectations as the dynamical quark loops act to screen the strong interaction.

Further comparisons can be made in the chiral limit. In Fig. 4 both quenched and dynamical data have been extrapolated to zero bare quark mass by a fit linear in the quark mass. In the dynamical case, the extrapolation was done for the case when the valence and light sea-quark

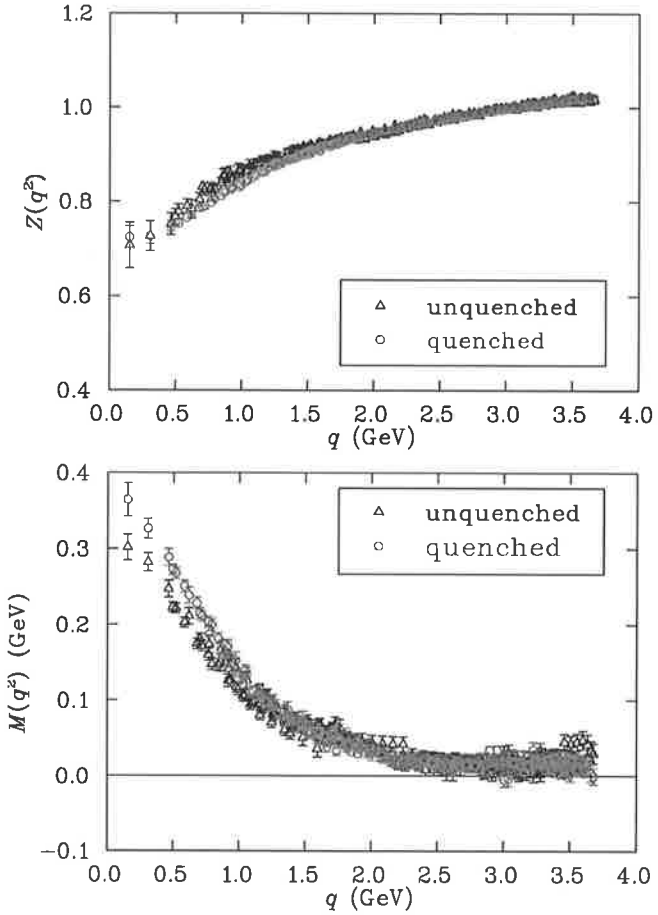

FIG. 4 (color online). Comparison of the unquenched (full QCD) and quenched quark propagator in the chiral limit. The renormalization function is renormalized at $q = 3$ GeV. Whereas little difference is observed in the renormalization function, the mass functions indicates that dynamical mass generation is suppressed by the addition of quark loops.

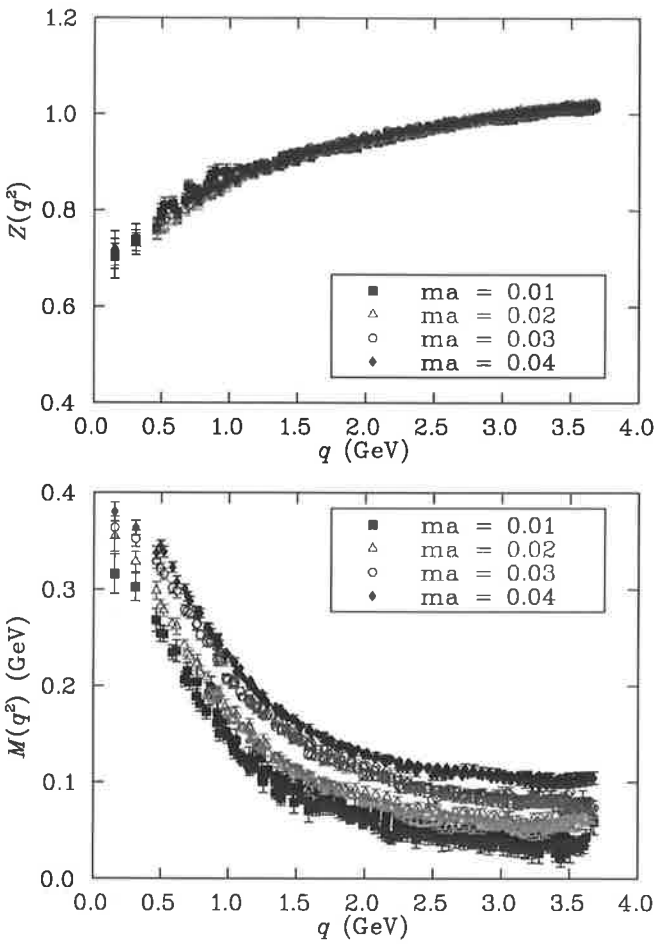

FIG. 5 (color online). Renormalization (top) and mass (bottom) functions for four different quark masses in full QCD, where the valence and light sea masses are matched. The wave-function renormalization function Z is renormalized at $q = 3$ GeV.

masses are identical. As discussed above, for a given bare quark mass, the running mass is larger in full QCD than in quenched QCD. This is apparent from the fact that the bare mass must be chosen smaller in the dynamical case in order that the running masses agree at large momenta e.g., see Fig. 3.

Figure 5 shows the mass and renormalization functions in the dynamical case for a variety of quark masses. Here the valence quark masses and the light sea-quark masses are matched. The results show that the renormalization function is insensitive to the bare quark masses studied here. The results for the mass function are ordered as expected with the larger bare quark masses, m, giving rise to a larger mass function.

Finally, we comment on the approach to the chiral limit. In Fig. 6 we show the mass function for five different momenta plotted as a function of the bare quark mass. The momenta considered include the lowest momentum of 0.155 GeV and 0.310, 0.495, 0.700 and 0.993 GeV to explore momentum dependent changes in the approach to the chiral limit. At larger momenta, the mass function is observed to be proportional to the bare quark mass. However, at small momenta, nonperturbative effects make this dependence more complicated. For example, a recent Dyson-Schwinger study predicts a downward turn as the bare mass approaches zero [5].

For the lowest momentum points, nonlinear behavior is indeed observed. For the quenched case, curvature in an upward direction is revealed as the chiral limit is approached, leading to the possibility of a larger infrared mass function for the lightest quark mass, despite the reduction of the input bare quark mass. In contrast, a hint of downward curvature is observed for the most infrared points of the full QCD mass function as the chiral limit is approached. It is interesting that the nature of the curvature depends significantly on the chiral dynamics of the theory which are modified in making the quenched approximation. Similar behavior is observed in the hadron mass spectrum where the coefficients of chiral nonanalytic be-

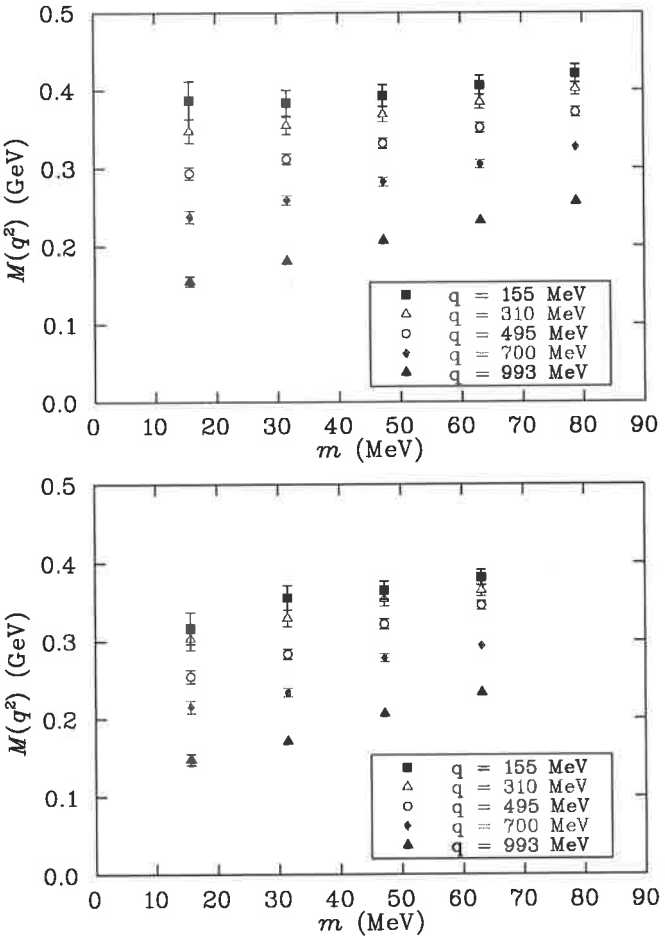

FIG. 6 (color online). The chiral limit approach of the mass function for selected momenta. Results from quenched QCD simulations are illustrated at top whereas full dynamical-fermion QCD results are illustrated at bottom. Nonlinear behavior is observed for the lowest momentum points, in opposite directions for quenched and full QCD.

havior can change sign in moving from quenched QCD to full QCD [21,22].

V. CONCLUSIONS

We have presented first results for the mass and wave-function renormalization functions of the quark propagator in which the effects of $2+1$ dynamical quark flavours are taken into account. In contrast to the significant screening suppression of the gluon propagator in the infrared [20], the quark propagator is not strongly altered by sea-quark effects. In particular, the renormalization function is insensitive to the light bare quark masses studied here, which range from 16 to 63 MeV, and also agrees well with previous quenched simulation results. Screening of dynamical mass generation in the infrared mass function is observed when comparing quenched and full QCD results at finite mass and in the chiral limit. The approach of the mass function to the chiral limit displays interesting non-trivial curvature for low momenta, with the curvature in quenched and full QCD in opposite directions.

ACKNOWLEDGMENTS

We thank the Australian Partnership for Advanced Computing (APAC) and the South Australian Partnership for Advanced Computing (SAPAC) for generous grants of supercomputer time which have enabled this project. This work is supported by the Australian Research Council.

APPENDIX: EXTRACTION OF THE SCALAR FUNCTIONS

The Asqtad quark action [16] is a staggered action using three-link, five-link and seven-link staples as a kind of "fattening" to minimize quark flavor (often referred to as "taste") changing interactions. The three-link Naik term [23] is included to improve rotational symmetry by improving the finite difference operator, and the five-link Lepage term [24] is included to correct errors at low momenta that may be introduced by the above mentioned staples. The coefficients are tadpole improved and chosen to remove all tree-level $\mathcal{O}(a^2)$ errors.

At tree level (i.e. no interactions, links set to the identity) the staples in this action make no contribution, so the action reduces to the tree-level Naik action,

$$S^{(0)} = \frac{1}{2}\sum_{x,\mu}\overline{\chi}(x)\eta_\mu(x)\Big[\frac{9}{8}(\chi(x+\mu)-\chi(x-\mu)) - \frac{1}{24}(\chi(x+3\mu)-\chi(x-3\mu))\Big] + m\sum_x \overline{\chi}(x)\chi(x), \tag{A1}$$

where the staggered phases are $\eta_\mu(x) = (-1)^{\zeta^{(\mu)}\cdot x}$ and

$$\zeta_\nu^{(\mu)} = \begin{cases} 1 & \text{if } \nu < \mu \\ 0 & \text{otherwise} \end{cases} \tag{A2}$$

In momentum space, the quark propagator with this action has the tree-level form

$$\begin{aligned} S^{(0)^{-1}}_{\alpha\beta}(p;m) &= i\sum_\mu(\overline{\gamma}_\mu)_{\alpha\beta}\Big[\frac{9}{8}\sin(p_\mu) - \frac{1}{24}\sin(3p_\mu)\Big] \\ &\quad + m\overline{\delta}_{\alpha\beta} \\ &= i\sum_\mu(\overline{\gamma}_\mu)_{\alpha\beta}\sin(p_\mu)\Big[1+\frac{1}{6}\sin^2(p_\mu)\Big] \\ &\quad + m\overline{\delta}_{\alpha\beta}, \end{aligned} \tag{A3}$$

where the α, β are themselves four-vectors: $\alpha_\mu = 0, 1$, and likewise for β; thus the quark propagator in Eq. (A3) is a 16×16 matrix. This familiar form is obtained by defining

$$\overline{\delta}_{\alpha\beta} = \Pi_\mu \delta_{\alpha_\mu\beta_\mu|\mathrm{mod}2}, \tag{A4}$$

$$(\overline{\gamma}_\mu)_{\alpha\beta} = (-1)^{\alpha_\mu}\overline{\delta}_{\alpha+\zeta^{(\mu)},\beta}. \tag{A5}$$

The mod2 in Eq. (A4) ensures its validity in Eq. (A5). The $\overline{\gamma}_\mu$ satisfy

$$\{\overline{\gamma}_\mu, \overline{\gamma}_\nu\}_{\alpha\beta} = 2\delta_{\mu\nu}\overline{\delta}_{\alpha\beta}, \tag{A6}$$

$$\overline{\gamma}_\mu^\dagger = \overline{\gamma}_\mu^T = \overline{\gamma}_\mu^* = \overline{\gamma}_\mu, \tag{A7}$$

forming a "staggered" Dirac algebra.

Staggered actions are invariant under translations of $2a$, and the momentum on this blocked lattice is

$$p_\mu = \frac{2\pi m_\mu}{L_\mu} \;\Big|\; m_\mu = 0, \ldots, \frac{L_\mu}{2} - 1. \tag{A8}$$

We calculate the quark propagator in coordinate space,

$$G(x, y) = \langle \chi(x)\overline{\chi}(y)\rangle, \tag{A9}$$

and obtain the quark propagator in momentum space by Fourier transform of $G(x, 0)$. To write the Fourier transform of the staggered field we write the momentum on the lattice

$$k_\mu = \frac{2\pi n_\mu}{L_\mu} \;\Big|\; n_\mu = 0, \ldots, L_\mu - 1 \tag{A10}$$

so that $k_\mu = p_\mu + \pi\alpha_\mu$ and define $\int_k \equiv \frac{1}{V}\sum_k$. Then

$$\int_k = \int_p \sum_{\alpha_\mu=0}^{1}, \tag{A11}$$

$$\chi(x) = \int_k e^{ik\cdot x}\chi(k) = \int_p \sum_\alpha e^{i(p+\pi\alpha)\cdot x}\chi_\alpha(p), \tag{A12}$$

and

$$G(x, y) = \sum_{\alpha\beta}\int_{p,l} \exp\{i(p + \alpha\pi)\cdot x - i(l + \beta\pi)\cdot y\} \times \langle \chi_\alpha(p)\overline{\chi}_\beta(l)\rangle \tag{A13}$$

$$= \sum_{\alpha\beta}\int_p e^{ip(x-y)}e^{i\pi(\alpha\cdot x - \beta\cdot y)}S_{\alpha\beta}(p). \tag{A14}$$

Now it will be convenient to rewrite this

$$G(k) = G(l + \pi\delta) \equiv G_\delta(l) = \sum_x e^{-ikx}G(x, 0)$$

$$= \sum_{\alpha\beta}\int_p \sum_x \exp\{-i(l + \pi\delta)x\} \times \exp\{i(p + \pi\alpha)x\}S_{\alpha\beta}(p)$$

$$= \sum_{\alpha\beta}\int_p \delta_{pl}\overline{\delta}_{\alpha\delta}S_{\alpha\beta}(p) \tag{A15}$$

$$= \sum_\beta S_{\delta,\beta}(l). \tag{A16}$$

In the interacting case, the quark propagator asymptotically approaches its tree-level value due to asymptotic freedom. At finite lattice spacing the actual behavior is closer to

$$S(q; m) \to \frac{1}{u_0}S^{(0)}(q; m/u_0), \tag{A17}$$

where u_0 is the tadpole (or mean-field) improvement factor defined by

$$u_0 = (\langle \mathrm{Tr}U_{\mathrm{plaq}}\rangle)^{1/4}. \tag{A18}$$

Assuming that the full lattice propagator retains its free form (in analogy to the continuum case) we write

$$S^{-1}_{\alpha\beta}(p) = i\sum_\mu(\overline{\gamma}_\mu)_{\alpha\beta}q_\mu(p_\mu)A(p) + B(p)\overline{\delta}_{\alpha\beta} \tag{A19}$$

$$= Z^{-1}(p)\left[i\sum_\mu(\overline{\gamma}_\mu)_{\alpha\beta}q_\mu(p_\mu) + M(p)\overline{\delta}_{\alpha\beta}\right], \tag{A20}$$

where q is the tree-level momentum, Eq. (6). Combining this with Eq. (A15) above, we can extract the scalar functions (which we now write in terms of q) as follows:

$$G_\alpha(q) = Z(q)\frac{-i\sum_\mu(-1)^{\alpha_\mu}q_\mu + M(q)}{q^2 + M^2(q)}, \tag{A21}$$

from which we obtain

$$\sum_\alpha \mathrm{Tr}G_\alpha(q) = 16N_c\frac{Z(q)M(q)}{q^2 + M^2(q)} = 16N_c\mathcal{B}(q), \tag{A22}$$

and

$$i\sum_\alpha\sum_\mu(-1)^{\alpha_\mu}q_\mu\mathrm{Tr}[G_\alpha(q)] = 16N_cq^2\frac{Z(q)}{q^2 + M^2(q)} = 16N_cq^2\mathcal{A}(q). \tag{A23}$$

Putting it all together we get

$$A(q) = Z^{-1}(q) = \frac{\mathcal{A}(q)}{\mathcal{A}^2(q)q^2 + \mathcal{B}^2(q_\mu)}, \tag{A24}$$

$$B(q) = \frac{M(q)}{Z(q)} = \frac{\mathcal{B}(p)}{\mathcal{A}^2(q)q^2 + \mathcal{B}^2(p)}, \tag{A25}$$

$$M(q) = \frac{\mathcal{B}(q)}{\mathcal{A}(q)}. \tag{A26}$$

By calculating $\mathcal{A}, \mathcal{B}$ instead of A, B, we avoid inverting the propagator. We calculate the ensemble average of $\mathcal{A}$ and $\mathcal{B}$ and then M and Z.

[1] P.O. Bowman, U.M. Heller, D.B. Leinweber, A.G. Williams, and J.B. Zhang, Nucl. Phys. B, Proc. Suppl. **128**, 23 (2004); **128**, 23 (2004)
[2] E. Ruiz Arriola, P.O. Bowman, and W. Broniowski, Phys. Rev. D **70**, 097505 (2004).
[3] D. Diakonov, Prog. Part. Nucl. Phys. **51**, 173 (2003).
[4] E. Ruiz Arriola and W. Broniowski, Phys. Rev. D **67**, 074021 (2003).
[5] M.S. Bhagwat, M.A. Pichowsky, C.D. Roberts, and P.C. Tandy, Phys. Rev. C **68**, 015203 (2003).
[6] R. Alkofer, W. Detmold, C.S. Fischer, and P. Maris, Phys. Rev. D **70**, 014014 (2004).
[7] J.I. Skullerud and A.G. Williams, Phys. Rev. D **63**, 054508 (2001).
[8] J. Skullerud, D.B. Leinweber, and A.G. Williams, Phys. Rev. D **64**, 074508 (2001).
[9] P.O. Bowman, U.M. Heller, and A.G. Williams, Phys. Rev. D **66**, 014505 (2002).
[10] P.O. Bowman, U.M. Heller, D.B. Leinweber, and A.G. Williams, Nucl. Phys. B, Proc. Suppl. **119**, 323 (2003).
[11] F.D.R. Bonnet, P.O. Bowman, D.B. Leinweber, A.G. Williams, and J.B. Zhang, Phys. Rev. D **65**, 114503 (2002).
[12] J.B. Zhang, P.O. Bowman, D.B. Leinweber, A.G. Williams, and F.D.R. Bonnet, Phys. Rev. D **70**, 034505 (2004).
[13] P.O. Bowman, U.M. Heller, D.B. Leinweber, A.G. Williams, and J.B. Zhang, Quark Propagator from LQCD and Its Physical Implications, in *Lattice Hadron Physics*, Lecture Notes in Physics (Springer-Verlag, to be published).
[14] C.W. Bernard *et al.*, Phys. Rev. D **64**, 054506 (2001).
[15] NERSC, Gauge connection, http://qcd.nersc.gov/
[16] K. Orginos, D. Toussaint, and R.L. Sugar, Phys. Rev. D **60**, 054503 (1999).
[17] M. Lüscher and P. Weisz, Commun. Math. Phys. **97**, 59 (1985); **98**, 433(E) (1985).
[18] C.T.H. Davies *et al.*, Phys. Rev. Lett. **92**, 022001 (2004).
[19] F.D.R. Bonnet, P.O. Bowman, D.B. Leinweber, A.G. Williams, and J.M. Zanotti, Phys. Rev. D **64**, 034501 (2001).
[20] P.O. Bowman, U.M. Heller, D.B. Leinweber, M.B. Parappilly, and A.G. Williams, Phys. Rev. D **70**, 034509 (2004).
[21] D.B. Leinweber, A.W. Thomas, A.G. Williams, R.D. Young, J.M. Zanotti, and J.B. Zhang, Nucl. Phys. **A737**, 177 (2004).
[22] R.D. Young, D.B. Leinweber, A.W. Thomas and S.V. Wright, Phys. Rev. D **66**, 094507 (2002).
[23] S. Naik, Nucl. Phys. **B316**, 238 (1989).
[24] G.P. Lepage, Phys. Rev. D **59**, 074502 (1999).

Scaling behavior of the quark propagator in full QCD

Maria B. Parappilly,[1] Patrick O. Bowman,[2] Urs M. Heller,[3] Derek B. Leinweber,[1] Anthony G. Williams,[1] and J. B. Zhang[1]

[1]*Special Research Center for the Subatomic Structure of Matter (CSSM) and Department of Physics, University of Adelaide 5005, Australia*

[2]*Nuclear Theory Center, Indiana University, Bloomington, Indiana 47405, USA*

[3]*American Physical Society, One Research Road, Box 9000, Ridge, New York 11961-9000, USA*

(Received 8 November 2005; published 13 March 2006)

We study the scaling behavior of the quark propagator on two lattices with similar physical volume in Landau gauge with $2+1$ flavors of dynamical quarks in order to test whether we are close to the continuum limit for these lattices. We use configurations generated with an improved staggered ("Asqtad") action by the MILC collaboration. The calculations are performed on $28^3 \times 96$ lattices with lattice spacing $a = 0.09$ fm and on $20^3 \times 64$ lattices with lattice spacing $a = 0.12$ fm. We calculate the quark mass function, $M(q^2)$, and the wave-function renormalization function, $Z(q^2)$, for a variety of bare quark masses. Comparing the behavior of these functions on the two sets of lattices we find that both $Z(q^2)$ and $M(q^2)$ show little sensitivity to the ultraviolet cutoff.

DOI: 10.1103/PhysRevD.73.054504 PACS numbers: 12.38.Gc, 11.15.Ha, 12.38.Aw, 14.65.−q

I. INTRODUCTION

Quantum Chromodynamics (QCD) is widely considered to be the correct theory of the strong interactions. Quarks and gluons are the fundamental degrees of freedom of this theory. The quark propagator contains valuable information about nonperturbative QCD. The systematic study of the quark propagator on the lattice has provided fruitful interaction with other approaches to hadron physics, such as instanton phenomenology [1], chiral quark models [2] and Dyson-Schwinger equation studies [3,4]. As a first principles approach lattice QCD has provided valuable constraints for model builders. In turn, such alternative methods can provide feedback on regions that are difficult to access directly on the lattice, such as the deep infrared and chiral limits.

The quark propagator has previously been studied using Clover [5,6], staggered [7,8] and Overlap [9–11] actions. For a review, see Ref. [12]. All these actions have different systematic errors and the combination of these studies has given us an excellent handle on the possible lattice artifacts in quenched QCD.

In this study we focus on the Landau gauge quark propagator in full QCD, and extend our previous work [13] to a finer lattice with lattice spacing $a = 0.09$ fm [14] but similar physical volume in order to test whether we are close to the continuum limit for these lattices. The scaling behavior of the momentum space quark propagator is examined by comparing the results on these two lattices. Our results show that there are no significant differences in the wave-function renormalization function and quark mass function on the two sets of lattices. Therefore the scaling behavior is good already at the coarser lattice spacing of $a = 0.12$ fm.

The configurations we use in this study were generated by the MILC collaboration [14,15] and are available from the Gauge Connection [16]. The dynamical configurations have two degenerate light fermions for the u and d quarks and a heavier one for the strange quark. Weighting for the fermion determinants is provided by the so-called, "fourth root trick.". While the current numerical results [17] provide compelling evidence that the fourth root trick gives an accurate estimate of the dynamical fermion weight, the formal issue of proving that this provides the determinant of a local fermion action from first principles remains unresolved.

II. DETAILS OF THE CALCULATION

The quark propagator is gauge dependent and we work in the Landau gauge for ease of comparison with other studies. Landau gauge is a smooth gauge that preserves the Lorentz invariance of the theory, so it is a popular choice. As derived in Ref. [18] an improved Landau-gauge-fixing functional, $\mathcal{F}^G_{\rm Imp} \equiv \frac{4}{3}\mathcal{F}^G_1 - \frac{1}{12u_0}\mathcal{F}^G_2$ is used where

$$\mathcal{F}^G_1[\{U\}] = \sum_{\mu,x} \frac{1}{2} \mathrm{Tr}\{U^G_\mu(x) + U^G_\mu(x)^\dagger\}, \tag{1}$$

$$\mathcal{F}^G_2 = \sum_{x,\mu} \frac{1}{2} \mathrm{Tr}\{U^G_\mu(x) U^G_\mu(x+\hat{\mu}) + \mathrm{h.c.}\}. \tag{2}$$

$$U^G_\mu(x) = G(x) U_\mu(x) G(x+\hat{\mu})^\dagger, \tag{3}$$

$$G(x) = \exp\left\{-i\sum_a \omega^a(x) T^a\right\}, \tag{4}$$

and u_0 is the plaquette measure of the mean link. We adopt a "steepest decents" approach. The functional derivative of $\mathcal{F}^G_{\rm Imp}$ with respect to ω^a provide

$$\Delta_1(x) \equiv \frac{1}{u_0}\sum_\mu [U_\mu(x-\mu) - U_\mu(x) - \mathrm{h.c.}]_{\rm traceless} \tag{5}$$

$$\Delta_2(x) \equiv \frac{1}{u_0^2}\sum_\mu [U_\mu(x-2\mu)U_\mu(x-\mu) - U_\mu(x)U_\mu(x+\mu) - \text{h.c.}]_{\text{traceless}} \quad (6)$$

and

$$\Delta_{\text{Imp}}(x) \equiv \tfrac{4}{3}\Delta_1(x) - \tfrac{1}{12}\Delta_2(x). \quad (7)$$

The resulting gauge transformation is

$$G_{\text{Imp}}(x) = \exp\left\{\frac{\alpha}{2}\Delta_{\text{Imp}}(x)\right\}, \quad (8)$$

where α is a tuneable step-size parameter. The gauge fixing algorithm proceeds by calculating the relevant Δ_i in terms of the mean-field-improved links, and then applying the associated gauge transformation, Eq. (8), to the gauge field. The algorithm using conjugate gradient Fourier acceleration is implemented in parallel, updating all links simultaneously, and is iterated until the Lattice Landau gauge condition

$$\theta_{\text{Imp}} = \frac{1}{VN_c}\sum_x \text{Tr}\{\Delta_{\text{Imp}}(x)\Delta_{\text{Imp}}(x)^\dagger\} \quad (9)$$

is satisfied with accuracy of $\theta_i < 10^{-12}$.

As this gauge fixing finds a local minimum of the gauge fixing functional, we are necessarily sampling from the first Gribov region. Our ensemble contains no gauge-equivalent configurations and hence has no Gribov copies as such. However, our configurations are local minima and *absolute* minima and therefore are not from the Fundamental Modular Region [19]. It is known from previous $SU(3)$ studies that neither the gluon nor quark propagator display any obvious Gribov noise above and beyond the ensemble statistical noise and so we do not consider it further here [20–22]. It will be interesting to repeat this calculation for the Gribov-copy free Laplacian gauge, and to do a systematic search for Gribov noise in Landau gauge , but these are left for future studies.

The MILC configurations were generated with the $\mathcal{O}(a^2)$ one-loop Symanzik-improved Lüscher-Weisz gauge action [23]. The dynamical configurations use the Asqtad quark action [24], an $\mathcal{O}(a^2)$ Symanzik-improved staggered fermion action which removes lattice artifacts up to order a^2g^2. We refer to the $a = 0.09$ fm lattice as the "fine" lattice and the $a = 0.12$ fm one as the "coarse" lattice.

We explore two light sea-quark masses, $ma = 0.0062$ ($m = 14.0$ MeV) and $ma = 0.0124$ ($m = 27.1$ MeV). The bare strange quark mass was fixed at $ma = 0.031$, or $m = 67.8$ MeV for $a = 0.09$ fm. The values of the coupling and the bare light sea-quark masses are matched such that the lattice spacing is held constant. The simulation parameters are summarized in Table I with the lattice spacings taken from [14].

On the lattice, the bare propagator $S(a; p^2)$ is related to the renormalized propagator $S^{\text{ren}}(\mu; p^2)$ through the renormalization constant [13]

TABLE I. Lattice parameters used in this study. The dynamical configurations each have two degenerate light quarks (up/down) and a heavier quark (strange). The light bare quark masses for the $28^3 \times 96$ lattice are 14.0 MeV and 27.1 MeV with a strange quark mass of 67.8 MeV. For the $20^3 \times 64$ lattice the bare quark masses range from 15.7 MeV to 78.9 MeV. The lattice spacing is $a \simeq 0.12$ fm for the $20^3 \times 64$ lattice and $a \simeq 0.09$ fm [14] for the $28^3 \times 96$ lattice.

	Dimensions	β	a	Bare Quark Mass	# Config
1	$28^3 \times 96$	7.09	0.086 fm	14.0 MeV, 67.8 MeV	108
2	$28^3 \times 96$	7.11	0.086 fm	27.1 MeV, 67.8 MeV	110
3	$20^3 \times 64$	6.76	0.121 fm	15.7 MeV, 78.9 MeV	203
4	$20^3 \times 64$	6.79	0.121 fm	31.5 MeV, 78.9 MeV	249
5	$20^3 \times 64$	6.81	0.120 fm	47.3 MeV, 78.9 MeV	268
6	$20^3 \times 64$	6.83	0.119 fm	63.1 MeV, 78.9 MeV	318

$$S(a; p^2) = Z_2(a; \mu)S^{\text{ren}}(\mu; p^2). \quad (10)$$

In the continuum limit, Lorentz invariance allows one to decompose the full quark propagator into Dirac vector and scalar pieces

$$S^{-1}(p^2) = Z^{-1}(p^2)[i\gamma \cdot p + M(p^2)], \quad (11)$$

where $M(p^2)$ and $Z(p^2)$ are the nonperturbative mass and wave-function renormalization functions, respectively. Asymptotic freedom implies that, as $p^2 \to \infty$, $S(p^2)$ reduces to the tree-level propagator

$$S^{-1}(p^2) \to i\gamma \cdot p + m, \quad (12)$$

up to logarithmic corrections. The mass function M is renormalization point independent and for Z we choose throughout this work the renormalization point as $\mu = 3.0$ GeV, i.e.,

$$S^{\text{ren}}(\mu; \mu^2) = \frac{S(a; \mu^2)}{Z_2(a; \mu)} = 1, \quad (13)$$

thus defining $Z_2(a; \mu)$.

The tree-level quark propagator with the Asqtad action has the form

$$S^{-1}(p) = i\sum_\mu \bar{\gamma}_\mu q(p_\mu) + m, \quad (14)$$

where $q(p_\mu)$ is the kinematic momentum given in [7]

$$q_\mu \equiv \sin(p_\mu)[1 + \tfrac{1}{6}\sin^2(p_\mu)]. \quad (15)$$

The $\bar{\gamma}_\mu$ form a staggered Dirac algebra (see Eq. (A.6) and (A.7) of Ref. [13]). Having identified the kinematic momentum, we define the mass and renormalization functions by

$$S^{-1}(p) = Z^{-1}(q)\left[i\sum_{\mu}(\bar{\gamma}_\mu)q_\mu(p_\mu) + M(q) \right]. \qquad (16)$$

Additional details can be found in Ref. [13]

III. NUMERICAL RESULTS

In Fig. 1 we show the results for the mass function $M(q^2)$ and wave-function renormalization function $Z(q^2)$ for the lightest of our light sea-quark masses for a variety of valence quark masses. In these figures, one valence quark mass (14.0 MeV) is identical to the light sea-quark mass, as in full QCD. The others are partially quenched results. The data are ordered as we expect, i.e., the larger the bare valence quark mass, the higher $M(q^2)$. The wave-function renormalization function, $Z(q^2)$, on the other hand, is infrared suppressed and the smaller the valence quark mass, the more pronounced the dip at low momenta. In Figs. 2 and 3 we instead hold the valence quark mass fixed and vary the sea-quark mass. Clearly the dependence over this small range of sea-quark masses is weak. Unfortunately we only have two dynamical sets to compare, and for the lightest valence quark the data are rather noisy.

Next we work on two lattices with different lattice spacing but similar physical volume. We compare the wave-function renormalization function $Z(q^2)$ and mass

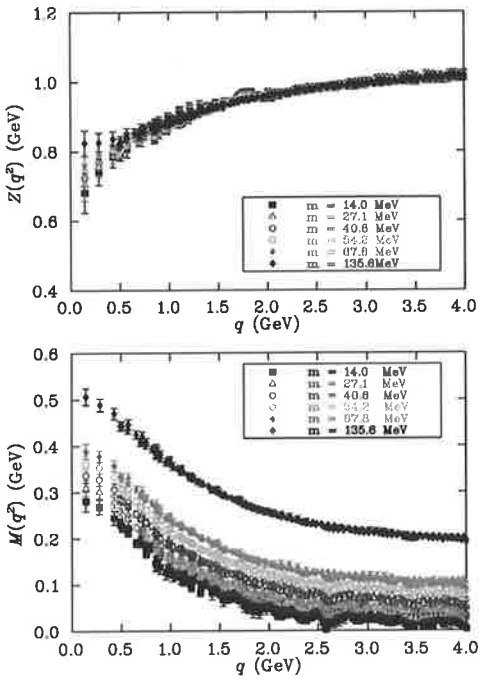

FIG. 1 (color online). The unquenched wave-function renormalization function $Z(q^2)$ and mass function $M(q^2)$ for a variety of valence quark masses (shown in the inset), with the light sea-quark mass fixed at $m = 14.0$ MeV. The renormalization function is renormalized at $q = 3.0$ GeV.

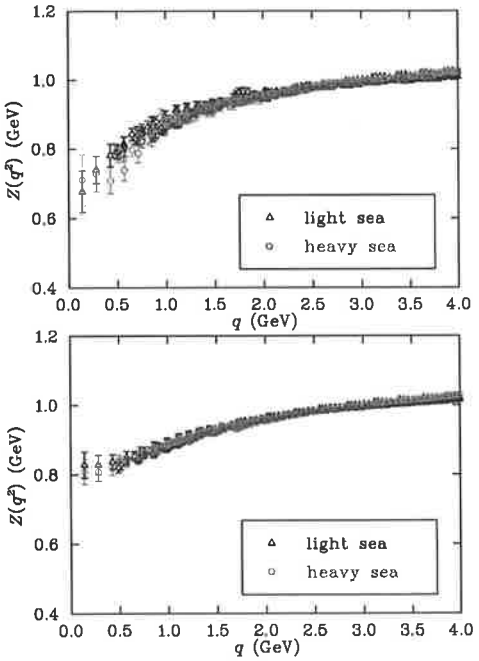

FIG. 2 (color online). The unquenched wave-function renormalisation function for the two different values of the light sea-quark mass on the fine lattice (14.0 MeV and 27.1 MeV). The valence quark masses are $m = 14.0$ MeV (top) and $m = 135.6$ MeV (bottom), the lightest and heaviest in our current sample, respectively. The renormalization function is renormalized at $q = 3.0$ GeV.

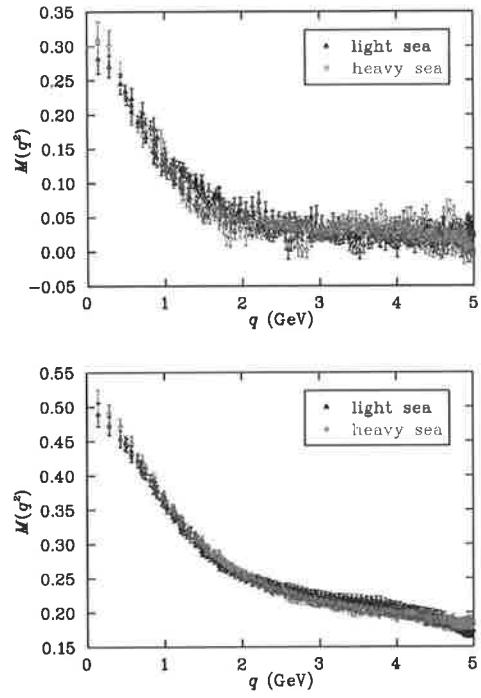

FIG. 3 (color online). The unquenched quark mass function for the two different values of the light sea-quark mass on the fine lattice (14.0 MeV and 27.1 MeV). The valence quark masses are $m = 14.0$ MeV (top) and $m = 135.6$ MeV (bottom), the lightest and heaviest in our current sample, respectively.

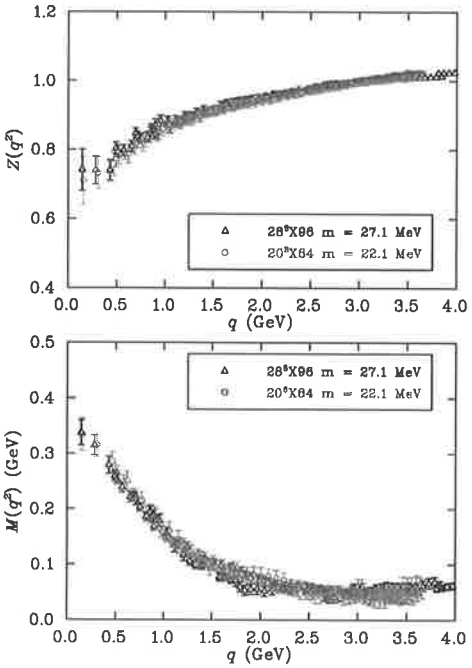

FIG. 4 (color online). Comparison of wave-function renormalization function $Z(q^2)$ and mass function $M(q^2)$ for two different lattices. Triangles correspond to the quark propagator at mass 27.1 MeV from $28^3 \times 96$ with lattice spacing $a = 0.09$ fm. The open circles are the data from $20^3 \times 64$ with lattice spacing $a = 0.12$ fm obtained by interpolating four different set of light quark masses making the $M(q^2)$ value matched for both lattices at $q = 3.0$ GeV. The renormalization point for $Z(q^2)$ is set at $q = 3.0$ GeV for both lattices.

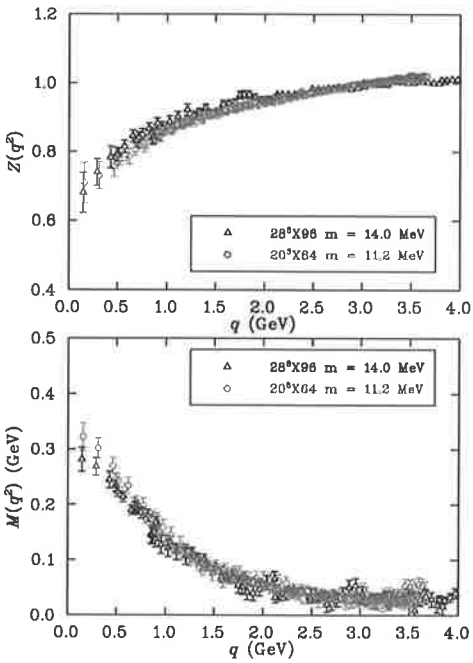

FIG. 5 (color online). This figure is same as Fig. 3, except the light quark mass of $28^3 \times 96$ with lattice spacing $a = 0.09$ fm is $m = 14.0$ MeV. The renormalization point for $Z(q^2)$ is set at $q = 3.0$ GeV for both lattices.

function $M(q^2)$ for two lattices with different lattice spacing a in full lattice QCD.

In Fig. 4, we show the quark propagator from the fine lattice for full QCD (light sea-quark mass and valence quark mass equal) with the light quark mass set to $m = 27.1$ MeV. This is compared with data from the coarse lattice by a simple linear interpolation from the four different data sets so the running masses are the same at $q^2 = 3.0$ GeV. Figure 5 repeats this for the lighter sea-quark, $m = 14.0$ MeV. The quark propagators are in excellent agreement, showing no dependence on the lattice spacing.

IV. CONCLUSIONS

In this study we performed a systematic comparison of the Asqtad quark propagator in full QCD for two lattices with different lattice spacing in order to establish how close these lattices are to the scaling region and hence to the contiuum limit. We compared the two functions $Z(q^2)$ and $M(q^2)$ on fine and coarse lattices and found them to be consistent within errors. We can thus deduce that for both lattices we are close to the scaling region for the quark propagator, which, for example, makes these lattices suitable for future studies attempting to determine quark masses [25].

ACKNOWLEDGMENTS

We thank the Australian Partnership for Advanced Computing (APAC) and the South Australian Partnership for Advanced Computing (SAPAC) for generous grants of supercomputer time which have enabled this project. POB thanks the CSSM for its hospitality during part of this work. This work is supported by the Australian Research Council.

[1] \D. Diakonov, Prog. Part. Nucl. Phys. **51**, 173 (2003); hep-ph/0212026.
[2] E. Ruiz Arriola and W. Broniowski, Phys. Rev. D **67**, 074021 (2003); hep-ph/0301202.
[3] M. S. Bhagwat, M. A. Pichowsky, C. D. Roberts, and P. C. Tandy, Phys. Rev. C **68**, 015203 (2003); nucl-th/0304003.
[4] R. Alkofer, W. Detmold, C. S. Fischer, and P. Maris, Phys. Rev. D **70**, 014014 (2004); hep-ph/0309077.

[5] J. I. Skullerud and A. G. Williams, Phys. Rev. D **63**, 054508 (2001); hep-lat/0007028.
[6] J. Skullerud, D. B. Leinweber, and A. G. Williams, Phys. Rev. D **64**, 074508 (2001); hep-lat/0102013.
[7] P. O. Bowman, U. M. Heller, and A. G. Williams, Phys. Rev. D **66**, 014505 (2002); hep-lat/0203001.
[8] P. O. Bowman, U. M. Heller, D. B. Leinweber, and A. G. Williams, Nucl. Phys. B, Proc. Suppl. **119**, 323 (2003); hep-lat/0209129.
[9] F. D. R. Bonnet, P. O. Bowman, D. B. Leinweber, A. G. Williams, and J. B. Zhang, Phys. Rev. D **65**, 114503 (2002); hep-lat/0202003.
[10] J. B. Zhang, F. D. R. Bonnet, P. O. Bowman, D. B. Leinweber, and A. G. Williams, Phys. Rev. D **70**, 034505 (2004); hep-lat/0301018.
[11] P. Boucaud *et al.*, Phys. Lett. B **575**, 256 (2003).
[12] P. O. Bowman, U. M. Heller, D. B. Leinweber, A. G. Williams, and J. B. Zhang, in *Lattice Hadron Physics*, Lecture Notes in Physics (Springer-Verlag, Berlin, 2005).
[13] P. O. Bowman, U. M. Heller, D. B. Leinweber, M. B. Parappilly, A. G. Williams, and J. B. Zhang, Phys. Rev. D **71**, 054507 (2005); hep-lat/0501019.
[14] C. Aubin *et al.*, Phys. Rev. D **70**, 094505 (2004); hep-lat/0402030.
[15] C. W. Bernard *et al.*, Phys. Rev. D **64**, 054506 (2001); hep-lat/0104002.
[16] NERSC, Gauge connection, http://www.qcd-dmz.nersc.gov.
[17] S. Dürr, Proc. Sci. LAT2005 (2005) 021 [hep-lat/0509026].
[18] F. D. R. Bonnet *et al.*, Aust. J. Phys. **52**, 939 (1999); hep-lat/9905006.
[19] A. G. Williams, Nucl. Phys. A, Proc. Suppl. **109**, 141 (2002); hep-lat/0202010.
[20] L. Giusti, M. L. Paciello, S. Petrarca, B. Taglienti, and N. Tantalo, Nucl. Phys. B, Proc. Suppl. **106**, 995 (2002); hep-lat/0110040.
[21] A. Sternbeck, E.-M. Ilgenfritz, M. Muller-Preussker, and A Schiller, AIP Conf. Proc. No. 756 (AIP, New York, 2005), pp. 284–286; hep-lat/0412011.
[22] A. Sternbeck, E.-M. Ilgenfritz, M. Muller-Preussker, and A Schiller, Nucl. Phys. B, Proc. Suppl. **140**, 653 (2005); hep-lat/0409125.
[23] M. Lüscher and P. Weisz, Commun. Math. Phys. **97**, 59 (1985); **98**, 433(E) (1985).
[24] K. Orginos, D. Toussaint, and R. L. Sugar, Phys. Rev. D **60**, 054503 (1999); G. P. Lepage, Phys. Rev. D **59**, 074502 (1999).
[25] D. Becirevic *et al.*, Phys. Rev. D **61**, 114507 (2000); hep-lat/9909082.

Bibliography

[A+97] H. Aiso et al. Towards understanding of confinement of gluons. *Nucl. Phys. Proc. Suppl.*, 53:570–573, 1997.

[A+04a] C. Aubin et al. Light hadrons with improved staggered quarks: Approaching the continuum limit. *Phys. Rev.*, D70:094505, 2004.

[A+04b] C. Aubin et al. Light pseudoscalar decay constants, quark masses, and low energy constants from three-flavor lattice qcd. *Phys. Rev.*, D70:114501, 2004.

[A+05] C. Aubin et al. Properties of light quarks from lattice qcd simulations. *J. Phys. Conf. Ser.*, 16:160–164, 2005.

[AdFF02a] C. Alexandrou, P. de Forcrand, and E. Follana. The gluon propagator without lattice gribov copies on a finer lattice. *Phys. Rev.*, D65:114508, 2002.

[ADFF02b] C. Alexandrou, P. De Forcrand, and E. Follana. The laplacian gauge gluon propagator in su(n(c)). *Phys. Rev.*, D65:117502, 2002.

[ADFM04] R. Alkofer, W. Detmold, C. S. Fischer, and P. Maris. Analytic properties of the landau gauge gluon and quark propagators. *Phys. Rev.*, D70:014014, 2004.

[AO03] Christopher A. Aubin and Michael C. Ogilvie. Lattice gauge fixing and the violation of spectral positivity. *Phys. Lett.*, B570:59–66, 2003.

[AO04] C. Aubin and Michael C. Ogilvie. Lattice gauge fixing as quenching and the violation of spectral positivity. *Phys. Rev.*, D70:074514, 2004.

[AvS01] Reinhard Alkofer and Lorenz von Smekal. The infrared behavior of qcd green's functions: Confinement, dynamical symmetry breaking, and hadrons as relativistic bound states. *Phys. Rept.*, 353:281, 2001.

[B+] Patrick O. Bowman et al. Qcd propagators: Some results from the lattice. *LC 2005 Proceedings.*

[B+95] Raymond Brock et al. Handbook of perturbative qcd: Version 1.0. *Rev. Mod. Phys.*, 67:157–248, 1995.

[B+98] Claude W. Bernard et al. Quenched hadron spectroscopy with improved staggered quark action. *Phys. Rev.*, D58:014503, 1998.

[B+99] D. Becirevic et al. Asymptotic behaviour of the gluon propagator from lattice QCD. *Phys. Rev.*, D60:094509, 1999.

[B+00a] D. Becirevic et al. Asymptotic scaling of the gluon propagator on the lattice. *Phys. Rev.*, D61:114508, 2000.

[B+00b] Claude W. Bernard et al. Scaling tests of the improved kogut-susskind quark action. *Phys. Rev.*, D61:111502, 2000.

[B+01] Claude W. Bernard et al. Quark loop effects with an improved staggered fermion action. *Nucl. Phys. Proc. Suppl.*, 94:237–241, 2001.

[B+05] Patrick O. Bowman et al. Unquenched quark propagator in landau gauge. *Phys. Rev.*, D71:054507, 2005.

[BBL+99] Frederic D. R. Bonnet, Patrick O. Bowman, Derek B. Leinweber, Anthony G. Williams, and David G. Richards. Discretisation errors in landau gauge on the lattice. *Austral. J. Phys.*, 52:939–948, 1999.

[BBL+01] Frederic D. R. Bonnet, Patrick O. Bowman, Derek B. Leinweber, Anthony G. Williams, and James M. Zanotti. Infinite volume and continuum limits of the landau-gauge gluon propagator. *Phys. Rev.*, D64:034501, 2001.

[BBL+02] Frederic D. R. Bonnet, Patrick O. Bowman, Derek B. Leinweber, Anthony G. Williams, and Jian-bo Zhang. Overlap quark propagator in landau gauge. *Phys. Rev.*, D65:114503, 2002.

[BBLW00] Frederic D. R. Bonnet, Patrick O. Bowman, Derek B. Leinweber, and Anthony G. Williams. Infrared behavior of the gluon propagator on a large volume lattice. *Phys. Rev.*, D62:051501, 2000.

[Ber06] C. Bernard. Staggered chiral perturbation theory and the fourth-root trick. 2006.

[BGLM00] Damir Becirevic, Vicente Gimenez, Vittorio Lubicz, and Guido Martinelli. Light quark masses from lattice quark propagators at large momenta. *Phys. Rev.*, D61:114507, 2000.

[BHL+04a] Patrick O. Bowman, Urs M. Heller, Derek B. Leinweber, Maria B. Parappilly, and Anthony G. Williams. Unquenched gluon propagator in landau gauge. *Phys. Rev.*, D70:034509, 2004.

[BHL+04b] Patrick O. Bowman, Urs M. Heller, Derek B. Leinweber, Anthony G. Williams, and Jian-bo Zhang. Infrared and ultraviolet properties of the landau gauge quark propagator. *Nucl. Phys. Proc. Suppl.*, 128:23–29, 2004.

[BHL+05] P. O. Bowman, U. M. Heller, D. B. Leinweber, A. G. Williams, and J. B. Zhang. Quark propagator from lqcd and its physical implications. *Lect. Notes Phys.*, 663:17–63, 2005.

[BHLW02] Patrick O. Bowman, Urs M. Heller, Derek B. Leinweber, and Anthony G. Williams. Gluon propagator on coarse lattices in laplacian gauges. *Phys. Rev.*, D66:074505, 2002.

[BHLW03] Patrick O. Bowman, Urs M. Heller, Derek B. Leinweber, and Anthony G. Williams. Modelling the quark propagator. *Nucl. Phys. Proc. Suppl.*, 119:323–325, 2003.

[BHW02] Patrick O. Bowman, Urs M. Heller, and Anthony G. Williams. Lattice quark propagator with staggered quarks in landau and laplacian gauges. *Phys. Rev.*, D66:014505, 2002.

[BMSY90] Claude W. Bernard, Daniel Murphy, Amarjit Soni, and Kenton K. Yee. Lattice quark propagator in fixed gauges. *Nucl. Phys. Proc. Suppl.*, 17:593–598, 1990.

[BO01] Claude Bernard and Others. The qcd spectrum with three quark flavors. *Phys. Rev.*, D64:054506, 2001.

[BP93] Vernon D. Barger and R. J. N. Phillips. Collider physics: 1993. 1993.

[BP95] Kirsten Buttner and M. R. Pennington. Infrared behavior of the gluon propagator: Confining of confined? *Phys. Rev.*, D52:5220–5228, 1995.

[BPRT03] M. S. Bhagwat, M. A. Pichowsky, C. D. Roberts, and P. C. Tandy. Analysis of a quenched lattice-qcd dressed-quark propagator. *Phys. Rev.*, C68:015203, 2003.

[BPS94] Claude W. Bernard, C. Parrinello, and A. Soni. A lattice study of the gluon propagator in momentum space. *Phys. Rev.*, D49:1585–1593, 1994.

[BT06] M. S. Bhagwat and P. C. Tandy. Analysis of full-qcd and quenched-qcd lattice propagators. *AIP Conference Proceedings*, 852:225–227, 2006.

[CMT03] Attilio Cucchieri, Tereza Mendes, and Andre R. Taurines. Su(2) landau gluon propagator on a 140**3 lattice. *Phys. Rev.*, D67:091502, 2003.

[CMT05] Attilio Cucchieri, Tereza Mendes, and Andre R. Taurines. Positivity violation for the lattice landau gluon propagator. *Phys. Rev.*, D71:051902, 2005.

[Cuc98] Attilio Cucchieri. Infrared behavior of the gluon propagator in lattice landau gauge. *Phys. Lett.*, B422:233–237, 1998.

[D+88] C. T. H. Davies et al. Fourier acceleration in lattice gauge theories. 1. landau gauge fixing. *Phys. Rev.*, D37:1581, 1988.

[D+04] C. T. H. Davies et al. High-precision lattice qcd confronts experiment. *Phys. Rev. Lett.*, 92:022001, 2004.

[DeG96] Thomas A. DeGrand. Lattice gauge theory for qcd. 1996.

[DeG04] Thomas A. DeGrand. Lattice qcd at the end of 2003. *Int. J. Mod. Phys.*, A19:1337–1394, 2004.

[Dia03] Dmitri Diakonov. Instantons at work. *Prog. Part. Nucl. Phys.*, 51:173–222, 2003.

[Dur05] Stephan Durr. Theoretical issues with staggered fermion simulations. *PoS*, LAT2005:021, 2005.

[Eck98] Gerhard. Ecker. Chiral symmetry. 1998.

[FA05] C. S. Fischer and R. Alkofer. Dynamical chiral symmetry breaking in landau gauge qcd. *AIP Conf. Proc.*, 756:275–277, 2005.

[FGMS03] F. Farchioni, C. Gebert, I. Montvay, and L. Scorzato. Lattice qcd with light dynamical quarks. *Nucl. Phys. Proc. Suppl.*, 119:344–349, 2003.

[Fis03] Christian S. Fischer. Non-perturbative propagators, running coupling and dynamical mass generation in ghost - antighost symmetric gauges in qcd. 2003.

[FN04] Sadataka Furui and Hideo Nakajima. What the gribov copy tells on the confinement and the theory of dynamical chiral symmetry breaking. 2004.

[FN05] Sadataka Furui and Hideo Nakajima. Confinement in the lattice landau gauge qcd simulation. *AIP Conf. Proc.*, 756:281–283, 2005.

[FN06] Sadataka Furui and Hideo Nakajima. Unquenched kogut-susskind quark propagator in lattice landau gauge qcd. *Phys. Rev.*, D73:074503, 2006.

[GC] Gauge connection.

[GLR04] Jochen Gattnar, Kurt Langfeld, and Hugo Reinhardt. Signals of confinement in green functions of su(2) yang- mills theory. *Phys. Rev. Lett.*, 93:061601, 2004.

[GLT+87] Steven A. Gottlieb, W. Liu, D. Toussaint, R. L. Renken, and R. L. Sugar. Hybrid molecular dynamics algorithms for the numerical simulation of quantum chromodynamics. *Phys. Rev.*, D35:2531–2542, 1987.

[Got97] Steven A. Gottlieb. Qcd spectrum - 1996. *Nucl. Phys. Proc. Suppl.*, 53:155–167, 1997.

[GPP+01] L. Giusti, M. L. Paciello, C. Parrinello, S. Petrarca, and B. Taglienti. Problems on lattice gauge fixing. *Int. J. Mod. Phys.*, A16:3487–3534, 2001.

[GPP+02] L. Giusti, M. L. Paciello, S. Petrarca, B. Taglienti, and N. Tantalo. Quark and gluon propagators in covariant gauges. *Nucl. Phys. Proc. Suppl.*, 106:995–997, 2002.

[Gri78] V. N. Gribov. Quantization of non-abelian gauge theories. *Nucl. Phys.*, B139:1, 1978.

[Gro99] David J. Gross. Twenty five years of asymptotic freedom. *Nucl. Phys. Proc. Suppl.*, 74:426–446, 1999.

[Gup97] Rajan Gupta. Introduction to lattice qcd. 1997.

[Haa] R. Haag. Local quantum physics: Fields, particles, algebras. Berlin, Germany: Springer (1992) 356 p. (Texts and monographs in physics).

[Had] A. Hadicke. Infrared behavior of gluon propagator in quarkless quantum chromodynamics and background field method. JENA-N-88-25.

[Hel06] U. M. Heller. Some results from full 2+1 flavor simulations of qcd. *PoS*, HEP2005:104, 2006.

[Jeg96] Beat Jegerlehner. Krylov space solvers for shifted linear systems. 1996.

[Kak] M. Kaku. Quantum field theory: A modern introduction. New York, USA: Oxford Univ. Pr. (1993) 785 p.

[Kan] T. Kaneko. Recent results from unquenched lattice qcd simulations. Prepared for 32nd International Conference on High-Energy Physics (ICHEP 04), Beijing, China, 16-22 Aug 2004.

[Kho04] Alexander Khodjamirian. Quantum chromodynamics and hadrons: An elementary introduction. 2004.

[KO99] Doug Toussaint Kostas Orginos, R.L. Sugar. Variants of fattening and flavor symmetry restoration. *Phys. Rev.*, D60:054503, 1999.

[KR04] A. Krassnigg and C. D. Roberts. Dyson-schwinger equations: An instrument for hadron physics. *Nucl. Phys.*, A737:7–15, 2004.

[L+04] D. B. Leinweber et al. Observing chiral nonanalytic behavior with flic fermions. *Nucl. Phys.*, A737:177–181, 2004.

[Lep96] G. Peter Lepage. Redesigning lattice qcd. 1996.

[Lep98] G. P. Lepage. Lattice qcd for novices. 1998.

[Lep99] G. Peter Lepage. Flavor-symmetry restoration and symanzik improvement for staggered quarks. *Phys. Rev.*, D59:074502, 1999.

[Leu94] H. Leutwyler. Principles of chiral perturbation theory. 1994.

[LRG02] K. Langfeld, H. Reinhardt, and J. Gattnar. Gluon propagators and quark confinement. *Nucl. Phys.*, B621:131–156, 2002.

[LS99] J. F. Lagae and D. K. Sinclair. Improved staggered quark actions with reduced flavour symmetry violations for lattice qcd. *Phys. Rev.*, D59:014511, 1999.

[LSWP98] Derek B. Leinweber, Jon Ivar Skullerud, Anthony G. Williams, and Claudio Parrinello. Gluon propagator in the infrared region. *Phys. Rev.*, D58:031501, 1998.

[LSWP99] Derek B. Leinweber, Jon Ivar Skullerud, Anthony G. Williams, and Claudio Parrinello. Asymptotic scaling and infrared behavior of the gluon propagator. *Phys. Rev.*, D60:094507, 1999.

[LW85] M. Luscher and P. Weisz. On-shell improved lattice gauge theories. *Commun. Math. Phys.*, 97:59, 1985.

[Ma00] J. P. Ma. A study of gluon propagator on coarse lattice. *Mod. Phys. Lett.*, A15:229–244, 2000.

[Man79] S. Mandelstam. Approximation scheme for qcd. *Phys. Rev.*, D20:3223, 1979.

[Man96] Aneesh V. Manohar. Effective field theories. 1996.

[Man99] Jeffrey E. Mandula. The gluon propagator. *Phys. Rept.*, 315:273–284, 1999.

[MM] I. Montvay and G. Munster. Quantum fields on a lattice. Cambridge, UK: Univ. Pr. (1994) 491 p. (Cambridge monographs on mathematical physics).

[MMS95] P. Marenzoni, G. Martinelli, and N. Stella. The gluon propagator on a large volume, at beta = 6.0. *Nucl. Phys.*, B455:339–356, 1995.

[MO87] J. E. Mandula and M. Ogilvie. The gluon is massive: A lattice calculation of the gluon propagator in the landau gauge. *Phys. Lett.*, B185:127–132, 1987.

[Mut87] T. Muta. Foundations of quantum chromodynamics: An introduction to perturbative methods in gauge theories. *World Sci. Lect. Notes Phys.*, 5:1–409, 1987.

[Mut98] T. Muta. Foundations of quantum chromodynamics. second edition. *World Sci. Lect. Notes Phys.*, 57:1–409, 1998.

[Nai89] Satchidananda Naik. On-shell improved lattice action for qcd with susskind fermions and asymptotic freedom scale. *Nucl. Phys.*, B316:238, 1989.

[Nec03] Silvia Necco. The static quark potential and scaling behavior of su(3) lattice yang-mills theory. 2003.

[Neu87] Herbert Neuberger. Nonperturbative brs invariance and the gribov problem. *Phys. Lett.*, B183:337, 1987.

[NF00] Hideo Nakajima and Sadataka Furui. A test of the kugo-ojima confinement criterion by lattice landau gauge qcd simulations. *Nucl. Phys.*, A680:151–154, 2000.

[P+06a] Maria B. Parappilly et al. Effects of dynamical sea-quarks on quark and gluon propagators. *AIP Conference Proceedings*, 852:237–239, 2006.

[P+06b] Maria B. Parappilly et al. Scaling behavior of quark propagator in full qcd. *Phys. Rev.*, D73:054504, 2006.

[Pap98] Alessandro Papa. Fixed point actions and on-shell tree-level symanzik improvement. *Phys. Lett.*, B437:123–130, 1998.

[Pen95] Olivier Pene. An introduction to lattice qcd. 1995.

[PS] Michael E. Peskin and D. V. Schroeder. An introduction to quantum field theory. Reading, USA: Addison-Wesley (1995) 842 p.

[RAB03] Enrique Ruiz Arriola and Wojciech Broniowski. Spectral quark model and low-energy hadron phenomenology. *Phys. Rev.*, D67:074021, 2003.

[Ric99] D. G. Richards. Lattice gauge theory: Qcd from quarks to hadrons. 1999.

[Rob03] C. D. Roberts. Aspects of dynamical chiral symmetry breaking. 2003.

[Rot05] H. J. Rothe. Lattice gauge theories: An introduction. *World Sci. Lect. Notes Phys.*, 74:1–605, 2005.

[RW94] Craig D. Roberts and Anthony G. Williams. Dyson-schwinger equations and their application to hadronic physics. *Prog. Part. Nucl. Phys.*, 33:477–575, 1994.

[SIMPS05a] A. Sternbeck, E. M. Ilgenfritz, M. Muller-Preussker, and A. Schiller. The gluon and ghost propagator and the influence of gribov copies. *Nucl. Phys. Proc. Suppl.*, 140:653–655, 2005.

[SIMPS05b] A. Sternbeck, E. M. Ilgenfritz, M. Muller-Preussker, and A. Schiller. The influence of gribov copies on the gluon and ghost propagator. *AIP Conf. Proc.*, 756:284–286, 2005.

[SLW01] Jonivar Skullerud, Derek B. Leinweber, and Anthony G. Williams. Nonperturbative improvement and tree-level correction of the quark propagator. *Phys. Rev.*, D64:074508, 2001.

[Smi02] J. Smit. Introduction to quantum fields on a lattice: A robust mate. *Cambridge Lect. Notes Phys.*, 15:1–271, 2002.

[Sti86] M. Stingl. Propagation properties and condensate formation of the confined yang-mills field. *Phys. Rev.*, D34:3863, 1986.

[SW01] Jon Ivar Skullerud and Anthony G. Williams. Quark propagator in landau gauge. *Phys. Rev.*, D63:054508, 2001.

[SW02] Rainer Sommer and Hartmut Wittig. Fundamental parameters of qcd. 2002.

[Sym83] K. Symanzik. Continuum limit and improved action in lattice theories. 1. principles and phi**4 theory. *Nucl. Phys.*, B226:187, 1983.

[TCM05] A. R. Taurines, A. Cucchieri, and T. Mendes. Temporal correlator in ym(2)(3) and reflection-positivity violation. *AIP Conf. Proc.*, 739:605–607, 2005.

[Tes98] M. Testa. Lattice gauge fixing, gribov copies and brst symmetry. *Phys. Lett.*, B429:349–353, 1998.

[vB97] Pierre van Baal. Gribov ambiguities and the fundamental domain. 1997.

[vSA00] Lorenz von Smekal and Reinhard Alkofer. What the infrared behavior of qcd green functions can tell us about confinement in the covariant gauge. 2000.

[WBB+] Anthony G. Williams, P. O. Bowman, F. D. R. Bonnet, D. B. Leinweber, and J. I. Skullerud. Gluon and quark propagators in landau gauge from the lattice. Prepared for Workshop on Light-Cone QCD and Nonperturbative Hadron Physics, Adelaide, Australia, 13-22 Dec 1999.

[Wil98] Anthony G. Williams. Lattice calculation of the gluon propagator and the strangeness magnetic moment of the nucleon. 1998.

[Wil99] Frank Wilczek. Quantum field theory. *Rev. Mod. Phys.*, 71:S85–S95, 1999.

[Wil02] Anthony G. Williams. Qcd, gauge fixing, and the gribov problem. *Nucl. Phys. Proc. Suppl.*, 109A:141–145, 2002.

[Wil03] Anthony G. Williams. Nonperturbative qcd, gauge-fixing, gribov copies, and the lattice. *Prog. Theor. Phys. Suppl.*, 151:154–160, 2003.

[YLTW02] R. D. Young, D. B. Leinweber, Anthony W. Thomas, and S. V. Wright. Chiral analysis of quenched baryon masses. *Phys. Rev.*, D66:094507, 2002.

[Ynd] F. J. Yndurain. The theory of quark and gluon interactions. Berlin, Germany: Springer (1999) 413 p.

[You04] Ross D. Young. Finite-range regularisation of chiral effective feild theory. *PhD thesis, The University of Adelaide*, 2004.

[ZBL+04] J. B. Zhang, Patrick O. Bowman, Derek B. Leinweber, Anthony G. Williams, and Frederic D. R. Bonnet. Scaling behavior of the overlap quark propagator in landau gauge. *Phys. Rev.*, D70:034505, 2004.

[Zwa91] D. Zwanziger. Vanishing of zero momentum lattice gluon propagator and color confinement. *Nucl. Phys.*, B364:127–161, 1991.

[Zwa94] Daniel Zwanziger. Fundamental modular region, boltzmann factor and area law in lattice gauge theory. *Nucl. Phys.*, B412:657–730, 1994.